Characterisation of engineered nanoparticles and their interaction with natural biological and non-biological material

Cameron Taylor

Linacre College

A thesis submitted for the degree of

Doctor of Philosophy

Department of Materials

Oxford University

October 2014

Abstract

Form, mobility, toxicity and the eventual fate of engineered nanomaterials in environmental ecosystems are currently not well defined and are needed to improve risk assessment and legislation. The present study subjected uncoated zinc oxide (ZnO) nanoparticles (30nm and 200nm) and coated silver (Ag) nanoparticles (Paraffin: 3-8nm and citrate/PVP: 50nm) to different ionic strength media and different types of algal/bacterial extracellular-polymeric species (EPS) at long (6 months) and short (2 weeks) timescales. Changes in particle size distribution and stability were examined using a multi-method approach. Sample concentration and sample polydispersity are important factors when selecting techniques. Uncoated ZnO nanoparticles aggregated heavily in water at high concentrations (1000mg/L). However silver nanoparticles (1-10mg/L) remained stable at all ionic strengths and EPS in this study due to the steric component of their coatings. Nano-toxicological experiments involving cyanobacteria *S.leopoliensis* and green algae *C.reinhardtii* showed size-dependent toxicity from coated nanosilver particles. Smaller nanoparticles (3-8nm) showed greater dissolution over 72h and greater toxicity to both species than 50nm particles indicating silver ions are an important toxicity mechanism. Nanoparticle coatings were likely important in controlling dissolution levels. Cell viability and production of reactive oxygen species (ROS) were shown to be important mechanisms of toxicity to phycological species. Species specific effects were noted for both silver nanoparticles. EPS from *S.leopoliensis* were noted to remove ionic silver from suspension and different types of *C.reinhardtii* EPS were produced when particles underwent different levels of toxic stress indicating that EPS could both affect particle toxicity and be affected by it. This work has demonstrated that coated nanoparticles could remain stable under various ionic strengths and with exposure to algal organic matter for timescales up to 6 months. This could result in adverse effects to aquatic organisms were they to reach environmental systems and is of concern to nanomaterial risk assessors.

Acknowledgements

I would like to start off by acknowledging the NanoFATE project for both funding my research for most of the past four years and for providing excellent opportunities to meet fellow academics and PhD students in my field as well as organising meetings in numerous countries and cities I had not had the occasion to visit before. I would also like to thank Oxford University Materials Department for funding the final 6 months of the PhD.

The first person I would like to thank is my main supervisor Dr Alison Crossley as without her patience, input, guidance, support and help this thesis would not have been written. I am especially grateful for her remaining positive about the project even when I was not, the help she provided in streamlining my writing by reading and re-reading the different chapters and for facilitating access to the different techniques and collaborators I worked with during my time at Oxford. Also big thanks to my second supervisor Professor Chris Grovenor who helped immensely in the latter stages of writing with his input into thesis structure and proofreading a number of chapters.

Special thanks must go to Dr Kerstin Jurkschat who helped me on this project immensely, providing supervision in the lab, advice and ideas on for using the particle sizing techniques as well as TEM help. Also I am supremely grateful to Dr Marianne Matzke who offered a lifeline on my project by agreeing to supervise the nanoecotoxicology aspects of my thesis. I want to thank her for her calm supervision, ideas and support while I was learning an entirely new discipline and for her friendship during the time I spent at CEH.

Further thanks need to go to Dr Claus Svendsen for managing the NanoFATE project and providing advice and help during the time I spent at CEH; Dan whose expertise in flow cytometry was invaluable and whose advice in Aveiro helped to put my project on the right

track. Elma, Carolin and Bill who made CEH a great place to work and who gave me advice about working in an ecotox lab.

Thanks must also go to Dr. Alexandra Kroll for analysing the EPS liquid chromatography samples and Rudo Verwij who processed my silver analytics samples. Gratitude must also go to the OMCS team and the Begbroke Microscopy team for being patient as I was learning many techniques and crashing the TEM vacuum every other session. Also to Nick Golding whose R and stats help was invaluable towards the end.

Further gratitude must also go to all those involved in NanoFate for letting me experience being part of an international team of scientists including Dr Dave Spurgeon, Prof. John Morgan, Dr Pete Kille, Prof Kees Van Gestel, Dr Susano Loureiro, Dr Filipa Calhoa, Lee Walker, Dr Steve Lofts (for his chemistry help), Dr Maria Diez-Ortiz plus fellow students Julian, Fabianne, Jacek, Paula and Pauline.

I also want to acknowledge some of the people who gave me support directly or indirectly and who helped me navigate the strange world of Oxford University and its sub-fuscs, bops, matriculations, balls and formals. Begbroke people especially Laura and Vince, thanks for being there for de-stressing cups of tea when machines broke and mutual moaning about politics and project management forms. Thanks must also go to the people I met and befriended in Linacre College Common Room over the years, you all made my time in Oxford very special (specifically Chauncey, Laird, Nick, Holly, Sarah Adam, Sara, Philly, Rob, Meleesa, Chloe, Nina, Linda, Gaia, Gagan, Claire, Jack, Sam, Aidan, David, Ben, Kat, Aled, Jen, Jon, Meredith, Claire, Rory, Dan, Rachel, Louie, Maddie, Ed, Jamie, Ben, Izzy, Sam, Ge, Ben, Rich, Janina). I could not have completed this thesis without the nights at the Star, wanders round Oxford, games of Catan, gigs, football (UK and USA) celebratory/concillatory drinks and Rusty pub quizzes.

Finally I have to thank my family whose support throughout my time in academia I greatly appreciated even though I forgot to phone home often.

Table of Contents

List of Figures

List of Tables

Common Abbreviations

µg/L – microgram per litre

AAS – Atomic Absorption spectroscopy

Ag – Silver

Ag^+ - Silver ion

AgCl – Silver chloride

$AgNO_3$- Silver Nitrate

AgNPs – Silver Nanoparticles

C.reinhardtii - *Chlamydomonas reinhardtii*

Cl or Cl^- - chloride

CO_2 – Carbon dioxide

CR^- - MBL media containing stressed *C.reinhardtii* EPS

CR^+ - MBL media containing unstressed *C.reinhardtii* EPS

d_{AGG} – cluster diameter (from TEM)

DCF – Dichlorofluorescein stain

DCS - Differential Centrifugal Sedimentation

dEPS – dissolved extra-cellular polymeric substances

d_H - Hydrodynamic diameter (DLS and NTA)

DIH_2O - De-ionised water

DLS - Dynamic Light Scattering

DLVO – Derjaguin-Landau-Verwey-Overbeek theory

d_{pp} – Primary particle diameter (from TEM)

d_s – Stoke's diameter (DCS)

EC_x – Effect Conctration X% - concentration at which X% of cells show an effect (e.g. EC_{50})

EDL – Electric double layer

EM – Electron Microscopy

EPS – extra-cellular polymeric substances – algal/cyanobacteria exudates

FC – Flow Cytometry

FDA - Fluorescein diacetate stain

FL1,2,3,4 – Flow cytometer measurement channel

h – Hour

H_2O_2 – Hydrogen Peroxide

HCO_3^- - Bicarbonate ion

HE – Hydroethidium stain

ISO – ISO bacterial medium

LC-OCD-OND - Liquid chromatography-organic carbon detection-organic nitrogen detection

MBL – Woodshole MBL algal medium

mg/L - milligram per litre – parts per million

min – minute

ml - millilitres

mon - months

MW – Molecular weight

ng/L – nanogram per litre

nm – nanometre

NOM – Natural organic matter

NP - Nanoparticle

NTA - Nano-Tracking Analysis

OM – organic matter

PECs - Predicted Environmental Concentrations

PNEC – Predicted No-Effect Environmental Concentration

PSD - Particle size distribution

PVP – Polyvinylpyrrolidone

ROS – Reactive oxygen species

S - Aspect Ratio

S.leopoliensis- Synechococcus leopoliensis

S_{AGG} – cluster aspect ratio (from TEM)

SEC – Size exclusion chromatography

sEPS – solid extra-cellular polymeric substances

SL^{+} - MBL media containing unstressed *S.leopoliensis* EPS

S_{pp} – Primary particle aspect ratio (from TEM)

SS – Side scatter (flow cytometry)

TEM – Transmission Electron Microscopy

UPH_2O - Ultrapure water

WWTP – Wastewater Treatment Plant

ZnO – Zinc Oxide

ZP- Zeta Potential

Chapter 1. Introduction

1.1 Introduction and Relevance of Nanotechnology

Ever since Richard Feynman popularised the concept of scaling down materials to almost atomic levels in a 1960 lecture, industry has been trying to unlock the novel properties of nanomaterials[1].

Nanotechnology, the creation and manipulation of materials at the nano-scale[2,3], has been identified as a key enabling technology by the European Commission for improving welfare, prosperity and security of citizens in countries through innovation and economic improvement[4]). It is estimated that the sector will grow to be worth 1 trillion dollars by the year 2015[5] encompassing a wide-ranging set of products (Figure 1-1).

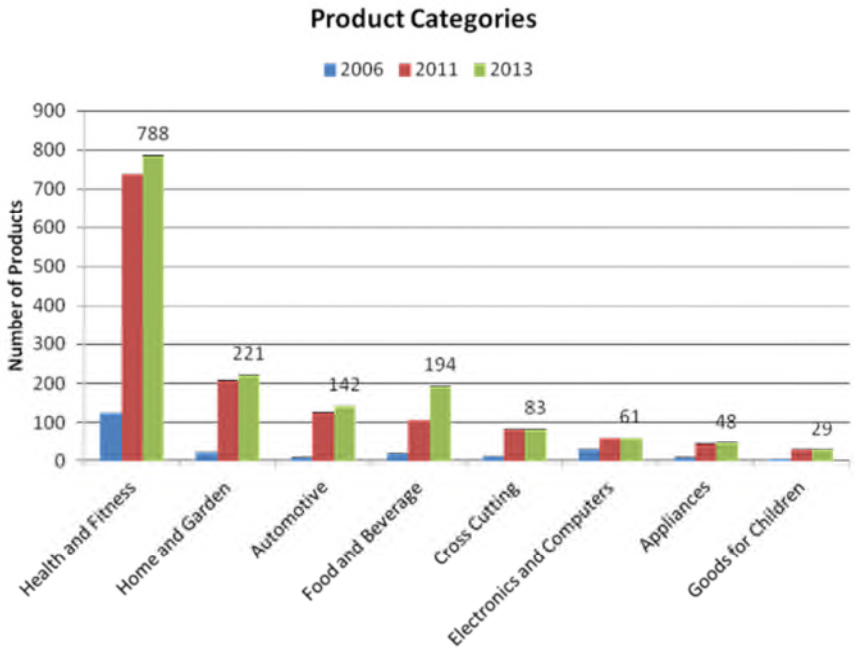

Figure 1-1. Number of products containing engineered nanomaterials per category per year up to 2011. Taken from Woodrow Wilson Database 2011[6]

The definition of 'nano' has been debated by standardisation committees and legislators. Current definitions refer to 'nano' as one dimension of an object being less than 100 nanometres[2,3,7,8]. Structures that fall under the 'nano' umbrella as defined by the British Standards Institution (BSI)[8] include:

- Nano-object: material with at least one dimension within the nanoscale (1-100nm)
- Nano-rod: nano-object that at least two dimensions in the nanoscale with a third longer than the other two (incorporates nano-fibres and nano-tubes)
- Nanoparticle (NP): nano-object that has all three of its outer dimensions within the nanoscale.

These definitions are based entirely on size measurements and do not include other factors such as size distribution, relationships between size and novel nanoscale properties or aggregation/agglomeration of individual particles to encompass larger structures[9].

Different physical and chemical (physicochemical) properties arise at the nano-scale including optical, thermal, strength, solubility, conductivity, electric, magnetic and photo-catalytic attributes desirable for use in many products (described in Table 2-1). Greater particle surface to volume ratio is thought to be a reason for the emergence of new properties as well as the presence of defects/edges on the nanoparticle surface. More atoms are present at the surface in relation to particle diameter at smaller sizes[10,11] (Figure. 1-2) resulting in greater levels of reactivity than larger non-nano (bulk) versions of the same material[10].

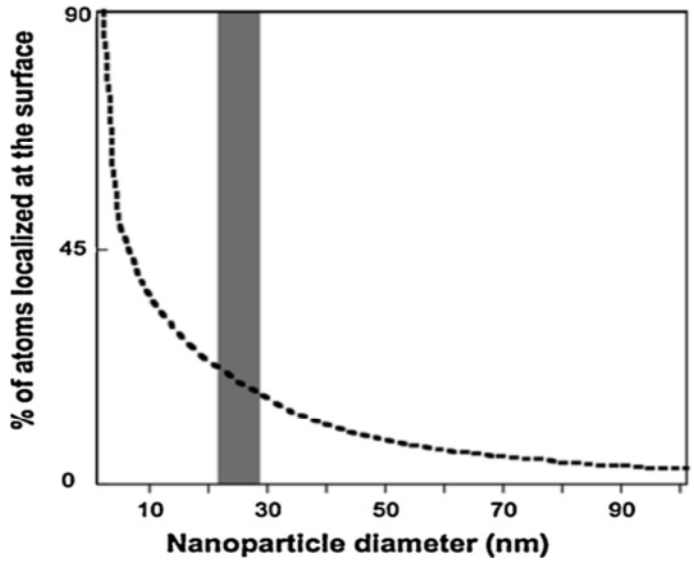

Figure 1-2. The percentage of atoms in a material localised at the surface increases as the diameter of the particle decreases. Taken from Handy et al. 2008[12].

Nano-scale reactivity has resulted in toxicity to a number of aquatic and terrestrial organisms[13,14] however the mechanisms that underpin toxic stress are not fully understood. A debate continues as to whether toxicity is caused by nanoparticle physical properties; ionic species released from surface dissolution of soluble particles or a combination of both for some particles.

1.2 Reasons for Research

As more consumer goods incorporating nanomaterials are developed, increasing amounts of Engineered Nanoparticles (ENPs) may find their way into environmental systems. There are many potential avenues for this, but the most effective anticipated pathway is via sewage treatment systems (as shown in Figure 1-3). These pathways and proven toxicity to microorganisms indicate a potential risk to environmental systems.

Form, mobility, toxicity and the eventual fate of engineered nanomaterials in environmental ecosystems is not well defined which makes assessing and legislating associated risk difficult[14]. A dearth of conclusive studies into behavioural aspects means improving the database of fate effects is imperative to improving risk assessment and hence safe development of nanomaterial products.

Characterisation of nanomaterials in relevant ecotoxicological and environment conditions is yet to be fully investigated and standardised. It is only very recently that nano-ecotoxicology studies have started to incorporate particle characterisation data, and laboratories may be relying on inappropriate methods. As such it is imperative to standardise the best techniques for characterising nano-suspensions for toxicology studies.

Zinc oxide (ZnO) and silver (Ag) nanoparticles are the most widely distributed materials in the environment[15]. Understanding changes which occur to industrially produced ZnO and Ag NPs in a range of media with time and in the presence of suspended organic material and linking this information to imparted toxic mechanisms to aquatic and terrestrial microorganisms is important to defining the risk of nanomaterials.

1.3 Aims of Thesis

This work was conceived within the NanoFATE project: a consortium of 12 partners from 9 different countries that investigated the life cycle analysis of engineered nanoparticles post-production through sewage treatment works and their eventual fate and toxicity to natural environments[16].

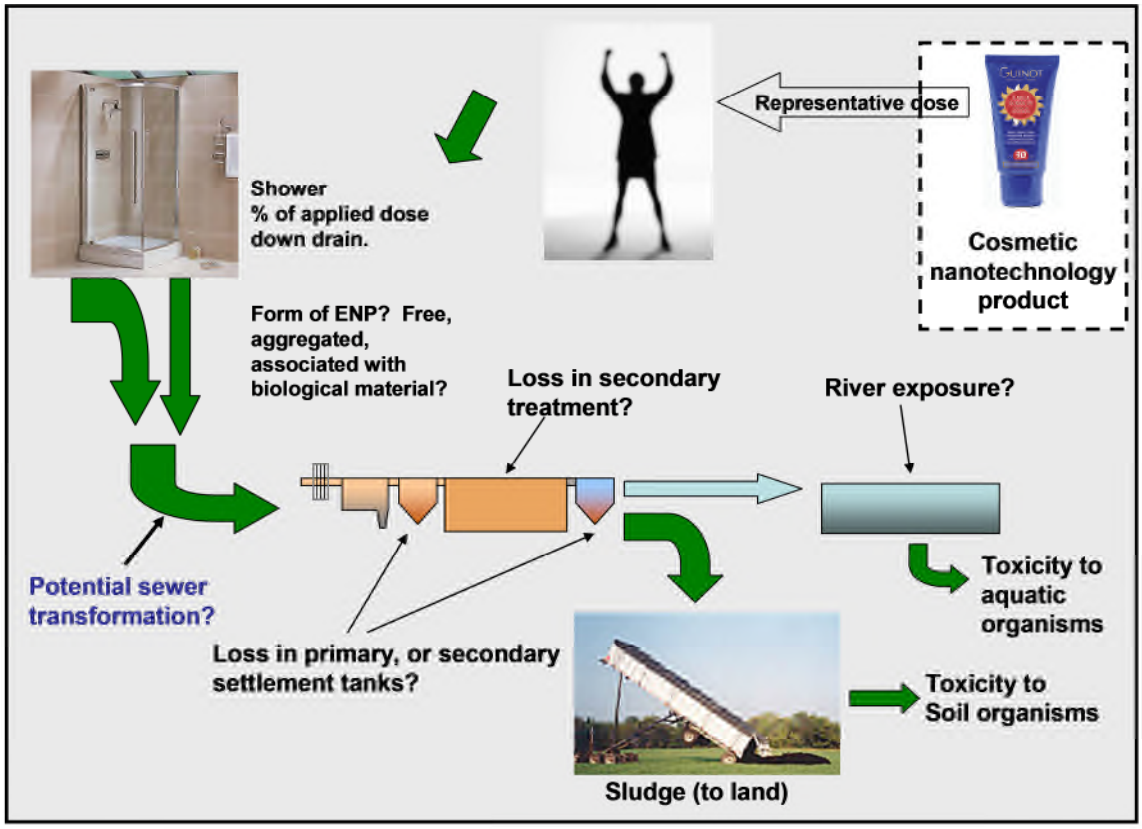

Figure 1-3. Diagram showing a possible pathway of nanoparticles into the environment. Particles from a cosmetic product (i.e. sunscreen) after washing may end-up in the sewage treatment process. The form of the nanoparticles, defined by their physico-chemical interactions with suspended and dissolved material in the surrounding material will specify their transport through the system. Depending on their outcome they can either end up in aquatic systems via effluent, or terrestrial systems via applied biosolids. Taken from NanoFATE website accessed 2014. (https://wiki.ceh.ac.uk/display/nanofate/General+Concepts+of+Project)

It was the intention of the work reported in this thesis to investigate nanoparticle properties and how these relate to toxicity in aquatic and terrestrial matrices relevant to eco-toxicity and realistic environmental scenarios. This gave rise to a number of aims:

- To investigate the applicability and effectiveness of different techniques to understand the size distribution, stability and morphology of zinc oxide and silver NPs in media of varying composition at long and short term timescales including exposure to algae produced extracellular polymeric substances (EPS)

- To investigate the influence and interrelatedness of particle concentration, surface coatings, media ionic strength and exudates from green algae and cyanobacteria on the stability of silver NPs over a two week period
- To investigate the magnitude and mechanism of toxicity of two coated silver NPs on green algae and cyanobacterial species and how this can be related to measured particle properties.

1.4 Thesis Structure

The thesis opens with an introduction to the topic and research aims of this work. A literature review of the theoretical basis, current knowledge and definitions relating to nanotechnology, particle properties, environmental risk assessment and associated eco-toxicology follows in Chapter 2. Chapter 3 acts as both an overview of the theory and limitations of characterisation techniques and an in-depth description of the laboratory methods, media preparation and equipment used in this thesis. Chapter 4 deals with the characterisation of ZnO and coated Ag nanoparticle suspensions in de-ionised water over 5-6 months using a suite of ensemble techniques and electron microscopy (EM). Ensemble techniques are those which derive size values from an average of many particles while single particle techniques measure individual particles separately. Chapters 5 and 6 show characterisation behaviour of two coated Ag nanoparticles in ultrapure water, algal eco-toxicology media and in the presence of different algal and cyanobacteria extracellular polymeric substances (EPS) using ensemble and single-particle techniques and EM. Chapter 7 investigates the magnitude and mechanisms of toxicity imparted on algae and cyanobacteria from the two coated nanoparticles using flow cytometry, analytical methods and fluorescent staining. Chapter 8 concludes this work with the thesis outcomes, how this data fits into

a wider environmental context and future recommendations for continuation of this work.

1.5 References

1. Feynman, R. P. There's plenty of room at the bottom. *Eng. Sci. XXIII* **35,** (1959).

2. RS/RAE. *The Royal Academy and Royal Society of Engineering: Nanoscience and nanotechnologies : opportunities and uncertainties*. (2004).

3. NNI [National Nanotechnology Initiative]. What Is Nanotechnology? (2014). at <http://www.nano.gov/nanotech-101/what/definition>

4. EuropeanComission. *Communication from the Comission to the European Parliament, The Council, The Europoean Economic and Social Committe of the Regions - "Preparing for our future: Developing a common strategy for key enabling technologies in the EU."*(2009).

5. Chowdhury, I., Hong, Y. & Walker, S. L. Container to characterization: Impacts of metal oxide handling, preparation, and solution chemistry on particle stability. *Colloids Surfaces A Physicochem. Eng. Asp.* **368,** 91–95 (2010).

6. Woodrow_Wilson_Database. Project on Emerging Nanotechnologies (2014): Consumer Products Inventory. (2014). at <http://www.nanotechproject.org/cpi/about/updates/ >

7. Lead, J. R. & Wilkinson, K. J. Aquatic Colloids and Nanoparticles: Current Knowledge and Future Trends. *Environ. Chem.* **3,** 159 (2006).

8. BSI. *British Standards Institution -PAS 136:2007 - Terminology for nanomaterials*. (2007).

9. Baalousha, M. & Lead, J. R. in *Environ. Hum. Heal. Impacts Nanotechnol.* 1–29 (John Wiley & Sons Ltd., 2009). doi:doi:10.1002/9781444307504.ch1

10. Tiede, K. *et al.* Detection and characterization of engineered nanoparticles in food and the environment. *Food Addit. Contam. Part A. Chem. Anal. Control. Expo. Risk Assess.* **25,** 795–821 (2008).

11. Moore, M. N. Do nanoparticles present ecotoxicological risks for the health of the aquatic environment? *Environ. Int.* **32,** 967 – 976 (2006).

12. Bottero, J. Y. *et al.* Manufactured metal and metal-oxide nanoparticles: Properties and perturbing mechanisms of their biological activity in ecosystems. *Comptes Rendus Geosci.* **343,** 168–176 (2011).

13. Fabrega, J., Luoma, S. N., Tyler, C. R., Galloway, T. S. & Lead, J. R. Silver nanoparticles: behaviour and effects in the aquatic environment. *Environ. Int.* **37,** 517–31 (2011).

14. Handy, R. D., Owen, R. & Valsami-Jones, E. The ecotoxicology of nanoparticles and nanomaterials : current status, knowledge gaps, challenges, and future needs. *Toxicology* **17,** 315–325 (2008).

15. Bondarenko, O. *et al.* Toxicity of Ag, CuO and ZnO nanoparticles to selected environmentally relevant test organisms and mammalian cells in vitro: a critical review. *Arch. Toxicol.* **87,** 1181–200 (2013).

16. NanoFATE. NanoFATE Website. (2014). at <https://wiki.ceh.ac.uk/display/nanofate/Home>

Chapter 2. Nanomaterials in the Environment: Literature Review

2.1 Introduction

The definition of nanomaterials is still being debated in the scientific and political communities. Current definitions tend to define nanomaterials as having at least one dimension in the range of 1-100nm with size being the key parameter (encompasses nanoparticles which have three dimensions under 100nm)[1–3]. However recently the European Commission has recommended the definition be updated to include size distribution (the full range of sizes present in the material) and particle properties to create a better definition for regulatory purposes[4], stating:

"*Nanomaterial' means a natural, incidental or manufactured material containing particles, in an unbound state or as an aggregate or as an agglomerate and where, for 50 % or more of the particles in the number size distribution, one or more external dimensions is in the size range 1 nm-100 nm*"[5].

Furthermore an aggregate is "*a particle comprising of strongly bound or fused particles*" and an agglomerate is "*a collection of weakly bound particles or aggregates*" [5] with these definitions being used in this thesis.

To put things in context 1nm is 10^{-9}m which is a thousand millionth of a metre and human hairs are ~80,000nm wide[6].

Companies which produce nanomaterials (such as Amepox who produced silver nanoparticles studied in this thesis or Sigma Aldrich) give various information but

usually refer to nanomaterials as nanoparticles, nanopowders or colloids usually giving the expected size distribution, concentration and stabilising agent[7,8]

The rationale for nanomaterial use in industry is that they exhibit novel and useful properties as a result of their small size. The Royal Academy of Engineering express their definition of nanotechnology as incorporating "*design, characterisation, production and application of structures, devices and systems by controlling shape and size at nanometre scale*"[6].

2.2 Historical Context of Nanotechnology

'Nano' materials were being utilised by humans way before the concept of 'nanotechnology' existed. Colloidal gold and silver nanoparticles have been found to be responsible for the dual colours present in ancient dichroic glasses such as the Lycurgus Cup from Rome thought to originate in the 4th century[9]. Between then and the 19th century nanomaterials were used to generate different colours for ceramics and stained glasses albeit in an unwitting manner. It was not until the late 19th century when investigation into these colour effects began and Michael Faraday stated in a lecture "The Bakerian Lecture: Experimental relations of Gold (and other metals) to Light" that colloidal gold was responsible for the red colour in ruby glass[10]. Since then the interesting effects of colloidal particles have been investigated from a huge number of angles including by physicists, chemists and materials scientists amongst others.

The modern concept of nanotechnology was outlined in 1959 in a lecture by physicist Richard Feynman called "There's plenty of room at the bottom"[11] in which he described the potential for manipulating material at a miniature scale; the famous example being fitting the entire Encyclopaedia Brittanica on the head of a pin. The term

'nanotechnology' was not coined for another 15 years until Norio Taniguchi in 1974 described an ion sputter machine's potential for nanometre precision[6].

Vast improvements in visualisation and manipulation technologies have allowed the conception and creation of a huge array of nano containing products. Developments in microscopy during the 20th century from the creation of field emission microscopes in the 1930s to the creation of atomic force microscopy in 1986[12] as well as materials milestones like the discovery of another carbon allotrope, fullerenes, in 1985 have all contributed to the understanding of nanotechnology. Fullerenes (C_n) or 'buckyballs', carbon materials named after the geodesic structures designed by Buckminster Fuller which they resemble, have preceded the discovery of a number of important carbon nanostructures including multi-walled carbon nanotubes in 1991[13,14] and graphene sheets in 2004[15]. These materials have hugely desirable mechanical and electrical properties and work is underway to incorporate them into numerous industries, including aerospace[16], environmental remediation[17], composite materials[17], hydrogen storage for clean energy applications[17,18], and biomedicine[19]. The innovations thus far and the potential for new commercial exploitation of nanomaterials mean it is necessary to understand their properties as a potential pollutant, and so fate studies are important.

2.3 Types of Nanoparticle

There are three main classifications of nanoparticle; natural, incidental and manufactured; of which the latter two are anthropogenic in origin and the former are produced by natural processes in the environment.

2.3.1 Natural Nanoparticles

Natural nanoparticles, or colloids as they were referred to until recently, have existed for billions of years and are created from natural environmental processes[1]. They are both organic and inorganic in nature and wide ranging in origin, from those produced by geologic processes such as erosion, weathering or sedimentation; air-borne particles from natural combustion that can influence atmospheric processes and natural organic matter produced and exuded by microbial or phycological organisms[20–22]. Due to their creation in the environment they are present at background levels in most natural settings such as marine/freshwater systems as well as soils and terrestrial environments. Whether organisms and humans are adapted to the presence of these particles is not yet fully understood, but it is thought to be a function of dose, exposure and rate of changes of habitats[21]. It may be that their existence in conjunction with the evolution of human/animal-kind may result in their being benign[21]. Due to ubiquity they can however play an important role in the fate and mobility of man-made substances such as pollutants that enter environmental settings. Biologically produced nanoparticles produced from plant material or microbial and algal organisms as fulvic/humic acids or extra-cellular polymeric substances (EPS) respectively are especially important when considering nanoparticle behaviour in this thesis and for their fate in the environment.

2.3.2 Incidental Nanoparticles

Incidental nanoparticles (also known as anthropogenic nanoparticles[22]) are formed inadvertently as a by-product of anthropogenic processes. The wearing down of man-made products such as car tyres can result in release of nanoscale products, while

combustion processes such as exhaust fumes and industrial emissions have also been shown to release microscopic particulate matter into the air[23]. It is thought that 50,000kg/year of these unintended particles are released into the environment [24] which means that they could become a problem in the future. The air-borne nature of many of these particles mean that they can become cloud-forming nuclei and as such have the ability to be transported long distances in certain weather conditions[25] and be deposited in a number of different environments including aquatic, marine and terrestrial systems. These products have been shown to cause respiratory problems amongst other adverse effects[26]. Work is being undertaken to distinguish these particles from other human-made manufactured particles in environmental systems[26].

2.3.3 Manufactured (Engineered) Nanoparticles

Manufactured or Engineered nanoparticles (ENPs) are materials which were produced intentionally and manipulated for a specific purpose[21]. Below 100nm ENPs have a wide variety of size (and size distributions), shapes, bulk chemistries and surface chemistries. They can also be formed from single elements or molecules such as silver or zinc-oxide or as composite particles such as gold core silver coated NPs[27] and doped particles used for tracking in the environment[28,29]. The huge range of properties leads to the novel attributes that make them so desirable to the nanotechnology industry and they have been incorporated into a wide range of applications as shown in Table 2-1.

Engineered nanoparticles (and other nanomaterials) can be separated into five main chemical classes[30,31]:

- Zero-valent metals: such as silver (AgNPs), gold (AuNPs) etc.

- Metal oxides: such as zinc oxide (ZnO NPs), cerium oxide (Ce_2O_3 NPs), titanium oxide (TiO_2 NPs)
- Carbons: such as fullerenes, carbon nanotubes (CNTs), graphene
- Quantum dots and semi-conductor materials: such as arsenides, tellurides, selenides, nitrides phosphates, sulphides combined with noble or transition metals[32]
- Nanopolymers: such as dendrimers[33]

When considering these classes for risk assessment purposes it is notable that they do not include many of the particle properties which could have an impact on fate and toxicity. Within each chemical class there is likely to be a wide range of morphologies, size/size distributions, crystal structures and surface types (coatings/stabilisers), and as such it would be difficult to group each set of chemicals based on this classification. Of these chemical classes, metals and metal-oxide NPs are the classes most relevant within this thesis as zinc oxide and silver NPs have been chosen for investigation.

2.3.4 Metal Oxides

Metal oxides are an important class of nanomaterials due to their photo-reactive and catalytic capabilities. Two of the most common materials that belong to this class are titanium dioxide and zinc oxide which tend to be incorporated into skin care products such as sunscreens and cosmetics due to their ability to absorb UV-light[31,34]. Cerium oxide, also included in this group, exhibits photo-catalytic properties which has made these metal oxides very popular for use in solar cells, paints and coatings[31,34].

Table 2-1. Types, Properties and Applications of Engineered Nanoparticles.

Chemical Class	Types	Properties	Uses	References
Metals	Ag, Au, Fe	high electrical and thermal conductivity, surface-enhanced Raman scattering, chemical stability, catalytic activity, non-linear optical behaviour, surface plasmonic resonance effects	inks, microelectronics, medical imaging, bacterial disinfectant (socks, plastics, soaps, pastes, metals and textiles, air filtration devices, toothpastes, baby products, vacuum cleaners, washing machines, fungicides and cosmetics), therapeutic applications (HIV, hepatitis and herpes inhibition), remediation + detoxifying pesticides (waters, sediments, and soils)	Fabrega et al. 2011 Klaine et al. 2008 Benn and Westerhoff 2008 Yu et al. 2013 Rizello and Pompa 2014 Lara et al. 2010 [31,35–39]
Metal Oxides	ZnO, TiO2, Ce2O3, CuO (most common) also CrO2, MoO3, Bi2O3, BaiO2, LiCoO2, INSnO	photocatalysts, UV-blocking, visible transparency, CuO: excellent thermophysical properties,	solar cells, paints, coatings, sun screens, cosmetics, toothpastes, beauty products, skin-care products, combustion catalyst to improve diesel fuel efficiency, gas sensors, oxygen pumps, glasses/ceramics , heat sensors, electronic chips, heat transfer nanofluids, face masks, wound dressings, socks, rubber manufacture, LCDs, pigments (as a whitener), chemical fibers, textiles, self-cleaning windows	Klaine et al. 2008 Auffan et al. 2008 Van Hoecke et al. 2009 Bondarenko et al. 2013 Dastjerdi and Montazer 2010 Martinson et al. 2007 Kenanakis et al. 2012 Kumari et al. 2010 [31,40–46]
Carbons	CNTs (single and multi-walled), Fullerenes, Grapene	excellent thermal and electrical conductance, high strength, hydrophobicity	Plastics, Catalysts, Electrodes, water purification, conductive coatings, batteries and fuel cells, supercapacitors, adhesives, composite	Klaine et al. 2008 [31]

			materials, sensors, electronic components in various transport industries	
Quantum Dots	Noble or Transition metals joined with: arsenides, tellurides, selenides, phosphates, sulphides (e.g. CdSe, CdTe, CdSeTe, InP, ZnSe)	Unique reactive core and optical properties derived from composition, controllable solubility and bioactivity	medical applications (imaging, targeted therapeutics), solar cells, photovoltaics, security inks, photonics, telecommunications, LED displays, data storage and quantum information processing	Klaine et al. 2008 Hardman et al. 2006 [31,32]
Polymers	Dendrimers	Multifunctional with controllable size, shape, space, flexibility and molecular weight	macrocapsules, nanoplastics and latex, glasses (colouring), chemical sensors, modified electrodes, therapeutic applications	Klaine et al. 2008 [31]

In addition cerium oxide has been incorporated as a combustion catalyst into diesel fuels as well as being assimilated into gas sensors and oxygen pumps due its oxygen storage and low redox properties[31,41]. Zinc oxide NPs are known to have the third largest production volumes of metal-containing nanoparticles (after SiO_2 and TiO_2) estimated to be between 550-33,400 tons[42]. As well as sunscreens they are also used heavily in a number of industries including rubber manufacture, solar cells[44], self-cleaning windows[45], LCD screens, whitening pigments and fibers[42,43]. This is due to their useful optical, mechanical, piezoelectric properties and their potential as a wide band-gap 3.37eV semiconductor, as well their ability to be synthesised in a number of different morphologies to maximise these properties[46].

2.3.5 Metals

Zero-valent metals include iron, gold and silver with the latter being the most commonly used metal nanomaterial in consumer products[31]. The Woodrow Wilson Database in the United States in 2011 stated that there of 1,317 NP-containing products 434 comprised of silver[47]. Specific industrial uses include bioaffinity sensing, conductive inks for circuit board creation, data storage devices and optoelectronics which utilise the high electrical and thermal conductivity, surface plasmonic resonance effects, chemical stability, catalytic activity and optical properties that occur for silver particles in the nanoscale[37,48,49]. However use of nano-silver as an antimicrobial agent remains its most potent application and this is estimated to make up 10% of the total commercial and research uses of the material[38]. Within the broad spectrum of antimicrobial applications, nano-silver has been utilised as: foot odour prevention in sock fibres; textiles; air filtration devices; toothpastes; baby products; vacuum cleaners; washing machines, fungicides and cosmetics[31,36,37]. Another highly relevant medical use of nanosilver has included therapeutic functions such as blocking HIV transmission, and inhibition of hepatitis B and herpes viruses[37,39].

2.4 Synthesis of Nanoparticles

To improve these products it is necessary to optimise the properties of the nanoparticles by finding novel fabrication methods and improving existing ones. There are two paradigms of nanoparticle synthesis: top down and bottom up. Top down fabrication is the creation of nanoparticles by reducing a larger piece of material to a smaller (nano) size, usually by cutting, milling or lithographic techniques but also by ion sputtering methods[33]. Bottom-up synthesis form NPs from growth of material from an

atomic/ionic level to nano-size[33]. These techniques are overwhelmingly chemistry based and include: formation over high temperature flames; self assembly in which the particles arrange themselves in particular structures according to their intrinsic properties[6,50]; atomic layer deposition whereby particles are deposited on a substrate and reacted to form structures[50] and other methods such as sol-gel synthesis and vapour deposition in which particles are grown or reacted to form nanoparticles[50]. Of the two, bottom-up methods control particle structure and composition more stringently and the NPs have fewer defects.

As nano-sized particles are inherently unstable they are inclined to come together to form larger clusters or particles, and manipulating synthesis methods to ensure the correct particle sizes form is necessary. During synthesis capping agents can be added to prevent this aggregation/larger particle formation occurring, and these include ligands (citrate, alkanethiols) which provide electrostatic stabilisation, or polymers (such as PEG/PVP) which provide both steric and electrostatic stability (discussed later)[51]. These coatings are especially important when considering particle interactions and fate in environmental contexts.

2.5 Characterisation of Nanoparticles

It is necessary to check the properties of particles once they have been synthesised and especially after they have been introduced to and interacted with new media and constituents. For this thesis the form of particles in a system relevant to eco-toxicology and fate studies is important. The inherent reactivity of NPs may mean that their physico-chemical properties have changed since they entered a new system and understanding these will elucidate mechanisms for persistence, mobility, transport or

dissolution in an aquatic environment. Ionic silver has been known for a long time to be highly toxic to aquatic species, as even low µg/L concentrations can have lethal effects[52], so particle dissolution effects need to be understood. The ability of nanoparticles to aggregate/agglomerate into larger clusters as well as interact with suspended salts, matter or ionic species in the dispersion media is also very important to understanding their fate[21,53].

It is also prescient for the nano-characterisation community to improve methods to detect, characterise and quantify NPs in soil environments. NPs may enter soils via applied biosolids or sewage sludge[54]. These environments are much more complex than aquatic systems as they have both a solid (soil) and a liquid state (soil pore water), and as such it is much more complicated to predict environmental behaviour in these systems[54].

Many of the studies into NP toxicology use different dose metrics, suspension media and characterisation techniques meaning that they cannot be compared easily with other similar experiments[21,53]. Some reviews have discussed the adoption of an all-inclusive framework of characterisation in which a minimum set of parameters are required when characterising particles for toxicity studies. Both pre and post exposure the mass, particle number, surface area, mean particle size/distribution, morphology of NPs and agglomerates, surface chemistry, stability (zeta potential) and dissolution were stated by Pettitt and Lead to be the minimum measurements needed for accurate exposure description[4]. As of yet however, there has been no consensus reached on what characteristics are the most important plus the time-consuming nature of characterisation studies can make this complex[55]. Figure 2-1 shows nanoparticle properties important to the understanding and classification of nanoparticle behaviour in suspension. These properties will likely affect NP interactions with other species and surfaces, and include size/size distribution, concentration, crystal structure,

composition, porosity/surface area, functionality of surface, surface charge and agglomeration state[56]. Most of these properties can be measured by one (if not many) physical or chemical characterisation methods either directly or indirectly with varying degrees of accuracy dependent on particle concentration, heterogeneity of the sample and stability of the sample. As a result, characterisation of the particles in relevant environment media is of paramount importance within the field. The techniques used in this thesis primarily consist of size/size distribution methods and imaging/composition methods, and are described in detail in Chapter 3. Fundamental theoretical differences between these techniques lead to specific advantages and limitations of each which are discussed in Chapter 3. Limitations include overestimation of NP size relating to light scatter effects (DLS, NTA), time consuming nature (DCS, TEM) and difficulty in measuring heterogeneous samples (DLS, NTA, DCS).

The use of contrasting methods with their own advantages and limitations in combination to locate properties of interest is becoming commonplace in characterisation studies. Most of these studies have been undertaken on polymer or ceramic particles, but some studies have begun to look into metallic NPs[57]. Montes-Burgos et al.[58] compared dynamic light scattering (DLS) and nano-tracking analysis (NTA) to study gold NPs and human plasma mixtures. Other studies have assessed polymeric NPs, polystyrene and gold NPs each using a selection of characterisation techniques[59–61]. A study by Mahl et al.[57] which looked at mixed dispersions of silver and gold NPs and another more recent study by Anderson et al.[61] using both monodisperse and polydisperse suspensions indicated that samples with multimodality are difficult to measure by most size distribution methods (DLS, DCS, NTA), and that much work is still needed to create new techniques and improve existing ones. A combination of methods will be used in this thesis (described in Chapter 3) to

demonstrate the need for a suite of techniques to truly understand NP behaviour in relevant matrices to toxicology and fate studies.

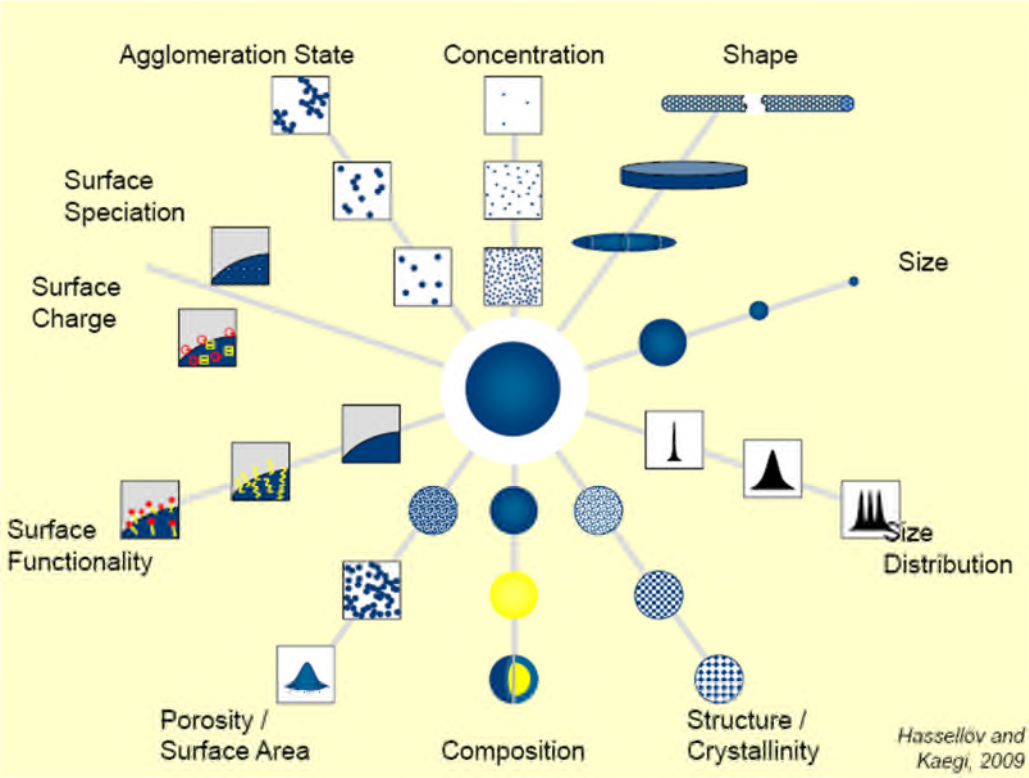

Figure 2-1. The important properties of manufactured nanoparticles that should be considered in characterisation studies. Taken from Hassellöv and Kaegi (2009)[56].

2.6 Environmental Impact and Risk Assessment of Nanomaterials

Further necessity for characterisation is driven by the regulation of nanomaterials. Currently REACH (Registration, Evaluation, Authorisation and Restriction of Chemicals) is about to be implemented in the EU accounting for a number of different chemicals, however discussion is ongoing as to whether nanomaterials are adequately provided for within the framework with regards to levels produced and whether the functionality of the nanomaterials makes their toxicity sufficiently different from bulk versions of the same material[4]. To improve nano-risk assessment it is necessary to

investigate both exposure routes of nanomaterials into environmental systems and also the intrinsic hazard to organisms in those ecosystems and how these facets change under different conditions:

Risk = Exposure x Hazard

2.6.1 Exposure

Exposure is the intensity and duration of contact between a potential stressor (nanomaterials) and an organism/ecosystem/environment[62]. Controlling the exposure will limit the contact to the hazard and therefore lower the risk of the material. Numerous aspects come into play when considering exposure. Greater production of NPs (e.g. ZnO and Ag) will increase the possibility of exposure due to the greater levels of materials in circulation. So too will particular pathways into the environment e.g. dumping of nanoproducts into a river will result in much greater exposure to aquatic organisms due to the high concentrations of these materials. NPs can enter the environment through different matrices (freshwaters, marine waters, soil, sediments, air). However, greater concentrations and direct pathways into the environment may not necessarily result in greater exposure depending on how the particles behave in that system. Aggregation of the particles into larger clusters lowering specific surface area or surface functionalization (such as coatings of organic matter or reaction with suspended/dissolved materials) could render the NPs benign to organisms in that environment. As such the form of NPs in a certain system may also decrease the potential for exposure, and work is required to understand and characterise particles in relevant matrices.

2.6.2 Silver Pathways into Environmental Systems

Some studies have investigated silver exposure pathways. Risk analysis of silver release into freshwaters from textiles and plastics predicted that 15% of all released silver will come from these sources[63]. If a nanoparticle is present within a cosmetic product (such as a sunscreen) an inevitable consequence will be washing the particles into the sewage system. Benn and Westerhoff[36] found that silver particles incorporated into socks for their antibacterial properties could be easily separated from the sock fibres just by washing with water. This was also noted by Geranio et al.[64], who detected greater leaching values using a water composition more relevant to everyday use. Risk assessment studies have identified sewage treatment plants as an important intermediary between anthropogenic and environmental system[63,65] with NPs having been shown to be amalgamated into treatment by-products such as sewage sludge[66]. Sewage sludge is often utilised as a fertiliser in agricultural lands and application is thought be the primary route of NPs into soils[65]. It could also be a secondary route as NPs could also be washed into nearby water bodies by runoff from rain[31,66].

It is difficult to assess the levels of NPs in complex environmental systems due to limitations of in situ characterisation and the inability of most affordable or common techniques to be able to detect and quantify the form and concentration of NPs above natural baseline levels. Further gaps in knowledge can be attributed to unmonitored sources and production levels making estimation of values difficult[67].

2.6.3 Microorganisms – Relevance and Biology

Algae and bacteria are important to environmental systems as they play a major role in nutrient cycling, contribute heavily to the carbon content of freshwater ecosystems and play a large role in primary production of organic matter from light energy[31]. Different types of algae exist classified by their chlorophyll content[68]. Green algae such as *Chlamydomonas reinhardtii* used in this thesis are known to contain chlorophyll a and b which can be used as marker for characterisation by flow cytometry. Algae are one of the key species on which toxicological risk assessments such as REACH or the EU Biocide Regulation are based[69]. This is due to their being one of the most sensitive markers for toxic study[69]. Algae will generally consist of a cellulose derived cell wall with 5-20nm pores which acts as a semi-permeable barrier to larger materials in the environment and acts to retain the algae's structure[70]. Cyanobacteria are single-celled microbial organisms that unlike other prokaryotic bacterial species gain their energy from photosynthesising. Their cell walls consist mainly of peptides[71] and a different membrane system compared to the green algae. Few nano-toxicology studies have been undertaken on cyanobacteria compared with other microorganisms, and as such cyanobacterium *Synechococcus leopoliensis* was used as a test organism in this thesis.

2.6.4 Hazard and Nano-ecotoxicology

With entry into environment systems a likely potential outcome, these highly reactive particles may induce a toxic effect on local species that live in these environments.

Much of the literature agrees that particle properties at the nanoscale are an important determinant of the potential hazards these particles could have on environmental health[72]. Determining the hazardous nature of nanoparticles, an intrinsic property of the material being measured, is important to improving risk assessment.

Ecotoxicology is the field of study that investigates chemical pollutants and their ecological and toxicological significance to biological organisms and communities with respect to their fate in the environment[73]. This includes nanoparticles. Nano-toxicology is an emergent field within this subject[74] and a large number of studies have been undertaken that encompass many different biological facets - among them dose studies and toxicogenomics. However, despite the increasing volume of studies the magnitude and modes of toxicity are still to be determined. It is still debated whether the nanoparticles themselves cause toxicity to aquatic microorganisms or whether dissolved ionic species released from the NP surface are responsible[70,75–7879,80]. On top of this the mechanisms of toxicity for either particles or ions is also still debated, with membrane damage and oxidative stress cited as the likely candidates[70,81,82]

Toxicity studies rely on acute (short term) and chronic (longer term) quantification of the concentrations that cause negative effects to a particular endpoint e.g. growth inhibition. Effect concentration (EC_x) values are used as markers for this information. For example EC_{50} for acute algal toxicity tests are the concentrations at which 50% of the algae's growth is inhibited. EC_x values are dependent on the properties of the exposure set-up and can be used in risk assessment. These values are incorporated into risk models to help predict damaging concentrations in the environment or to assess species sensitivity. Most of these experiments occur in the lab in simulated conditions and as such it may be difficult to extrapolate data to a realistic environmental ecosystem with variable ionic and chemical conditions.

2.6.5 Silver Toxicity to Aquatic Microorganisms

A number of eco-toxicology studies have been devoted to silver nanoparticles, of which many use algae and bacterial species as test organisms. Table 2-2 outlines many of these studies. Aquatic microorganisms are among the most sensitive to NP toxicity and hence should 'drive' the risk assessment[69].

Adverse effects on microbial growth have been noted for both gram-positive and negative bacterial species[83–85], photosynthesising bacterial species (cyanobacteria)[7971] and both freshwater and marine algae and diatoms[70,76–78,80].

Mechanisms of toxicity to bacterial species were thought to relate to direct particle attachment to the cell surface causing damage to cell membranes, nanoparticle internalisation through the membrane or release of silver ions. Particle properties including oxidation potential, size and {111} planar surface area were proposed to effect *E.coli* toxicity[83–86], but the particle surface area effects on toxicity were not appraised [73]. Sotiriou and Pratsinis[87] have shown that the antibacterial activity of smaller Ag NP (<10nm) is dominated by Ag^+ ion release as opposed to larger NPs which can elicit toxic effect from the particle itself.

Studies into mechanisms of toxicity to algae species are still sparse in the literature and this subject is still being debated. Some studies indicate that silver NP toxicity to algae and cyanobacterial species is influenced heavily by the release of ionic silver from NP dissolution[70,75–78] while others indicate that particle properties are also likely playing a role[79,80].

There is worry that smaller NPs could enter through these cell wall pores to cause toxic stress to the algae/cyanobacteria. One study indicated that the cell wall was an important barrier to silver uptake into the organism[88]. Within the cell wall a membrane

bilayer made from lipids governs endocytosis[70,76]. There is worry that NPs or ions that breach the cell wall will damage the cell membrane. Examples of membrane integrity loss and cell lysis have been noted in the literature[76,82,83,89–92].

Oxidative stress is also thought to be a major mechanism for algal toxicity as nanoparticles, due to their high reactivity, are thought to form oxygen free radicals at their surface[93]. Most algal species have anti-oxidant mechanisms but excess reactive oxygen species (ROS) will cause damage to algal cell components such as DNA[94].

The modes and magnitude of toxicity are thought to be particle and species specific and so extensive characterisation accompanying each toxicity test is required. On top of this studies into more complex environs through microcosm/mesocosm experiments are needed (some of which have already been undertaken[71,95,96]) to understand toxicity at an ecosystem level. More information will aid in understanding hazard and therefore risk to environmental systems.

2.6.6 Applying Toxicity Data to Risk Assessment

Predicted Environmental Concentrations (PECs) are the expected concentration values for chemicals in an environmental compartment. Due to the difficulties in characterisation in environmental systems there is very little actual concentration data for NPs in realistic scenarios and therefore modelling using known physicochemical characterisation and degradation information is needed to create PECs[97,98]. PNECs (Predicted No Effect Concentrations) are the concentrations at which no adverse effects are noted for the pollutant and require knowledge and extrapolation of EC_x values in nanoparticle toxicology studies. For PNECs, an assessment or safety factor is applied to ensure that the high uncertainty in toxicity assessment is accounted for[99]. A

ratio of PEC/PNEC can be used to assess the risk of a pollutant in a particular environment. A PEC/PNEC ration of <1 will indicate that there is little risk, 1-100 indicate possible risk but more data is needed, while >100 indicates that there is risk and it should be lowered immediately[67].

Numerous models have been used to predict PECs/PNECs by a number of different laboratories[98] although owing the constantly improving data-sets the assessed values alter fairly rapidly. The gaps in modelling studies are beyond the scope of this thesis but are outlined in the literature[98] and include the way that models incorporate physic-chemical properties as well as differing estimations of NP production. The most recent models have begun to look at impacts of spatial and temporal properties of NP inputs and sinks towards PECs[100]. These have indicated that levels will rarely reach above 20ng/L (Nano-Ag) or 300ng/L (Nano-ZnO) in high population density and low water flow areas in Europe, including the Rhine and Po river basins, south-east England and densely populated Mediterranean areas considering information from 1971-2000[100]. In a review of recent modelling studies Gottschalk et al.[98] indicated predicted environmental concentrations of AgNPs in surface waters (10^{-5}-10^{0}µg/L), WWTP effluents (10^{-3}-10^{2}µg/L) and biosolids/sediments (10^{-4}-10^{2}µg/L). However most of the models reviewed only touch on Ag NP transformations and shape/agglomeration behaviour which are necessary to understand the form, toxicity and mobility of these particles in the environment[98]. Another study noted that silver levels in many rivers around the world reached levels which would cause toxicity to environmental bacterium *Pseudomonas putida*[69].

2.7 Properties That Affect Stability and Nanoparticle Interactions in an Environmental Setting

2.7.1 Size, Surface Area, Shape

Nanoparticulates (<100nm) develop different optical, thermal, strength, solubility, conductivity, electric, magnetic and photo-catalytic attributes compared to bulk phase of the same materials[101]. The size and surface area of nanoparticles are intrinsically linked, with smaller sized NPs resulting in greater surface area per unit mass and hence a greater proportion of atoms present at the surface and a higher surface energy and reactivity[22,101,102] (Figure 2-2). At sizes below 20-30nm, particles are thermodynamically unstable and recrystallization can occur to reduce the surface free energy and much more stable configurations[40].

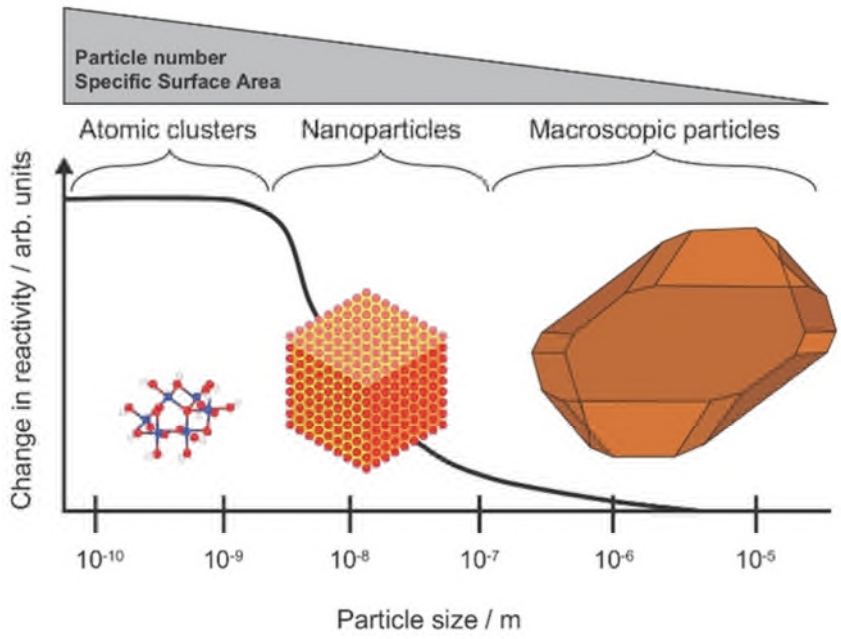

Figure 2-2. Demonstrating the change in surface area and reactivity as particles become larger or smaller. Taken from Hartland et al. 2013 (adapted from Wigginton et al. 2007)[20,103].

These changes in particle size and surface area may influence the interaction with other suspended species or the toxicity with organisms. Greater reactivity at the surface may result in greater toxicity if in contact with organisms which could be exacerbated by the possible ability of the smaller particles to enter cell membranes through pores. Instability resulting from the high energies involved could result in cluster and aggregation actually lowering bioavailability[24]. It has also been noted that dissolution can increase as reactivity increases down into the nanoscale according to the Ostwald-Freundlich equation at least to sizes down to a few nm[104].

The morphology of the particles play a role in the formation of aggregates, with diffusion, attachment efficiency and prominence of surface crystal faces all properties likely to affect particle interactions and toxicity[105].

2.7.2 Colloids

To discuss particles dispersed in a liquid media including the algal eco-toxicology media used in this thesis and natural waters it is necessary to understand the colloidal theories that underpin the relationship between NPs and their stability in dispersion. Dispersions of NPs can be considered as a colloidal system. This is a close mixture of substances in which at least one phase is homogenously dispersed (the colloid) amongst a larger continuous liquid phase (the dispersion medium)[106]

Most colloidal systems (particularly nanoparticle suspensions) are thermodynamically unstable and therefore when creating a colloid, energy must be supplied to disperse the particles in the medium[107]. As a result the system will constantly be trying to get back to its initial energetically favourable non-dispersed state[108]. NPs within the system

will collide with each other and constantly stick together and separate, as well as sediment out of the liquid[21,53].

Suspended particles will be subject to a number of forces which will affect their stability regardless of any chemical or physical interactions with other suspended matter: Gravity, buoyancy/frictional forces and stochastic Brownian motion (random movements caused by particle interaction)[109].

2.7.3 Stability of Particles in Natural Waters

Intrinsic physical properties are likely to be dynamic when the NP is in suspension as the size, shape and surface area will change upon interaction with other suspended/dissolved materials or through dissolution of the particles. Homo-aggregation (interaction with other particles of the same type) or hetero-aggregation (interaction with other materials and sizes) will likely also occur when in realistic suspensions[110].

2.7.4 Electrical Double Layer and DLVO Theory

The surface charge of a nanoparticle is predominantly governed by the techniques used to synthesise it and is important when considering behaviour when in suspension. Particles can have either an intrinsic charge as a result of their atomic structure and crystalline defects or be given one by placing it into a polar medium[111].

Table 2-2. Toxic effect of Ag NPs to Algal, Cyanobacterial and Bacterial Species. n/a: not mentioned in study. Based on Fabrega et al. 2011[35] and Romer Roche 2012[112]

Organism	NP size (distribution)	Capping Agent	Shape	Toxic Concentrations	Toxicity Endpoint	Dosing Length	Media/Matrix	Results and NP Effects	Reference
ALGAE									
Chlamydomonas reinhardtii	10-200nm (median 40nm) Volume: 98% were 25±13 nm	Carbonate Coated	Spherical	EC50: 1h: 3300±572nM 2h: 1049±396nM 3h: 879±159nM 4h: 801±84nM 5h: 829±69nM	Growth Inhibition	1-5 days	MOPS media	Toxicity caused by Ag^+ ions released from Ag NP surface when in contact with algal cells	Navarro et al. 2008[76]
Chlamydomonas reinhardtii	40nm	Citrate	n/a	5mg/L: Toxicity greater over 3-5 day period at younger (fast) growth stages than latter (slower growth stages)	Chlorophyll Concentraiton	5-25 days	COMBO Media	Growth phase dependent toxicity. Algal exudates thought to mitigate toxicity of NPs and ion. Both NP specific and ion specific toxic effects	Stevenson et al. 2013[80]
Chlorella vulgaris	Primary NPs: 50nm Agglomerates: 307.3 nm	uncoated	spherical	1mg/L: 34% 10mg/L: 51%	Total Chlorophyll Content (%)	24h	BG-11 media	Decreased cell viability and increased	Oukarroum et al. 2012 [92]

								ROS production and lipid peroxidation also noted. Nothing about mechanisms.	
Pseudokirchneriella subcapitata	Ag-Cit: 14nm Ag-PVP: 15nm	Ag-Cit: citrate Ag-PVP: PVP	n/a	Ag–Cit: 3.0 ± 0.7µg/L Ag–Cit+4 mg/L SRHA: 5.2 (4.6–5.8)µg/L Ag–Cit+8 mg/L SRHA: 5.6 (5.5–5.7)µg/L Ag–PVP: 19.5 ± 6.1µg/L Ag–PVP+4 mg/L SRHA: 36.7 (33.8–38.8)µg/L Ag–PVP+8 mg/L SRHA: 48.9µg/L	Growth Inhibition (%)	72h	synthetic fresh water (SFW) prepared using a modified USEPA medium – SRHA was added to media as proxy for organic matter	Ag^+ ions generally more toxic than Ag–Cit and Ag–PVP. Presence of NOM: Stabilisation and reduced toxicity	Angel et al. 2013 [78]
Pseudokirchneriella subcapitata	26.6±8.8nm	Sodium Citrate	Spherical	EC50: 0.19mg/L	Growth Inhibition	96h	Moderately hard freshwater	Ag ions more toxic than Ag NPs	Griffitt et al. 2008 [113]
Pseudokirchneriella subcapitata	3–8 nm	Alkane Coating	Spherical	EC50: 32.40 µg/L	Growth Inhibition	72h	Woods Hole MBL culture medium	Different in toxicity between NP and $AgNO_3$ relate to rate of interaction between released Ag^+ ions, chloride in media and algae exudate.	Ribeiro et al. 2013 [114]

CYANOBACTERIA									
Synechococcus Sp.	20nm, 40nm, 100nm	Not stated but electrostatically stabilised during synthesis (synthesised with maltose)	spherical	10µM after 72h – 100% Growth Inhibition at all NP sizes	Growth Inhibition	72h	blue−green11 (Bg1150) cyanobacterial medium	Below 10µM size dependent toxic effects. Possible ion and NP combined toxic mechanism	Burchardt et al. 2012 [79]
Microcystis aeruginosa	20-50nm	No capping agent (synthesised with Tannic Acid)	n/a	0.001mg/L: 2.5% 0.01mg/L: 14% 0.1mg/L: 37% 1 mg/l: 87%	Growth Inhibition	24h	natural eutrophic lake water (from Lake Ilgam, Seoul, Korea)	NPs possible penetrated thin cyanobacterial cell wall.	Park et al. 2010 [71]
MARINE									
Thalassiosira pseudonana	20nm, 40nm, 100nm	Not stated but electrostatically stabilised during synthesis (synthesised with maltose	spherical	10µM after 72h - 20nm :50% 40nm: 60% 100nm: 40%	Growth Inhibition	72h	Artifical Sea Water	Below 10µM size dependent toxic effects. Possible ion and NP combined toxic mechanism	Burchardti et al. 2012 [79]
Dunaliella tertiolecta	Primary NPs: 50nm Agglomerates: 448.9 nm	Uncoated	spherical	1mg/L: 45% 10 mg/L: 75%	Total Chlorophyll Content (%)	24h	McLachlan Media	Decreased cell viability and increased ROS production and lipid peroxidation also noted. Nothing about mechanisms. No cell wall therefore	Oukarroum et al. 2012 [92]

								potentially greater effect .	
Thalassiosira weissflogi	60-70nm	Polyvinylpyrrolidone (PVP)	n/a	No toxicity observed from NPs	n/a	48h	Media with variable C, N and P nutrients	Toxicity was observed for Ag^+ released from AgNPs after samples were filtered <22µm	Miao et al. 2009 [77]
BACTERIA									
Escherichia coli	4-24nm Mode: 12nm	Daxad 19	n/a	10 µg/cm^3: 70% inhibition of bacterial growth (CFU) 50-60µg/cm: 100% inhibition of bacterial growth inhibition (CFU) 10, 50, and 100 µg/cm^3 caused delay in bacterial growth	Growth Inhibition of colony forming units (CFU) and growth delay of suspended bacteria	9h-24h	Luria–Bertani (LB) medium + Agar Plates	Pits were observed in the bacterial cell wall after interaction with NPs	Sondi & Salopek-Sondi 2004 [83]
Escherichia coli	Spherical/Triangular: 39-40nm Rod-shaped: average edge length >100 nm and mean diameters of ~16 nm	Citrate	Spherical, Rod-shaped, (truncated) triangular	Truncated: 100% inhibition of growth: 1µg. Spherical: 12.5µg reduced the number of colonies significantly, 50 to 100µg/L caused 100% inhibition Rod-shaped: No complete	Inhibition of Growth	0-26h	Difco nutrient broth (NB) + Agar Plates	Truncated NPs more toxic than other forms of NP	Pal et al. 2007 [85]

				inhibition at any concentration.					
Escherichia coli	9.2 ± 2.8 nm	citrate	Spherical	Silver sensitive strain: 2 nM Silver resistant strain >80 nM	Minimum inhibitory concentration	24h	(Hepes) buffer + Luria–Bertani medium	Antibacterial acitivty of AgNPs due to surface forming Ag^+ ions after oxidation	Lok et al. 2007 [86]
Gram Negative Bacteria species	16±8nm	n/a	Icosahedral, twinned, decahedral	>75 μg/ml no significant growth	Bacterial Growth (CFU)	30 minutes	Luria–Bertani (LB) medium and Agar plates	AgNPs attached to the cells and [111] crystal facet more toxic	Morones et al. 2005 [84]
Escherichia coli	4-16nm	n/a	Spherical, moncrystalline	1mg/L – greater Ag/SiO_2 results in more toxicity	Growth Inhibition	330minutes	Luria-Bertani (LB) broth	stronger antibacterial activity for smaller nanosilver particles, smaller nPs more release of $Ag^=$ deciding toxicity	Sotirou and Pratsinis 2010 [87]

2.7.4.1 Electrical Double Layer

The Electrical Double Layer (EDL) model proposed by Helmholtz in 1853[106] and further amended by Guoy, Chapman and Stern respectively over time has become fundamental in describing the nature of charged particles within a liquid media[115] (Figure 2-3). Charged surfaces in ionic solution will attract and repel oppositely charged surfaces and similarly charged surfaces respectively, and as such are responsible for electrostatic stabilisation[111].

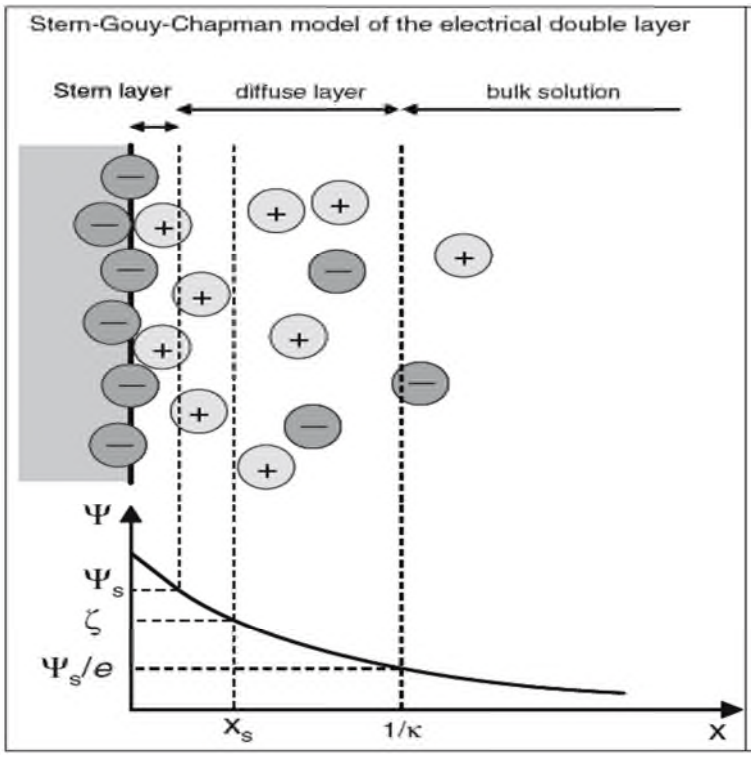

Figure 2-3. Diagram of the electrical double layer (EDL) around nanoparticles: 1/κ is the Debye length, zeta potential (ζ), electrostatic potential (ψ), electrostatic potential at the stern layer (ψs), Euler's number (e), Boltzmann constant (k). X is a distance from the surface, Xs is the distance where ions and molecules are mobile and can be sheared off (shear plane), and potential here is measured as the zeta potential. Taken from Handy et al. 2008 [53].

Theoretically a particle surface in suspension has two demarcated layers: an inner Stern layer which is split into inner and outer Helmholtz planes (IHP and OHP respectively); and an outer diffuse (Guoy-Chapman) layer[53,111]. IHP is the boundary within which ions are specifically adsorbed onto the NP surface (i.e. not readily removed by ion exchange)[53]. OHP

is the closest that the central point of a hydrated (water coated) species can get to the particle surface. The diffuse layer contains excess ionic species that are non-specifically adsorbed and as a result, although attracted to the particle surface, they are able to move around in that particular area, known as the slipping plane[53].

The thickness of the entire EDL can be measured by utilising the Debye length (1/κ, κ^{-1})[116]:

$$\kappa^{-1} = \left(\frac{e^{e}\sum \rho_i z_i^2}{\varepsilon_0 \varepsilon_r kT}\right)^{-1/2} = \left(\frac{\varepsilon_0 \varepsilon_r kT}{2e^2 I}\right)$$

Where e is the electronic charge, ρ_i is the number density of ion species (i), z_i is the valence of those ionic species, ε_0 is the dielectric permittivity of a vacuum, ε_r is the dielectric constant of the surrounding medium, k is the Boltzmann constant and T is absolute temperature in Kelvin. The EDL will be compressed (shorter Debye length) as the ionic strength of the surrounding media is increased. Standard colloidal dispersions will have a Debye length of less than a nanometre, up to 100nm[107].

When characterising the stability of a suspension, zeta potential (ZP), the electrical potential present at the Stern layer/slipping plane is used and this is controlled by the reciprocal of the Debye length[117]. This value can also be used as a proxy value for the charge of a suspended particle; however technically it is the voltage that results from the surface charge and flow dynamics near the surface of a particle[53].

2.7.4.2 DLVO Theory

EDL theory applies to one particle suspended in an ionic medium and this can be incorporated into the DLVO theory developed by Derjaguin, Landau, Verwey and Overbeek in the 1940s, and used to explain the stability of interacting particles in suspension[53,116,118–120]. In DLVO theory there are attractive and repulsive forces acting at different length scales

on the particle by other particles and the surrounding media[53]. Van der Waals attractive forces are constant when an NP is in suspension acting over a range comparable to the colloidal particle radius[116]. The strength of these forces relate to the composition of the suspended material with respect to a Hamaker constant[53,108,115,117,121].

Repulsive forces relate to the EDL of a particle in suspension and can be thought of as screening direct interaction with other suspended particles. Stabilisation occurs when the ionic strength of the media is decreased enough to allow the Debye length to increase and prevent interactions[108,122]. The Guoy-Chapman layer of the EDL will overlap and result in ionic species in the layer mixing and causing a repulsive interaction[108,116]. Particles will be held in suspension when the electrostatic repulsive force (which acts on a much shorter length scale) is greater than the attractive force.

Aggregation (irreversible attachment of particles) or agglomeration (weaker bonding and reversibility) will occur if interacting particles have sufficient collision energy to overcome an energy barrier (maximum activation potential) defined by the balance of attractive/repulsive forces[108,117] (Figure 2-4). Particles which completely overcome the barrier are likely to be permanently aggregated as opposed to reversible agglomeration. As per aggregation kinetics, particles can reach a sufficient energy to overcome the energy barrier and will no longer be repelled by electrostatic forces (critical coagulation concentration – CCC)[123]. In terms of energy, this point is known as fast or diffusion-limited aggregation as the k_BT is greater than the barrier energy. Aggregation is rapid and is limited only by the diffusion rate of the particles and collisions between the particles through the media[121,124]. At balanced attraction and repulsive forces, particles in suspension can require many collisions before reaching enough energy to aggregate i.e. they are limited by probability to overcome the energy barrier and are known as slow or reaction-limited[121,124]. Abe et al.[123] studied aggregation effects of silica nanoparticles when exposed to Ca^{2+} and natural humic acids from the Suwannee River using dynamic light scattering. It was seen that the NPs

aggregation behaviour followed the diffusion limited regime rather than the faster aggregation regime caused by bridging mechanisms of the materials.

The effects and outcome of the forces involved in colloidal systems is still being developed today and there are a number of inconsistencies present. DLVO does not account for: short particle separation distances (< a few nm), particle specific effects such as discrete size, morphology and chemistry[115], non-constant charge throughout a particle; and differences in particle surface textures (such as coatings) which may alter the collision efficiency in suspension[53].

In addition, there are forces which are not considered by DLVO interactions such as hydration forces and steric stabilisation.

2.7.4.3 Hydration Forces

In suspension, the density of water surrounding the particle decays out towards the bulk solution leaving a layered hydration structure around the particle[118]. Upon particle interaction water layers between them are squeezed out and repulsive forces occur[115].

2.7.4.4 Steric Stabilisation

Some organic or polymeric NP coatings prevent direct contact between two NPs in suspension due to a barrier effect similar to hydration forces and this is known as steric stabilisation[108,122]. Polymeric molecules have chains that stretch out into the bulk solution and when particles coated in the steric materials approach, the entropy of confining these chains results in a repulsive force[115].

This generally results in more effective stabilisation than just electrostatic (EDL) forces[108]. Steric stabilisation is not fully understood, but the degree of the repulsive force is thought to be governed by the amount and the coverage of the coating, the strength of adsorption to the surface (reversible or irreversible) and the chemical makeup and quality of the bulk

medium[115]. Sterically stabilised particles can remain in suspension even under high ionic strength that under purely DLVO conditions would cause aggregation[53].

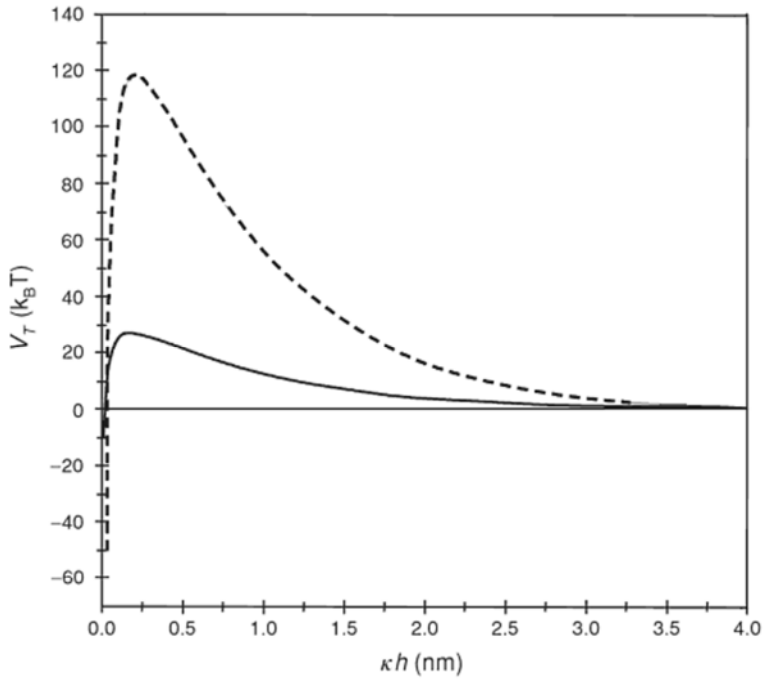

Figure 2-4. Addition of electrostatic and repulsive potential to the attractive potential gives a superposition leaving a primary maximum that is the barrier for stability between colloidal particles. Graph shows two example curves. Potential (VT) is plotted in kBT which allows relation of the height of the maximum with Brownian energy collisions. Distance (κh) is in nanometres. Figure is taken from[117]. For aggregation energy must be input to a level that can overcome the primary maximum.

2.7.5 Aggregation of Nanoparticles in Natural Waters

The aggregation state of particles in natural media is important to understand as particles that do not remain nano-sized will have lower reactive surface area to interact with organisms likely causing their toxic effects to be lessened[35,125].

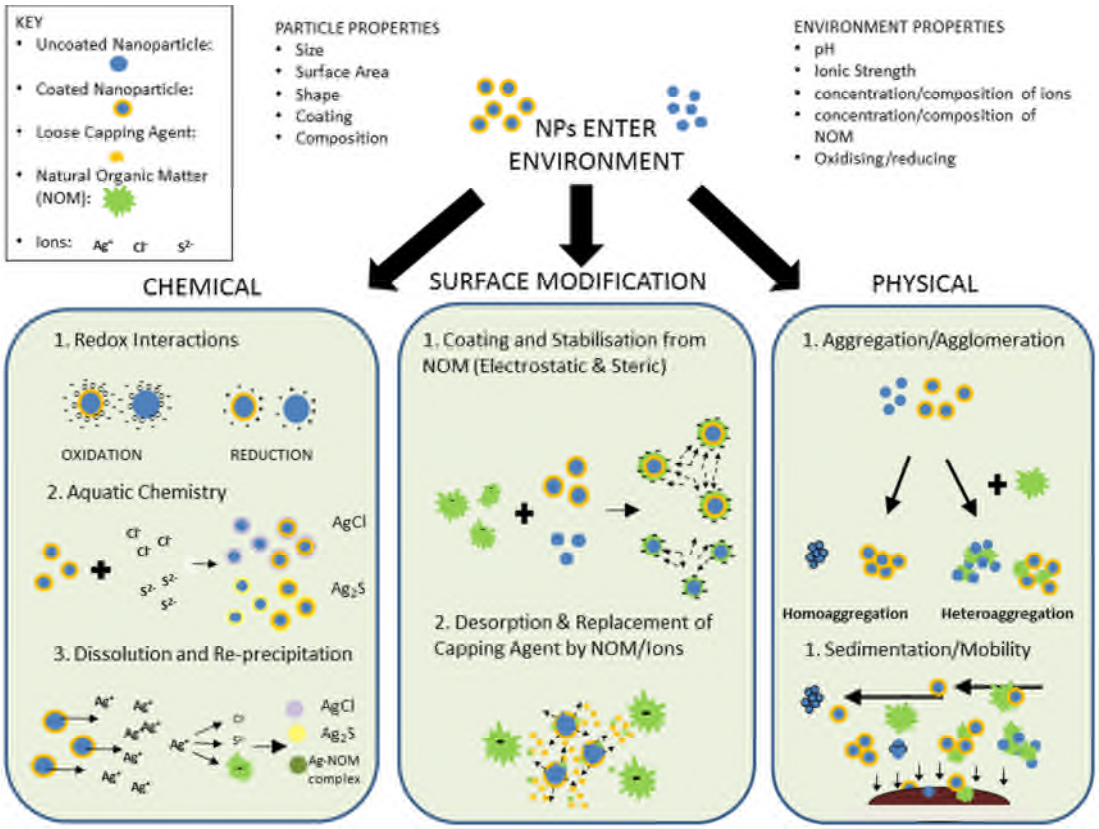

Figure 2-5. Likely chemical, physical and surface interaction of nanoparticles in an aquatic system.

Aggregation/stabilisation mechanisms in natural water are influenced by both the particles and the surrounding media conditions (Figure 2-5). Both the pH and ionic strength are important in this regard.

The pH of suspension controls the level of ionisation of the suspended NP which is positive/negative in natural waters dependent on the surface functional groups, and as such affects the charge dependent electrostatic forces acting on the NP[111,122]. El Badawy et al.[126] indicated agglomeration of NPs under acidic conditions. The point of zero charge (PZC) can be found by manipulating the pH of a suspension to the point where the particle surface charge becomes neutral. Above the PZC, surfaces becomes negatively charged due to surface group dissociations creating cationic (positive charged) conditions[22]. Depending on

the pH in environmental systems, particles will exhibit particular charge and behaviour therefore understanding NP character in relation to pH is important.

Ionic strength is also important to particle stability in environmental waters[125]. Higher ionic strength leads to screening of the EDL charge and lowers the energy barrier, allowing NPs to aggregate. There will be differences in the ionic strength between freshwaters, sea waters and estuarine waters therefore aggregation behaviour would vary between these environments, with aggregation likely quicker in greater ionic concentrations. NPs have been seen to aggregate much more rapidly in seawater than freshwater presumably due to greater concentration of salts in the water and hence greater levels of ionic species present (10mg/L, CeO_2 and TiO_2 aggregated to greater than nano-size within minutes)[125]. Dilutions (2 and 10 fold) of ionic ecotoxicity media caused greater toxicity of AgNPs to *Dapnia Magna* as less aggregation occurred than in standard strength media[127]. Silver NPs have been noted to aggregate at high ionic strength in a number of studies[126,128,129]. In addition polyvalent cations have caused greater suppression of electrostatic charge and increased aggregation compared to monovalent cations, indicating higher valency ions have a greater effect on aggregation[118,129].

2.7.6 Transformations of Nanoparticles in Natural Waters

Nanoparticles are often transformed in the environment, for example ZnO NPs are converted to different forms of ZnS, $Zn_2(PO_4)_2$ and Zn/Fe oxy/hydroxides of varying persistence in biosolids relating to different conditions[130].

There are a huge number of environment conditions that will result in the transformation of silver NPs, including aggregation, flocculation, redox state, dissolution, sulfidation, interaction with ionic species and interaction with suspended organic material[131] (Figure 2-5). As such, predicting NP behaviour in natural waters is complex owing the number of

simultaneous effects occurring. Furthermore in toxicity testing it is necessary to constrain as many of these properties as possible to fully understand particle behaviour[127].

NPs made from Class B soft metal ions (e.g. Ag and Zn) will be especially culpable to dissolution and sulfidation due to their likelihood to form partially soluble metal oxides and their affinity to inorganic and organic ligands[110]. As such the redox state may be the defining medium property when assessing fate[4]. In oxidised freshwaters, silver NPs will be oxidised causing the formation of an Ag_2O surface layer which is partially soluble. In reducing environments Ag_2S would likely be the predominant species which is much less soluble and may affect future transformations[110,132]. Oxidised silver NPs as per thermodynamic conditions will preferentially interact with chloride (Cl^-) and reduced sulphur species in suspension depending on the availability of these ligands and the redox state of the surrounding environment[133]. Sulphur groups are the most thermodynamically favourable species after oxidation of the silver, but in low sulphur environments and in most algal growth media monovalent chloride ions will possibly result in AgCl NP surface layers[134]. NP interaction with chloride ions is currently being assessed and the ratio of Cl/Ag in the system has been noted to determine dissolution levels of NPs and their stability[134,135]. It has been shown that in environments with low chloride in relation to silver (low Cl/Ag) dissolution is likely prevented by an insoluble AgCl layer on the particle surface while high chloride in relation to silver (high Cl/Ag) results in the production of soluble AgCl species[132]. The surface capping agent of the material is also likely to determine the chemical composition of the surface layer.

Transformed NPs will likely have different properties to their previous pristine state. For example in environments with low Cl/Ag ratio solid AgCl NPs will be formed which are less bioavailable to environmental organisms. But the same particles in higher Cl/Ag ratio environments may be soluble and therefore more bioavailable and potentially toxic[134]. Therefore fully understanding the effects of ionic species in suspension on NP fate are

necessary, especially when NPs are present with capping agents which will make environmental chemical reactions more complex.

The life cycle analysis of particles is important to consider as the route in which particles take into environmental systems are important to their eventual fate. For example AgNPs were seen to form Ag_2S NPs after travelling through a WWTP, the most likely entry point for AgNPs into the environment[130].

2.7.7 Interaction of Nanoparticles with Capping Agents and Organic Materials

The surface properties of NPs control their behaviour in natural media[70]. As mentioned earlier surface capping by ligands of polymers will result in the stability of NPs either through charge based electrostatic stabilisation, steric stabilisation by physically preventing NPs coming together. Whilst many particles have capping agents added at the synthesis stage, it has also been proposed that when NPs enter an environmental setting they may interact with organic substances in suspension. These substances could coat the particle surface and convey electro-steric stabilisation by surface charge alteration or physical suppression of the EDL[21,22,95] or destabilise particles by aggregation, bridging mechanisms or stripping of the pre-existing particle coating[95,136–139] (Figure 2-5).

Suspended natural organic matter (NOM) derived from plant and algal material in the environment (one of the 'natural' nanoparticles) has been shown to interact with nanoparticles and will likely affect their stability in real aquatic systems[96]. Due to NOM being formed from many different types of plant algal material it consists of numerous anionic ligands including humic/fulvic substances, peptides, proteins, peptidoglycans and polysaccharides and each of these materials will likely interact differently with NPs in the environment[103].

Humic/fulvic substances are the most studied of these classes and have been seen to attach and cover the surface of nanoparticles keeping NPs of various compositions in suspension, including AgNPs and fullerenes[21,33,53,95,96,128,140], although in some cases ionic species in suspension such as Ca^{2+} have been seen to destabilise these materials[128]. Addition of humic substances to unstable citrate stabilised AgNPs and stable PVP coated AgNPs in media containing NaCl and $CaCl_2$ resulted in further steric stabilisation to both particles[129].

Of the biological NOM, those produced as algal and cyanobacterial extracellular polymeric substances (EPS) are of particular interest as they form a large part of the in situ autochthonous (indigenous) fraction of the dissolved organic matter (DOM) pool in the environment[141]. These substances are metabolically exuded by aquatic microorganisms and they consist of mostly polysaccharides as well as proteins, lipids and nucleic acids of varying molecular weights[77,139] and it has been stated that different forms of EPS will be excreted under different external conditions (such as toxic stress)[77,142].

These substances (EPS) have been shown to bind with ionic metal species in environmental systems rendering suspended metal species less bioavailable and also increasing the organisms metal tolerance[77,114,141]. Understanding EPS interaction with nanoparticles is of paramount importance. Different NOM types have various structures with polysaccharides being fibrillar in nature and proteins globular and less degraded than humic substances[103].

As with other forms of NOM there is evidence for both enhancement of particle stability through coating and steric stability and for destabilisation through aggregation and gel formation by EPS[77,103,138,143], although this is not fully understood as of yet. As such it useful to characterise the types of EPS that are produced by algae/cyanobacteria and understand how they interact with NPs to gain an idea of their fate in algae rich freshwater environments.

It is also important to understand the interaction of differently synthesised NP coatings and suspended organic material such as EPS, as coatings will provide different surface

chemistries for interaction and as such stability or aggregation could depend on these properties[96,136,139]. For example one study noted Gum Arabic and PVP coatings exhibited different stability, dissolution and aggregation in the same microcosm[96].

Coatings in some cases have also been seen to either alter dissolution of the particle surface or bind. Gao et al.[144], using nano-silver in different water types noted lower toxicity to zooplankton in higher ionic strength waters, possibly due to prevention of Ag^+ ion release. The same was noted in Liu and Hurt[145] when citrate-stabilised silver nanoparticles were coated with humic/fulvic species.

More work is needed to investigate these interactions to understand the fate of NPs in environmental matrices with a large DOM pool and the surface interactions between NP surfaces (including those coated with organic or manufactured capping agents).

2.8 Conclusions

It can be noted from the literature that knowledge of the form, behaviour and toxicity of nanoparticles is still required to gain a complete picture of their fate in environmentally relevant systems. More information on nanoparticle toxicity and mechanisms of action to algal species is still required as it is still not determined whether ions or solid nanoparticles (or both) are the cause for toxic stress. Further toxic modes proposed include direct particle attachment to the surface of the organism, generation of reactive oxygen species and other biological mechanisms. It may be that numerous toxic mechanisms will occur at once depending on the prevalent particle and media properties.

Furthermore the impact of coatings and of organic materials such as those exuded from algal and cyanobacterial species are thought to play a major role in the stability and toxicity of NPs, with different combinations of capping agents and types of organic matter causing

aggregation or stabilisation. The interaction between these properties on top of other particle properties (size, size distribution, shape, surface area, dissolution, charge) and environmental parameters such as pH, ionic strength and chemical composition are required to gain a holistic knowledge of NP behaviour in realistic scenarios. This will also improve risk and fate modelling and will answer questions about long-term nanoparticle persistence in aquatic systems.

This research project will extend the understanding of long and short-term behaviour of zinc oxide and silver nanoparticles in suspension in DI water as well as how silver nanoparticles behave in the relevant eco-toxicology media at different ionic strengths and in the presence/absence of different types of algal/cyanobacterial extracellular polymeric substances. The toxicity mechanisms involved in two silver nanoparticles will be also investigated with the characterised properties of particles given consideration. A number of the different techniques will be used throughout the thesis including: DLS, NTA, DCS, TEM, SEM, EDX and Flow Cytometry which will characterise particles/algae in suspension and will demonstrate the effectiveness of using a suite of techniques to fully understand colloidal properties of NPs such as size distribution, stability and morphology.

2.9 References

1. Lead, J. R. & Wilkinson, K. J. Aquatic Colloids and Nanoparticles: Current Knowledge and Future Trends. *Environ. Chem.* **3,** 159 (2006).

2. BSI. *British Standards Institution -PAS 136:2007 - Terminology for nanomaterials*. (2007).

3. NNI [National Nanotechnology Initiative]. What Is Nanotechnology? (2014). at <http://www.nano.gov/nanotech-101/what/definition>

4. Pettitt, M. E. & Lead, J. R. Minimum physicochemical characterisation requirements for nanomaterial regulation. *Environ. Int.* **52,** 41–50 (2013).

5. EuropeanComission. “Commission recommendation of 18 October 2011 on the definition of nanomaterial.” *Off. J. Eur. Union* 38–40 (2011).

6. RS/RAE. *The Royal Academy and Royal Society of Engineering: Nanoscience and nanotechnologies : opportunities and uncertainties*. (2004).

7. Amepox. Amepox. (2015). at <http://www.amepox-mc.com/>

8. SigmaAldrich. Sigma Aldrich - Nanomaterial Products. (2015). at <http://www.sigmaaldrich.com/materials-science/nanomaterials/nanomaterials-products.html>

9. NNI [National Nanotechnology Initiative]. Nanotechnology Timeline. (2014). at <http://www.nano.gov/timeline>

10. Sharma, V., Park, K. & Srinivasarao, M. Colloidal dispersion of gold nanorods : Historical background, optical properties, seed-mediated synthesis, shape separation and self-assembly. *Mater. Sci. Eng. R* **65,** 1–38 (2009).

11. Feynman, R. P. There's plenty of room at the bottom. *Eng. Sci. XXIII* **35,** (1959).

12. Binnig, G. & Quate, C. F. Atomic Force Microscope. *Phys. Rev. Lett.* **56,** 930–934 (1986).

13. Kroto, H. W., Heath, J. R., O'Brien, S. C., Curl, R. F. & Smalley, R. E. C60: Buckminsterfullerene. *Lett. to Nat.* **318,** 162–163 (1985).

14. Iijima, S. Helical microtubules of graphitic carbon. *Lett. to Nat.* **354,** 56–58 (1991).

15. Novoselov, K. S. *et al.* Electric Field Effect in Atomically Thin Carbon Films. *Science* **306,** 666–669 (2004).

16. Gohardani, O., Elola, M. C. & Elizetxea, C. Potential and prospective implementation of carbon nanotubes on next generation aircraft and space vehicles: A review of current and expected applications in aerospace sciences. *Prog. Aerosp. Sci.* **70,** 42–68 (2014).

17. Mauter, M. S. & Elimelech, M. Critical Review Environmental Applications of Carbon-Based Nanomaterials. *Environ. Sci. Technol.* **42,** 5843–5859 (2008).

18. Liu, C. & Cheng, H. Carbon nanotubes for clean energy applications. *J. Phys. D. Appl. Phys.* **38,** 231–252 (2005).

19. Liu, Z., Tabakman, S., Welsher, K. & Dai, H. Carbon Nanotubes in Biology and Medicine: In Vitro and in vivo Detection, Imaging and Drug Delivery. *Nano Res.* **2,** 85–120 (2009).

20. Wigginton, N. S., Haus, K. L. & Hochella, M. F. Aquatic environmental nanoparticles. *J. Environ. Monit.* **9,** 1306–16 (2007).

21. Handy, R. D., Owen, R. & Valsami-Jones, E. The ecotoxicology of nanoparticles and nanomaterials : current status, knowledge gaps, challenges, and future needs. *Toxicology* **17,** 315–325 (2008).

22. Christian, P., Von Der Kammer, F., Baalousha, M. & Hofmann, T. Nanoparticles: structure, properties, preparation and behaviour in environmental media. *Ecotoxicology* **17,** 326–43 (2008).

23. Handy, R. D. & Shaw, B. J. Toxic effects of nanoparticles and nanomaterials: Implications for public health, risk assessment and the public perception of nanotechnology. *Health. Risk Soc.* **9,** 125–144 (2007).

24. Borm, P. J. a *et al. The potential risks of nanomaterials: a review carried out for ECETOC. Part. Fibre Toxicol.* **3,** 11 (2006).

25. Charron, A. & Harrison, R. M. in *Environ. Hum. Heal. Impacts Nanotechnol.* 163–201 (John Wiley & Sons Ltd., 2009). doi:doi:10.1002/9781444307504.ch5

26. Peters, T. M. *et al.* Airborne Monitoring to Distinguish Engineered Environmental Nanomaterials from Incidental Particles for Environmental Health and Safety. *J. Occup. Environ. Hyg.* **6,** 73–81 (2009).

27. Uppal, M. A., Ewing, M. B. & Parkin, I. P. One-Pot Synthesis of Core-Shell Silver-Gold Nanoparticle Solutions and Their Interaction with Methylene Blue Dye. *Eur. J. Inorg. Chem.* 4534–4544 (2011). doi:10.1002/ejic.201100536

28. Crossley, A., Jurkschat, K. & Lojkowski, W. *NanoFate D1.5. Method report on the use and analysis of tagged ZnO ENPs in fate and toxicity studies*. (2011).

29. Lojkowski, W. *et al.* Solvothermal synthesis of nanocrystalline zinc oxide doped with Mn2+, Ni2+, Co2+ and Cr3+ ions. *J. Nanoparticle Res.* **11,** 1991–2002 (2009).

30. Bhatt, I. & Tripathi, B. N. Chemosphere Interaction of engineered nanoparticles with various components of the environment and possible strategies for their risk assessment. *Chemosphere* **82,** 308–317 (2011).

31. Klaine, S. J. *et al.* Nanomaterials in the environment: Behavior, fate, bioavailability, and effects. *Environ. Toxicol. Chem.* **27,** 1825–1851 (2008).

32. Hardman, R. A Toxicologic Review of Quantum Dots: Toxicity Depends on Physicochemical and Environmental Factors. *Environ. Health Perspect.* **114,** 165–172 (2006).

33. Baalousha, M. & Lead, J. R. in *Environ. Hum. Heal. Impacts Nanotechnol.* 1–29 (John Wiley & Sons Ltd., 2009). doi:doi:10.1002/9781444307504.ch1

34. Auffan, M. *et al.* Structural degradation at the surface of a TiO(2)-based nanomaterial used in cosmetics. *Environ. Sci. Technol.* **44,** 2689–94 (2010).

35. Fabrega, J., Luoma, S. N., Tyler, C. R., Galloway, T. S. & Lead, J. R. Silver nanoparticles: behaviour and effects in the aquatic environment. *Environ. Int.* **37,** 517–31 (2011).

36. Benn, T. M. & Westerhoff, P. Nanoparticle Silver Released into Water from Commercially Available Sock Fabrics. *Environ. Sci. Technol.* **42,** 4133–4139 (2008).

37. Yu, S., Yin, Y. & Liu, J. Silver nanoparticles in the environment. *Environ. Sci. Process. Impacts* **15,** 78 (2013).

38. Rizzello, L. & Pompa, P. P. Nanosilver-based antibacterial drugs and devices: Mechanisms, methodological drawbacks, and guidelines. *Chem. Soc. Rev.* **43,** 1501–1518 (2014).

39. Lara, H. H., Ixtepan-turrent, L., Garza-treviño, E. N. & Rodriguez-padilla, C. PVP-coated silver nanoparticles block the transmission of cell-free and cell-associated HIV-1 in human cervical culture. *J. Nanobiotechnology* 1–11 (2010).

40. Auffan, M., Rose, J., Wiesner, M. R. & Bottero, J.-Y. Chemical stability of metallic nanoparticles: a parameter controlling their potential cellular toxicity in vitro. *Environ. Pollut.* **157,** 1127–33 (2009).

41. Van Hoecke, K. *et al.* Fate and Effects of CeO 2 Nanoparticles in Aquatic Ecotoxicity Tests. *Environ. Sci. Technol.* **43,** 4537–4546 (2009).

42. Bondarenko, O. *et al.* Toxicity of Ag, CuO and ZnO nanoparticles to selected environmentally relevant test organisms and mammalian cells in vitro: a critical review. *Arch. Toxicol.* **87,** 1181–200 (2013).

43. Dastjerdi, R. & Montazer, M. A review on the application of inorganic nano-structured materials in the modification of textiles: focus on anti-microbial properties. *Colloids Surf. B. Biointerfaces* **79,** 5–18 (2010).

44. Martinson, A. B. F. *et al.* ZnO Nanotube Based Dye-Sensitized Solar Cells. *Nano Lett.* **7,** 2183–2187 (2007).

45. Kenanakis, G., Vernardou, D. & Katsarakis, N. Light-induced self-cleaning properties of ZnO nanowires grown at low temperatures. *Appl. Catal. A Gen.* **411-412,** 7–14 (2012).

46. Kumari, L., Li, W. Z., Vannoy, C. H., Leblanc, R. M. & Wang, D. Z. Zinc oxide micro- and nanoparticles : Synthesis , structure and optical properties. *Mater. Res.* **45,** 190–196 (2010).

47. Woodrow_Wilson_Database. Project on Emerging Nanotechnologies (2014): Consumer Products Inventory. (2014). at <http://www.nanotechproject.org/cpi/about/updates/ >

48. Fabrega, J., Fawcett, S. R., Renshaw, J. C. & Lead, J. R. Silver Nanoparticle Impact on Bacterial Growth : Effect of pH , Concentration , and Organic Matter. *Environ. Sci. Technol.* 7285–7290 (2009).

49. Chinnapongse, S. L., MacCuspie, R. I. & Hackley, V. a. Persistence of singly dispersed silver nanoparticles in natural freshwaters, synthetic seawater, and simulated estuarine waters. *Sci. Total Environ.* **409,** 2443–50 (2011).

50. Biswas, A. *et al.* Advances in top-down and bottom-up surface nanofabrication: techniques, applications & future prospects. *Adv. Colloid Interface Sci.* **170,** 2–27 (2012).

51. Ju-Nam, Y. & Lead, J. R. Manufactured nanoparticles: an overview of their chemistry, interactions and potential environmental implications. *Sci. Total Environ.* **400,** 396–414 (2008).

52. Farkas, J. *et al.* Characterization of the effluent from a nanosilver producing washing machine. *Environ. Int.* **37,** 1057–1062 (2011).

53. Handy, R. D., von der Kammer, F., Lead, J. R., Owen, R. & Crane, M. The ecotoxicology and chemistry of manufactured nanoparticles. *Ecotoxicology* **17,** 287–314 (2008).

54. Whitley, A. R. *et al.* Behavior of Ag nanoparticles in soil: Effects of particle surface coating, aging and sewage sludge amendment. *Environ. Pollut.* **182,** 141–149 (2013).

55. Stone, V. *et al.* Nanomaterials for environmental studies: classification, reference material issues, and strategies for physico-chemical characterisation. *Sci. Total Environ.* **408,** 1745–54 (2010).

56. Hassellöv, M. & Kaegi, R. in *Environ. Hum. Heal. Impacts Nanotechnol.* 211–266 (John Wiley & Sons, Ltd, 2009). doi:10.1002/9781444307504.ch6

57. Mahl, D., Diendorf, J., Meyer-Zaika, W. & Epple, M. Possibilities and limitations of different analytical methods for the size determination of a bimodal dispersion of metallic nanoparticles. *Colloids Surfaces A Physicochem. Eng. Asp.* **377,** 386–392 (2011).

58. Montes-Burgos, I. *et al.* Characterisation of nanoparticle size and state prior to nanotoxicological studies. *J. Nanoparticle Res.* **12,** 47–53 (2010).

59. Bootz, A., Vogel, V., Schubert, D. & Kreuter, J. Comparison of scanning electron microscopy, dynamic light scattering and analytical ultracentrifugation for the sizing of poly(butyl cyanoacrylate) nanoparticles. *Eur. J. Pharm. Biopharm.* **57,** 369–75 (2004).

60. Braun, a. *et al.* Validation of dynamic light scattering and centrifugal liquid sedimentation methods for nanoparticle characterisation. *Adv. Powder Technol.* **22,** 766–770 (2011).

61. Anderson, W., Kozak, D., Coleman, V. A., Jämting, Å. K. & Trau, M. A comparative study of submicron particle sizing platforms: Accuracy, precision and resolution analysis of polydisperse particle size distributions. *J. Colloid Interface Sci.* **405,** 322–330 (2013).

62. Aitken, R. J., Galea, K. S., Tran, C. L. & Cherrie, J. W. in *Environ. Hum. Heal. Impacts Nanotechnol.* 307–356 (John Wiley & Sons, Ltd, 2009). doi:10.1002/9781444307504.ch8

63. Blaser, S. A., Scheringer, M., MacLeod, M. & Hungerbuhler, K. Estimation of cumulative aquatic exposure and risk due to silver: Contribution of nano-functionalised plastics and textiles. *Sci. Total Environ.* **390,** 396–409 (2008).

64. Geranio, L. & Heuberger, M. The Behavior of Silver Nanotextiles during Washing. *Environ. Sci. Technol.* **43,** 8113–8118 (2009).

65. Gottschalk, F., Sonderer, T., Scholz, R. W. & Nowack, B. Modeled Environmental Concentrations of Engineered Nanomaterials (TiO2, ZnO, Ag, CNT, Fullerenes) for Different Regions. *Environ. Sci. Technol.* **43,** 9216–9222 (2009).

66. Kim, H., Park, C., Murayama, M. & Hochella. Jr, M. F. Discovery and Characterization of Silver Sulfide Nanoparticles in Final Sewage Sludge Products. *Environ. Sci. Technol.* **44,** 7509–7514 (2010).

67. Mueller, N. C. & Nowack, B. Exposure Modeling of Engineered Nanoparticles in the Environment. *Environ. Sci. Technol.* **42,** 4447–4453 (2008).

68. South, G. R. & Whittick, A. *An Introduction to Phycology*. (Blackwell Scientific Publications, 1996).

69. Matzke, M., Jurkschat, K. & Backhaus, T. Toxicity of differently sized and coated silver nanoparticles to the bacterium Pseudomonas putida: risks for the aquatic environment? *Ecotoxicology* **23,** 818–829 (2014).

70. Navarro, E. *et al.* Environmental behavior and ecotoxicity of engineered nanoparticles to algae, plants, and fungi. *Ecotoxicology* **17,** 372–386 (2008).

71. Park, M.-H., Kim, K.-H., Lee, H.-H., Kim, J.-S. & Hwang, S.-J. Selective inhibitory potential of silver nanoparticles on the harmful cyanobacterium Microcystis aeruginosa. *Biotechnol. Lett.* **32,** 423–428 (2010).

72. Labille, J. *et al.* Aging of TiO(2) nanocomposites used in sunscreen. Dispersion and fate of the degradation products in aqueous environment. *Environ. Pollut.* **158,** 3482–9 (2010).

73. Apte, S. C., Rogers, N. J. & Batley, G. E. in *Environ. Hum. Heal. Impacts Nanotechnol.* 267–305 (John Wiley & Sons, Ltd, 2009). doi:10.1002/9781444307504.ch7

74. Oberdörster, G., Oberdörster, E. & Oberdörster, J. Nanotoxicology : An Emerging Discipline Evolving from Studies of Ultrafine Particles. *Environ. Health Perspect.* **113,** 823–839 (2005).

75. He, D., Dorantes-Aranda, J. J. & Waite, T. D. Silver Nanoparticle - Algae Interactions: Oxidative Dissolution, Reactive Oxygen Species Generation and Synergistic Toxic Effects. *Environ. Sci. Technol.* **46,** 8731–8738 (2012).

76. Navarro, E. *et al.* Toxicity of Silver Nanoparticles to Chlamydomonas reinhardtii. *Environ. Sci. Technol.* **42,** 8959–8964 (2008).

77. Miao, A.-J. *et al.* The algal toxicity of silver engineered nanoparticles and detoxification by exopolymeric substances. *Environ. Pollut.* **157,** 3034–41 (2009).

78. Angel, B. M., Batley, G. E., Jarolimek, C. V & Rogers, N. J. The impact of size on the fate and toxicity of nanoparticulate silver in aquatic systems. *Chemosphere* **93,** 359–365 (2013).

79. Burchardt, A. D. *et al.* Effects of Silver Nanoparticles in Diatom Thalassiosira pseudonana and Cyanobacterium Synechococcus sp. *Environ. Sci. Technol.* **46,** 11336–11344 (2012).

80. Stevenson, L. M. *et al.* Environmental feedbacks and engineered nanoparticles: mitigation of silver nanoparticle toxicity to Chlamydomonas reinhardtii by algal-produced organic compounds. *PLoS One* **8,** e74456 (2013).

81. Rodea-Palomares, I., Boltes, K. & Fernández-, F. Physicochemical Characterization and Ecotoxicological Assessment of CeO2 Nanoparticles Using Two Aquatic Microorganisms. *Toxicol. Sci.* **119,** 1–25 (2010).

82. Oukarroum, A., Barhoumi, L., Pirastru, L. & Dewez, D. Silver nanoparticle toxicity effect on growth and cellular viability of the aquatic plant Lemna gibba. *Environ. Toxicol. Chem.* **32,** 902–7 (2013).

83. Sondi, I. & Salopek-Sondi, B. Silver nanoparticles as antimicrobial agent: a case study on E. coli as a model for Gram-negative bacteria. *J. Colloid Interface Sci.* **275,** 177–182 (2004).

84. Morones, J. R. *et al.* The bactericidal effect of silver nanoparticles. *Langmuir* **16,** 2346–2353 (2005).

85. Pal, S., Tak, Y. K. & Song, J. M. Does the Antibacterial Activity of Silver Nanoparticles Depend on the Shape of the Nanoparticle? A Study of the Gram-Negative Bacterium Escherichia coli. *Appl. Environ. Microbiol.* **73,** 1712–1720 (2007).

86. Lok, C.-M. *et al.* Silver nanoparticles : partial oxidation and antibacterial activities. *J. Biol. Inorg. Chem.* **12,** 527–534 (2007).

87. Sotiriou, G. a & Pratsinis, S. E. Antibacterial activity of nanosilver ions and particles. *Environ. Sci. Technol.* **44,** 5649–54 (2010).

88. Piccapietra, F., Allué, C. G., Sigg, L. & Behra, R. Intracellular silver accumulation in Chlamydomonas reinhardtii upon exposure to carbonate coated silver nanoparticles and silver nitrate. *Environ. Sci. Technol.* **46,** 7390–7 (2012).

89. Karlsson, H. L., Cronholm, P., Gustafsson, J. & Möller, L. Copper oxide nanoparticles are highly toxic: a comparison between metal oxide nanoparticles and carbon nanotubes. *Chem. Res. Toxicol.* **21,** 1726–32 (2008).

90. Rodea-Palomares, I. *et al.* Physicochemical characterization and ecotoxicological assessment of CeO2 nanoparticles using two aquatic microorganisms. *Toxicol. Sci.* **119,** 135–45 (2011).

91. Rodea-Palomares, I. *et al.* An insight into the mechanisms of nanoceria toxicity in aquatic photosynthetic organisms. *Aquat. Toxicol.* **122-123,** 133–43 (2012).

92. Oukarroum, A., Bras, S., Perreault, F. & Popovic, R. Inhibitory effects of silver nanoparticles in two green algae, Chlorella vulgaris and Dunaliella tertiolecta. *Ecotoxicol. Environ. Saf.* **78,** 80–5 (2012).

93. Nel, A., Xia, T., Madler, L. & Li, N. Toxic Potential of Materials. *Science* **311,** 622–627 (2006).

94. Zhao, H. *et al.* Detection and characterization of the product of hydroethidine and intracellular superoxide by HPLC and limitations of fluorescence. *PNAS* **102,** 5727–5732 (2005).

95. Bone, A. J. *et al.* Biotic and abiotic interactions in aquatic microcosms determine fate and toxicity of Ag nanoparticles: part 2-toxicity and Ag speciation. *Environ. Sci. Technol.* **46,** 6925–33 (2012).

96. Unrine, J. M., Colman, B. P., Bone, A. J., Gondikas, A. P. & Matson, C. W. Biotic and abiotic interactions in aquatic microcosms determine fate and toxicity of Ag nanoparticles. Part 1. Aggregation and dissolution. *Environ. Sci. Technol.* **46,** 6915–24 (2012).

97. Gottschalk, F., Sonderer, T., Scholz, R. W. & Nowack, B. Possibilities and limitations of modeling environmental exposure to engineered nanomaterials by probabilistic material flow analysis. *Environ. Toxicol. Chem.* **29,** 1036–48 (2010).

98. Gottschalk, F., Sun, T. & Nowack, B. Environmental concentrations of engineered nanomaterials: review of modeling and analytical studies. *Environ. Pollut.* **181,** 287–300 (2013).

99. Rocks, S. A. *et al.* in *Environ. Hum. Heal. Impacts Nanotechnol.* 389–421 (John Wiley & Sons, Ltd, 2009). doi:10.1002/9781444307504.ch10

100. Dumont, E., Keller, V., Williams, R. J. & Johnson, A. C. *NanoFate D6.6. Maps of regional risk assessment of selected ENPs; including and representation of PECs and exceedances of threshold effect values for a range of endpoints PNECS for taxa or sub-groups, biomarker endpoints) under different usage scenarios*. (2013).

101. Tiede, K. *et al.* Detection and characterization of engineered nanoparticles in food and the environment. *Food Addit. Contam. Part A. Chem. Anal. Control. Expo. Risk Assess.* **25,** 795–821 (2008).

102. Bottero, J.-Y. *et al.* Manufactured metal and metal-oxide nanoparticles: Properties and perturbing mechanisms of their biological activity in ecosystems. *Comptes Rendus Geosci.* **343,** 168–176 (2011).

103. Hartland, A., Lead, J. R., Slaveykova, V. I., O'Carroll, D. & Valsami-Jones, E. The Environmental Significance of Natural Nanoparticles. *Nat. Educ. Knowl.* **4,** 7 (2013).

104. Ma, R. *et al.* Size-Controlled Dissolution of Organic-Coated Silver Nanoparticles. *Environ. Sci. Technol.* **46,** 752–759 (2011).

105. Zhou, D. & Keller, A. a. Role of morphology in the aggregation kinetics of ZnO nanoparticles. *Water Res.* **44,** 2948–56 (2010).

106. Weiser, H. B. *Colloid Chemistry*. 226–233 (John Wiley & Sons, Inc. New York. Chapman & Hall Ltd. London, 1949).

107. Klupp Taylor, R. N. Phd Thesis: Self-Assembled Colloidal Multifunctional Nanostructures. (2009).

108. Lu, K. Theoretical analysis of colloidal interaction energy in nanoparticle suspensions. **34,** 1353–1360 (2008).

109. Christian, P. in *Environ. Hum. Heal. Impacts Nanotechnol.* 31–77 (John Wiley & Sons, Ltd, 2009). doi:10.1002/9781444307504.ch2

110. Lowry, G. V, Gregory, K. B., Apte, S. C. & Lead, J. R. Transformations of nanomaterials in the environment. *Environ. Sci. Technol.* **46,** 6893–9 (2012).

111. Fermin, D. & Riley, J. in *Colloid Sci. Princ. Methods Appl.* (ed. Cosgrove, T.) 23–44 (John Wiley & Sons Ltd., 2010).

112. Romer Roche, I. PhD Thesis: The ecotoxicological and environmental behaviour and transformations of silver nanoparticles. (2012).

113. Griffitt, R. J., Luo, J., Gao, J., Bonzongo, J.-C. & Barber, D. S. Effects of particle composition and species on toxicity of metallic nanomaterials in aquatic organisms. *Environ. Toxicol. Chem.* **27,** 1972–1978 (2008).

114. Ribeiro, F. *et al.* Silver nanoparticles and silver nitrate induce high toxicity to Pseudokirchneriella subcapitata, Daphnia magna and Danio rerio. *Sci. Total Environ.* **466-467C,** 232–241 (2013).

115. Liang, Y., Hilal, N., Langston, P. & Starov, V. Interaction forces between colloidal particles in liquid : Theory and experiment. *Adv. Colloid Interface Sci.* **135,** 151 – 166 (2007).

116. Briscoe, W. in *Colloid Sci. Princ. Methods Appl.* (ed. Cosgrove, T.) 329–361 (John Wiley & Sons Ltd., 2010).

117. Eastman, J. in *Colloid Sci. Princ. Methods Appl.* (ed. Cosgrove, T.) 1–30 (John Wiley & Sons Ltd., 2010).

118. Baalousha, M. Aggregation and disaggregation of iron oxide nanoparticles: Influence of particle concentration, pH and natural organic matter. *Sci. Total Environ.* **407,** 2093–101 (2009).

119. Derjaguin, B. V. & Landau, L. D. Theory of the stability of strongly charged lyophobic sols and of the adhesion of strongly charged particles in solutions of electrolytes. *Acta Physicochim URSS* **14,** 633 (1941).

120. Verwey, E. J. . & Overbeek, J. T. G. *Theory of the stability of lyophobic colloids*. (Elsevier Publishing Company, Inc., 1948).

121. Petosa, A. R., Jaisi, D. P., Quevedo, I. R., Elimelech, M. & Tufenkji, N. Aggregation and deposition of engineered nanomaterials in aquatic environments: role of physicochemical interactions. *Environ. Sci. Technol.* **44,** 6532–49 (2010).

122. Everett, D. H. *Basic Principles of Colloid Science*. (Royal Society of Chemistry, 1989).

123. Abe, T., Kobayashi, S. & Kobayashi, M. Aggregation of colloidal silica particles in the presence of fulvic acid, humic acid, or alginate: Effects of ionic composition. *Colloids Surfaces A Physicochem. Eng. Asp.* **379,** 21–26 (2011).

124. Lin, M. . *et al.* Universal Reaction-Limited Colloid Aggregation. *Phys. Rev. A* **41,** 2005–2020 (1990).

125. Keller, A. a *et al.* Stability and aggregation of metal oxide nanoparticles in natural aqueous matrices. *Environ. Sci. Technol.* **44,** 1962–7 (2010).

126. El Badawy, A. M. *et al.* Impact of environmental conditions (pH, ionic strength, and electrolyte type) on the surface charge and aggregation of silver nanoparticles suspensions. *Environ. Sci. Technol.* **44,** 1260–6 (2010).

127. Römer, I. *et al.* The critical importance of defined media conditions in Daphnia magna nanotoxicity studies. *Toxicol. Lett.* **223,** 103–108 (2013).

128. Cumberland, S. A. & Lead, J. R. Particle size distributions of silver nanoparticles at environmentally relevant conditions. *J. Chromatogr. A* **1216,** 9099–105 (2009).

129. Huynh, K. A. & Chen, K. L. Aggregation kinetics of citrate and polyvinylpyrrolidone coated silver nanoparticles in monovalent and divalent electrolyte solutions. *Environ. Sci. Technol.* **45,** 5564–71 (2011).

130. Ma, R. *et al.* Fate of zinc oxide and silver nanoparticles in a pilot wastewater treatment plant and in processed biosolids. *Environ. Sci. Technol.* **48,** 104–12 (2014).

131. Sharma, V. K., Siskova, K. M., Zboril, R. & Gardea-Torresdey, J. L. Organic-coated silver nanoparticles in biological and environmental conditions: fate, stability and toxicity. *Adv. Colloid Interface Sci.* **204,** 15–34 (2014).

132. Lowry, G. V *et al.* Long-term transformation and fate of manufactured ag nanoparticles in a simulated large scale freshwater emergent wetland. *Environ. Sci. Technol.* **46,** 7027–36 (2012).

133. Levard, C. *et al.* Sulfidation of silver nanoparticles: natural antidote to their toxicity. *Environ. Sci. Technol.* **47,** 13440–8 (2013).

134. Levard, C. *et al.* Effect of Chloride on the Dissolution Rate of Silver Nanoparticles and Toxicity to E. coli. *Environ. Sci. Technol.* **47,** 5738–5745 (2013).

135. Li, X., Lenhart, J. J. & Walker, H. W. Dissolution-Accompanied Aggregation Kinetics of Silver Nanoparticles. *Langmuir* **26,** 16690–16698 (2010).

136. Yang, X., Lin, S. & Wiesner, M. R. Influence of natural organic matter on transport and retention of polymer coated silver nanoparticles in porous media. *J. Hazard. Mater.* **264,** 161–168 (2014).

137. Gondikas, A. P. *et al.* Cysteine-Induced Modifications of Zero-valent Silver Nanomaterials: Implications for Particle Surface Chemistry, Aggregation, Dissolution, and Silver Speciation. *Environ. Sci. Technol.* **46,** 7037–7045 (2012).

138. Liu, X., Jin, X., Cao, B. & Tang, C. Y. Bactericidal activity of silver nanoparticles in environmentally relevant freshwater matrices : Influences of organic matter and chelating agent. *J. Environ. Chem. Eng.* **2,** 525–531 (2014).

139. Lau, B. L. T., Hockaday, W. C., Ikuma, K., Furman, O. & Decho, A. W. A preliminary assessment of the interactions between the capping agents of silver nanoparticles and environmental organics. *Colloids Surfaces A Physicochem. Eng. Asp.* **435,** 22–27 (2013).

140. Chen, K. L. & Elimelech, M. Influence of humic acid on the aggregation kinetics of fullerene (C60) nanoparticles in monovalent and divalent electrolyte solutions. *J. Colloid Interface Sci.* **309,** 126–134 (2007).

141. McIntyre, a M. & Guéguen, C. Binding interactions of algal-derived dissolved organic matter with metal ions. *Chemosphere* **90,** 620–6 (2013).

142. Ozturk, S. & Aslim, B. Modification of exopolysaccharide composition and production by three cyanobacterial isolates under salt stress. *Environ. Sci. Pollut. Res.* **17,** 595–602 (2010).

143. Planchon, M. *et al.* Exopolysaccharides protect Synechocystis against the deleterious effects of titanium dioxide nanoparticles in natural and artificial waters. *J. Colloid Interface Sci.* **405,** 35–43 (2013).

144. Gao, J. I. E. *et al.* Dispersion and Toxicity of Selected Manufactured Nanomaterials in Natural River Water Samples : Effects of Water Chemical Composition. *Environ. Sci. Technol.* **43,** 3322–3328 (2009).

145. Liu, J. & Hurt, R. H. Ion release kinetics and particle persistence in aqueous nano-silver colloids. *Environ. Sci. Technol.* **44,** 2169–75 (2010).

Chapter 3. Methodology and Laboratory Techniques

3.1 Introduction

To gain a complete holistic understanding of the behaviour and character of nanoparticles for fate, toxicity and transport studies it is necessary to fully characterise the nanoparticles in relevant media. This behaviour is affected by the intrinsic physical and chemical properties of the nanoparticle such as size, shape, surface coatings, structure and charge as well by the external properties of the surrounding medium such as pH, charge and ionic composition. There is no one single technique which provides a complete picture and as such it is necessary to use a suite of techniques which complement each other to reduce bias, improve accuracy, make data comparable between other scientific studies and understand multiple nanoparticle properties at the same time.

In this chapter the theoretical underpinning of multiple techniques (DLS, NTA, DCS, TEM and FC) is described along with any advantages and limitations that the techniques exhibit in the literature and for the data in this thesis (Table 3-1). Following this the equipment and protocols used in sample preparation, experimental design and post-experiment statistical analysis are described.

Table 3-1. A list of the Characterisation techniques used in this thesis and their measured parameter, resolution, advantages and disadvantages.

Technique	Parameter Measured	Resolution	Advantages	Disadvantages
DLS (size)	Z-average hydrodynamic diameter: d_H (nm), volume and number particle size distribution (PSD)	~1nm to several microns	- Simple user interface - rapid, in-situ measurements. - Widely used, so results potentially comparable.	- Interpretation of intensity weighted results for polydisperse samples is difficult - affected presence of dust and aggregates
Zetasizer (zeta potential)	Zeta Potential (mV)	Same as DLS	- Simple user interface, - rapid, in-situ measurements. - Widely used, so results potentially comparable.	- not an exact measurement of surface charge therefore requires interpretation
NTA	Particle hydrodynamic diameter (d_H), particle size distribution (PSD) Particle number concentreation	50nm (15nm for high RI materials such as Ag)	- Higher resolution than DLS for polydisperse samples - simple, quick and low cost	- Requires skilled operator - affected by high concentrations - can overestimate particle size in polydisperse samples - poor for low-refractive index samples
DCS	Stoke's diameter: d_h, Particle Size Distribution (PSDs)	nm-75µm	- High resolution	- Requires prior knowledge of particle parameters - poor for heterogeneous materials - time consuming
TEM	Size visualisation, morphology, composition	<1nm	- Very high resolution - visualisation of sample - can be used in conjunction with EDX	- Time-consuming - difficult to get statistically significant data for PSDs - sample preparation technique can create artefacts
EDX	Composition, semi-quantitative	nm-µm	- Rapid technique - used in conjunction with EM techniques - compositional information	- Requires good surface preparation to obtain complete and meaningful counts
FC	Cell counts, cell size, fluorescence information	µm	- Allows separation of cell populations - gives subtle information on cell properties when used in conjunction with fluorochromes	- Results complex to interpret - slow interface

3.2 Methods

3.2.1 Dynamic Light Scattering

3.2.1.1 Theory

Dynamic Light Scattering (DLS) (also known as photo correlation spectroscopy: PCS) is a technique used to measure particle size distributions from suspensions of suspended material. Laser light is transmitted through a sample which is then scattered by the objects present in suspension and picked up by a detector. Depending on the random Brownian movement of the suspended material in suspension the signals are constructive or destructive and will fluctuate in intensity[1]. These are processed using an autocorrelation function which is used to calculate the intensity weighted z-average diffusion coefficient of the particles in suspension[2]. This diffusion coefficient is then put into the Stokes-Einstein Equation (Equation 3-1) which is used to calculate an intensity weighted z-average hydrodynamic diameter (d_H) of the particles in suspension:

$$d_H = \frac{kT}{f} = \frac{kT}{3\pi\eta D} = \frac{(x,y)^2}{4}$$

Equation 3-1. Stokes-Einstein Equation. d_H is the hydrodynamic diameter; k is the Boltzmann constant, f is the particle frictional coefficient, η is the solvent viscosity, T is the absolute temperature and D is the diffusion coefficient. x,y are particle displacement in the x and y axis (NTA).

Volume and number particle size distributions (PSDs) can also be obtained by conversion of the intensity weighted distribution using the refractive index of the suspended material using Mie theory[1,3].

3.2.1.2 Advantages and Limitations

DLS is a commonly used technique when characterising nanoparticles suspensions mainly due to the simplicity of use and speed of analysis[3,4]. The technique is non-destructive allowing re-measurement of the same sample and only low volumes of sample are needed for measurements (~1ml). Temperature and measurement time are controlled during analysis. According to the specifications given by the manufacturer (Malvern Instruments Ltd.) particles between one nanometre up to several micrometres can be detected by DLS[5].

However DLS also has limitations. As DLS results are intensity weighted, results from polydisperse samples (multiple particle sizes present in suspension) are difficult to interpret. Larger, slower moving suspended particles scatter more light than smaller particles and will overwhelm the signal and result in a larger size being reported than is predominant in the sample[3,6–8]. A particle of 50nm compared to a particle of 5nm in the same suspension will scatter 1 million times as much light according to the Rayleigh approximation ($I \alpha d^6$)[1,3,9]. Particles in suspension are assumed spherical[8,10] therefore high aspect ratio particles could also result in skewed size detection.

As most nanoparticle suspension have some degree of polydispersity and non-sphericity owing to the difficulty of creating truly monodisperse and monomodal samples. DLS interpretation would be difficult.

Concentration is an important parameter to consider for DLS measurements. Low concentrations and hence fewer particles result in a weaker signal (Figure 3-1) and hence more variability. However aggregation is more likely at high concentrations owing to greater frequency of collisions caused by more particles present in suspension[11]. DLS hydrodynamic diameters are nearly always higher than other characterisation techniques with aggregation and data skewing likely to be the main causes[3,10,12].

3.2.1.3 Method

Mean Z-average hydrodynamic diameters (d_H) and PSDs for all samples were obtained using a Malvern Zetasizer Nano ZS (Figure 3-2 A) with software version 7.03. Refractive indices for each particle are shown in Table 3-4. A 1ml aliquot of the sample was transferred to a disposable sizing cuvette (Figure. 3-10 B) using a pipette. The cuvette was inserted into the Zetasizer unit and the sample was run using the pre-loaded software. The machine was run using a 4mW 633nm He-Ne laser at a measurement angle of 173°. Up to 10 repeat measurements were obtained for each sample to account for the reproducibility of the measurements.

3.2.2 Zeta Potential

3.2.2.1 Theory

Zeta-potential is used as a proxy for particle suspension stability[4]. A solid material with a surface (or surface coating) that is exposed to an aqueous solution (such as a nanoparticle suspension in a medium) attracts ions of opposite charge. This interaction and arrangement of the charges at the interface between the particle and surrounding medium is known as the Electric Double Layer (EDL). The EDL is theoretically comprised of an inner (Stern) layer where opposing ions are strongly bound to surface of the material and an external diffuse layer where ions are still associated but not as strongly attached (known as the slipping plane)[13,14] (Figure. 3-3). The zeta-potential is the potential that exists at the edge of the slipping plane (diffuse layer)[4].

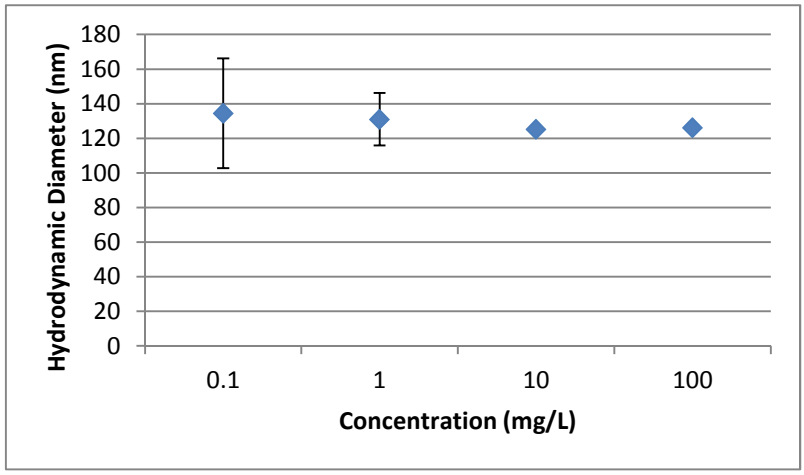

Figure 3-1. Concentration against d_H for AG1 particles in deionised water. Little change in mean d_H is seen but greater variability is present at lower concentrations.

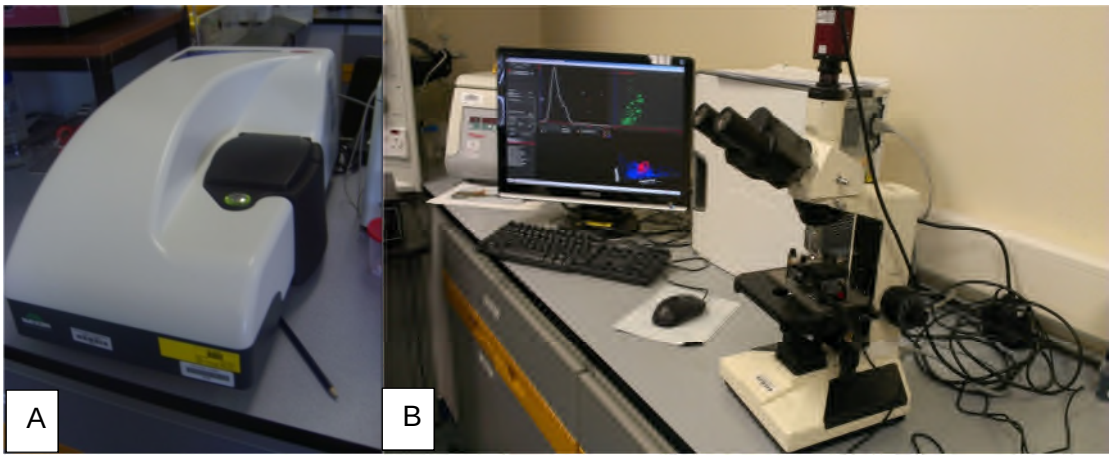

Figure 3-2. A: Malvern Zetasizer used for DLS and Zeta measurements, B: NanoSight system used for NTA.

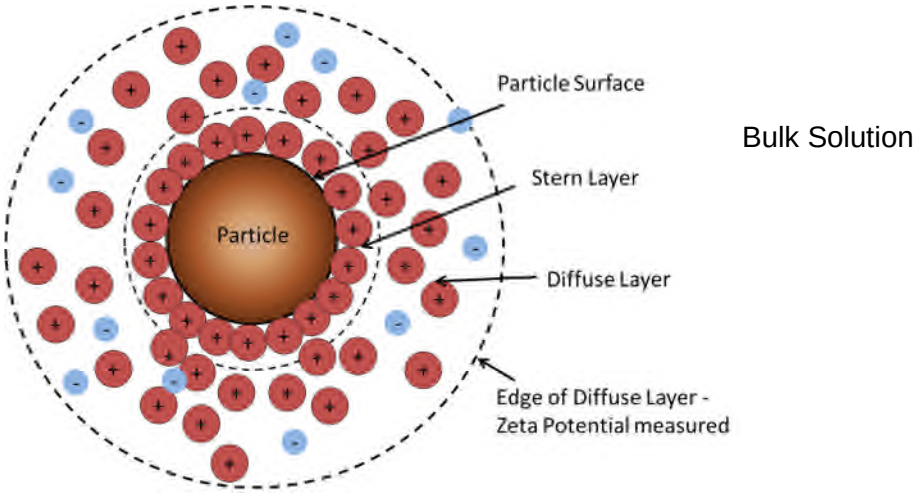

Figure 3-3. Electrical Double Layer around a particle in suspension.

Electrophoretic mobility is used to obtain zeta-potential values. An electric field applied across the sample causes charged particles in suspension to move towards the electrode of opposite charge. Particle movement across this field is known as electrophoresis[2]. Electrophoretic mobility ($m^2V^{-1}S^{-1}$) is obtained by measuring the frequency shift in scattered laser light caused by the particles undergoing electrophoresis in a known electric field considering the wavelength of the laser and the scattering angle[2]. Electrophoretic mobility is calculated using Henry's equation (equation 3-2) which can be rearranged to obtain the zeta potential.

$$U_E = \frac{2\varepsilon z f(Ka)}{3\eta}$$

Equation 3-2. z is the zeta potential, U_E is the electrophoretic mobility, ε is the dielectric constant of the medium, η is the viscosity of the medium and f(Ka) is Henry's function**.**

Henry's function is determined by particle radius (a) and the ratio of the radius to the EDL thickness (ka)[15,16]. Thickness of the EDL is controlled by the ionic makeup of the surrounding medium. f(Ka) is usually given a value based upon one of two theoretical approximations:

Smoluchowski (1.5) and Hückel (1). Which approximation is chosen comes down to the type of colloid and polarity of the medium. The Smoluchowski approximation was used for samples in this thesis as it is generally used for aqueous suspensions[15].

As the zeta-potential is based heavily on the ionic composition of the medium, it is affected by changes in pH and composition of surrounding media[17]. From Derjaguin, Landau, Verwey and Overbeek (DLVO) theory (described in Chapter 2), low pH and greater ionic strength cause compression of the EDL, meaning decreased repulsion and increased potential for aggregation or sedimentation of the particles[2,18].

A high zeta-potential value of >30mV (positive or negative) implies interparticle repulsion and that little flocculation is occurring. A low zeta value approaching zero (<30mV) implies instability and hence potential for aggregation/flocculation to occur[1,2].

3.2.2.2 Advantages and Limitations

Zeta potential calculation by analysis of electrophoretic mobility is a commonly used technique owing to its fairly rapid analysis time (~30 seconds per measurement). Malvern Zetasizer software is simple to use. Only small amounts of sample are needed for analysis (~1ml) with no sample preparation necessary. It is important to note that the zeta potential measurement is not an exact measurement of the surface charge of the suspended particles, rather it is measurement of the voltage at the edge of the slipping plane[4]. This is important when interpreting the results of this technique as they can be affected by surface coatings on the particles[19].

3.2.2.3 Method

Zeta potential measurements for all samples were undertaken using a Malvern Zetasizer Nano ZS as per 3.2.1.3. Disposable zeta cuvettes (Figure 3-10 C) were primed by rinsing through with ethanol and three times with deionised water. Malvern Zeta Standards (-68mV+/-6.8mV) were used to calibrate and check that the zeta cell gave reasonable values

during analysis. Following calibration, cuvettes were again rinsed with ethanol and deionised water before measurement.

For analysis, approximately 1.5ml of sample suspension was transferred into the zeta cuvette of which 0.5ml was discarded to rinse out any leftover deionised water. The cuvette was inserted into the Zetasizer unit and the sample was run using the Zetasizer software. Up to 10 repeat measurements were obtained for each sample to account for reproducibility of the measurements. Results were given as zeta-potential in mV as a function of pH.

3.2.3 Nano-tracking Analysis

3.2.3.1 Theory

Nano-tracking analysis (NTA) is used to measure particle size distributions (PSDs) of colloidal nanoparticle suspensions. It is similar to DLS, it utilises light scattering to obtain information, but differs in that instead of an intensity weighted measurement it tracks individual particles (point scatterers) that have been illuminated by scattered laser light using a CCD camera attached to an optical microscope. Samples are injected onto the surface of a glass prism which acts as a conduit for the laser light (Figure 3-4). A video of the illuminated particles undergoing Brownian motion is obtained over a user defined length of time (usually 30-90 seconds) and the displacement of individual particles between video frames is tracked[3,20,21].

The software tracks each individual particle in x and y position allowing the particles diffusion coefficient to be calculated (D), and this along with the Boltzmann constant (k) and the known temperature (T) and viscosity (η) of the medium allows the hydrodynamic diameter of the particle to be calculated using the Stokes-Einstein equation (Equation 3-2)[3,7,20]. However, as measurements are recorded in 2-D and Brownian motion occurs in 3-dimensions the Stokes-Einstein equation is modified when calculating the diffusion coefficient (equation 3.1)[21].

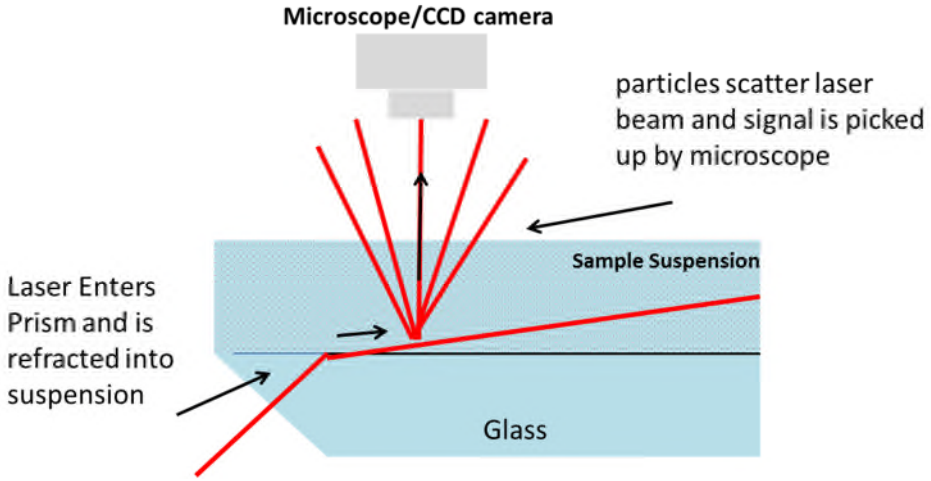

Figure 3-4. The Theory Behind NTA

3.2.3.2 Advantages and Limitations

Advantages of NTA include the small sample volume required (~0.5ml), the simple user interface of the software, the relative rapidity of the measurements and minimal sample preparation. As NTA data is not obtained via intensity-weighted detection of scattered light, the effects from particle size are much less pronounced than in DLS[7,8,20,22]. Larger particles still scatter more light but as just the movement of the particle is collected rather than signal intensity, skewing of the d_H is mitigated and polydisperse samples can be more accurately dealt with[3]. Furthermore, as the technique counts each individual point scatterer it can be used to calculate the particle concentrations (particle no/ml), which is useful when the concentration of the sample is not known. The temperature of the sample can be measured and input into the software.

However, the technique is prone to user error as the software must be optimised to obtain an accurate number of particles in the field of view. This can lead to misestimation of the particle sizes present in suspension[3,21,23]. Concentrations that are too high will result in less

accurate tracking of particles. If multiple particles cross tracks during analysis the software can become confused as to which one it was tracking at that time. As a result it is necessary to keep concentrations low[8,21]. Approximately 10^7-10^{10} particles per ml (roughly 30 particles per field of view) was deemed to be the optimum concentration to obtain reasonable results for the NTA[7]. Very polydisperse or heterogeneous samples can result in the scattering from larger particles drowning out the signal from smaller particles[12,21]. This can result in overestimation of d_H as well as misrepresentation of the concentration of the suspension. Particle refractive index also will affect the amount of light a particle will scatter. Samples containing both biological material and nanoparticulate material will be particularly susceptible to this error. Finally, high aspect ratio particles can cause a blinking affect due to their rotational motion and this can cause difficulty in interpretation[21].

3.2.3.3 Method

PSDs and d_H were obtained using a Halo™ NanoSight LM10 with NanoSight NTA software version 2.3 (Figure 3-2). A Marlin CCD camera was used to collect video data and a 655nm laser was used for light scattering. Temperature values were obtained using a CKY 505 RTD thermometer with thermocouple. ~0.5-1ml of sample was inserted into the viewing unit using a disposable 1ml syringe until overspill occurred (to prevent pressure effects from air bubbles affecting the measurement). The sample was aligned visually using the optical microscope to the recommended optimal measurement point (to the right of the optical 'thumbprint'). The CCD camera was inserted and the particle viewing area was focused so as to include as many particles as possible in focus. Software parameters were set and videos were obtained (Table 3-2). Up to 10 videos of length 30-60 seconds were obtained for each sample to account for reproducibility of the measurements. Videos were also processed using the NanoSight software with set parameters to ensure comparability between samples. Hydrodynamic diameter (d_H) was defined as the mode particle size detected in each suspension (i.e. the peak of the PSD) while PSD was taken to be the spread of all the particle sizes.

3.2.4 Differential Centrifugal Sedimentation

3.2.4.1 Theory

Differential centrifugal sedimentation (DCS) is used to obtain particle size distributions (PSDs). Particles are injected into a spinning disc containing a sucrose density gradient (Figure 3-5). The time taken for particles to settle through the gradient is recorded by a detector[8]. The detector analyses the drop in intensity as a particle travels past and breaks a laser beam, recording the time. Changes in intensity correspond to changes in voltage, and the software converts these voltages to an absorption value and then into weight based particle size distributions. Mie theory can be used to convert results in number or volume based PSDs[3].

Table 3-2. Software parameters for NTA measurements. *software assigned values, others are user defined.

Software Section	**Parameter**	**Values used for AG1 and AG2 characterisation experiments (Chapter 5 + 6)**
Capture	Camera Shutter	Variable dependent on sample
	Camera Gain	Variable dependent on sample
	Capture Duration	Dependent on sample: 30-60 seconds
Pre-Processing	Screen Gain	1.00
	Detection Threshold *	5 – 10
	Blur *	Usually 3x3 (dependent on sample)
	Min Track Length *	Usually 10 (dependent on sample)
	Min. Expected Particle Size *	3 – 50nm (dependent on sample)
Calibration	Temperature	~22°C (from thermometer)
	Viscosity of liquid	~1 (water)

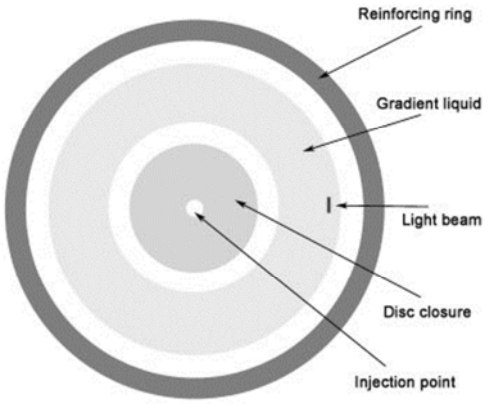

Figure 3-5. Theory behind DCS. Taken from CPS Intruments Ltd Operating Manual [24].

The size, shape and density of the particles will determine their velocity through the gradient so particles of different properties will settle out at different rates according to Stoke's law[3,7] . The Stoke's diameter (or the equivalent spherical diameter) of a particle undergoing sedimentation (d_S) is calculated using an equation (equation 3.3a) which, owing the fact that all parameters except D and t are constant during a DCS measurement can be simplified (equation 3.3b).

$$d_S = \left(\frac{18\eta \ln(\frac{R_f}{R_0})}{t(\rho_p - \rho_f)\omega^2} \right)^{0.5} = \left(\frac{K}{t}\right)$$

(a) (b)

Equation 3.3. d_S is the Stoke's diameter, η is the medium viscosity, R_f is the radial position of the detector, R_0 is the radial position of the surface of the density gradient fluid, t is the time taken for the particle to travel through the gradient to the detector, ρ_p is the density of the particle, ρ_f is the density of the fluid and ω is the rotation speed of the spinning disc. K is a combination of the constants.

Diameter of the particles is calculated relative to a calibration standard of known size and density as the machine is unable to discern particle size from first principles. It can measure objects that range in size from a few nanometers up to 75 micrometres[24].

3.2.4.2 Advantages and Limitations

The main advantages of the DCS technique is its resolution which is very good for detecting separation between particle sizes to ~2-3nm even within a broad distribution of diameters[23]. It also requires little sample preparation as the suspension can be injected into the centrifuge as is.

However, it is necessary to know the density of the material in suspension[23,25]. This can be issue if the material is unknown or if it is a composite material[8]. Environmentally relevant samples tend to be heterogeneous with multiple materials present and one density would not adequately describe all of them. Polydisperse samples where the size distribution is wide are likely to exhibit large density changes also making these samples difficult to interpret.

It can take a while for the smallest samples to make their way through the gradient to the detector and as such it can be time-consuming to measure the entire particle distribution in a polydisperse sample[23]. The technique fares much better with monodisperse distributions.

Table 3-3. Standard Operating Procedure for each NP in DCS. Note: Particle Absorption values estimated based on the colour of suspension silver suspensions were coloured (0.1) while zinc-oxide NPs were white (0.001)[24]. Non-sphericity factors for these particles were assigned 1.1 indicating particles were not purely circular. Fluid density, refractive index and viscosity were estimated for sucrose in water between 8-24%[24].

Standard Operating Procedure	**Silver NPs**	**Zinc Oxide NPs**
Particle Density	10.5g/ml[26]	5.61g/ml[27]
Particle Refractive Index	0.54[28]	2.1[29]
Particle Absorption	0.1	0.001
Non-sphericity factor	1.1	1.1
Calibration Peak Diameter	0.371µm	0.371µm
Calibration Particle Density	1.385g/ml	1.385g/ml
Fluid Density	1.05g/ml	1.05g/ml
Fluid Refractive Index	1.35	1.35
Fluid Viscosity	1.3cps[24]	1.3cps[24]

Method

d_S and PSDs were obtained using a CPS Disc Centrifuge (Figure. 3-6) with software version 9.5c. A standard operating procedure was set up for the different NP samples (Table 3-3). Samples were analysed at a disc speed of ~24,000rpm and sample upper and lower size limits were input (assessed by preliminary measurements of the samples before the experiment began – data not included).

Two sucrose solutions with granulated sucrose (Sigma-Aldrich 99% pure) dissolved into deionised water were created at 8% and 24%. The density gradient was created by injecting 1.6ml of increasing combinations of the two solutions into the spinning disc followed by 0.5ml of dodecane to prevent evaporation and was left to stabilise for an hour.

0.1ml of 0.371µm polystyrene latex beads suspended in SEB (CPS instruments) was injected into the spinning disc as a calibration and processed. The sample was then injected and measured. Most measurements took in the range of 15 minutes to 1 hour depending on the polydispersity of the sample.

Figure 3-6. CPS Disc Centrifuge

3.2.5 Transmission Electron Microscopy

3.2.5.1 Theory

Transmission Electron Microscopy (TEM) is one of the most powerful methods of nanoparticle characterisation as it allows direct visual analysis of nano-sized objects. It is able to visualise such small objects compared with light microscopy because the wavelengths of electrons are much smaller than that of light allowing a much greater spatial resolution[30–32].

The technique works by using electrons to create images and diffraction patterns of thin samples in an ultra-high vacuum (UHV). Electrons are generated by thermionic emission from a filament (usually made of tungsten or lanthanum hexaboride, LaB_6) connected to a high voltage source in the range of ~100-300kV. Electrons produced by the filament or field emission gun (FEG) are accelerated by the applied voltage and travel through the column and are focussed by electro-magnetic lenses and apertures to either form an electron beam interacting with the sample or to form a small probe which is scanned over the sample (Scanning Transmission Electron microscopy - STEM)[30]. Upon interaction with the sample the electrons behave in a number of different ways. They can travel through the specimen unaffected or they can be scattered. The extent and direction of this scattering depends on the thickness, density and crystallinity of the specimen (taking into account the atomic number and weight of individual atoms) as well as the energy of the electron beam[33]. Scattering at an atomic level relates to the interaction of incident electrons with the nucleus or the electron cloud surrounding the nucleus, the former usually resulting in greater emergent scatter angle than the latter[33]. Standard TEM imaging utilises electrons that travel through the sample either unaffected or by forward scattering (electrons scattered within 90° angle of the incident beam)[33]. Other signals such as secondary electrons and back-scattered electrons (electrons scattered at >90° angle from the incident beam) can be studied using TEM but are mainly the preserve of SEM. The sample is visualised onto a fluorescent screen (and/or a CCD camera) by converting the transmitted electron signal that emerges

from the sample into an image using a detector[6,33]. Greater atomic numbers and sample thicknesses will result in greater contrast between the material being imaged and its background[33].

3.2.5.2 Advantages and Limitations

The advantage of TEM in relation to other particle suspension characterisation methods is the ability to visually analyse individual nanoparticles themselves rather than a proxy[6] down to a resolution of ~0.07nm for high resolution instruments[34]. Shape, size and even internal structure can be accurately obtained to a good spatial resolution. Furthermore the technique can be used in conjunction with spectroscopic techniques such as energy-dispersive x-ray spectroscopy (EDX) to obtain qualitative chemical information, or with appropriate standards, semi quantitative data.

However, it is very difficult to get statistically conclusive quantitative particle size distribution data owing to the time-consuming nature of the technique and the costs involved in producing and analysing a large number of TEM images[6,35]. Ideally it would be necessary to measure as many particles as feasible, ideally many thousands[30,36]. In addition automatic particle size distribution analysis is often difficult or impossible due to the low contrast of overlapping particles in aggregates or agglomerates. To obtain a statistically significant number of particles, the concentration of the sample cannot be too low, but greater concentrations may not be environmentally comparable.

Samples were created using the drop deposition technique (Section 3.3.6.2.). Evaporation can cause the particles on the surface to be dragged towards the edges of the TEM grid, generating association of previously non-interacting particles and altered particle structures hence creating artefacts[6,30]. Samples are also left open to impurities present in the laboratory air which can settle on the grid whilst drying. Other sample preparation techniques

are available such as cryo-sectioning and ultra-centrifugal harvesting which mainly apply to biological tissues[6,30], but these were not used owing to the nature of the sample analysis required and time available.

Figure 3-7. JEOL 2010 TEM.

3.2.5.3 Method

Sample grids were analysed using a JEOL 2010 analytical TEM (Figure 3-7), which has a LaB_6 electron gun and can be operated between 80 and 200kV. The majority of measurements were obtained at 200kV. The instrument has a resolution of 0.19nm, an electron probe size down to 0.5nm and maximum specimen tilt of ±10 degrees along both axes.

3.2.6 Flow Cytometry

Flow Cytometry (FC) has become over the past few decades an important technique used in characterisation of biological samples[37,38]. In this thesis it was used to quantify toxicological effects on algal and bacterial species.

3.2.6.1 Theory

FC measures the size and fluorescence of objects in a suspension via laser interaction (Figure 3-8). Objects in suspension are directed towards the laser using hydrodynamic focusing in which a pressurised sheath fluid containing the sample is streamlined so objects are moving in single file. This ensures that the sample is analysed one object at a time[38].

Objects are characterised through the scattering of laser light, collected in the same direction as the laser beam (forward scatter) and at 90 degrees (side scatter), and also by emission of fluorescence at different light wavelengths[39]. Cells can be grouped or 'gated' based upon their size and fluorescence, and visualised in dot plots and histograms. Flow cytometers typically have multiple detectors in which fluorescence emissions at different wavelengths are picked up[38]. Gating allows the populations to be quantified when compared with a fluorescence bead stock of known quantity[38].

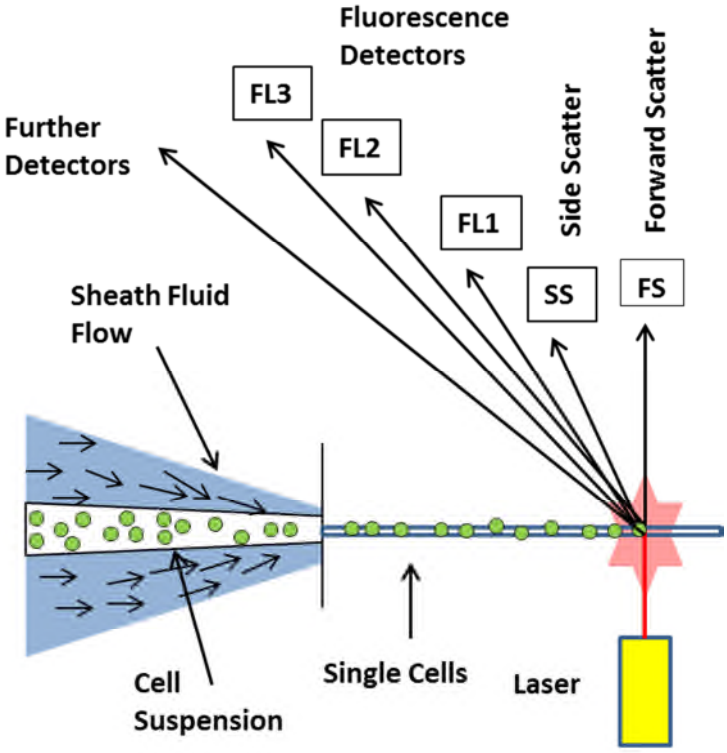

Figure 3-8. Theory behind Flow Cytometry

Intrinsic cellular properties can be assessed such as cell size, population size, chlorophyll levels and internal structure. The addition of fluorochrome stains to samples allow further properties to be understood, such as the generation of reactive oxygen species (ROS) and cell viability[37,40]. Stains work by absorbing light at a particular wavelength and then emitting it at a higher wavelength if certain biological conditions are met. The fluorochromes used in this thesis are described in Section 3.3.5.5.

3.2.6.2 Advantages and Limitations

The ability of FC to separate out different cell populations in a heterogenous population as well as detect changes in population dynamics over time is the technique's real strength, as size and fluorescence characterisation allows subtle differences to be detected which would not be possible using other cell counting techniques[39]. This is particularly useful when assessing sample contamination.

The output from the technique can be difficult to interpret, requiring a skilled operator. Slow through-put of the machine compared to other cell counting techniques can also be a disadvantage, but this was not an issue in this thesis owing to the small number of samples measured.

3.2.6.3 Method

Cell population counts were obtained using a Beckman Coulter Flow Cytometer (Figure 3-9) with Multi tube carousel loader and 488nm, 638nm, 405nm wavelength lasers. Measurements were obtained using Gallios^{TM} Cytometry List Mode Data Acquisition and Analysis Software 1.2. Sample volumes (1ml) were pipetted into 5ml PP tubes (Figure 3-10 G) along with 10µl of Fluoresbrite^{TM} 1.568±0.026µm carboxylate latex microspheres for

calibration. A cleaning protocol consisting of rinses of 10% bleach, 70% ethanol and deionised water was run after each set of samples to prevent biological contamination of the system. Data was exported to Microsoft Excel spreadsheets which were further processed to produce charts.

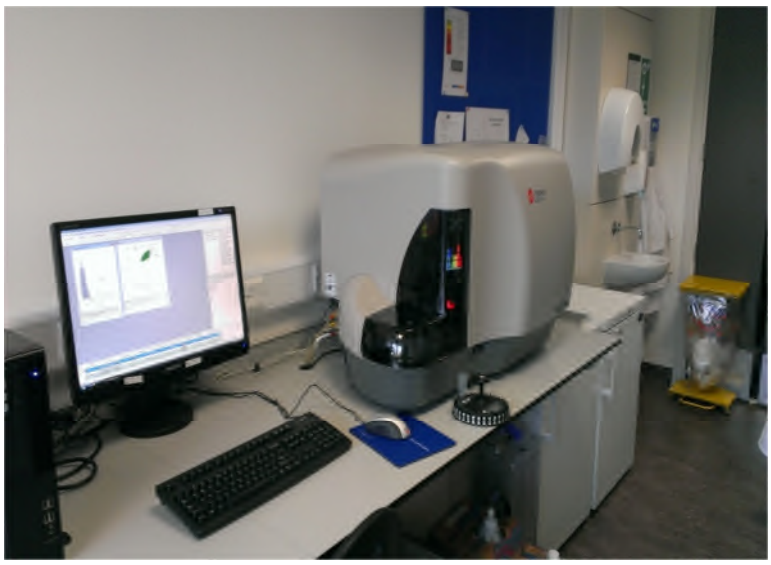

Figure 3-9. Beckman Coulter Flow Cytometer

3.3 Laboratory Methods and Experimental Setup

3.3.1 Safety

In both characterisation and biological laboratories, when handling nanoparticle suspensions or powders and biological materials latex gloves and laboratory coats were always worn. Laboratory coats were never removed from their specific laboratory and gloves were disposed into autoclave bins after use. When handling dry nanoparticles, face masks and eye protection were used to prevent inhalation and eye contact of airborne materials. Hands were thoroughly washed to prevent carrying of algal or bacterial species outside the laboratory.

3.3.2 Containers and Laboratory Equipment

3.3.2.1 Containers

Nanoparticle suspension samples for physical characterisation were created and stored in glass vials (Figure 3-10 A). All glassware used for characterisation samples was rinsed three times with deionised water and dried in an oven set to 30°C. Nanoparticle and $AgNO_3$ stocks for eco-toxicity experiments were stored and mixed in sterile polypropylene centrifuge tubes (15 and 50mL: Figure 3-10 F). Algal and cyanobacterial stock cultures were grown in sterile TC Easy Flasks, 75cm^2 for suspension cultures (VWR, UK) with a working volume of 50mL (Figure 3-10 D). Exposed eco-toxicity samples were grown in sterile TC Easy Flasks, 25cm^2 for suspension cultures (VWR, UK) with a working volume of 10mL (Figure 3-10 E). Stocks of fluorescence markers used in mechanistic eco-toxicity tests were stored in Star-lab/Simport 2ml sterile Cryovials® at -20 degrees Celsius (not shown). Flow cytometry samples were measured in Greiner-Bio-One 5ml PP tubes (Figure 3-10 G).

3.3.2.2 Centrifugation Tubes

Merck Millipore Amicon® Ultra-15 Centrifugal Filter devices with 10kD molecular weight cut off (MWCO) were used in the silver dissolution analytics experiments (Figure 3-10 H and I). Tubes were copper-loaded with 3ml of copper nitrate solution (0.1M) and centrifuged for ~10minutes at 4000rpm to ensure all the moisture travelled through the filter. This step was repeated with MilliQ water for a washing step. This was done to ensure that silver ions did not bind to the filter before analytics experiments.

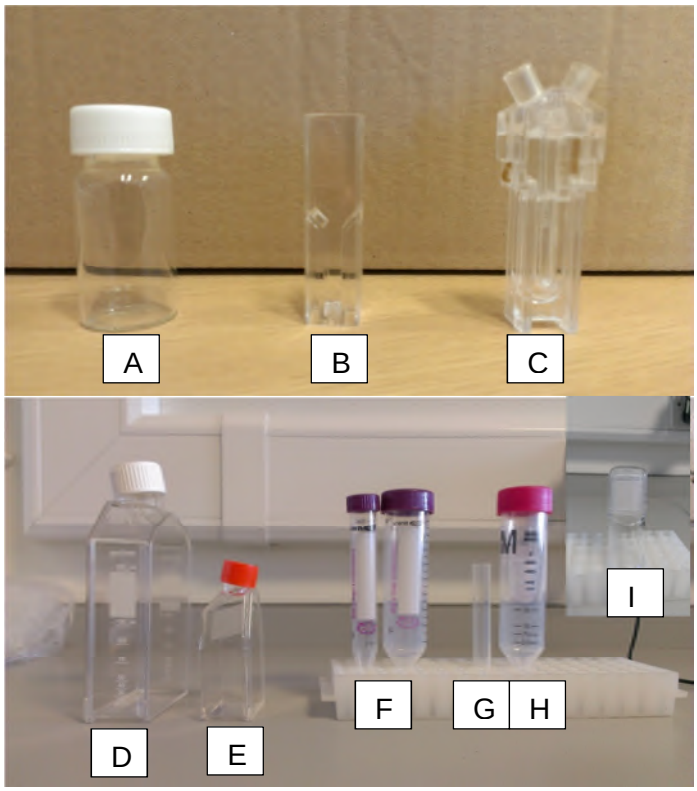

Figure 3-10. Glassware and containers used in this thesis. A. Glass vials for characterisation samples. B. Disposable DLS sizing cuvette. C. Disposable Zeta-cell. D. Culture flask. E. Exposure Flask. F. Polypropylene tubes for mixing and storing NP stocks. G. PP tubes for FC. H. Ultrafiltration Tube. I. 10kD MWCO filter.

3.3.2.3 Pipetting

Pipetting was accomplished using pre-calibrated Biohit Proline Plus pipettes of 10, 100, 1000, 5000 and 10000µl volume. Pipettes were rinsed with 10% ethanol and de-ionised water between measurements that involved algal cultures to prevent cross-contamination of the different species.

3.3.2.4 pH Readings

Measurements of pH for the characterisation samples were undertaken using both a pre-calibrated Hanna Instruments H19025 pH meter and Fisherbrand pH paper. Measurements

of pH for eco-toxicity media were taken by a Sartorius Professional pH meter PP-25. Calibration was checked using pH standard buffers at pH4 and pH7. Glass electrodes for both pH meters were rinsed with de-ionised water before each measurement and were left for 5 minutes to gain stable pH readings. Glass electrodes have been shown to be reasonably accurate for AgNP suspensions although spurious effects have been noted for glass adsorbing NPs species such as TiO_2[41].

3.3.2.5 Weighing

Nanoparticles for characterisation samples were weighed out using a Sartorius ME mass balance. Media constituents and fluorescence stains were measured using a Sartorius MC1 Research RC 250 S mass balance

3.3.3 Waste

After analysis, nanoparticle suspensions were stored in 1L glass bottle which when filled were subsequently disposed of. Algal suspensions were collected and autoclaved.

3.3.4 Particles

Particles were obtained by a number of suppliers, some commercial and some from industrial partners of the NanoFate project. Information is given in Table 3-4.

Table 3-4. Particle Identification, compositional material, supplier and expected primary particle size. *obtained from Malvern Zetasizer software [42]

Particle ID	Material	Supplier	Manufacturer Stated Size	Coating	Refractive Indices used for DLS*	Absorption Values used for DLS*
ZN1	Zinc Oxide	NanoTrade	30nm	None	2.004	0.001
ZN2	Zinc Oxide	NanoTrade	200nm	None	2.004	0.001
AG1	Silver	Amepox	3-8 nm	Organic Paraffin-type coating	0.140	3.140
AG2	Silver	Institut Català de Nanotecnologia	50 nm	Both citrate and PVP	0.140	3.140

3.3.5 Media Preparation

3.3.5.1 Ultrapure and De-ionised Water

De-Ionised water was obtained from the de-ionised water tap in the characterisation laboratory. Ultrapure water was obtained in both labs by a Milli-Q water purification system.

3.3.5.2 MBL Woodshole Medium

MBL Woodshole medium was prepared from a recipe on the CSIRO website which was adapted from Nichols[43] for freshwater samples. Stock solutions were created by dissolving a specific mass of chemical into distilled water (stock solutions shown in Table 3-5, media preparation shown in Table 3-6). Stock solutions were stored in borosilicate glass jars and refrigerated at 4°C to be used whenever new MBL media batches were required.

Table 3-5. Stock solutions used in the creation of MBL Woods Hole media and masses of chemical added to distilled water to create them.

Stock Solution	Constituent	Mass of constituent chemical added to 1L distilled water (dH_2O) (g)	
1	$CaCl_2.2H_2O$	36.76	
2	$MgSO_4.7H_2O$	36.97	
3	$NaHCO_3$	12.60	
4	K_2HPO_4	8.71	
5	$NaNO_3$	85.01	
6	$Na_2SiO_3.9H_2O$	28.42	
7	Na_2EDTA	4.36	
8	$FeCl_3.6H_2O$	3.15	
9	Metal Mix		Additional instructions: Add each constituent chemical separately to ~750mL of dH_2O, fully dissolve between each addition. Finally make up to 1L with dH_2O.
	$CuSO_4.5H_2O$	0.01	
	$ZnSO_4.7H_2O$	0.022	
	$CoCl_2.6H_2O$	0.01	
	$MnCl_2.4H_2O$	0.18	
	$Na_2MoO_4.2H_2O$	0.006	
10	H_3BO_3	28.4	
11	Tris stock	250.0	

Table 3-6. Preparation steps for eco-toxicity media

Preparation Step	MBL Woods Hole Media	ISO Testmedium
1	Distilled water was autoclaved to prevent contamination	Distilled water was autoclaved to prevent contamination
2	1ml of MBL stocks 1-8, 10 and 11 and 5ml of stock 9 added to 1L of autoclaved distilled water	6.2mL of ISO stocks 1 and 2, 12.4ml of ISO stock 3 added to 200mL of autoclaved distilled water
3	pH was adjusted to 7.2 (usually begins ~8.3) using hydrochloric acid and mixed using magnetic stirrer	n/a

3.3.5.3 ISO Bacterial Growth Medium

ISO bacterial growth media was created according to ISO guidelines[44]. Stock solutions were created by dissolving a specific mass of chemical into pre-autoclaved distilled water (stock solutions shown in Table 3-7, media recipe shown in Table 3-6). As with MBL media, stock solutions were stored in borosilicate glass jars and refrigerated at 4°C until new media was required.

Table 3-7. Stock solutions used in the creation of ISO Bacterial media and masses of chemical added to distilled water to create them.

Stock Solution	Constituents	Mass of constituent chemical added to 500ml distilled water (dH_2O) (g)
1	$NaNO_3$ $K_2HPO_4 \times 3H_2O$ KH_2PO_4	10.0 3.14 1.20
2	$C_6H_{12}O_6$	36.6
3	$MgSO_4 \times 7H_2O$ Granulated Iron(III) Citrate	4.0 0.01

3.3.5.4 MBL Woods hole media with algae and cyanobacteria EPS.

The impact of algal and cyanobacterial extra polymeric substances (EPS) on particle stability and characterisation was investigated in Chapter 6. EPS were obtained from 2 species, the green algae *Chlamydomonas reinhardtii* and cyanobacteria *Synechococcus leopoliensis.* The different media treatments are shown in Table 3-9. Part of the investigation was to assess EPS produced with and without exposure to a chemical stressor. Unstressed EPS was obtained for both *C.reinhardtii* (CR^+) and *S.leopoliensis* (SL^+) by culturing the organisms in plain MBL Woods Hole medium (described above) for 72 hours, the length of an algal growth inhibition test (as per 3.3.7.3.). After 72 hours the samples underwent a number of preparation steps seen in Table 3-8.

Table 3-8. Preparation steps for unstressed EPS samples.

Preparation Step	Activity
1	72 hours of exposure
2	Initial centrifugation of sample for 10mins at 4000rpm to separate the main algal biomass from the EPS
3	Removal of the supernatant containing the dissolved and smaller suspended material
4	Addition of a further 5ml of plain MBL medium to the biomass pellet followed by re-suspension
5	Centrifugation for a further 10 minutes at 4000rpm
6	Supernatant was again collected and combined with the supernatant collected on Step 3. This was used for the characterisation experiments in Chapter 6

Stressed *C.reinhardtii* EPS (CR^-) were obtained in a similar manner to unstressed EPS, but the organisms were exposed to a low concentration of $AgNO_3$ (5µg/L) in the MBL media for the 72 hour experimental duration before separation of the EPS.

Table 3-9. Nomenclature for the different EPS media treatments and the constituents of the treatments.

Media	Constituents
CR^+	Plain MBL + Unstressed *C.reinhardtii* EPS
CR^-	Plain MBL + stressed *C.reinhardtii* EPS
SL^+	Plain MBL + Unstressed *S.Leopoliensis* EPS

3.3.5.5 Fluorescence Stains

Mechanisms of toxicity for two AgNPs (AG1 and AG2) were investigated in Chapter 7 and were assessed by measuring changes in fluorescence caused by interaction with a toxicant for three different fluorescence stains. FDA, HE and DCF were purchased from Sigma Aldrich and Molecular Probes respectively. The different stains are shown in Table 3-10 along with their preparation protocols. Differences in fluorescence signal are caused by changes in organism's biological state.

3.3.6 Characterisation Sample Preparation

3.3.6.1 Nanoparticle Suspensions

Nanoparticle suspensions for physical characterisation were created using a modified technique as per PROSPECT protocol[45]. Particles initially in powder form were weighed into a receptacle at the mass for the desired suspension concentration. A few drops of suspension medium were added to create a paste which was stirred with a spatula. More suspension medium was added to make up the desired suspension concentration. AG1

particles from a stock suspension were pipetted into a receptacle and diluted to desired concentration with suspension medium. After creation and before each measurement the samples were sonicated in an ultrasonic bath for 30 seconds and shaken by hand for 30 seconds to make sure the particles were suspended.

3.3.6.2 TEM samples

TEM samples were created by pipetting 20-40µl of nanoparticle suspension onto holey copper grid coated with carbon film placed upon filter paper. These were left to dry under a cover until fully dry. TEM samples were taken monthly for Chapter 4 and at 0 hours and 336 hours for experiments in Chapters 5 and 6.

3.3.6.3 Storage

All characterisation samples were stored in a dry, dark fridge at 4°C to prevent light and temperature affecting the samples.

3.3.7 Exposure Methods

3.3.7.1 Organisms

Biological exposures were carried out at the Centre for Ecology and Hydrology (CEH) in Wallingford. *C. reinhardtii* (strain number CCAP 11/45) was obtained from the Culture Collection of Algae and Protozoa (CCAP, Scottish Marine Institute, Oban, United Kingdom), *S. leopoliensis* (strain number 1402-1) was obtained from the Culture Collection of Algae, University of Gottingen, Germany. The former was selected over recommended OECD guideline species (*P.subcapitata*) due to its short life cycle allowing the possibility for several generations in a single test and its use as a model organism in metal toxicity testing[46–48]. It

also has a fully sequenced genome which makes it ideal for detailed follow up studies involving toxicity mechanisms and it has also been used in previous nanoparticle toxicity tests[49,50].

3.3.7.2 Growth Inhibition Test

Using an adapted OECD 201 guideline[51] the growth rate inhibition of the green algae and cyanobacteria were calculated. The main adaptions to the OECD guideline were use of MBL Woodshole media as opposed to the recommended OECD/AAP media to simplify potential NP interactions with media constituents and use of green algal species *C.reinhardtii* as opposed to recommended species *P.subcapitata*. Growth rate inhibition tests are used in ecotoxicology to measure the effect of a toxicant on aquatic microorganisms[52,53]. Growth rate was measured as the change of cell numbers (measured by flow cytometry) between cultures exposed to a toxicant and that of an untreated control. Data was plotted as dose-response curves which allow effect concentration (EC_X) values to be obtained. Dose-response curves were obtained for AG1 and AG2 nanoparticles plus H_2O_2 and $AgNO_3$ in MBL medium. $AgNO_3$ was used as a control to assess the effect of silver ions in relation to silver in nanoparticulate form. H_2O_2, a non-radical reactive oxygen species (ROS), is a known stressor[54] and was used as a positive control in fluorescence experiments for ROS formation.

3.3.7.3 Growth Inhibition Test Methodology

Prior to starting the experiment, the cell density of the stock cultures was checked using the flow cytometer. 1ml of culture grown to desired cell density was added to 9ml serial dilutions of the toxicant. Serial dilutions were used to assess a range of concentrations and were set up by calculating the dilution factor and pipetting volume for each toxicant (Equations 3-4, 3-5). A number of different concentration ranges were assessed to understand and obtain the

full dose-response curve for each toxicant on each species. Three controls for each species were set up as well as one replicate per serial dilution concentration.

Equation 3-4. Serial Dilution Factor

$$\text{Dilution Factor (dl)} = \sqrt[n-1]{\frac{\text{Maximum Concentration}}{\text{Minimum Concentration}}}$$

Equation 3-5. Serial Dilution Pipetting Volume

$$\text{Pipetting volume (pv)} = \frac{\text{Volume of media in each vessel (ml)}}{\text{Dilution factor}-1}$$

Exposures were left for 72h in specific growth conditions modified from those recommended in OECD 201 guideline[51] – shown in Table 3-11. After 72h the cell numbers of the controls and replicates were measured.

Table 3-10. Conditions for cell culture incubations

Condition	Description
Temperature	22°C
Light Conditions	16 hours light, 8 hours dark
Light Intensity	~9000 lux
Shaking	80-95 rpm
Test volume	10ml per exposure replicate
Age of Organisms	~3 days
Initial Cell count	~10^4 for green algae, ~10^5 for cyanobacteria (cells per ml)
Algal medium	MBL Woods Hole
Test Duration	72 hours
Measurement parameter	Cell growth inhibition – measured from changes in cell growth rate

Table 3-11. Fluorescence staining preparation protocols.

Stain	Stock Preparation	Sample Preparation	Incubation Time	Measures	Flow Cytometer Detection Channel	Mechanism
Fluorescein diacetate (FDA)	10mg powder into 10ml of dimethyl sulfoxide (DMSO). Store at -20°C	1. Add 1ml of ultrapure water to 500µl of DMSO stock. 2. Pipette 30µl into 1ml sample 3. Incubate until measurement	10 minutes in cool, dark place	Cell Viability	FL1	- Inherently non-fluorescent, non-polar and lipophilic but can easily enter cells through membranes and cell walls [40,48]. - Upon entering the cell, unspecific acetates in the stain will be removed by unspecific cellular esterases leaving hydrophilic and polar fluorescein unable to leave the cell unless cell wall/membranes are damaged [39,40,55,56] - Greater decreases in cell viability results in higher fluorescence detected in flow cytometry data
Hydroethidium (HE)	25mg powder into 15.92ml DMSO. Store at -20°C	1. Pipette 1µl DMSO stock into 1ml sample 2. Incubate until measurement	10 minutes in cool, dark place	Reactive Oxygen Species (ROS)	FL2	- Oxidised by free radical species such as H_2O_2 and NO_3^- - Blue fluorescent dye to red fluorescent hydroethidine [37] - associates with RNA and DNA in the cell's nucleus and causes fluorescence [57,58]
Dichlorofluorescein (DCF)	10mg powder into 17.3ml DMSO. Store at -20°C	1. Pipette 10µl DMSO stock into 1ml sample 2. Incubate until measurement	80 minutes in cool, dark place	Reactive Oxygen Species (ROS)	FL1	- Non-polar H_2DCFDA (2',7'-dichlorodihydrofluorescein diacete transformed into non-fluorescent form 2',7'-dichlorodihydrofluorescein (H_2DCF) by entering the cell through an intact cell wall and interacting with esterases. - Further transformed into fluorescent 2',7'-dichlorofluorescein (DCF) upon interaction with ROS [40,59,60]

The average growth rate over 72 hours was calculated using the difference in cell numbers obtained by the flow cytometer. Figure 3-11a shows a typical flow cytometer output for *C.reinhardtii.* Cell numbers and calibration bead numbers were obtained from the gates using the flow cytometer software.

$$\mu_i - j = \frac{lnC_j - lnC_i}{t_j - t_i}$$

Equation 3-6. $\mu_i - j$ is the average specific growth rate from time *i* to time *j*, t_i is the initial time of the exposure period, t_j is the final time of the exposure period, C_i is the biomass (cell number) at time *i* and C_j is the biomass (cell number) at time *j*.

Percentage inhibition of growth was calculated using equation 3-7:

$$\%\mathrm{Ir} = \frac{\mu_C - \mu_T}{\mu_C} \mathrm{x}\, 100$$

Equation 3-7. %Ir is the percent inhibition of the average specific growth rate, μC is the mean value for average specific growth rate (μ) in the control group and μT is the average specific growth rate for the treatment replicate.

3.3.7.4 Fluorescence Staining Experiments

For fluorescence experiments a cell density of ~10^5-10^6 cells per ml was obtained by growing the algae and cyanobacterial populations for 3-4 days. EC_{70} values (the concentration at which growth inhibition has been decreased by 70%) were calculated from dose-response curves obtained in previous exposures for the two silver NPs AG1 and AG2 as well as $AgNO_3$ and H_2O_2. Again $AgNO_3$ was used as a control to compare the effects of silver ions and silver NPs while H_2O_2 is a proven stressor and producer of ROS and was used as a positive control.

6ml of culture was exposed to EC_{70} values of each toxicant (estimated using R from dose-response curves) and incubated under the same conditions as the dose-response

experiments (Table 3-11) for 30-40mins to elicit a toxic response. Following this, samples were exposed to each fluorescence stain for the required incubation time as described in Table 3-10. While samples were incubating they were stored in the dark at 4°C. The Flow Cytometer was gated to assess the movement of the detected cell populations upon production of ROS (HE and DCF) and loss of cell viability (FDA). Figure 3-11b+c shows example flow cytometer outputs for *C.Reinhardtii* stained with FDA exposed to no stressor and H_2O_2 respectively with the effect of a stressor evident by the numbers present in each gate. The flow cytometer was set up to run each sample for 60 seconds or to detect 10,000 events so as to have comparable populations between samples.

3.3.7.5 Analytics Experiments

To give greater insight into the mechanism of nanoparticle toxicity, specifically the effect of ions vs. solid nanoparticulate silver[41], the dissolution of the AG1 and AG2 initially and after 72 hours was assessed. Both *C.reinhardtii* and *S.leopoliensis* were exposed to ~EC_{20} and ~EC_{50} (the nominal concentration at which growth inhibition has decreased by 20% and 50% respectively, estimated by eye from dose-response curves for AG1 and AG2. Samples were set up the same way as the dose-response experiments with 1ml of culture added to 9ml of spiked media and stored under the same conditions for 72 hours as stated in Table 3-12. Note: EC_x values were drastically different when estimated from dose-response curve fitting as more data was collected after these samples were analysed.

Table 3-12. Concentrations of each particle used for total and dissolved silver analytics analysis for both species of microorganism and particle type.

Species	Toxicant	Concentrations
C.reinhardtii (green algae)	AG1	EC_{20} 700µg/L, EC_{50} 800µg/L
	AG2	EC_{20} 1500µg/L EC_{50} 1700µg/L
S.leopoliensis (cyanobacteria)	AG1	EC_{20} 97µg/L EC_{50} 225µg/L
	AG2	EC_{20} 502.5µg/L EC_{50} 1100µg/L

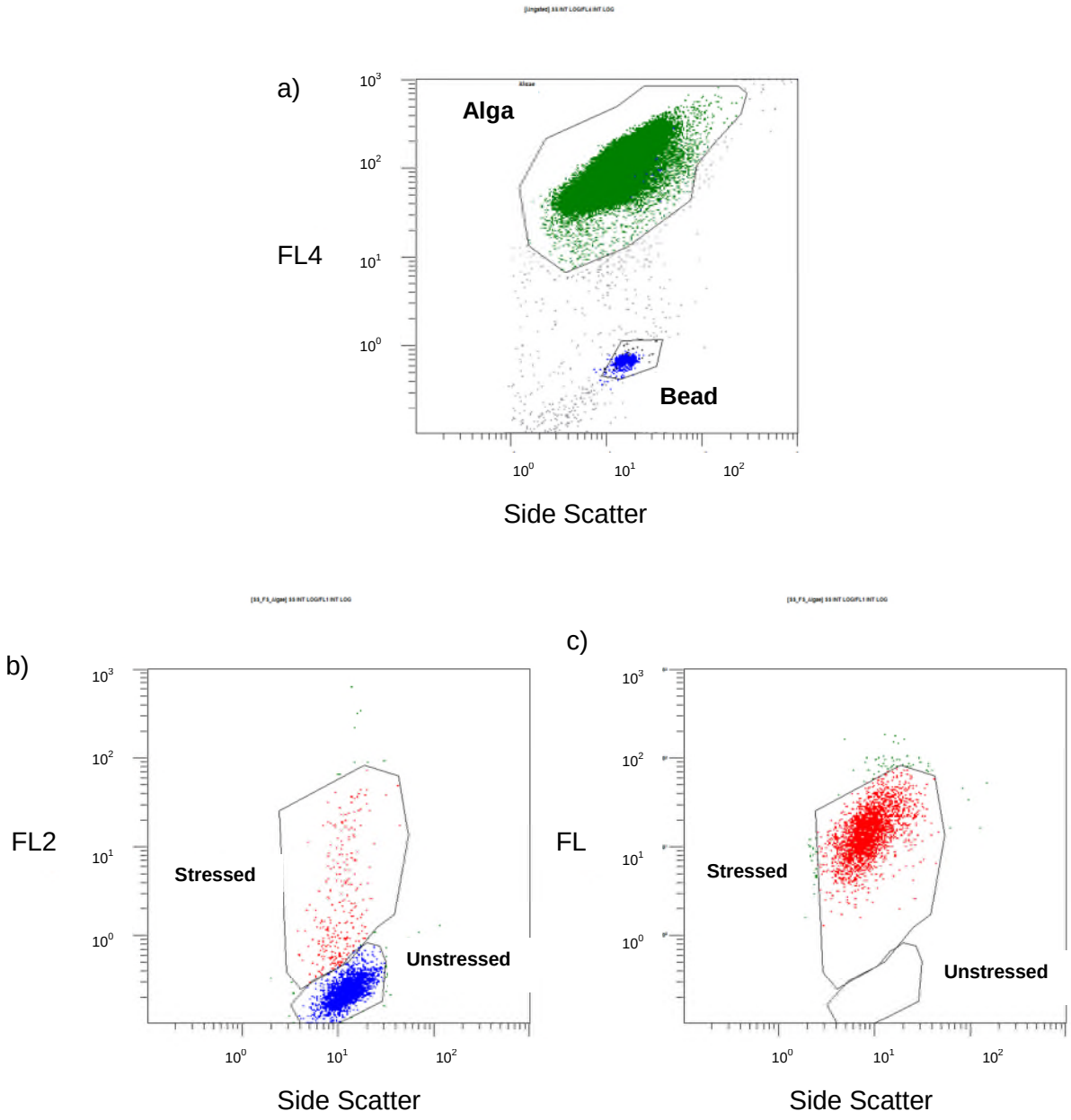

Figure 3-11. Example flow cytometer distributions. All show side scatter on X-axis (used to designate size) and the wavelength channel (Fluorescence) on the y-axis. Algal cell numbers and calibration bead numbers were obtained from the gates. a) *C.reinhardtii* and calibration beads. Y-axis = FL4 b) Unstressed *C.reinhardtii* stained with FDA. Y-axis = FL2 c) Stressed *C.reinhardtii* exposed to EC_{70} H_2O_2 stained with FDA. Y-axis = FL2.

For total silver samples at 0 hours and 72 hours, 5ml was taken from each culture and 0.15ml of 69% nitric acid was added to acidify the sample for analytics. Samples were

sealed with parafilm and stored at 4°C in the dark. Dissolved silver samples at 0 hours and 72 hours were obtained by taking the remaining 5ml of each sample and centrifuging at 4000rpm for 30-60mins through 10kDa centrifugal filter devices to separate out dissolved silver from total silver. The supernatant containing dissolved silver acidified with 0.15ml 69% nitric acid was sealed with parafilm and stored at 4°C.

Samples were sent to the Vrije Universiteit Amsterdam, Department of Animal Ecology in the Netherlands for Atomic Absorption Spectroscopy (AAS) analysis.

3.3.7.6 Biological Exudates Characterisation

Samples were sent away for chemical analysis of the concentration and composition of EPS of both stressed and unstressed *C.reinhardtii* and *S.leopoliensis.* Exposures were created for both species exposed to variable doses of AG1, AG2, $AgNO_3$ plus a control (values picked to incorporate a wide range of concentrations). Doses are shown in Chapter 7. Three replicates were set up for each toxicant. Samples were set-up in the same manner as dose-response curves with 1ml of culture added to 9ml of spiked MBL medium. After 72 hours, samples were processed for chemical analysis in the same way as MBL-EPS physical characterisation samples (Section 3.3.5.4. Table 3-8) however after the second centrifugation step both the pellet and the supernatant of these samples were retained. Pellets were stored at -20°C. 3% Sodium Azide (NaN_3) was added at a 1:100 dilution to the supernatant to preserve the sample and this was refrigerated until analysis.

Samples were sent to the Swiss Federal Institute of Water Research (EAWAG), Dubendorf, Switzerland, Department of Environmental Toxicology for analysis by liquid chromatography-organic carbon detection-organic nitrogen detection (LC-OCD-OND). This technique involved separation of different molecular weight fractions of organic matter based upon retention times through a size exclusion column[61].

3.3.8 Statistics and Data Analysis

Characterisation data from DLS, NTA, DCS and TEM techniques was analysed using Microsoft Excel 2010. Error bars in charts were set to one standard deviation of the mean obtained from at least 3 replicates. Flow cytometry data was viewed initially in Microsoft Excel and then converted into a form that would allow analysis by R[62].

R in standard mode was used to plot the dose-response data while the *drc* package[63,64] was used to fit a four-parameter log-logistic regression curve to the data to obtain EC_x values (equation shown in 7.2.6). R was also used to fit a linear model to fluorescence data to assess the significance of each treatment on each endpoint.

3.4 References

1. Malvern Instruments Ltd. Zetasizer Nano Series User Manual. (2004).

2. Jiang, J., Oberdörster, G. & Biswas, P. Characterization of size, surface charge, and agglomeration state of nanoparticle dispersions for toxicological studies. *J. Nanoparticle Res.* **11,** 77–89 (2009).

3. Anderson, W., Kozak, D., Coleman, V. A., Jämting, Å. K. & Trau, M. A comparative study of submicron particle sizing platforms: Accuracy, precision and resolution analysis of polydisperse particle size distributions. *J. Colloid Interface Sci.* **405,** 322–330 (2013).

4. Xu, R. Progress in nanoparticles characterization: Sizing and zeta potential measurement. *Particuology* **6,** 112–115 (2008).

5. Kaszuba, M. *et al.* Measuring sub nanometre sizes using dynamic light scattering. *J. Nanoparticle Res.* **10,** 823–829 (2007).

6. Hassellöv, M., Readman, J., Ranville, J. F., Tiede, K. & Tiede, Æ. K. Nanoparticle analysis and characterization methodologies in environmental risk assessment of engineered nanoparticles. *Ecotoxicology* **17,** 344–361 (2008).

7. Hassellöv, M. & Kaegi, R. in *Environ. Hum. Heal. Impacts Nanotechnol.* 211–266 (John Wiley & Sons, Ltd, 2009). doi:10.1002/9781444307504.ch6

8. Mahl, D., Diendorf, J., Meyer-Zaika, W. & Epple, M. Possibilities and limitations of different analytical methods for the size determination of a bimodal dispersion of metallic nanoparticles. *Colloids Surfaces A Physicochem. Eng. Asp.* **377,** 386–392 (2011).

9. Boyd, R. D., Pichaimuthu, S. K. & Cuenat, A. New approach to inter-technique comparisons for nanoparticle size measurements; using atomic force microscopy, nanoparticle tracking analysis and dynamic light scattering. *Colloids Surfaces A Physicochem. Eng. Asp.* **387,** 35–42 (2011).

10. Karlsson, H. L., Gustafsson, J., Cronholm, P. & Möller, L. Size-dependent toxicity of metal oxide particles--a comparison between nano- and micrometer size. *Toxicol. Lett.* **188,** 112–8 (2009).

11. Kallay, N. & Zalac, S. Stability of nanodispersions: a model for kinetics of aggregation of nanoparticles. *J. Colloid Interface Sci.* **253,** 70–6 (2002).

12. Domingos, R. F. *et al.* Characterizing Manufactured Nanoparticles in the Environment : Multimethod Determination of Particle Sizes. *Environ. Sci. Technol.* **43,** 7277–7284 (2009).

13. Klaine, S. J. *et al.* Nanomaterials in the environment: Behavior, fate, bioavailability, and effects. *Environ. Toxicol. Chem.* **27,** 1825–1851 (2008).

14. Weiser, H. B. *Colloid Chemistry*. 226–233 (John Wiley & Sons, Inc. New York. Chapman & Hall Ltd. London, 1949).

15. Tantra, R., Schulze, P. & Quincey, P. Effect of nanoparticle concentration on zeta-potential measurement results and reproducibility. *Particuology* **8,** 279–285 (2010).

16. Fermin, D. & Riley, J. in *Colloid Sci. Princ. Methods Appl.* (ed. Cosgrove, T.) 23–44 (John Wiley & Sons Ltd., 2010).

17. Dougherty, G. M. *et al.* The zeta potential of surface-functionalized metallic nanorod particles in aqueous solution. *Electrophoresis* **29,** 1131–9 (2008).

18. El Badawy, A. M. *et al.* Impact of environmental conditions (pH, ionic strength, and electrolyte type) on the surface charge and aggregation of silver nanoparticles suspensions. *Environ. Sci. Technol.* **44,** 1260–6 (2010).

19. Handy, R. D., von der Kammer, F., Lead, J. R., Owen, R. & Crane, M. The ecotoxicology and chemistry of manufactured nanoparticles. *Ecotoxicology* **17,** 287–314 (2008).

20. Malloy, A. & Carr, B. NanoParticle Tracking Analysis - The Halo^{TM} System. *Part. Part. Syst. Charact.* **23,** 197–204 (2006).

21. Gallego-Urrea, J. a., Tuoriniemi, J., Hassellöv, M. & Hassello, M. Applications of particle-tracking analysis to the determination of size distributions and concentrations of nanoparticles in environmental, biological and food samples. *TrAC Trends Anal. Chem.* **30,** 473–483 (2011).

22. Saveyn, H. *et al.* Accurate particle size distribution determination by nanoparticle tracking analysis based on 2-D Brownian dynamics simulation. *J. Colloid Interface Sci.* **352,** 593–600 (2010).

23. Calzolai, L., Gilliland, D. & Rossi, F. Measuring nanoparticles size distribution in food and consumer products: a review. *Food Addit. Contam. Part A. Chem. Anal. Control. Expo. Risk Assess.* **29,** 1183–93 (2012).

24. CPS Instruments Inc. CPS Disc Centrifuge Operating Manual. 1–78 (2004). at <http://www.cpsinstruments.eu/pdf/Manual.pdf>

25. Hu, W. *et al.* Toxicity of copper oxide nanoparticles in the blue mussel, Mytilus edulis: A redox proteomic investigation. *Chemosphere* **108,** 289–299 (2014).

26. RSC. Royal Society of Chemistry: Periodic Table. (2014). at <http://www.rsc.org/periodic-table>

27. IHPP. Institute of High Pressure Physics: Properties of Zinc. (2014). at <http://www.unipress.waw.pl/index.php?option=com_content&view=article&catid=70:descriptions&id=301:properties-of-zno>

28. Sadowski, Z., Maliszewska, I. H., Grochowalska, B., Polowcyzk, I. & Kozlecki, T. Synthesis of silver nanoparticles using microorganisms. *Mater. Sci.* **26,** 419–424 (2008).

29. Buxbaum, G. & Pfaff, G. *Industrial Inorganic Pigments*. (Wiley-VCH Verlag GmbH & Co KGaA, 2005).

30. Mavrocordatos, D., Perret, D. & Leppard, G. G. in *Environ. Colloids Part. Behav. Sep. Characterisation* (eds. Wilkinson, Kevin, J. & Lead, Jamie, R.) 345–405 (2007).

31. Weinberg, H., Galyean, A. & Leopold, M. Evaluating engineered nanoparticles in natural waters. *TrAC Trends Anal. Chem.* **30,** 72–83 (2011).

32. Klang, V., Matsko, N. B., Valenta, C. & Hofer, F. Electron microscopy of nanoemulsions: an essential tool for characterisation and stability assessment. *Micron* **43,** 85–103 (2012).

33. Williams, D. B. & Carter, C. B. *Transmission Electron Microscopy: A Textbook for Materials Science*. *Mater. Sci.* **V1-V4,** 703 (1996).

34. Dudkiewicz, A. *et al.* Characterization of nanomaterials in food by electron microscopy. *TrAC Trends Anal. Chem.* **30,** 28–43 (2011).

35. Tiede, K., Hassellöv, M., Breitbarth, E., Chaudhry, Q. & Boxall, A. B. A. Considerations for environmental fate and ecotoxicity testing to support environmental risk assessments for engineered nanoparticles. *J. Chromatogr. A* **1216,** 503–509 (2009).

36. Vigneau, E., Loisel, C., Devaux, M. F. & Cantoni, P. Number of particles for the determination of size distribution from microscopic images. *Powder Technol.* **107,** 243–250 (2000).

37. Cid, A., Herrero, C. & Abalde, J. Functional analysis of phytoplankton by flow cytometry a study of the effect of copper on a marine diatom. *SCI. MAR.* **60,** 303–308 (1996).

38. Díaz, M., Herrero, M., García, L. a. & Quirós, C. Application of flow cytometry to industrial microbial bioprocesses. *Biochem. Eng. J.* **48,** 385–407 (2010).

39. Dunker, S., Jakob, T. & Wilhelm, C. Contrasting effects of the cyanobacterium Microcystis aeruginosa on the growth and physiology of two green algae, Oocystis marsonii and Scenedesmus obliquus , revealed by flow cytometry. *Freshw. Biol.* **58,** 1573–1587 (2013).

40. Hyka, P., Lickova, S., Přibyl, P., Melzoch, K. & Kovar, K. Flow cytometry for the development of biotechnological processes with microalgae. *Biotechnol. Adv.* **31,** 2–16 (2013).

41. Handy, R. D. *et al.* Ecotoxicity test methods for engineered nanomaterials: practical experiences and recommendations from the bench. *Environ. Toxicol. Chem.* **31,** 15–31 (2012).

42. Malvern Instruments Ltd. Zetasizer Software. (2012).

43. Nichols, H. W. in *Handb. Phycol. Methods* (ed. Stein, J. R.) 16–17 (Cambridge University Press, 1973). at <http://www.marine.csiro.au/microalgae/methods/Media CMARC recipes.htm#MBL>

44. ISO 10712. Water quality -- Pseudomonas putida growth inhibition test (Pseudomonas cell multiplication inhibition test). (1995). at <http://www.iso.org/iso/catalogue_detail.htm?csnumber=18800>

45. PROSPECT. Protocol for Nanoparticle Dispersion. (2010). at <http://www.nanotechia.org/sites/default/files/files/PROSPECT_Dispersion_Protocol.pdf>

46. Melegari, S. P., Perreault, F., Costa, R. H. R., Popovic, R. & Matias, W. G. Evaluation of toxicity and oxidative stress induced by copper oxide nanoparticles in the green alga Chlamydomonas reinhardtii. *Aquat. Toxicol.* **142-143,** 431–40 (2013).

47. Lee, D.-Y., Fortin, C. & Campbell, P. G. C. Contrasting effects of chloride on the toxicity of silver to two green algae, Pseudokirchneriella subcapitata and Chlamydomonas reinhardtii. *Aquat. Toxicol.* **75,** 127–35 (2005).

48. Jamers, A. *et al.* Flow cytometric analysis of the cadmium-exposed green alga Chlamydomonas reinhardtii (Chlorophyceae). *Eur. J. Phycol.* **44,** 541–550 (2009).

49. Merchant, S. S. *et al.* The Chlamydomonas genome reveals the evolution of key animal and plant functions. *Science* **318,** 245–50 (2007).

50. Navarro, E. *et al.* Toxicity of Silver Nanoparticles to Chlamydomonas reinhardtii. *Environ. Sci. Technol.* **42,** 8959–8964 (2008).

51. OECD. Test No 201: Freshwater Alga and Cyanobacteria, Growth Inhibition Test. *OECD Guidel. Test. Chem.* **Section 2,** 25 (2011).

52. Ribeiro, F. *et al.* Silver nanoparticles and silver nitrate induce high toxicity to Pseudokirchneriella subcapitata, Daphnia magna and Danio rerio. *Sci. Total Environ.* **466-467C,** 232–241 (2013).

53. Debenest, T. *et al.* Monitoring of a flame retardant (tetrabromobisphenol A) toxicity on different microalgae assessed by flow cytometry. *J. Environ. Monit.* **12,** 1918–23 (2010).

54. Von Moos, N. & Slaveykova, V. I. Oxidative stress induced by inorganic nanoparticles in bacteria and aquatic microalgae – state of the art and knowledge gaps. *Nanotoxicology* **8,** 605–630 (2014).

55. Hadjoudja, S. *et al.* Short term copper toxicity on Microcystis aeruginosa and Chlorella vulgaris using flow cytometry. *Aquat. Toxicol.* **94,** 255–64 (2009).

56. Michels, M. H. a, van der Goot, A. J., Norsker, N.-H. & Wijffels, R. H. Effects of shear stress on the microalgae Chaetoceros muelleri. *Bioprocess Biosyst. Eng.* **33,** 921–7 (2010).

57. Prado, R., Rioboo, C., Herrero, C., Suárez-Bregua, P. & Cid, A. Flow cytometric analysis to evaluate physiological alterations in herbicide-exposed Chlamydomonas moewusii cells. *Ecotoxicology* **21,** 409–20 (2012).

58. Zhao, H. *et al.* Superoxide reacts with hydroethidine but forms a fluorescent product that is distinctly different from ethidium: potential implications in intracellular fluorescence detection of superoxide. *Free Radic. Biol. Med.* **34,** 1359–1368 (2003).

59. Saison, C. *et al.* Effect of core-shell copper oxide nanoparticles on cell culture morphology and photosynthesis (photosystem II energy distribution) in the green alga, Chlamydomonas reinhardtii. *Aquat. Toxicol.* **96,** 109–14 (2010).

60. Yoshida, K., Igarashi, E., Mukai, M., Hirata, K. & Miyamoto, K. Induction of tolerance to oxidative stress in the green alga, Chlamydomonas reinhardtii, by abscisic acid. *Plant, Cell Environ.* **26,** 451–457 (2003).

61. Stewart, T. J., Traber, J., Kroll, A., Behra, R. & Sigg, L. Characterization of extracellular polymeric substances (EPS) from periphyton using liquid chromatography-organic carbon detection-organic nitrogen detection (LC-OCD-OND). *Environ. Sci. Pollut. Res. Int.* **20,** 3214–23 (2013).

62. R Development Core Team. R: A Language and Environment for Statistical Computing. (2013). at <www.r-project.org>

63. Ritz, C. & Streibig, J. C. Bioassay Analysis using R. *J. Stat. Softw.* **12,** 1–21 (2005).

64. Ritz, C. & Streibig, J. Analysis of Dose Response Data. (2013).

Chapter 4. Long-term characterisation of Silver and Zinc Oxide Nanoparticle Suspensions

4.1 Introduction

Fate studies are dependent on the understanding of nanomaterial behavior in suspension which can be used to improve environmental risk assessment. The toxicity of engineered nanoparticles is dependent on the physicochemical properties of the both the particles and the surrounding media. Particle specific properties include size (and size distribution), morphology, extent of aggregation/agglomeration (tight clustering/loose clustering), chemical makeup and solubility[1–4] while media specific properties include ionic strength, ionic composition, pH, stabilisers/coatings and concentration of suspended material[5–8].

When in suspension these properties may alter over time and this can have a knock-on effect on their bioavailability and possible toxic potency[9]. As such it is necessary to characterize these properties.

4.1.1 Aims and Objectives

The purpose of this part of the study was to assess the long-term stability (5-6 months) of metal and metal oxide nanoparticles in de-ionised water (*DI*H_2O) with respect to particle hydrodynamic diameters (d_H & d_{pp}), particle size distributions (PSD), zeta potential (ZP) and morphological changes (aspect ratio S_{pp}). This data is useful in understanding the particles persistence and form in environmental systems.

This study also aimed to assess the capability of a selection of suspension characterisation methods to analyse long-term changes in particle character. Most toxicology laboratories are

unlikely to have access to high-end techniques such as electron microscopy and will more commonly use widespread cost-effective techniques such as dynamic light scattering or differential centrifugal sedimentation. As such it is important to assess techniques limitations and gauge the accuracy of their outputs. Most studies utilize only one or two of these common techniques without taking their technical limitations (discussed in Chapter 3) into account therefore it is useful to investigate these issues using a suite of techniques concurrently[10]. The techniques used in this study were dynamic light scattering (DLS), differential centrifugal sedimentation (DCS) and transmission electron microscopy (TEM) while zeta potential (ZP) was also analysed using a Malvern Zetasizer.

.

4.1.2 Materials and Methods

4.1.2.1 Particles

Two uncoated ZnO nanoparticle samples (ZN1 and ZN2) with different sizes and aspect ratios were used as well as organic paraffin coated Ag-NPs (AG1) as described in Chapter 3.

4.1.2.2 Preparation of Media

Deionised water (*DI*H_2O) from the tap in the laboratory was used as suspension medium.

4.1.2.3 Preparation of Suspensions

Preparation of NP suspensions was based on PROSPECT: Protocol for Nanoparticle Dispersion [11] and described in Chapter 3.

4.1.2.4 Characterisation

Each suspension was measured monthly from 0-6 months to understand any time dependent effects. Light scattering technique DLS (Malvern Zetasizer Nano) and DCS (CPS disc centrifuge) were used to obtain hydrodynamic/Stoke's diameters (d_H/d_s) and particle size distributions (PSDs) respectively. ZP data was calculated from electrophoretic mobility using a Malvern Zetasizer. Complementary pH values were obtained using pH paper. TEM was used to obtain qualitative morphological information for particles at 0 and 6 months as a counterpoint to the other characterisation techniques. Experimental techniques and measurement protocols are described in greater detail in Chapter 3.

4.2 Results

4.2.1 DLS: Hydrodynamic Diameter

The z-averaged d_H of AG1 NPs at both 10mg/L and 100mg/L remained stable within a margin of ~30nm for the duration of the experiment with low standard deviation (Figure 4-1a). 10mg/L d_H increased to 140nm at 6 months with larger standard deviation (SD) than previous measurements. Both 1000mg/L zinc oxide nanoparticles (ZN1 and ZN2) showed large mean d_H (between 500 and 4600nm) and large standard deviation which prevented a definitive d_H for these samples (Figure 4-1b,c). At no point in the measurements were the stated primary particle size of any of the studied nanoparticles seen in DLS (AG1: 3-8nm, ZN1: 30nm, ZN2: 200nm).

4.2.2 DLS: Polydispersity Index

Polydispersity index (PDI) is a dimensionless factor that gives an idea into the width of particle sizes present in a suspension. High polydispersity Index (PDI >0.4) indicates that

samples have a large distribution of particle sizes and are therefore polydisperse whereas a low PDI (up to 0.4) indicates a more monodisperse distribution.

PDI for AG1 remained low (below 0.3) for the experiment duration with a shallow increasing trend indicating that size distribution of the sample although relatively constrained was increasing in width (Figure 4-2a). PDI for ZN1, ZN2 were variable and remained medium to high (0.35-1) with large standard deviation at all stages indicating that there was a large spread of particle sizes for these samples (Figure 4-2b, c). High standard deviation in PDI indicates variability in PSD over the duration of each measurement.

To get an idea of the range in diameters in the each suspension DLS intensity plots are shown for 10mg/L AG1 particles. Initial measurements (0 months: Figure 4-2d) show a single peak corroborating the low PDI (~0.12: Figure 4-2a) whilst at 6 months (Figure 4-2e) higher PDI (~0.33: Figure 4-2a) corresponds to the presence of a second peak in the distribution at ~345nm making the distribution wider. Distributions for ZN1 (Figure 4-2f) and ZN2 (data not shown) show a single narrow peak lower than the Z-average value however this is an artefact. Much of the ZnO material in suspension was much larger than the Zetasizer detection limits and was sedimenting during the measurements complicating the intensity distribution. It should be noted that these intensity distributions show the data for one replicate out of ten repeat measurements and are used as a qualitative example to show the width of the distribution.

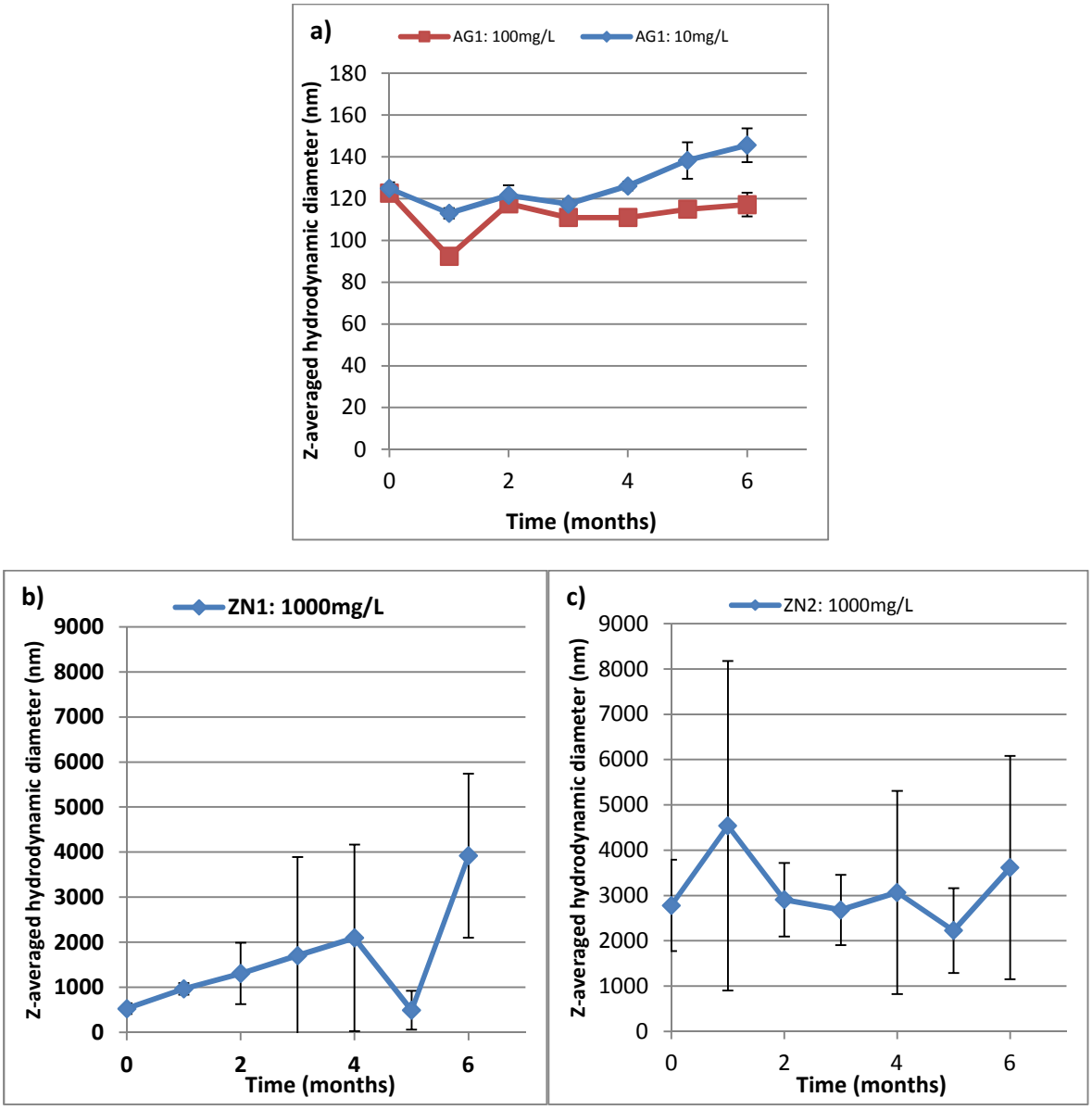

Figure 4-1. Z-averaged hydrodynamic diameters (d_H) over the duration of the experiment (5-6months). a) AG1 b) ZN1 c) ZN2. Error bars indicate one standard deviation of 10 repeat measurements.

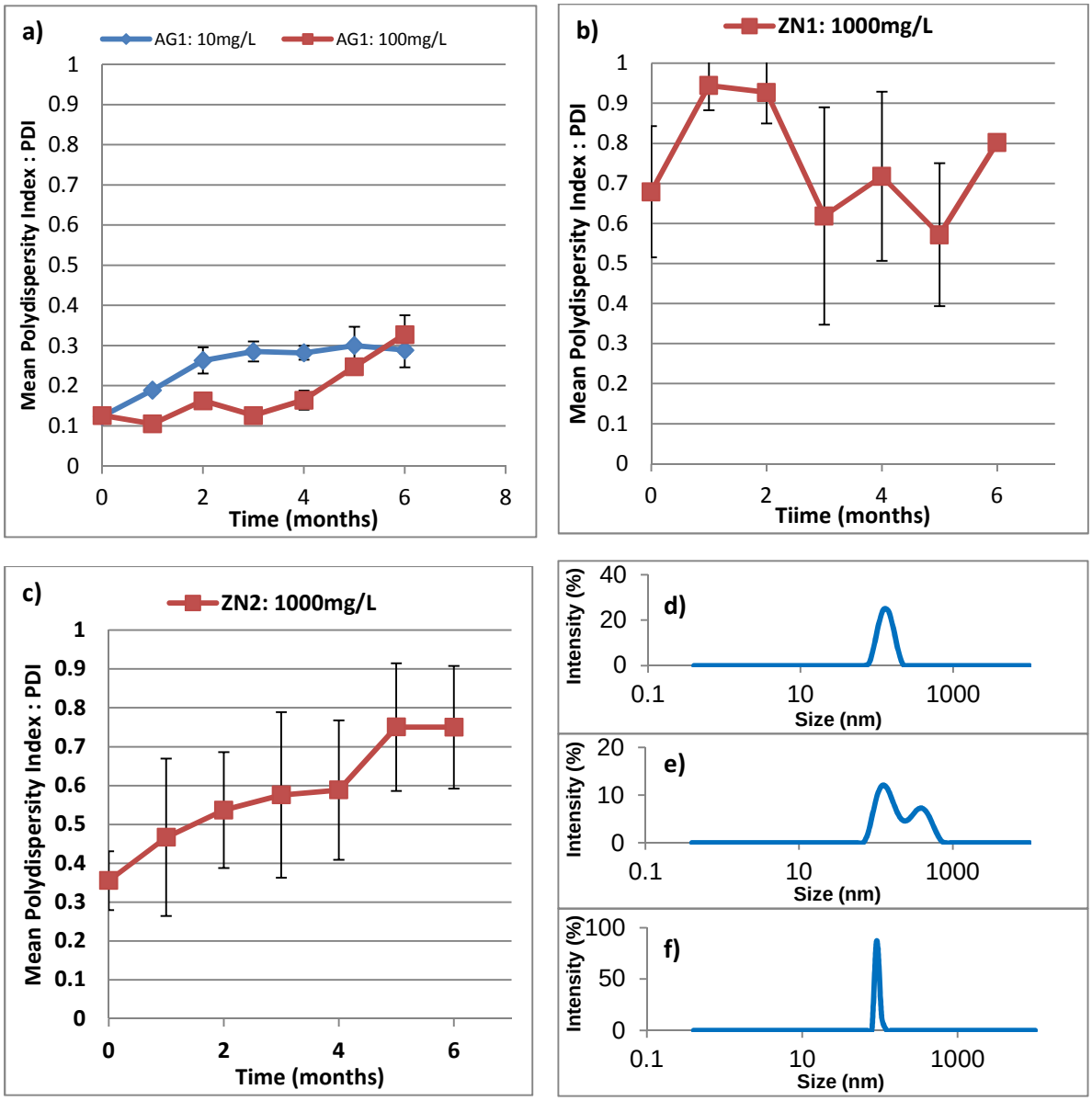

Figure 4-2. Polydispersity Index (PDI) over the duration of the experiment (5-6months) for a) AG1 b) ZN1 c) ZN2. Example DLS measurement showing size distribution by intensity signal for one replicate of d) AG1 0 months e) AG1 6 months f) ZN1 6 months. ZN2 data was similar to ZN1 and is not shown. Error bars indicate one standard deviation of 10 repeat measurements.

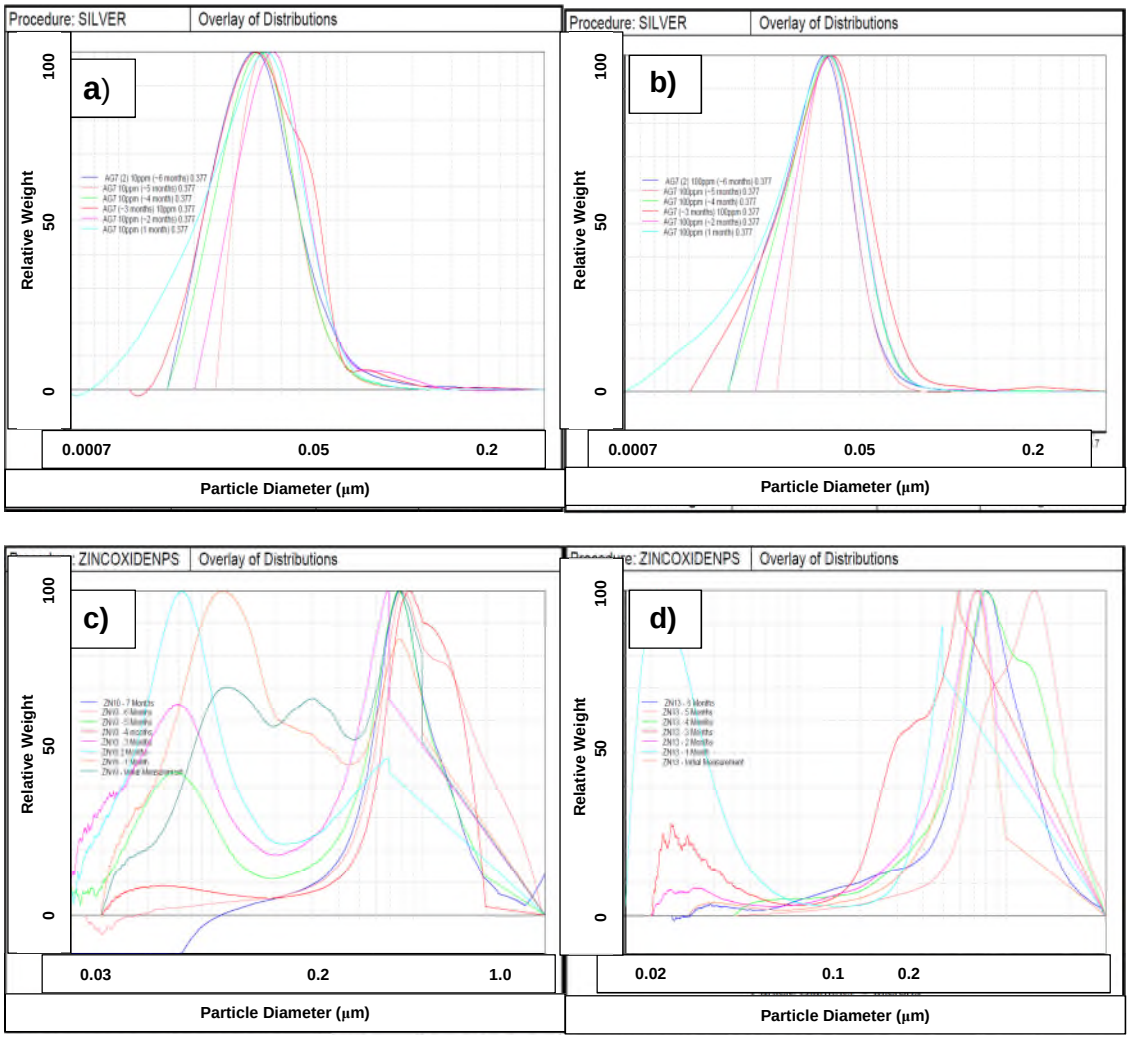

Figure 4-3. DCS Relative Weight Particle Size Distributions over the duration of the experiment (5-6months). a) AG1 10mg/L b) AG1 100mg/L c) ZN1 1000mg/L d) ZN2 1000mg/L. X-axis shows particle diameter in microns while the Y-axis gives the relative weight of each diameter in relation to the other diameters in distribution. Data for c) and d) is very noisy.

4.2.3 DCS: Particle Size Distribution

There was little difference in DCS results for AG1 PSDs between the two concentrations 10mg/L and 100mg/L and for the 6 month duration of the experiment. Data suggested suspended materials were between 20-100nm with peak d_s at ~40nm (Figure 4-3a,b). The DCS data for ZN1 and ZN2 show very wide PSDs which were 0-3µm and it was difficult to pick out specific d_s from the peaks present in the distribution due to noise (Figure 4-3c, d). Both ZnO samples indicate the presence of two peaks in the distribution showing that these

particles are multimodal. As with DLS the manufacturer stated particle sizes are not seen for any of the particles.

4.2.4 TEM: Particle Size and Aspect Ratio

Table 4-1 shows particle size data from the analysis of TEM images for each particle shown in Figures 4-4 - 4-6. From the table it can be seen that none of the primary particles showed an increase in primary particle diameter (d_{pp}), size range or aspect ratio (S_{pp}) for the duration of the experiment over the influence of error bars (1 standard deviation).

AG1 had the smallest diameter of the measured particles as expected remaining between 4.9 and 23nm diameter throughout the experiment. Particles were ellipsoid and present in loosely associated clusters (size not measured) (Figure. 5-6a, 4-4). The average diameter increased slightly after 6 months from 9.58 to 11.38nm however this cannot be stated conclusively due to large error bars for both data sets. No change in average aspect ratio (S_{pp}) of the primary particles was noted for AG1 indicating that particles did not undergo definitive morphological change.

Both ZN1 and ZN2 particles indicated no change in their respective d_{pp}, diameter range and S_{pp} from 0 to 6 months (Table 4-1). Both were similar size to their stated manufacturer sizes of ~30nm and ~200nm respectively. ZN1 particles were mainly oblate with some hexagonal (Figure 4-5). ZN2 NPs were much more angular and from 0-6 months were seen to become more rounded at the edges (Figure. 4-6) however this did not alter the S_{pp} of the particles. Both particles were present in very large clusters indicating that extreme agglomeration (loosely associated particle clusters) and likely some aggregation (tightly bound particles fused together) occurred in suspension or during TEM sample preparation due to high concentrations. If dissolution has occurred it is not to the extent that average primary particle size or even particle size range has been affected greatly for either particle.

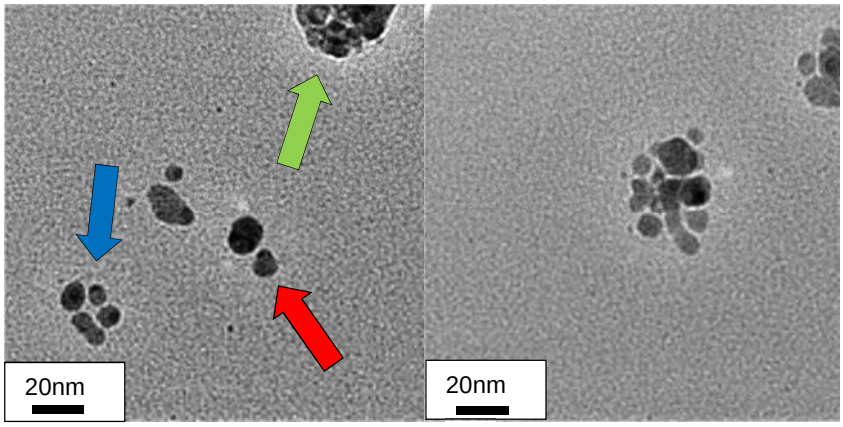

Figure 4-4. TEM images of 100mg/L AG1 NPs in *DI*H_2O at 6 months (scale bars 20nm and 20nm). Arrows indicate primary particles (red), loose clusters (agglomerates) (blue) and tight clusters (aggregates) (green)

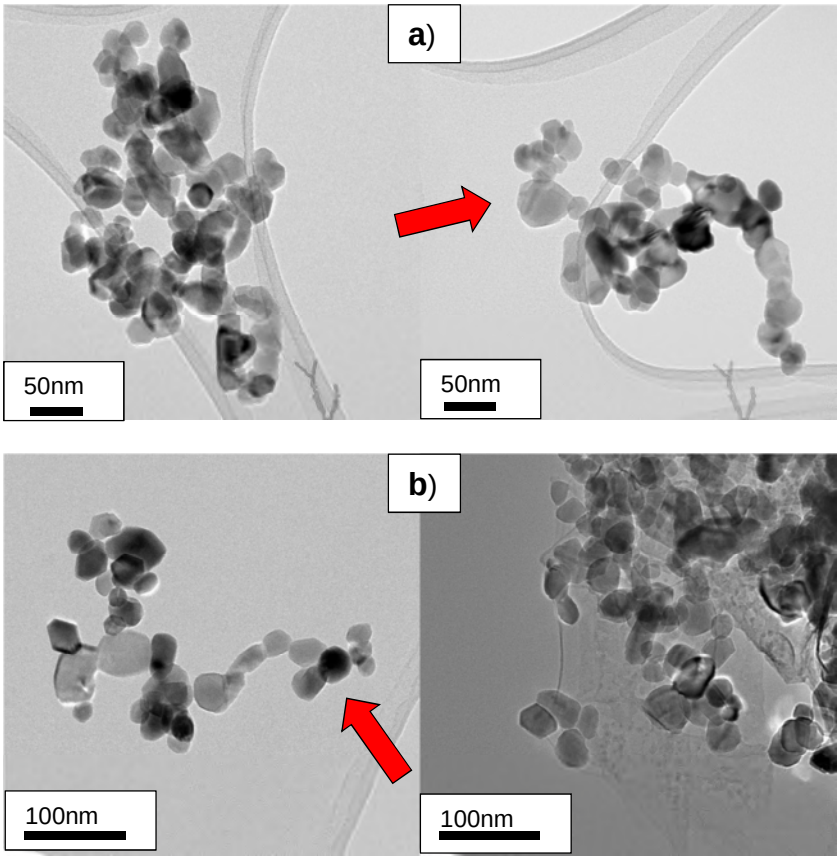

Figure 4-5. TEM images of 1000mg/L ZN1 NPs in *DI*H_2O at a) 0 and b) 6 months (scale bars a) 50nm b) 100nm). Arrows indicate primary particles (red).

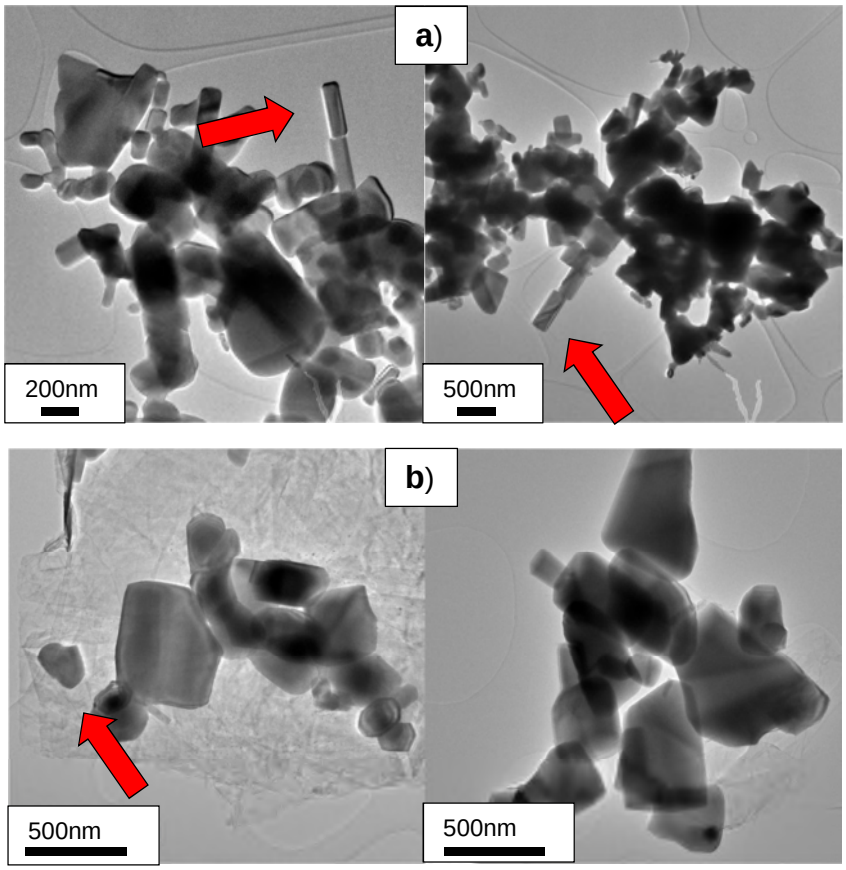

Figure 4-6. TEM images of 1000mg/L ZN2 NPs in *DI*H_2O at a) 0 and b) 6 months (scale bars a) 200nm and 500nm b) 500nm). Arrows indicate primary particles (red).

Table 4-1. TEM data AG1, ZN1, ZN2 nanoparticles in *DI*H_2O. Primary particle (d_{pp}), size ranges and aspect ratios of primary particles (S_{pp}).

Particle	Time (months)	Conc. (mg/L)	d_{pp} (nm/no)	range (nm)	S_{pp} (range)	Notes
AG1	0	10	9.55±3.66/102	4.9-18.16	1.24±0.41 (1.00-2.24)	*Ultrapure water rather than *DI*H_2O (data from Ch. 5)
	6	100	11.38±3.26/51	5.80-23.52	1.25±0.18 (1.02-1.91)	
ZN1	0	1000	32.75±10.61/ 81	17.06-66.16	1.33±0.27 (1.00-2.34)	
	6	1000	30.94±10.14/66	10.64-60.30	1.35±0.24 (1.02-2.49)	
ZN2	0	1000	283.32±137.50/60	101.7-707.5	1.79±0.65 (1.01-3.76)	
	6	1000	293.73±141.34/60	103.04-707.59	1.76±0.99 (1.03-7.11)	

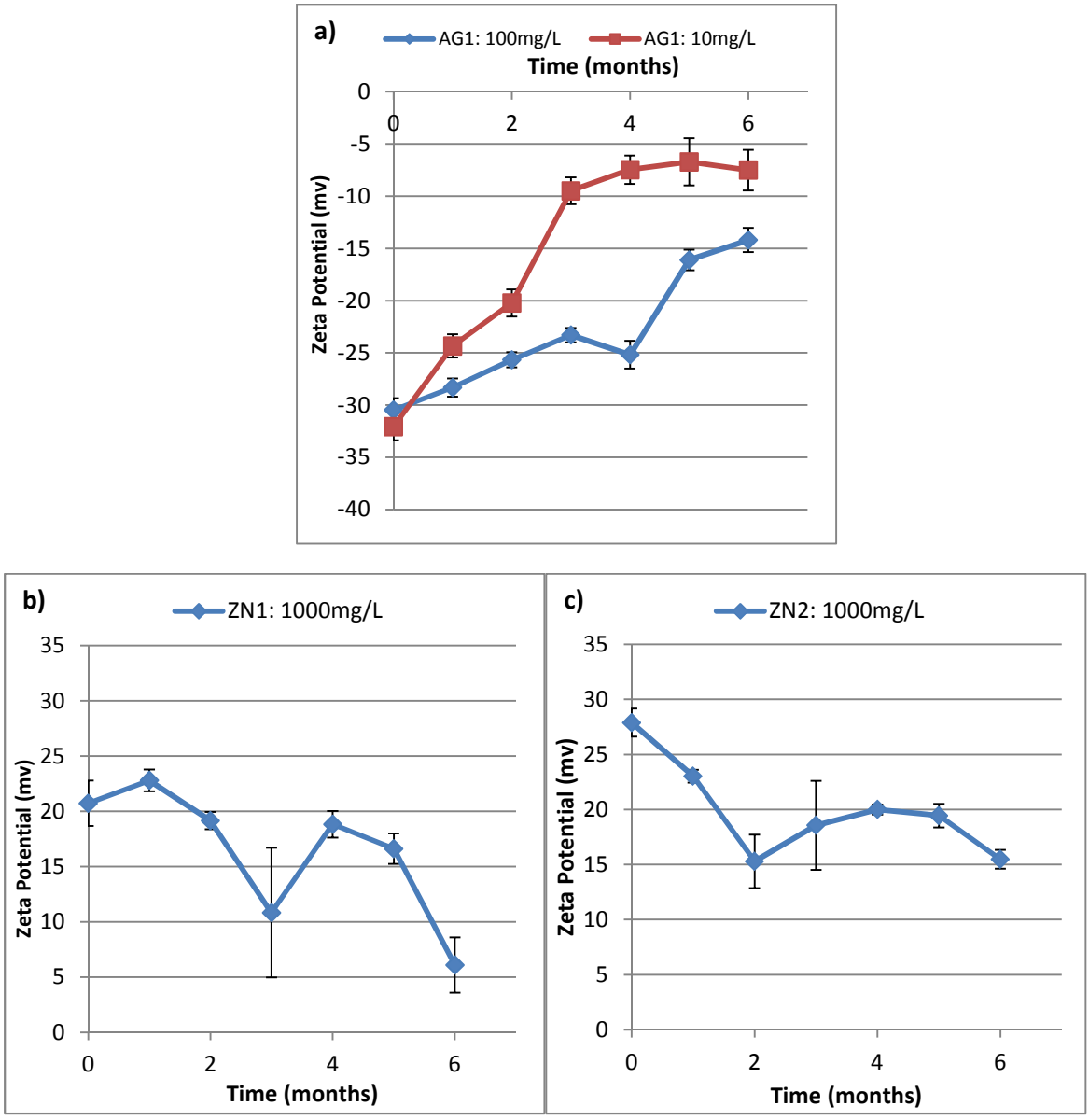

Figure 4-7. Zeta Potential (ZP) measured from electrophoretic light scattering over the duration of the experiment (5-6months). a) AG1 b) ZN1 c) ZN2. Error bars indicate one standard deviation of 10 repeat measurements. pH was 7 for all samples for the experiment duration.

4.2.5 Zeta Potential (ZP)

Zeta potential data showed different trends for each of the particles. AG1 NPs at both 10 and 100mg/L showed high negative electrostatic stability at the beginning of the experiment (~-30mV) which increased towards 0mV (instability) over the 6 month experimental duration (Figure 4-7a). ZN1, and ZN2 showed medium to high positive electrostatic stability at the beginning (20-45mV) after which all the particles ZPs decreased over the experimental duration (figure 4-7b,c). Zeta Potential data for all of the particles show a decrease in the overall electrostatic stability regardless of particle surface charge. pH for all the suspensions remained constant for the experimental duration at 7. Subtle incremental changes that may have been occurring could not be detecting using the pH paper.

4.2.6 DLS: Percentage of Number Distributions in Each Size Fraction

As an aside the percentage of each samples number distribution that was above and below 100nm were assessed. Intensity particle size distributions (PSDs), the default measurement by DLS were converted by the zetasizer software to number PSDs using Mie theory[12,13]. Both concentrations of AG1 NPs show there were always more particles <100nm than >100nm during the experiment (Figure 4-8a, b). The opposite was true of both ZnO NPs (ZN1 and ZN2) in which the majority of the sample was >100nm throughout (Figure 4-8c, d)

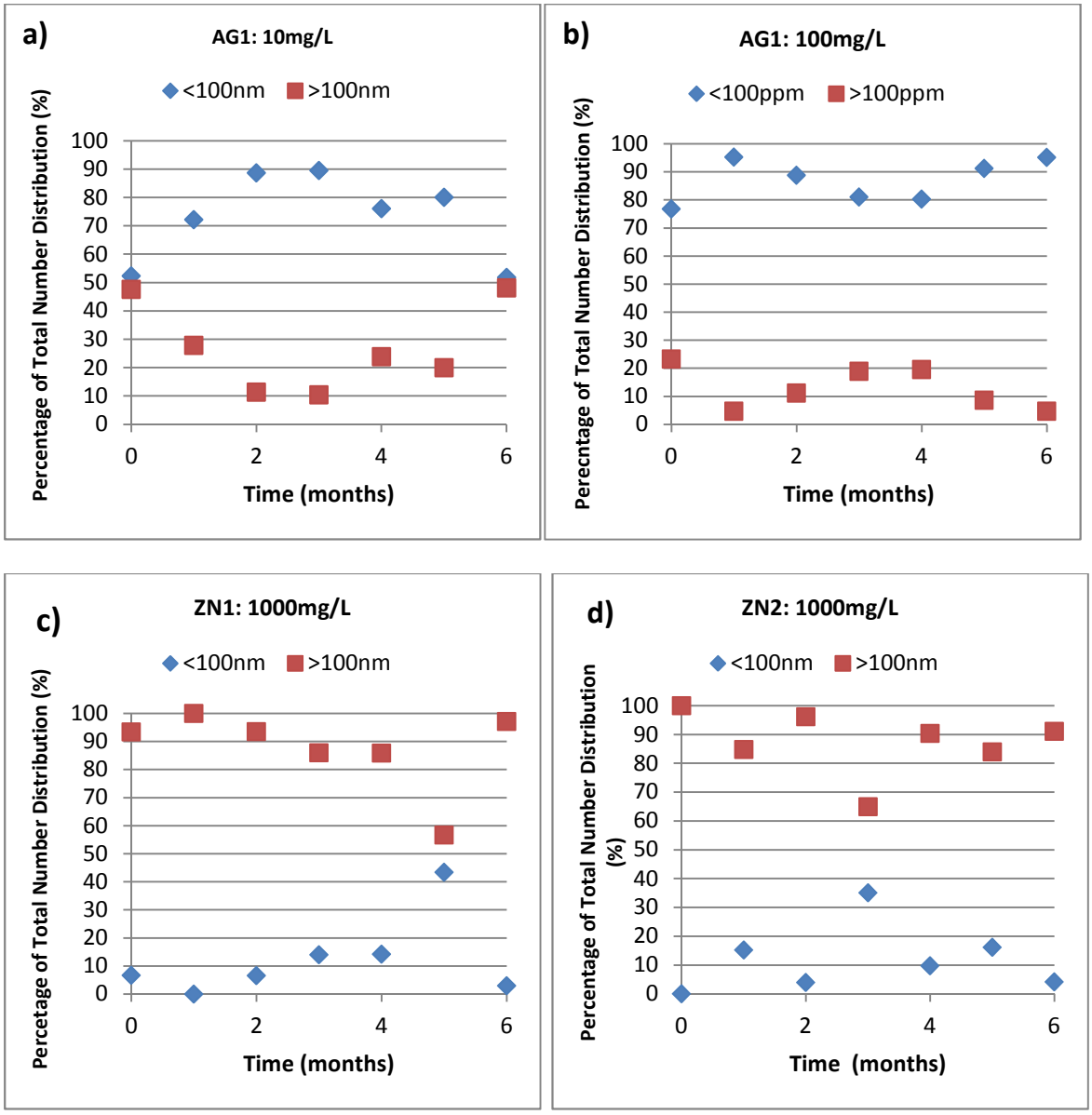

Figure 4-8. Percentage of number particle size distribution less than 100nm (<100nm) and greater than 100nm (>100nm). a) AG1 10mg/L b) AG1 100mg/L c) ZN1 1000mg/l d) ZN2 1000mg/L.

4.3 Discussion

4.3.1 DLS – Detection and Stability

Results for ZN1 and ZN2 highlight the difficulty in interpreting DLS data at high concentrations. ZN1 and ZN2 especially have standard deviations so large as to make discerning any trends in particle size very hard (Figure 4-1b, c).

These difficulties arose due to a number of reasons. As mentioned in Chapter 3 the DLS technique works by measuring light intensity from particle scattered laser light. High concentrations of the samples resulted in aggregation/agglomeration and sedimentation which caused the light intensity scattering to fluctuate rapidly between each replicate due to variable intra-suspension particle concentration. This resulted in variable d_H values and high standard deviations for these samples. Sedimentation could also be observed by eye (data not included). Greater aggregation resulted in greater polydispersion and wide size range multi-modal distributions which made the sample susceptible to light intensity skewing effects and overestimation of d_H[14]. PDI information for ZN1 and ZN2 was high for the duration of the experiment with some variability likely due to sedimentation of particles (Figure 4-2b, c, f). As the particles in suspension were seen to sediment they were shaken and sonicated before each measurement. This caused turbidity and as such it is possible that multiple-scattering events were occurring in which the incoming laser light is scattered multiple times before reaching the detector. This should result in underestimation of particle sizes however as can be seen the d_H values are still very high (Figure 4-1b, c). All of these aforementioned effects are probably occurring to some extent in the 1000mg/L samples. As a result it is difficult to draw many conclusions for high concentration DLS measurements other than aggregation/agglomeration and sedimentation occurred which caused highly variable d_H.

Stable d_H data, inter-replicate comparability and low PDI (<0.4) for AG1 particles (Figure 4-1a, 4-2a) indicated that whilst the particles were polydisperse it is a much smaller distribution than for the higher concentration samples. Although values are low (<0.4) the slight increase in PDI over the experiment duration for both concentrations of AG1 particles indicates that some aggregation may be occurring over time resulting in an increase in the width of the distribution (Figure 4-2d, e). These samples are much more suitable for analysis by DLS.

4.3.2 Zeta Potential – Detection and Stability

Zeta potential (ZP) data indicated particle specific behavior. AG1 ZP values and therefore the particle surface charges were negative for the experimental duration while ZN1 and ZN2 were positive. This was likely due to differing chemical makeup of the particles as the positively charged NPs were metal oxides and AG1 particles silver with an organic stabilizer. Different surface chemistries confer different levels of surface charge and hence affect the ZP. All four of the particles showed an initial moderate to high electrostatic stability (-20mV<X>20mV) and all indicated a trend in which the ZP potential moves towards instability (0mV) over the experiment duration.

Dependence of zeta potential measurements on concentration has been noted at low concentrations[15,16]. After a certain dilution level, artefacts occurred in the Zetasizer owing to the greater influence of extraneous particles in the media and due to the effects of heterodyne light scattering when the instrument was in homodyne mode[15]. However DLS samples at higher concentrations have not been comprehensively studied experimentally. Tantra et al.[15] looked at high concentrations (0.1% wt) of gold nanoparticles at similar concentration to the 1000mg/L ZnO NPs used in this study and the Zetasizer was seen to give accurate results. However another study stated that particles concentrations of 262nm polystyrene latex beads above 0.01% wt (similar to AG1 concentrations in this study) underwent multiple scattering and results were inaccurate[17]. 0.1% wt. samples were so turbid as to prevent light transmittance through the suspension[17]. It was not possible to discern if the ZN1 and ZN2 ZP data was affected by concentration as comparison at a different concentrations was not undertaken but comparison with the other techniques is possible[18].

Therefore it is useful to question the validity of ZP results as a proxy for stability at concentrations high enough to cause aggregation and sedimentation. If concentration is so high that particles can overcome the charge barrier surrounding NPs then the value obtained for electrostatic stability tells us little of the suspension behavior. So while the zeta potential of both ZN1 and ZN2 are around 20mV it is still unlikely that the suspensions were stable owing to the large aggregations and sedimentation noted in the other characterization techniques seen visually. It may be that the ZP signal was picked up from unsedimented particles left in suspension after the rest of the sample had aggregated and settled to the bottom of the cell. In this case the ZP per overall suspension concentration is not accurate. It would be useful in future studies to assess whether the particles left in suspension were stable after precipitation.

Both AG1 samples are at lower concentrations than the other particles but it is likely that the presence of the organic paraffin stabilizer in these samples is also contributing to the zeta potential. The effect on particle stabilisers on zeta potential is discussed in Chapter 5.

The trend of all ZP values towards 0mV (and therefore electrostatic instability) in these samples likely results from a number of different potential effects. Change in ZP implies a change in the ionic composition of the media during the experiment which occurs from reactions of the suspension media with the particle surfaces (protonation/deprotonation[19]) resulting in release of ionic species via dissolution. This should be noted by pH changes however owing to the poor resolution of the pH paper smaller incremental changes could not be assessed. Small decreases in solution pH have been seen to show an increase in a positive manner for TiO_2 NPs ZP at high particle concentrations (500mg/L)[20] which could explain the increase in AG1 ZP. Other NPs ($Fe(OH)_2$ and Al/TiO_2 NPs in *DI*H_2O have been shown to show no difference in pH with concentration therefore chemical composition of the suspension media and the NP surfaces likely result in variable effects on ZP depending on the particle investigated[19]. This was seen in this study with each NP showing different ZP behavior. It is also likely that interaction of the ambient laboratory air and the particle

suspension medium (*DI*H_2O) is playing a part. It has been shown that a number of counter-ions can influence the ionic composition of suspension media in contact with ambient air of which it has been shown that HCO_3^- has the biggest effect. HCO_3^- has been noted to cause a negative shift in ZP upon interaction with suspended NPs[19] possibly accounting for the decrease towards zero in ZN1 and ZN2. Differences with AG1 may relate to more complex interactions with the particle coating. However with the data available none of these effects can be definitively constrained.

4.3.3 DCS – Detection and Stability

PSDs obtained for ZN1 and ZN2 were highly variable and it was not possible to ascertain definitive values or trends. As DCS calculates the PSD from comparison of particle movement through a density gradient and across a light detector to that of a sphere of the same density the technique works on some assumptions. Sample movement across the detector is affected by particle diameter, refractive index and shape therefore variable PSDs for ZN1 and ZN2 likely result from high polydispersity in the samples due to aggregation[21]. High concentration samples with heavy particles or aggregates such as those in ZN1 and ZN2 can result in the dispersion travelling as a 'heavy liquid' in which the particles move as one through the detection zone resulting in miscalculation of size values[21]. Also high aspect ratio particles such as ZN2 can travel differently to rounded particles in the density gradient. Diffusion coefficients and frictional forces depend on the centre of mass, centre of buoyancy and centre of hydrodynamic stress of the particles which can alter orientation and travel through the disc gradient and light detector. The large clusters present in the high concentration samples may have also had variable aspect ratios and movement through the gradient. Results for these particles using this technique were inconclusive however AG1 particles gave a reasonably stable PSD at both concentrations which may relate to the narrow multimodal distribution of these particles as well as their lower concentrations.

4.3.4 TEM – Detection of Morphological Effects and Stability

TEM data cannot be used to measure stability due to the need to evaporate suspensions before measurements. However it can give useful information on the morphological changes of individual particles/clusters. Hydrodynamic diameter (d_{pp}) of all analysed particles (AG1, ZN1 and ZN2) showed little difference between 0 and 6 months. Any subtle changes that may be occurring to primary particles were likely masked by high standard deviation due to the wide range in particle size as well as poor statistics. Due to the time consuming nature of the technique only a small number of particles were counted (50-100) which is too low to give a statistically relevant picture. In ZN2 samples a change in morphology could be clearly seen after 6 months (Figure 4-6b) as the sharper edges of the particles became rounded possibly due to dissolution. Some re-growth may have also occurred during this morphological change. However this did not lead to a change in d_{pp}, range or aspect ratio (S_{pp}). Using aspect ratio to understand morphological behavior is crude and as such more sophisticated particle analysis procedures are useful to understand some of the subtleties in the information. ZN1 and ZN2 were also present in large particles associations up to several microns in size which were likely the cause for the large d_H and d_s seen in both DLS and DCS respectively for these particles. These large associations likely result from aggregation/agglomeration of the NPs due to high concentrations used[22].

4.4 Conclusions

It is important to conduct characterization experiments for each batch of new material to define technique limitations for that sample[15] as well as for comparison with behaviour in eco-toxicity and natural media. It is also useful to undertake the same experiments to check materials in storage. It is possible that nano-particle samples both dry and in suspension

may change over time and it is valuable to check the sample is the same as used in previous experiments.

It is possible to study the long-term stability of four distinct nanomaterials using these four techniques. However the concentration of the particles must be within range of each machines detection limits. This throws up issues when considering that too high a concentration for one machine may be within the detection limits of another. Were distinct concentrations of NPs used for each machine as per their detection limits then the data would not be comparable as concentration has shown to be an important facet when understanding NP behavior. At 1000mg/L the DLS, ZP and DCS were shown to be unsuitable for accurate characterization of ZN1 and ZN2 NPs but were reasonable when analyzing the AG1 particles at 10mg/L and 100mg/L. The instability of the ZnO particles are also likely having a major effect in detection of stable values between replicates as aggregation and sedimentation will affect both the local concentration and the polydispersity of the sample. TEM can be used to detect changes in size and morphology which are valuable information when considering the particle behavior however sophisticated morphological analysis is necessary to gain maximum information from the images. Particle stabilisers are also likely important in these techniques as stabilized AG1 particles gave the lowest PDI and most consistent results. The increase in PDI for AG1 particles could have resulted from loss of particle stabiliser over time causing some aggregation. Particle stabilisers are discussed more thoroughly in the next chapter.

4.4.1 Environmental Relevance

Studies into long-term stability of engineered nanomaterials in the environment are important to risk assessment. While some nanomaterials may be in a stable form over a short time

period it may be that after a certain period of time they become aggregated or move into a non-bioavailable form.

The EU commission recently updated its definition of nanomaterial to encompass size distribution and stated a nanomaterial is one in which 50% or more of the substance in a number size distribution have constituents which have an external dimension <100nm[23]. A rough assessment of this was undertaken using DLS and it was noted that AG1 had at least 50% of its distribution <100nm while ZN1 and ZN2 had very little of the number distribution below <100nm (Figure 4-8). This indicates that ZN1 and ZN2 upon entering an environmental system would likely aggregate/agglomerate into non-nano sizes and remain in this range for months. Therefore they would not need to be legislated under nano-risk assessment measures whereas AG1 would need to be due to their stability at small sizes throughout the experiment. This could mean greater bioavailability for the AG1 particles than the ZnO NPs. There would however be caveats to this as the agglomerates/aggregates may have nanostructures within that could cause toxicity, for example the high aspect ratio parts of ZN2.

It may also be that particles dissolve after a subsequent period of aging upon introduction to an environmental system. It was not possible to accurately predict the behavior of these samples over the time-frame with these techniques but changes to the samples were seen. It is possible that any subtle changes in morphology and size in the ZnO particles could result from dissolution but as no spectroscopic composition techniques were undertaken in this study it was not possible to say this for certain. Increase in AG1 PDI over the experiment duration could indicate that aggregation of these particles might occur after a certain timeframe in an environmental setting and therefore a temporal aspect needs to be investigated especially in relation to interactions between the NPs and the surrounding media.

DIH_2O as a suspension media is unlikely to be representative of natural matrices which tend to consist of a greater diversification of suspended organic and ionic species which would interact with nanomaterials present in suspension. Further chapters will investigate the effect of different ionic composition (Chapter 5), suspended organic material (Chapter 6) and mechanisms of particle toxicity in these media (Chapter 7).

Whilst the high concentrations used in this study for ZN1 and ZN2 NPs (1000mg/L) are much greater than would be commonly seen in the environment for these particles (ng/L-μg/L[24]) it is useful to characterize particle behavior at these concentrations when taking into account potential chemical spills and hazards. With the anticipated growth in nanomaterial utilizing industries it is possible that the likelihood of a spillage will increase. While some study has gone into assessing the detection capabilities of DLS and DCS when observing nanomaterials the anticipated effects on actual industry particles are still to be completely constrained, especially when considering information used in ecotoxicology or risk assessment studies. Therefore it is useful to question the validity of the results obtained when measuring NP suspensions.

4.5 References

1. Oberdörster, G. *et al.* Principles for characterizing the potential human health effects from exposure to nanomaterials : elements of a screening strategy. *Part. Fibre Toxicol.* **35,** 1–35 (2005).

2. Hassellöv, M. & Kaegi, R. in *Environ. Hum. Heal. Impacts Nanotechnol.* 211–266 (John Wiley & Sons, Ltd, 2009). doi:10.1002/9781444307504.ch6

3. Johnston, B. D. *et al.* Bioavailability of Nanoscale Metal Oxides TiO2, CeO2, and ZnO to Fish. *Environ. Sci. Technol.* **44,** 1144–1151 (2010).

4. Griffitt, R. J., Luo, J., Gao, J., Bonzongo, J. C. & Barber, D. S. Effects of particle composition and species on toxicity of metallic nanomaterials in aquatic organisms. *Environ. Toxicol. Chem.* **27,** 1972–1978 (2008).

5. El Badawy, A. M. *et al.* Impact of environmental conditions (pH, ionic strength, and electrolyte type) on the surface charge and aggregation of silver nanoparticles suspensions. *Environ. Sci. Technol.* **44,** 1260–6 (2010).

6. Dasari, T. P. & Hwang, H.-M. The effect of humic acids on the cytotoxicity of silver nanoparticles to a natural aquatic bacterial assemblage. *Sci. Total Environ.* **408,** 5817–23 (2010).

7. Gondikas, A. P. *et al.* Cysteine-Induced Modifications of Zero-valent Silver Nanomaterials: Implications for Particle Surface Chemistry, Aggregation, Dissolution, and Silver Speciation. *Environ. Sci. Technol.* **46,** 7037–7045 (2012).

8. Bone, A. J. *et al.* Biotic and abiotic interactions in aquatic microcosms determine fate and toxicity of Ag nanoparticles: part 2-toxicity and Ag speciation. *Environ. Sci. Technol.* **46,** 6925–33 (2012).

9. Pinto, V. V. *et al.* Long time effect on the stability of silver nanoparticles in aqueous medium: Effect of the synthesis and storage conditions. *Colloids Surfaces A Physicochem. Eng. Asp.* **364,** 19–25 (2010).

10. Domingos, R. F. *et al.* Characterizing Manufactured Nanoparticles in the Environment : Multimethod Determination of Particle Sizes. *Environ. Sci. Technol.* **43,** 7277–7284 (2009).

11. PROSPECT. Protocol for Nanoparticle Dispersion. (2010). at <http://www.nanotechia.org/sites/default/files/files/PROSPECT_Dispersion_Protocol.pdf>

12. Anderson, W., Kozak, D., Coleman, V. A., Jämting, Å. K. & Trau, M. A comparative study of submicron particle sizing platforms: Accuracy, precision and resolution analysis of polydisperse particle size distributions. *J. Colloid Interface Sci.* **405,** 322–330 (2013).

13. Malvern Instruments Ltd. Zetasizer Nano Series User Manual. (2004).

14. Tomaszewska, E. *et al.* Detection Limits of DLS and UV-Vis Spectroscopy in Characterization of Polydisperse Nanoparticles Colloids. *J. Nanomater.* **2013,** 1–10 (2013).

15. Tantra, R., Schulze, P. & Quincey, P. Effect of nanoparticle concentration on zeta-potential measurement results and reproducibility. *Particuology* **8,** 279–285 (2010).

16. Medrzycka, K. B. The effect of particle concentration on zeta potential in extremely dilute solutions. *Colloid Polym. Sci.* **269,** 85–90 (1991).

17. Xu, R. Progress in nanoparticles characterization: Sizing and zeta potential measurement. *Particuology* **6,** 112–115 (2008).

18. Kaszuba, M., Corbett, J., Watson, F. M. & Jones, A. High-concentration zeta potential measurements using light-scattering techniques. *Philos. Trans. R. Soc. A* **368,** 4439–4451 (2010).

19. Wang, N., Hsu, C., Zhu, L., Tseng, S. & Hsu, J.-P. Influence of metal oxide nanoparticles concentration on their zeta potential. *J. Colloid Interface Sci.* **407,** 22–8 (2013).

20. Suttiponparnit, K. *et al.* Role of Surface Area, Primary Particle Size, and Crystal Phase on Titanium Dioxide Nanoparticle Dispersion Properties. *Nanoscale Res. Lett.* **6,** 27 (2010).

21. Gallego-Urrea, J. A., Hammes, J., Cornelis, G. & Hassellöv, M. Multimethod 3D characterization of natural plate-like nanoparticles: shape effects on equivalent size measurements. *J. Nanoparticle Res.* **16,** 2383 (2014).

22. Baalousha, M. *et al.* Characterization of cerium oxide nanoparticles-part 1: size measurements. *Environ. Toxicol. Chem.* **31,** 983–93 (2012).

23. EuropeanComission. "Commission recommendation of 18 October 2011 on the definition of nanomaterial."*Off. J. Eur. Union* 38–40 (2011).

24. Fabrega, J., Luoma, S. N., Tyler, C. R., Galloway, T. S. & Lead, J. R. Silver nanoparticles: behaviour and effects in the aquatic environment. *Environ. Int.* **37,** 517–31 (2011).

Chapter 5. Characterisation of Silver Nanoparticles in plain eco-toxicology media

5.1 Introduction

Understanding behaviour of nanomaterials in suspension is both a media and a particle specific issue and as such is a multifaceted problem. Properties of colloidal nanoparticles have been shown to alter over time changing their character and toxic potential[1]. Fate, behavior and therefore potential toxicity of nanomaterials in an environmental setting will be dependent on these properties and as such a comprehensive characterization approach is needed.

5.2 Aims and Objectives

The purpose of this part of the study was to understand the influence of suspension media and particle coating on the stability of NPs. Characterisation of NPs in suspension complements toxicity research.

Changes in nanoparticle properties between different media, and at different concentrations were assessed over a 2 week duration that encompasses most eco-toxicity tests with emphasis on particle diameter, size distribution and aggregation state. The effect of coating was also observed in order to understand if these properties affect particle stability over the length of the experiment.

As with Chapter 4 this study aimed to demonstrate the effectiveness of a multi-method approach for characterizing two types of coated Ag NPs (3-8nm capped with organic paraffin coating, ~50nm stabilized with both PVP and citrate) in algal (MBL Woods Hole) and bacterial (ISO) exposure media and ultrapure water (*UP*H_2O), three media with differing ionic strengths and chemical compositions. The characterization techniques used included:

dynamic light scattering (DLS), nano-tracking analysis (NTA), differential centrifugal sedimentation (DCS) and transmission electron microscopy (TEM). Zeta Potential (ZP) was also analysed using a Malvern Zetasizer.

5.2.1 Materials and Methods

5.2.1.1 Particles

Organic paraffin coated Ag-NPs (AG1) and Ag-NPs stabilised with both citrate and PVP simultaneously (AG2) as described in Chapter 3 were used for these experiments.

5.2.1.2 Preparation of Media

Two environmental eco-toxicity media were used as suspension medium. MBL Woodshole algal media[2] and ISO media 10712[3]. Preparation and composition is described in Chapter 3. Ultrapure water (*UP*H_2O) was used as a control media owing to its lack of ionic species.

5.2.1.3 Preparation of Suspensions

Preparation of NP suspensions was based on PROSPECT: Protocol for Nanoparticle Dispersion[4] and described in Chapter 3.

5.2.1.4 Characterisation

Table 5-1. Summary Table of Characterisation Measurements

Technique	Parameters Measured	Measurement Times	Notes
DLS (Dynamic Light Scattering)	Hydrodynamic diameter (d_H), Particle Size Distribution (PSD) (nm)	0h, 24h, 48h, 72h, 168h, 336h	Used Malvern Zetasizer
ZP (Zeta Potential)	Zeta Potential (mv)	0h, 24h, 48h, 72h, 168h, 336h	Used Malvern Zetasizer. Complimentary pH values taken using electron pH meter
NTA (Nano-Tracking Analysis)	Mode Hydrodynamic diameter (d_H), Particle Size Distribution (PSD)	0h, 24h, 48h, 72h, 168h, 336h	Used Nanosight

	(nm)		
DCS (Differential Centrifugal Sedimentation)	Stokes diameter (d_s), Particle Size Distribution (PSD) (nm)	0h, 24h, 48h, 72h, 168h, 336h	Used CPS Disc Centrifuge
TEM (Transmission Electron Microscopy)	Particle Size, Aspect Ratio, Cluster Size, %age Aggregates	0h, 336h	Used Jeol 2010 TEM. Qualitative visual counterpoint to other techniques

Overview of characterisation measurements is given in Table 5-1. Experimental techniques and measurement protocols are described in greater detail in Chapter 3.

5.3 Results

5.3.1 Dynamic Light Scattering (DLS) and Zeta Potential (ZP)

For AG1 there was no statistically conclusive increase or decrease in the measured d_H over the duration of the experiment in any media (Figure. 5-1). Hydrodynamic diameters were measured in the range of 120-200nm with only 1mg/L in *UP*H_2O giving a much larger d_H around 337-394nm possibly due to stock suspension dilution effects or uncompressed double layer effects discussed in 5.3.1.1. Manufacturer stated primary particle size of 3-8nm was not observed for any suspension in DLS. Measurements in all media at 1mg/L gave larger d_H values than those at 10mg/L, possibly relating to coating effects discussed in 5.3.2.

ZP data (Figure. 5-2) shows particles in all three media were negatively charged for the experimental duration and remained between -27 and -62mV. Slight increases in zeta potential over time were seen in all media at all concentrations except 1mg/L in *UP*H_2O (Figure. 5-2) indicating decreasing stability over the duration of the experiment for those samples. ZPs remained within the required stability threshold to indicate electrostatic stabilisation. pH fluctuated slightly for each sample rising for *UP*H_2O 10mg/L, MBL 1mg/L and decreased for 1mg/L in *UP*H_2O, 10mg/L in MBL and 1-10mg/L in ISO for the duration of the experiment for all media. The pH of 100mg/L AG1 in MBL media remained stable

although this sample was measured using pH paper which is less sensitive to small incremental changes than a pH meter.

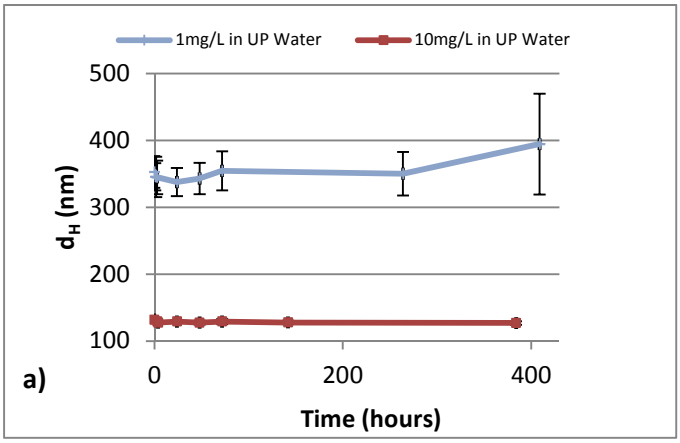

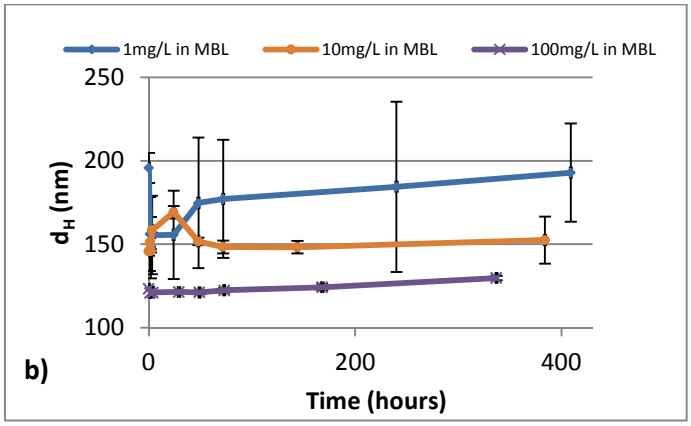

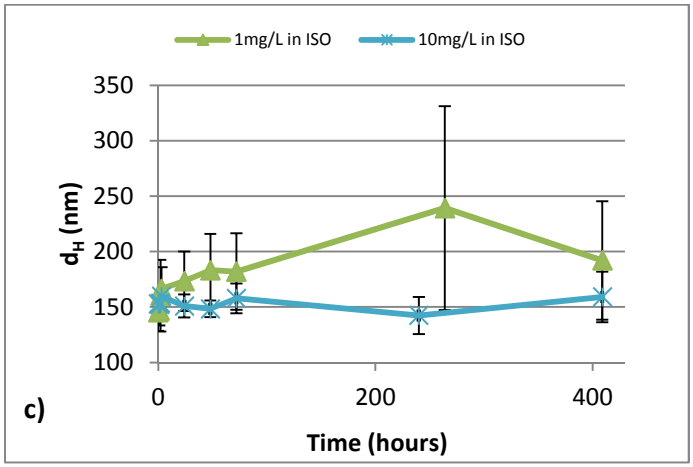

Figure 5-1. AG1 Mean Z-average d_H (nm) vs. time (hours) in: a) *UP*H_2O b) MBL c) ISO

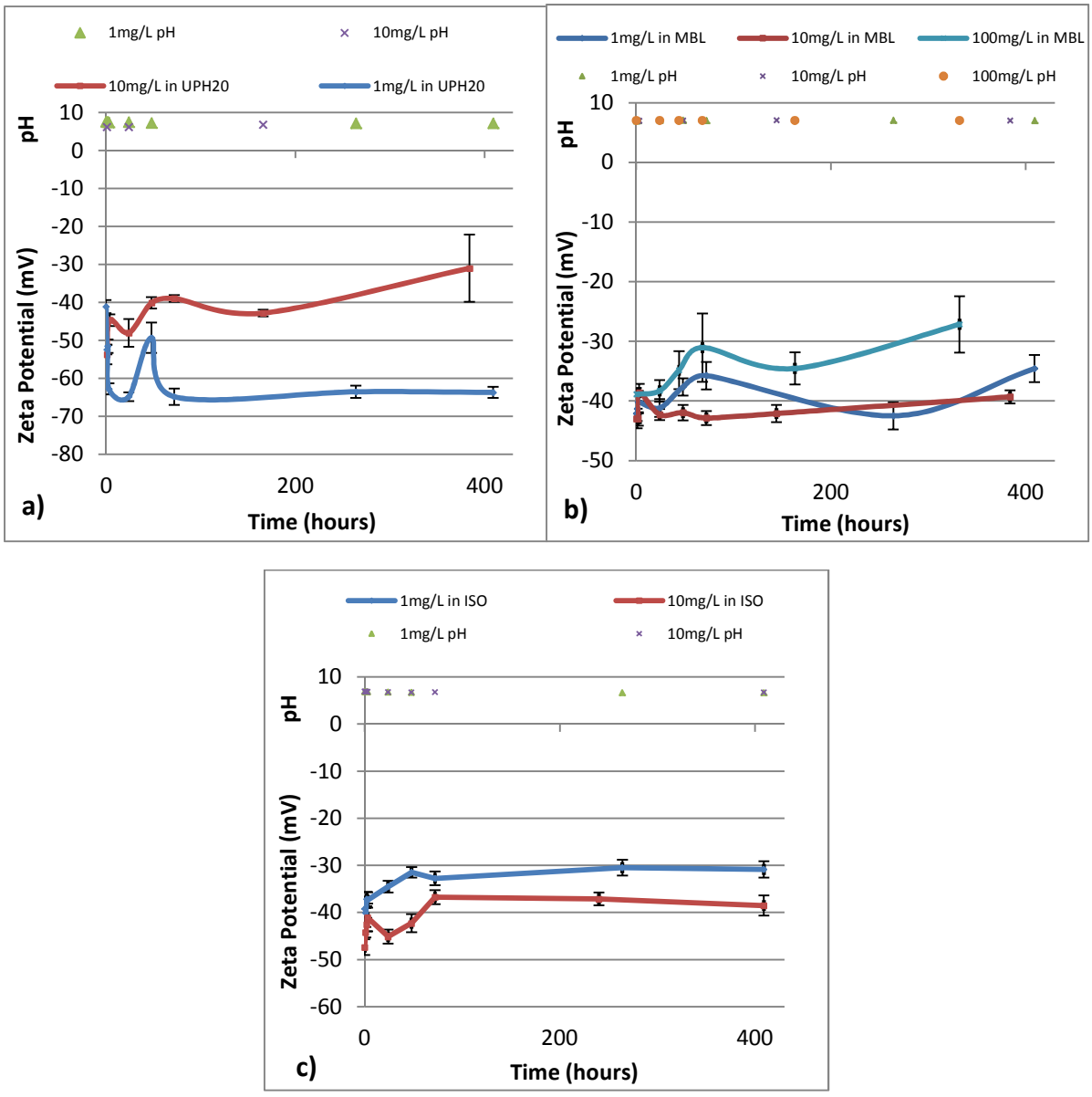

Figure 5-2. AG1 Mean Zeta Potential (mV) and pH values vs. time (hours) in: a) *UP*H_2O b) MBL c) ISO

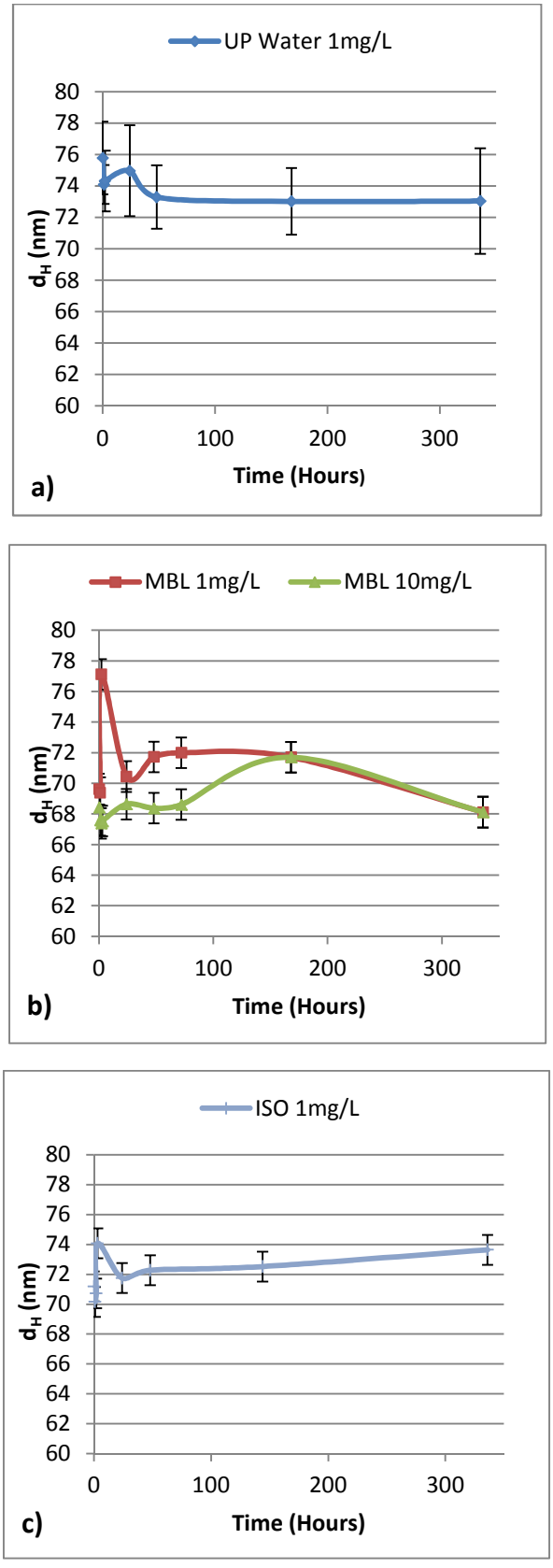

Figure 5-3. AG2 Mean Z-average d_H (nm) vs. time (hours) in: a) *UP*H_2O b) MBL c) ISO

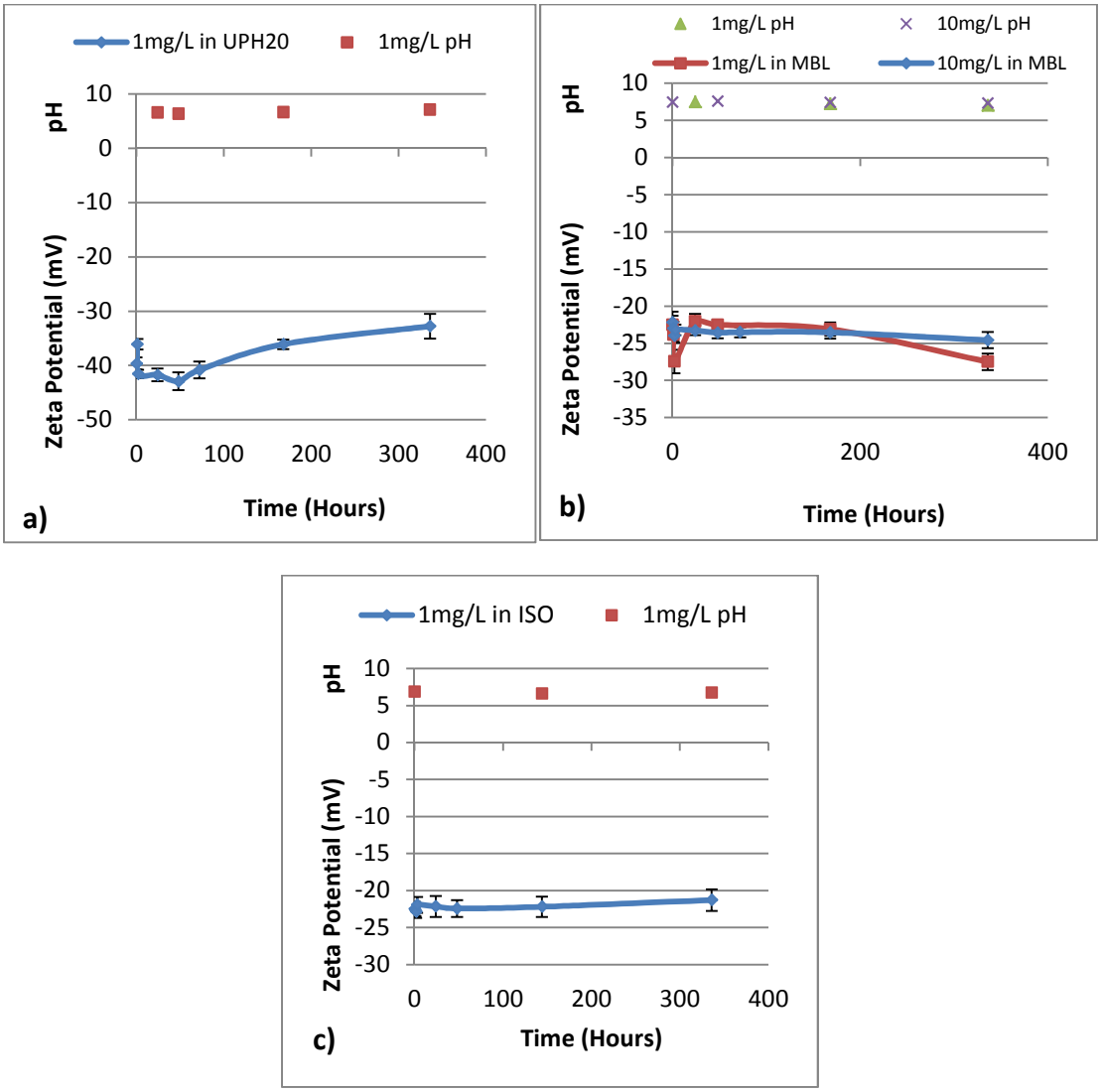

Figure 5-4. AG2 Mean Zeta Potential (mV) and pH values vs. time (hours) in: a) *UP*H_2O b) MBL c) ISO

PVP-stabilised AgNPs (AG2) in all three media gave d_H at roughly 68-78nm (Figure. 5-3) which were stable within 10nm for the duration of the experiment. The reasons for these values are discussed in 5.3.1.1. Little difference was seen in d_H between the 3 media and concentrations in MBL media.

The data also shows NPs were negatively charged in the three media (Figure. 5-4). ZPs for 1mg/L in *UP*H_2O fluctuated between -42mV and -32mV showing an increasing trend, remaining at high electrostatic stability (Figure. 5-4). Particles at 1mg/L in ISO and 1-10mg/L in MBL media were stable between -27mV and -22mV for the duration of the experiment

implying medium electrostatic stability. pH increased slightly in *UP*H_2O and decreased slightly in MBL and ISO media though never changed more than 0.5. These small changes in pH possibly relate to interaction of suspension properties such as media, coating, particles and dissolved ionic species with each other and with constituents in the air. It may also relate to the sensitivity and stabilisation of the pH during each measurement using the pH meter as it took up 10 minutes for readings to stabilise during each measurement.

5.3.2 Nano-Tracking Analysis (NTA)

Table 5-2. NTA data AG1: d_H (nm) and PSD (nm) values which remain unchanged over the duration of the experiment.

Media	Conc. (mg/L)	d_H Range (Mode diameter: nm)	PSD range (nm)
UPH_2O	1mg/L	~23-30nm	~4-120nm
UPH_2O	10mg/L	~30-33nm	~5-120nm
MBL medium	1mg/L	~24-30nm	~3-166nm
MBL medium	10mg/L	~30-35nm	~3-212nm
ISO Testmedium	1mg/L	~22-30nm	~6-110nm
ISO Testmedium	10mg/L	~27-34nm	~4-110nm

NTA shows PSDs and the software calculates the d_H of particles in suspension based upon individual particle counts (method discussed in 3.2.3.). Data is given in d_H range and PSD range which are the ranges in which the mode particle size and the particle size distributions remained over the experimental duration.

AG1 showed an unchanging mode d_H around ~20-35nm and a PSD between 0-120nm for all media and concentrations for the duration of the experiment (Table 5-2).

The manufacturer stated particle size of 3-8nm fell within the measured particle size distribution in all media however the d_H was larger at ~20-35nm. There was no significant difference in the measured PSD or d_H between the two concentrations of 1mg/L and 10mg/L in any media (Table 5-2).

Table 5-3. NTA data AG2: d_H (nm) and PSD (nm) values which remain unchanged over the duration of the experiment.

Media	Conc. (mg/L)	d_H Range (Mode diameter: nm)	PSD range (nm)
UPH_2O	1mg/L	~15-20nm	0-60nm
MBL medium	1mg/L	~20nm	0-60nm
	10mg/L	~20nm	0-60nm
ISO testmedium	1mg/L	~20nm	0-60nm

Mode d_H (~15-20nm) and PSD values (0-60nm) for AG2 NPs for the duration of the experiment showed no differences between the three separate media or between different concentrations in MBL media (Table 5-3). NTA data for AG2 shows that the mode d_H was less than the expected manufacturer stated diameter (50nm) for the duration of the experiment (discussed in 5.3.1.1).

5.3.3 Differential Centrifugal Sedimentation (DCS)

Table 5-4. DCS data: Particle Size Distributions (nm) and d_s (nm) values which remain unchanged over the duration of the experiment.

Particle	Media	Conc (mg/L)	PSD (nm)	d_s (Mode diameter: nm)
AG1	*UP*H_2O	1	~10-90	~10-20 (variable)
	UPH_2O	10	~6-70	~8-15 (variable)
	MBL	1	~10-90	~10-25 (variable)
	MBL	10	~10-90	~15
	ISO	1	~10-90	~15-30 (variable)
	ISO	10	~10-90	~15
AG2	*UP*H_2O	1	~20-100	~45
	MBL	1	~20-100	~45
	MBL	10	~20-120	~45
	ISO	1	~20-100	~45

AG1 suspensions showed the same PSD (6-90nm) and roughly the same d_s (~10-25nm) for the duration of the experiment (although *UP*H_2O had a slightly smaller PSD at ~6-70nm) in all media at both concentrations (Table 5-4).

AG2 particles also showed a constant PSD (~20-120nm) and peak (~45nm) in all media (and both concentrations in MBL media) (Table 5-4).

5.3.4 Transmission Electron Microscopy (TEM)

5.3.4.1 AG1 Particles

Table 5-5 shows particle size data from the analysis of TEM images (Fig 5-6ab, 5-7ab, 5-8ab) of AG1 in *UP*H_2O, MBL and ISO media at 0h and 2 weeks (336h). All the images show primary particles (d_{pp} ~8-9nm) as well as two types of clusters: loosely associated clusters (agglomerates) and tightly bound spherical clusters (aggregates).

The primary particle diameter (d_{pp}) remained around 8-9nm in all the media at both measurement times however a decrease was seen in *UP*H_2O while an increase was noted in MBL and ISO media from 0h to 336h. Similar trends were noted for the cluster diameter (d_{AGG}). The changes in both properties cannot be stated conclusively as the standard deviation for the particles is high and allows for overlap in diameters. The size range in d_{AGG} increased over time in both MBL and ISO but not in *UP*H_2O indicating the presence of much larger aggregates in the more ionic media.

The average aspect ratio (S_{pp}) of the primary particles stayed comparable over the experiment duration at ~1.2 in all media. This indicated a shape that was slightly elongated rather than purely spherical (S=1) and did not change by a significant amount. However, the S_{pp} range in MBL and ISO increased indicating that more particles were present with a longer aspect ratio and hence more elongated morphology after two weeks, but not enough

to affect the average. A decrease was noted in *UP*H_2O for the same property. The average cluster aspect ratio (S_{AGG}) decreased over two weeks in MBL and ISO but increased in *UP*H_2O (although in all media the range in aspect ratios increased showing greater variety in morphologies). The percentage of clusters that were tightly bound (aggregates) as opposed to loosely bound (agglomerates) decreased over the experiment duration in *UP*H_2O but increased in MBL and ISO. This indicated that clusters may have been becoming more tightly bound in the latter media but less so in the former. The changes in particles as measured by TEM are discussed in 5.3.8.

Table 5-5. AG1 in *UP*H_2O, MBL and ISO: TEM data. Primary particle (d_{pp}) and cluster diameters (d_{AGG}), size ranges, aspect ratios of primary particles (S_{pp}) and clusters (S_{AGG}) and percentage of clusters in aggregate form (tightly bound and fused together).

Media	Time (h)	Conc. (mg/L)	d_{pp} (nm/no particles)	d_{pp} range (nm)	S_{PP} (range)	d_{AGG} (nm/no particles)	d_{AGG} range (nm)	S_{AGG} (range)	% Aggregates (no particles)
UPH_2O	0	10	9.55±3.66/ 102	4.9-18.16	1.24±0.41 (1.00-2.24)	44.59±19.71 /38	15.92-98.46	1.21±0.20 (1.00-1.90)	57.89% (38)
	336	10	9.01±2.85/ 105	4.23-19.45	1.22±0.28 (1.00-1.72)	40.27±20.70 /33	15.81-97.62	1.22±0.24 (1.00-2.21)	42.42% (33)
MBL	0	10	8.43±3.71/ 102	2.43-23.4	1.14±0.26 (1.00-1.46)	51.22±26.24 /17	22.86-96.08	1.32±0.25 (1.01-1.69)	58.8% (17)
	336	10	9.62±4.95/ 110	3.45-33.74	1.25±0.23 (1.00-2.08)	120.45±85.20/17	32.35-313.69	1.20±0.24 (1.00-1.90)	82.35% (17)
ISO	0	10	7.91±3.40/ 104	2.79-28.18	1.18±0.35 (1.00-1.69)	42.74±19.71 /27	20.34-95.89	1.54±0.77 (1.04-5.00)	37.04% (27)
	336	10	9.04±3.70/ 131	2.47-18.36	1.26±0.40 (1.00-2.40)	69.61±47.99 /35	17.82-225.72	1.52±0.83 (1.014-5.57)	45.7% (35)

The stock suspension of 1000mg/L AG1 showed 5-10nm primary particles, loosely associated larger ~30-40nm agglomerates and occasional tightly bound circular aggregates of ~50-100nm (Fig. 5-8)

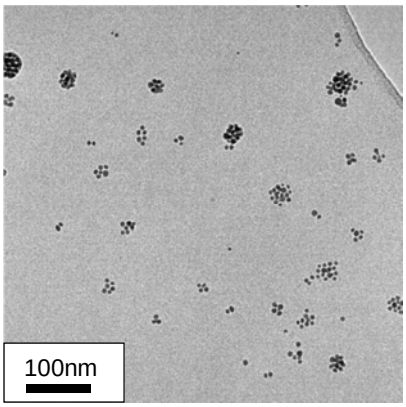

Figure 5-5. TEM image of 1000mg/L stock suspension of AG1

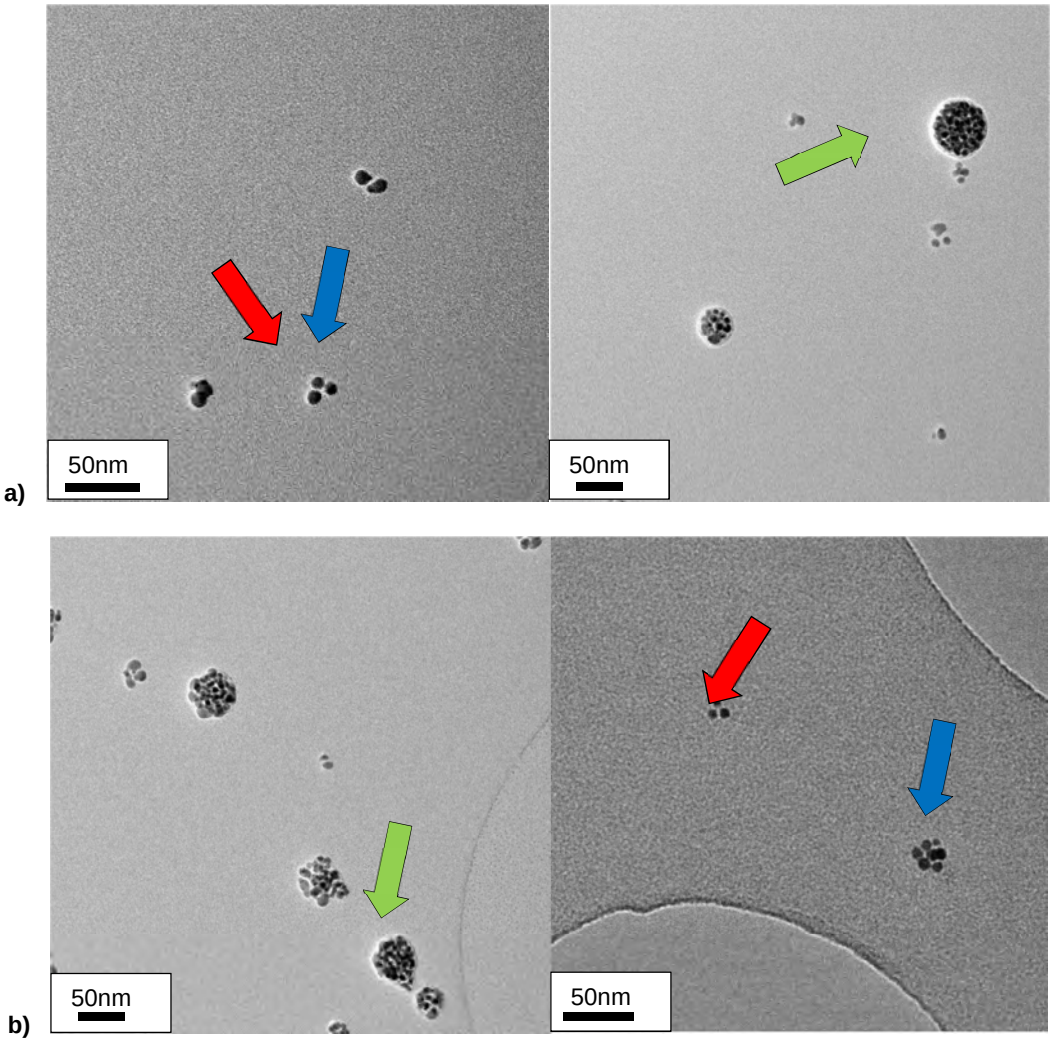

Figure 5-6. TEM image of 10mg/L AG1 in *UP*H_2O: a) 0 h (scale bars 50nm & 10nm) b) 2 weeks (scale bars 50nm and 50nm). Arrows indicate primary particles (red), loose clusters (agglomerates) (blue) and tight clusters (aggregates) (green)

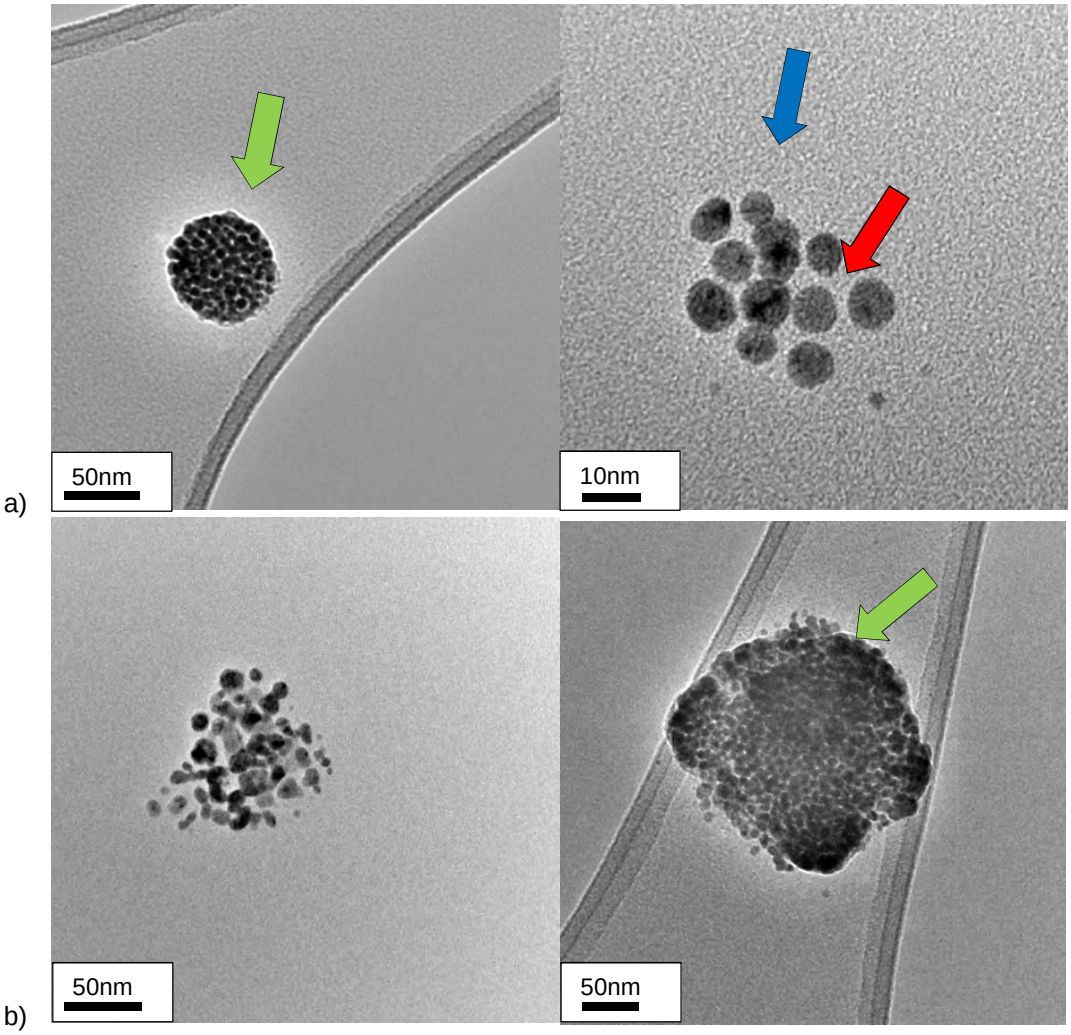

Figure 5-7. TEM image of 10mg/L AG1 in MBL Media: a) 0 h (scale bars 50nm & 10nm) b) 2 weeks (scale bars 50nm and 50nm). Arrows indicate primary particles (red), loose clusters (agglomerates) (blue) and tight clusters (aggregates) (green)

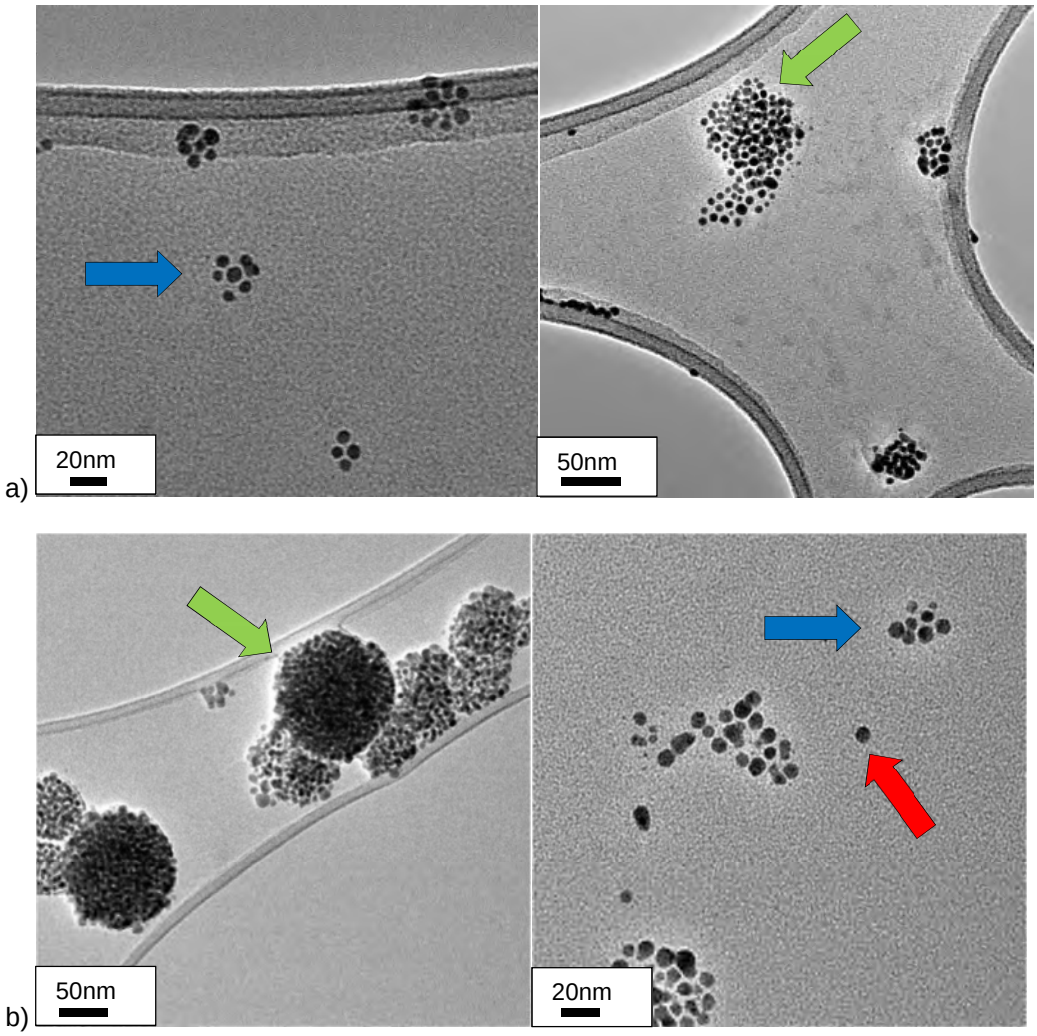

Figure 5-8. TEM image of 10mg/L AG1 in ISO media: a) 0h (scale bars 20nm & 50nm) b) 2 weeks (50nm & 50nm). Arrows indicate primary particles (red), loose clusters (agglomerates) (blue) and tight clusters (aggregates) (green).

5.3.4.2 AG2 Particles

Table 5-6 shows particle size data from the analysis of TEM images (Fig 5-9ab, 5-10ab, 5-11ab) of AG2 in *UP*H_2O, MBL and ISO media at 0h and 2 weeks (336h). NPs were present mainly as primary particles of ~50nm and any clusters were loosely associated agglomerates of primary particles (Figures 5-9, 5-10, 5-11). The images show that the majority of the particles had a thin coating present on the outside of the primary particles and clusters which was probably PVP. The d_{pp} for AG2 in all three media at both times was

always between 43-57nm and no significant difference could be seen after 336h for any of the samples. Similarly the range of primary particle sizes, the aspect ratio (S_{pp}) and range in aspect ratios showed similar behaviour with little obvious difference between 0h and 336h and between the three media. There were very few clusters in most of the samples and they were all loosely associated i.e. agglomerates not aggregates. The size and aspect ratio were comparable in all the treatments.

Table 5-6. AG2 in *UP*H_2O MBL and ISO: TEM data. Primary particle (d_{pp}) and cluster diameters (d_{AGG}), size ranges, aspect ratios of primary particles (S_{pp}) and clusters (S_{AGG}) and percentage of clusters in aggregate form (tightly bound and fused together).

Media	Time (h)	Conc. (mg/L)	d_{pp} (nm/no particles	d_{pp} range (nm)	S_{PP} (range)	d_{AGG} (nm/no particles)	d_{AGG} range (nm)	S_{AGG} (range)	%Aggregates (no particles)
UPH_2O	0	10	52.88±16.72/42	26.83-104.96	1.23±0.14 (1.03-1.54)	77.62±0/1	77.62-77.62	1.85±0 (1.85-1.85)	0% (1)
	336	10	57.06±15.79/34	34.64-98.34	1.19±0.12 (1.02-1.45)	86.48±0/1	86.48-86.48	1.48±0 (1.48-1.48)	0% (1)
MBL	0	10	43.20±17.07/55	9.56-104.73	1.29±0.21 (1.01-1.87)	102.77±50.49/8	56.16-195.39	1.64±0.43 (1.06-2.22)	0% (8)
	336	10	46.99±17.65/45	19.13-86.37	1.28±0.20 (1.00-2.08)	71.03±16.51/5	52.13-90.55	1.81±0.52 (1.29-2.58)	0% (5)
ISO	0	10	51.38±18.52/76	12.88-105.15	1.24±0.18 (1.01-2.23)	101.43±31.79/10	73.69-162.46	2.14±0.39 (1.69-2.90)	0% (10)
	336	10	49.59±11.87/52	26.60-84.23	1.22±0.14 (1.01-1.63)	0/0	0	0 (0)	0% (0)

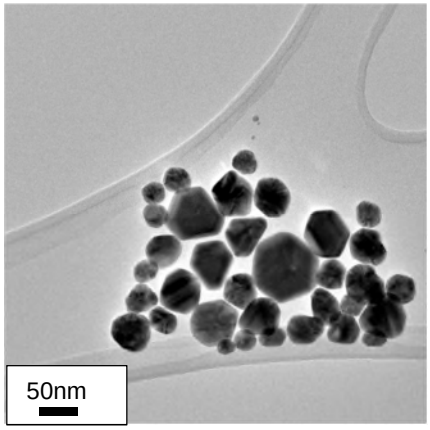

Figure 5-9. 1000mg/L AG2: PVP stabilised Ag NP stock suspension

The stock suspension of 1000mg/L AG2 NPs showed 30-50nm spherical and hexagonal particles (Fig. 5-9).

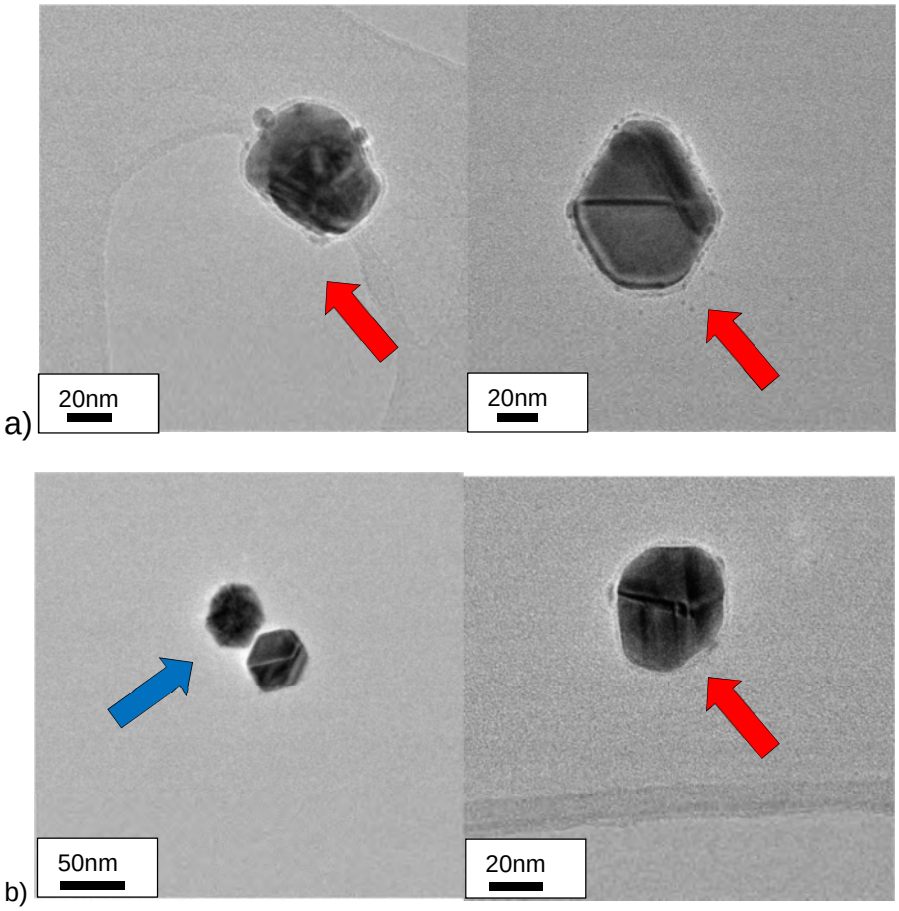

Figure 5-10. TEM image of 10mg/L AG2 in *UP*H_2O: a) 0h (scale bars 20nm & 50nm) b) 2 weeks (50nm & 50nm). Arrows indicate primary particles (red), loose clusters (agglomerates) (blue) and tight clusters (aggregates) (green).

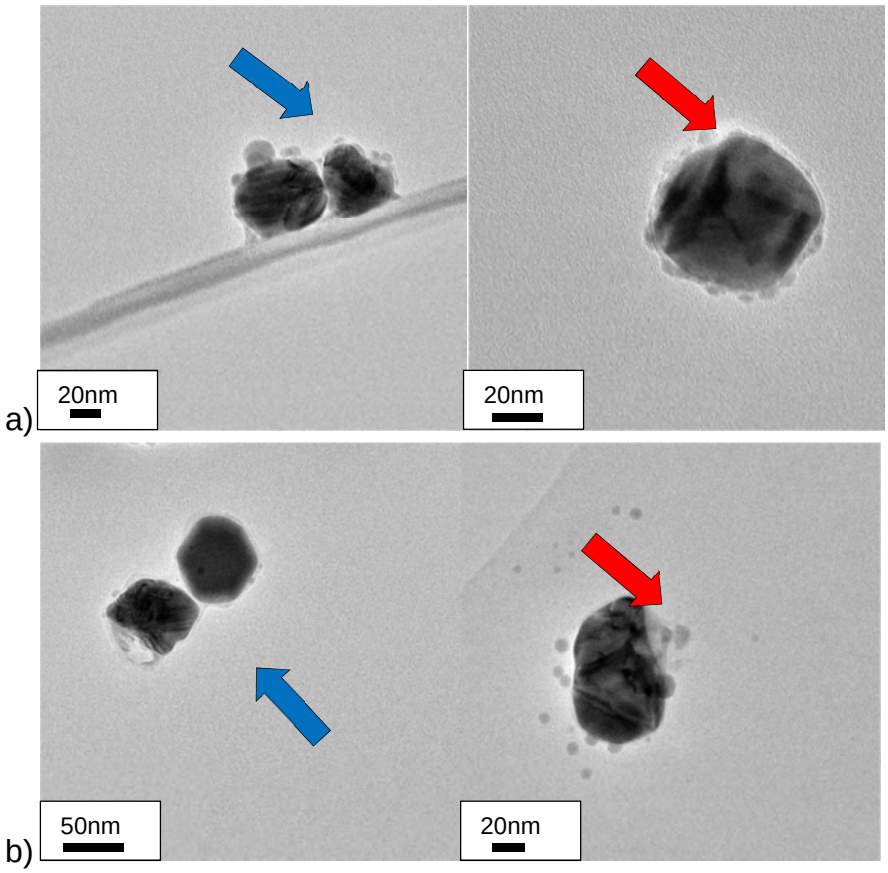

Figure 5-11. TEM image of 10mg/L AG2 in MBL media: a) 0h (scale bars 20nm & 50nm) b) 2 weeks (50nm & 50nm). Arrows indicate primary particles (red), loose clusters (agglomerates) (blue) and tight clusters (aggregates) (green).

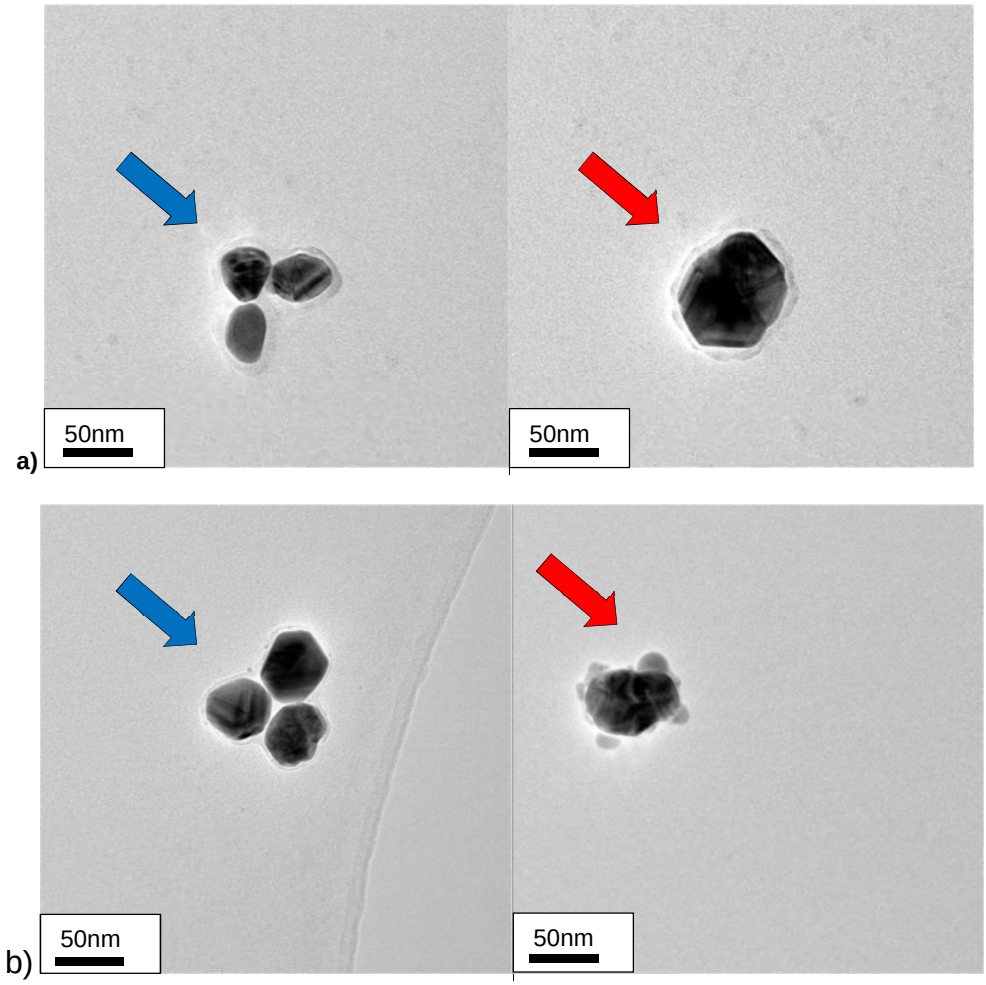

Figure 5-12. TEM image of 10mg/L AG2 in ISO media: a) 0h (scale bars 20nm & 50nm) b) 2 weeks (50nm & 50nm). Arrows indicate primary particles (red), loose clusters (agglomerates) (blue) and tight clusters (aggregates) (green).

5.4 Discussion

5.4.1 Comparison of Techniques

A number of different characterisation techniques commonly used in nanoparticle stability tests[5] were used to investigate the stability of both uncoated and coated silver NPs. These utilise different theoretical bases to look at size of particles in a suspension as described in Chapter 3. The results obtained from each technique give different size/size distribution values. Indeed, no single particle sizing technique proved definitive in understanding the

behaviour of either nanoparticle suspension, a conclusion also stated by Domingos et al.[6] who compared 6 different sizing techniques. Suspensions would have to be completely monodisperse to get perfectly agreeable size values which is not the case for samples measured in this study[6].

5.4.1.1 Light-scattering methods (DLS and NTA)

Different techniques each have their own specific limitations and advantages which need to be taken into consideration when comparing the data. These techniques are described in Chapter 3. DLS and NTA can overestimate particle size in polydisperse samples due to intensity weighted particle scattering and masking effects respectively[5]. Here, the z-average hydrodynamic particle diameters observed in DLS for all concentrations of AG1 in all three media (Figure. 5-1) are larger than the expected 3-8nm and are likely skewed due to larger clusters of primary particles seen in the corresponding TEM images (Figures 5-5, 5.6, 5-7, 5-9). Corresponding NTA values are also likely affected by these clusters however the smaller diameters (30-45nm; Table 5-2) are closer to TEM observed sizes due to theoretical differences in the techniques mentioned above. Differing DLS d_H values in *UP*H_2O to those in ionic media (Figure. 5-1) are possibly related to small numbers of large clusters in suspension at low concentration skewing size values upwards. In ultrapure water there are less charged ionic species and hence the electronic double layer around particles is likely to be less compressed and larger sizes could be picked up by this technique for this media compared to the other media. However, the larger sizes were not seen in the 10mg/L suspension which could indicate that the coating is having a prominent effect (discussed in 5.3.3. and 5.3.5).

AG2 NPs DLS results in all three media may also be affected by the larger particles as initial Z-average sizes are slightly larger than the expected 30-50nm particles seen in TEM (Table

5-6, Figures 5-9 to 5-12). This could relate to the PVP coating on the surface of the NPs which will likely increase the d_H of the particle. AG2 NPs measured by NTA show a lower d_H (~20-30nm; Table 5-3) than that obtained by DLS. It is also lower than the manufacturer stated primary particle size of ~50nm which is seen in TEM (Figure. 5-9). This is unexpected as the diameter measured by NTA should not be less than that of the particle core assuming that the media parameters are input correctly and because the particle coatings should in theory increase the diameter. Closer inspection of PSD data in DLS (intensity and volume) also indicates the presence of a peak around 20nm (Figure. 5-13) which dominates the sample volume. TEM and DCS (Figure. 5-9, Table 5-4) do not pick up this 20nm peak. It may be that the PVP coating on the particles is 'washed off' when the stock suspension is exposed to the more dilute eco-toxicity media forming smaller 15-20nm PVP micelles. If this is the case, there is still a good coverage of PVP remaining on the silver cores NPs as they continue to remain stable over the duration of the experiment.

5.4.1.2 DCS

Differential centrifugal sedimentation or DCS analysis does not suffer from the same biases as the light scattering techniques as size is calculated from the density of the particles[7]. It therefore provides a good analytical counterpoint when assessing d_H[8]. The main limitation for DCS is based upon its dependence on the particle density input by the user[5] which becomes an issue when particles are coated in a material that alters their overall density. Other studies have shown that the hydrodynamic diameter of silver and gold core nanoparticles when coated by both polymers and biological proteins was underestimated by DCS for this very reason[8–10].

a)

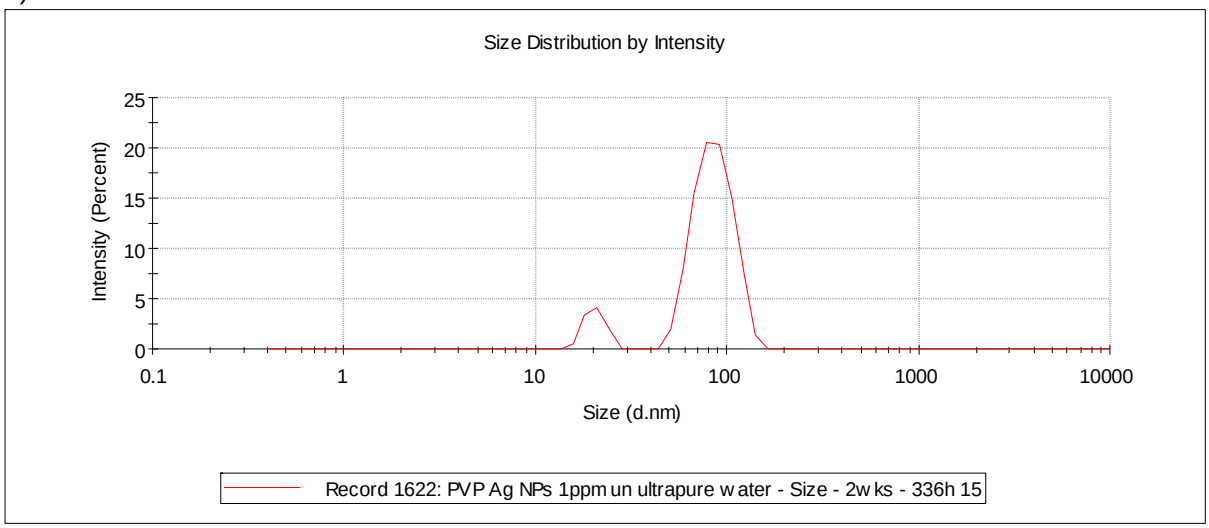

b)

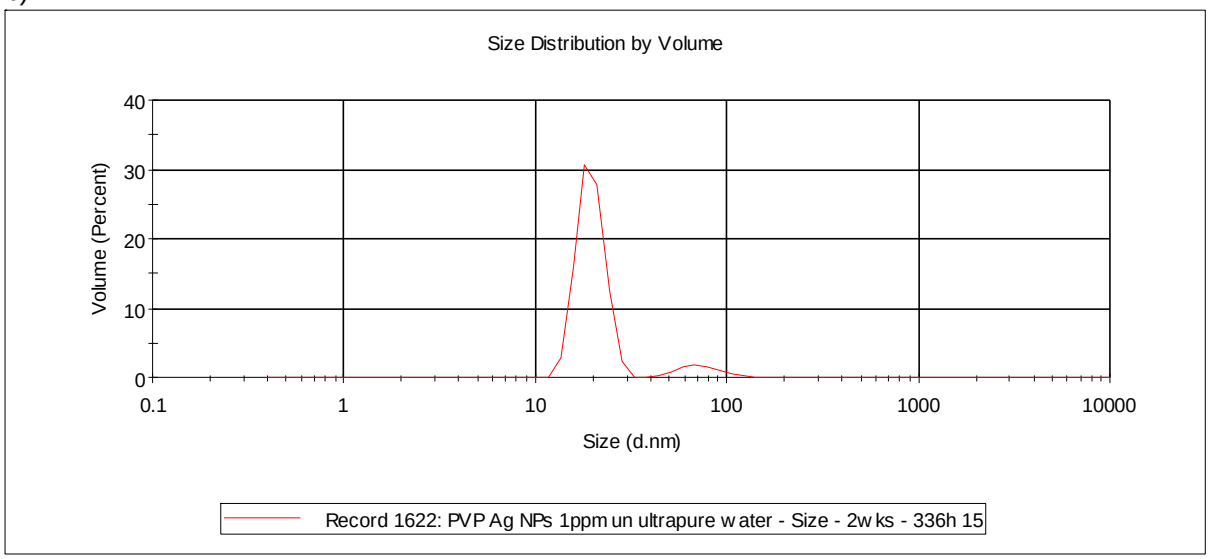

Figure 5-13. PVP stabilised Ag NP stock suspension (AG2) measured in DLS a) PSD intensity weighted b) PSD volume weighted

This does not seem to be the case in this study as the AG2 NPs in all three media are very similar to those seen by TEM (Table 5-3) when using a density for pure silver (10.5g/ml). This implies that although the particles are double stabilised with citrate and PVP, the coating is not thick enough to drastically affect the density of the particles. The coating of the AG1 particles also seem to be having a negligible effect on the particle density as the distributions and peak size seen by all three media (Table 5-3) do seem to correspond to values obtained by TEM (5-50nm Figures. 5-5 to 5-8). Any changes in size detection due to

density are drowned out by actual variations in particle size. The technique is also likely to show greater resolution for bigger particles such as AG2 as the smallest particles are liable to be affected by Brownian motion. This causes particles to diffuse and therefore the time at which particles of similar size reach the detector to vary slightly within a distribution causing peak broadening[7]

5.4.1.3 TEM

TEM, while excellent as a visual counterpoint to other sizing techniques is subject to preparation issues due to requirement for dry or 'fixed' samples. This means samples are subject to evaporative meniscus effects which cause the particles to be dragged together[6]. This cannot be discounted as the AG1 are present in clusters on the TEM grids and as such the diameter (d_{AGG}) and aspect ratio (S_{AGG}) are likely to have been affected. AG1 TEM data show primary particles at about ~8-9nm diameter (confirming the manufacturer stated particle size was reasonably accurate) as well as large circular clusters which are likely the reason for overestimated hydrodynamic diameters in the other techniques (Figures. 5-5 to 5-8). TEM images of the stock suspension of the AG2 particles (Figure. 5-9) show particles around 40-60nm confirming the manufacturer stated particle size of 50nm. Some particles are present in loosely associated agglomerates however there are few of these explaining the comparable results seen in the other characterisation techniques.

It should also be noted that analysis of TEM images is time-consuming and while 50-100 particles were chosen as the baseline minimum number of particles for measurement this value is still low and stating any conclusive trends is still difficult.

5.4.2 Influence of nanoparticle concentration on detection

No differences were seen in NTA or DCS when comparing the different concentrations of AG1 and AG2 particles. Both showed consistent PSDs and diameters ($d_{H,}$ d_s) values. DLS results for AG2 showed no difference in diameter between 1 and 10mg/L particles in MBL (Figure. 5-3) however AG1 show a larger particle size for 1mg/L than higher concentrations (Figure. 5-1). As this effect is not seen for the AG2 particles at 1mg/L and in the other techniques, especially NTA which has a greater resolution at lower concentrations[6], it is likely due to a combination of different factors. It is possible that upon mixing of the stock suspension and the media that instantaneous equilibration of the particles, coating and media occurs. At lower concentrations more coating is stripped off the particles (see 5.3.4.) and more agglomeration/aggregation of the particles occurs resulting in the presence of larger clusters and hence greater d_H measured by DLS. NTA would not have detected this due to its different theoretical basis.

Concentration is important to consider when characterising particles as can be seen from the results obtained in this study. The particle concentrations used in this study (1-100mg/L) were higher when considering predicted concentrations of silver (ionic) in the aquatic environment are around 0.01-0.08µg/L[11,12]. They were adopted so that they were within the optimum range for detection in all the characterisation techniques (Technique limitations described in Chapter 3). Nevertheless high concentrations could apply to situations in which an environmental chemical spill occurs.

5.4.3 Influence of nanoparticle coating on stability and detection

Both particles suspensions in all three media remained stable over the length of the experiment. This is likely due to their stabilising coatings. Engineered nanoparticles (or NP

aggregates) are normally stabilised against aggregation to maintain their desired nano-specific properties by adsorption/covalent attachment of organic or inorganic compounds[13]. Types of suspension include electrostatic (purely ionic) stabilisation that utilises the electric double layer (EDL) theory and steric stabilisation whereby a coating provides physical stabilisation (Figure 5-14a,b). These can be combined to create electro-steric stabilisation either by doubly stabilising the NP or by combining the two effects in one coating (Figure 5-14c).

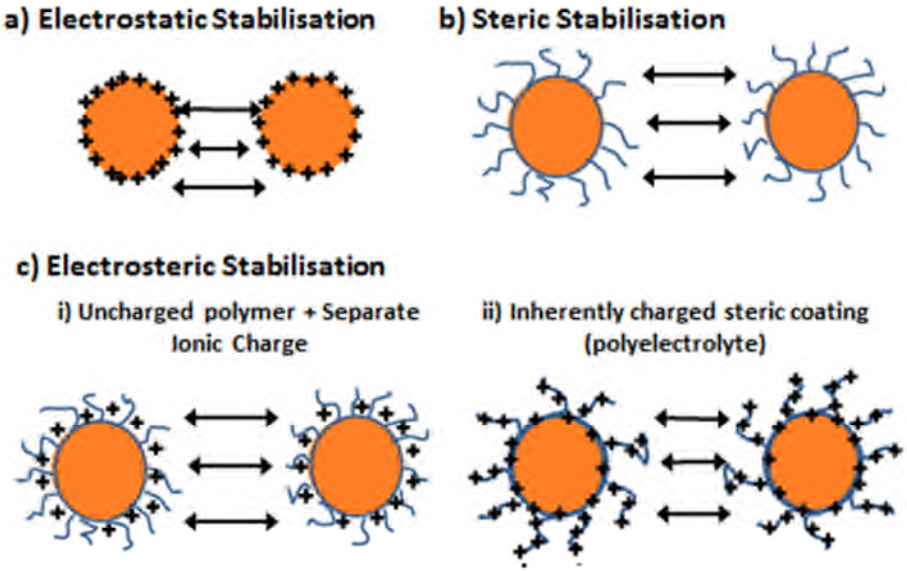

Figure 5-14. Different forms of NP stabilisation in suspension. a) Electrostatic (ionic stabilisation). b) Steric stabilisation. c) Electrosteric Stabilisation (i) separate ionic and steric stabilisation (i.e. two seperate coatings) (ii) charged (polyelectrolyte[14]) coating - combined ionic and steric stabilisation (i.e. one coating). Note charged component can be positive (+) or negative (-)

The NPs in this study are both electro-sterically stabilised. AG2 NPs are coated by non-ionic Polyvinylpyrrolidone (PVP) and stabilised in ionic citrate (Figure 5-14c (i)). The latter two are common coatings in industry, they provide a steric and an electrostatic component to stabilisation[9,15,16]. Steric polymers are known to be a highly effective particle stabilisers[13,17], more so than purely electrostatic stabilisers like citrate. This is likely in part due to the

strength of interaction of the coating with the particles in suspension. Citrate is known to be weakly bound to the surface of nanoparticles[13] and citrate has been observed to desorb from the surface of suspended nanoparticles upon dilution of the stock suspension[18].

AG1 particles came suspended in organic paraffin stabiliser at 1000mg/L. AG1 were seen to exhibit a charge in all media however paraffin is non-polar and would unlikely be charged[19]. Therefore any charge coming from the NPs must have come from the silver NP core through the coating. This could indicate that the paraffin coating was thin or not evenly spread around the Ag core (possibly due to concentration effects whereby the coating desorbs upon creation of AG1 suspensions in diluting media). The stability of the NPs in ionic media for the entire experimental duration indicates that the coating also likely had a steric component to its stability and hence AG1 were also electro-sterically stabilised.

TEM data for AG1 after 2 weeks in suspension in both MBL and ISO media shows possible changes in morphology due to dissolution of individual particles and clusters (Table 5-5) indicating that the organic paraffin type coating may be disintegrating allowing individual particles to interact, though not enough to cause full destabilisation.

Light scattering data for AG2 shows a peak present at ~20nm, smaller than the 50nm core diameter of the particles (Table 5-3, Figure. 5-13). The peak could be due to desorbed citrate or free/weakly bound PVP micelles in suspension. Fatisson et al.[20] found peaks in fluorescence correlation microscopy data which could be attributed to albumin (another common protein stabiliser) present in NP suspensions giving credence to this theory. This ‘desorbed PVP’ peak was present throughout the experiment at all measurement times indicating that it formed upon sample creation and was stable throughout. TEM images for AG2 particles in all media indicated that these particles were present mainly as primary particles and a coating could be seen around the outside of individual particles which is likely the PVP (Figures 5-9 to 5-12).

5.4.4 Influence of nanoparticle concentration on stability

Stability was unaffected by differences in concentration with both particles in all media showing unchanging values in DLS, NTA and DCS for the duration of the experiment. While for uncoated nanoparticles it would be expected that greater concentrations of particles in suspension would result in greater aggregation due to the higher probability of collisions, it has been noted for coated nanoparticle suspensions that higher concentrations result in stronger stability[21]. This relates to the fact that at greater dilutions (lower suspension concentrations) the new equilibrium between the particle stock suspension and the surrounding media results in stripping of the coating off the surface of the particles hence less of a stabilising effect[21]. The concentrations observed in this study are likely still high enough to prevent too much coating from being 'washed' off and therefore the particles remain stable.

5.4.5 Influence of coatings on zeta potential

As ZP is inextricably tied to particle stability it is affected by many of the same properties including pH, ionic strength of the media and particle coatings[22,23]. The ZP plot for AG1 at all concentrations in all three media shows that ZP values never go above the -30mV high stability threshold (-30mV<0>-30mV) (Figure. 5-2) agreeing with the stable d_H values and PSDs seen in the other characterisation methods. AG1 give a strong negative stabilising charge from the silver core which is allowed through the neutral organic paraffin coating.

For AG2 particles the negative ZPs in all media (Figure. 5-4) are likely caused by depronation of the carboxylic groups on the citrate coating which occurs at ~pH7 providing a negative charge[16]. Charge from the silver core is likely being blocked by the tightly bound non-ionic PVP coating. Charge may also be emanating from defects in the PVP coating or

additional charged surface adsorbed materials on the particles[16]. Differences between the ZP of AG2 in MBL/ISO (~-20mV) and in *UP*H_2O (-43-33mV) are likely due to ionic species in the surrounding media as discussed below. ZP of -20mV are in the moderately stable realm and therefore aggregation would be expected to occur however as no agglomeration/aggregation was observed in any characterisation techniques (with the exception of TEM which could relate to sample preparation artefacts) over the duration of the experiment this likely pertains to the steric stabilisation effect of the PVP.

5.4.6 Influence of pH on stability

The pH of either particle in suspension showed no consistent trend relating to concentration or media and all were within a reasonably neutral zone of 6.34-7.57 for the majority of the experiment (Figure 5-2, 5-4). It has been noted that nanoparticle suspensions have greater stability at higher pH due to more OH^- ions and therefore greater electrostatic repulsion[24]. The stability of particles in this study is seemingly unaffected by slight changes in pH, likely due to their coatings providing a greater electrostatic stabilisation than destabilisation from the pH (AG1) or from uncharged steric stabilisation (AG1, AG2). Note: the *UP*H_2O was seen to be 6.14-7.12 for the experiment duration (Figure 5-2, 5-4) which implies that either little carbon dioxide (CO_2) from the ambient laboratory air was dissolving into the suspensions or that the particles themselves had an alkaline effect as CO_2 has been shown to result in a lower pH of 5.5[25].

5.4.7 Influence of media ionic strength on stability

Three different media were used to create nanoparticle suspensions. Ultrapure water was used as a control due to its low concentration of ions and un-reactivity. Woodshole MBL

media and standard ISO media are both used in algae and bacterial eco-toxicity studies[2,3] and in this study have ionic strengths of 5.53mM and 10.54mM respectively.

Media of higher ionic strength would be expected to cause aggregation/agglomeration of the nanoparticles due to charge balance effects. Both Romer et al.[26] and Tejamaya et al.[15] have shown that certain iterations of standard *D.magna* OECD media caused aggregation of coated-silver NPs at high concentrations. Citrate capped silver nanoparticles were seen to aggregate extensively within 24 hours when suspended in 8.84μM OECD daphnia media, a much lower ionic strength than used in this study[27]. DLVO theory states that negatively charged particles in suspension are held in suspension when the repulsive forces generated by charged surface groups are greater than attractive van der Waals forces[13]. Media with high counter-ionic strength will compress the electric double layer (EDL) on the surface of the particle decreasing repulsive forces and causing particles to aggregate[28]. This likely explains the higher negative zeta potential of both silver nanoparticles in *UP*H_2O than in MBL and ISO media as the former has less ionic species and therefore less compressed EDL and greater negative charge (Figure. 5-2 and Figure. 5-4)[20]. Electrostatically stabilised Ag NPs have been shown to remain stable and unagglomerated in de-ionised water for weeks[29]. Indeed, in this study all nanoparticles in *UP*H_2O show constant size for the duration of the experiment. However, little aggregation is occurring in the ionic media either, likely due to the coatings on both nanoparticles which override the double layer compression.

As stated above PVP is a steric coating and is unlikely affected by changes in ionic strength[30]. The organic paraffin coating on the AG1 also has a steric stabilising effect as these particles were not destabilised. Any differences in size and PSD between 10.54mM ISO media and 5.53mM MBL media for both silver NP species are too subtle to be picked up using any of the particle characterisation techniques in this study.

5.4.8 Influence of media composition on stability

Chemical make-up of the media could be expected to have an effect on the behaviour of particles. Mono-valent and di-valent ionic species would be expected to impact the ionic strength of a media differently. Studies have shown that divalent electrolytes are much more likely to cause destabilisation by aggregation when compared to monovalent electrolytes[16,31]. The two media investigated in this study have differing chemical makeups with MBL having a more complex mix of salts than ISO but at much lower concentrations giving a lower ionic strength. One major difference between the two media is the presence of chloride in the MBL media but not ISO. Chloride is known to have a strong affinity for silver with complexes of AgCl known to form in the presence of silver ions in solution as seen in equations (i) and (ii)[32].

Ratios of chloride concentration to silver concentration (Cl/Ag) have been shown to be a determinant factor for dissolution to occur[9,32] and even show greater importance to dissolution than ionic strength[33]. Silver ions produced by oxidation of the silver surface and subsequent dissolution will form complexes with ionic species in the medium of which chloride is prevalent (sulphide ions would also complex with the silver however these were not present in either medium). Soluble silver ions and soluble chloride ions would complex to form insoluble silver chloride salts which are initially nano-sized (Eqn (i)). Greater levels of chloride in relation to silver (high Cl/Ag ratios) would convert insoluble solid silver chloride into soluble silver-chloride ions ($AgCl_x^{(x-1)}$) such as $AgCl_2^-$.(Eqn (ii)).

(i) $Ag^+_{(aq)} + Cl^-_{(aq)} \rightarrow AgCl_{(s)}$

(ii) $AgCl_{(s)} + Cl^-_{(aq)} \rightarrow AgCl_2^-{}_{(aq)}$

While dissolution was not quantified in this study, TEM images of AG1 after 2 weeks in both chloride containing MBL media and non-chloride ISO media show changes in morphology and distribution of particles that point to the possibility of dissolution occurring (Table 5-5).

Work in Chapter 7 of this thesis indicates that AG1 particles are soluble to some extent therefore it is probable that dissolution is occurring.

It is likely that the concentration of chloride in MBL is so low that dissolution behaviour of the particles in MBL media doesn't vary much from the ISO medium over the experiment duration. It was not possible to check if morphological changes in solid silver noted in TEM images was due to precipitated $AgCl_{(s)}$ but in future studies Energy dispersive x-ray spectroscopy (EDX) could be used in conjunction with TEM to check the surface chemistry of these masses. Similar morphological and distribution behaviour was not noticed in the *UP*H_2O likely due to the much lower concentration/composition of ionic species present facilitating dissolution.

Increasing ZP of AG1 at all concentrations in most media except 1mg/L *UP*H_2O (Figure. 5-2, 5-4) could be due to interaction of the medium with ambient laboratory air. Interaction of NP suspensions with ambient air was not controlled for in our experiments and it may be that airborne species are dissolving into the suspensions and slowly altering the composition/charge. CO_2 has been shown to dissolve in ultrapure water resulting in a pH decrease and HCO_3^- has resulted in a lowering of ZP[25]. Whilst a major pH change was not noted in these experiments it could be that complex interactions between the ambient laboratory air, medium composition and dissolution of the NPs is resulting in gradually increasing zeta potential and this should be investigated further in future work.

It is clear that the salts present in exposure media and their ionic strengths are important to the subsequent understanding particle-media interactions. The two nanoparticles show little change over the duration of the experiment therefore the stabilising force conferred by their coatings overcomes any effects from media ionic strength and keeps the particles in suspension. It would be expected that the stability of sterically coated particles like AG1 and AG2 would not be affected by changes in ionic strength as they are keep in suspension by purely physical means.

5.5 Conclusion

It was the aim of this chapter to determine if and how the stability of multiple concentrations of two types of coated silver nanoparticles commonly used in industry change over a 2 week duration in ultrapure water and two common eco-toxicity media or varying composition and ionic strength. This was assessed using a selection of different characterisation techniques (DLS, NTA, DCS and TEM) and it was shown that multiple complementary characterisation techniques are necessary during toxicity testing as they each have specific strengths and weaknesses. It was seen that both nanoparticles were very stable in all three media for the 2 week duration of the experiment likely due to their coatings (paraffin and PVP). The concentration of the particle suspensions, while shown to have an effect in the literature was found to have little effect on the overall stability of these suspensions, although it was seen to affect detection in some of the particle sizing techniques. The ionic strength and composition of the different media while shown to be important in the literature did not cause any changes in the stability of these particles although subtler effects may be occurring such as dissolution. Dissolution of the particles was not directly investigated in this study however it can be seen that the AG1 particles in TEM show subtle changes in particle morphology over the duration of the experiment in ISO and MBL medium. It is possible that the stability of these particles along with their size differences and coatings could have a toxic effect to aquatic organisms. Smaller size particles are thought to be able to enter cell walls and the physico-chemical form and surface chemistry will dictate the interaction between particles and aquatic species. Toxicity testing must be undertaken to understand this.

5.5.1 Future Work

The influence of coatings and the properties of eco-toxicity test media on silver nanoparticle stability still remains to be completely understood.

Studies which isolate and fully understand each media and nanoparticle specific property are still needed. MBL and ISO media properties such as the ionic species, salt composition and pH need to be measured and compared in a systematic manner to isolate the effect of each property on silver nanoparticle stability. While studies have been undertaken to understand the effect of common electrostatic and steric coatings such as citrate and PVP respectively on the stability of NPs, less work has been done to properly characterise less common coatings used in industry to stabilise NPs such as the organic paraffin coating on the AG1. As was shown in this study they have both an electrostatic and a steric component to their stability. In industry it can be the case that the coating is patented and information about the composition is not freely given to risk assessors. Additional work may require more in depth chemical testing to ascertain the composition and concentration of these coatings as well as washing experiments.

Most importantly it is becoming abundantly clear that dissolution is one of, if not the main factor influencing silver nanoparticle toxicity on micro-organisms[34,35]. More analysis is needed to understand the mechanisms of dissolution of silver nanoparticles in specific ecotoxicity media with special consideration given to its salt concentration and ionic strength as well as the influence of particle size, shape and especially coating. Further to this characterisation of particles in more realistic environmental conditions (e.g. turbidity, biological material, environmentally applicable concentrations) is needed to illuminate the fate of NPs in real-world situations.

5.6 References

1. Pinto, V. V. *et al.* Long time effect on the stability of silver nanoparticles in aqueous medium: Effect of the synthesis and storage conditions. *Colloids Surfaces A Physicochem. Eng. Asp.* **364,** 19–25 (2010).

2. Nichols, H. W. in *Handb. Phycol. Methods* (ed. Stein, J. R.) 16–17 (Cambridge University Press, 1973). at <http://www.marine.csiro.au/microalgae/methods/Media CMARC recipes.htm#MBL>

3. ISO 10712. Water quality -- Pseudomonas putida growth inhibition test (Pseudomonas cell multiplication inhibition test). (1995). at <http://www.iso.org/iso/catalogue_detail.htm?csnumber=18800>

4. PROSPECT. Protocol for Nanoparticle Dispersion. (2010). at <http://www.nanotechia.org/sites/default/files/files/PROSPECT_Dispersion_Protocol.pdf>

5. Anderson, W., Kozak, D., Coleman, V. A., Jämting, Å. K. & Trau, M. A comparative study of submicron particle sizing platforms: Accuracy, precision and resolution analysis of polydisperse particle size distributions. *J. Colloid Interface Sci.* **405,** 322–330 (2013).

6. Domingos, R. F. *et al.* Characterizing Manufactured Nanoparticles in the Environment : Multimethod Determination of Particle Sizes. *Environ. Sci. Technol.* **43,** 7277–7284 (2009).

7. CPS Instruments Inc. CPS Disc Centrifuge Operating Manual. 1–78 (2004). at <http://www.cpsinstruments.eu/pdf/Manual.pdf>

8. Coradeghini, R. *et al.* Size-dependent toxicity and cell interaction mechanisms of gold nanoparticles on mouse fibroblasts. *Toxicol. Lett.* **217,** 205–16 (2013).

9. Angel, B. M., Batley, G. E., Jarolimek, C. V & Rogers, N. J. The impact of size on the fate and toxicity of nanoparticulate silver in aquatic systems. *Chemosphere* **93,** 359–365 (2013).

10. Mahl, D., Diendorf, J., Meyer-Zaika, W. & Epple, M. Possibilities and limitations of different analytical methods for the size determination of a bimodal dispersion of metallic nanoparticles. *Colloids Surfaces A Physicochem. Eng. Asp.* **377,** 386–392 (2011).

11. Boxall, A. B. A., Tiede, K. & Chaudhry, Q. Engineered nanomaterials in soils and water: how do they behave and could they pose a risk to human health? *Nanomedicine* **2,** 919–927 (2007).

12. Mueller, N. C. & Nowack, B. Exposure Modeling of Engineered Nanoparticles in the Environment. *Environ. Sci. Technol.* **42,** 4447–4453 (2008).

13. Levard, C., Hotze, E. M., Lowry, G. V & Brown, G. E. Environmental Transformations of Silver Nanoparticles: Impact on Stability and Toxicity. *Environ. Sci. Technol.* **46,** 6900–6914 (2012).

14. Cosgrove, T. in *Colloid Sci. Princ. Methods Appl.* (ed. Cosgrove, T.) 135–150 (John Wiley & Sons Ltd., 2010).

15. Tejamaya, M., Römer, I., Merrifield, R. C. & Lead, J. R. Stability of Citrate, PVP, and PEG Coated Silver Nanoparticles in Ecotoxicology Media. *Environ. Sci. Technol.* **46,** 7011–7017 (2012).

16. Huynh, K. A. & Chen, K. L. Aggregation kinetics of citrate and polyvinylpyrrolidone coated silver nanoparticles in monovalent and divalent electrolyte solutions. *Environ. Sci. Technol.* **45,** 5564–71 (2011).

17. Kvitek, L. *et al.* Initial Study on the Toxicity of Silver Nanoparticles (NPs) against Paramecium caudatum. *J. Phys. Chem. C* **113,** 4296–4300 (2009).

18. Cumberland, S. A. & Lead, J. R. Particle size distributions of silver nanoparticles at environmentally relevant conditions. *J. Chromatogr. A* **1216,** 9099–105 (2009).

19. Briscoe, W. H. & Horn, R. G. Direct Measurement of Surface Forces Due to Charging of Solids Immersed in a Nonpolar Liquid. *Langmuir* **18,** 3945–3956 (2002).

20. Fatisson, J., Quevedo, I. R., Wilkinson, K. J. & Tufenkji, N. Physicochemical characterization of engineered nanoparticles under physiological conditions: effect of culture media components and particle surface coating. *Colloids Surf. B. Biointerfaces* **91,** 198–204 (2012).

21. Piccapietra, F., Sigg, L. & Behra, R. Colloidal stability of carbonate-coated silver nanoparticles in synthetic and natural freshwater. *Environ. Sci. Technol.* **46,** 818–25 (2012).

22. Khan, S. S., Mukherjee, A. & Chandrasekaran, N. Impact of exopolysaccharides on the stability of silver nanoparticles in water. *Water Res.* **45,** 5184–90 (2011).

23. Khan, S. S., Mukherjee, A. & Chandrasekaran, N. Studies on interaction of colloidal silver nanoparticles (SNPs) with five different bacterial species. *Colloids Surf. B. Biointerfaces* **87,** 129–38 (2011).

24. Prathna, T. C., Chandrasekaran, N. & Mukherjee, A. Studies on aggregation behaviour of silver nanoparticles in aqueous matrices: Effect of surface functionalization and matrix composition. *Colloids Surfaces A Physicochem. Eng. Asp.* **390,** 216–224 (2011).

25. Wang, N., Hsu, C., Zhu, L., Tseng, S. & Hsu, J.-P. Influence of metal oxide nanoparticles concentration on their zeta potential. *J. Colloid Interface Sci.* **407,** 22–8 (2013).

26. Römer, I. *et al.* Aggregation and dispersion of silver nanoparticles in exposure media for aquatic toxicity tests. *J. Chromatogr. A* **1218,** 4226–33 (2011).

27. Römer, I. *et al.* The critical importance of defined media conditions in Daphnia magna nanotoxicity studies. *Toxicol. Lett.* **223,** 103–108 (2013).

28. Briscoe, W. in *Colloid Sci. Princ. Methods Appl.* (ed. Cosgrove, T.) 329–361 (John Wiley & Sons Ltd., 2010).

29. El Badawy, A. M. *et al.* Surface charge-dependent toxicity of silver nanoparticles. *Environ. Sci. Technol.* **45,** 283–7 (2011).

30. Hitchman, A., Smith, G. H. S., Ju-Nam, Y., Sterling, M. & Lead, J. R. The effect of environmentally relevant conditions on PVP stabilised gold nanoparticles. *Chemosphere* **90,** 410–6 (2013).

31. Li, X., Lenhart, J. J. & Walker, H. W. Dissolution-Accompanied Aggregation Kinetics of Silver Nanoparticles. *Technology* **26,** 16690–16698 (2010).

32. Levard, C. *et al.* Effect of Chloride on the Dissolution Rate of Silver Nanoparticles and Toxicity to E. coli. *Environ. Sci. Technol.* **47,** 5738–5745 (2013).

33. Chambers, B. A. *et al.* Effects of Chloride and Ionic Strength on Physical Morphology, Dissolution, and Bacterial Toxicity of Silver Nanoparticles. *Environ. Sci. Technol.* **48,** 761–769 (2013).

34. Sondi, I. & Salopek-Sondi, B. Silver nanoparticles as antimicrobial agent: a case study on E. coli as a model for Gram-negative bacteria. *J. Colloid Interface Sci.* **275,** 177–182 (2004).

35. Navarro, E. *et al.* Toxicity of Silver Nanoparticles to Chlamydomonas reinhardtii. *Environ. Sci. Technol.* **42,** 8959–8964 (2008).

Chapter 6. Characterisation of Silver Nanoparticles in eco-toxicology media exposed to algal extra-cellular polymeric substances (EPS)

6.1 Introduction

In the previous chapter the influence of media ionic strength and composition on the stability of silver nanoparticles when suspended in different eco-toxicity test media was investigated. Algal species have been seen to exude cellular materials in the form of exo-polymeric substances (EPS) consisting mainly of carbohydrates (polysaccharides) and proteins which contribute to the autochthonous (or indigenous) fraction of the dissolved organic carbon (DOC) pool in aquatic environments[1]. Some of the literature has suggested that this happens to a greater extent when exposed to an environmental stressor e.g. ions or NPs[2–4]. Algal exudates are known to be an effective metal binding agent[5] and are thought to decrease toxicity through the alteration of NP surface chemistry[6]. Exposure of biological exudates to CuO and ZnO NPs has been shown to cause metal ion chelation[7,8]. However the exact mechanisms and magnitude of interaction of these materials with nanoparticles (especially silver) and their effect on stability is still relatively unknown.

6.1.1 Aims and Objectives

The purpose of this study was to analyse the behavior of two engineered silver nanoparticles (AG1: 3-8nm in paraffin and AG2: ~50nm in PVP/citrate) suspended in MBL Woodshole media with organic carbon efflux from a green algae and a cyanobacterial species. These organisms are prevalent in aquatic ecosystems so provided a useful test organism to investigate.

The same suite of characterisation techniques used in Chapter 5 (dynamic light scattering: DLS, zeta potential: ZP, nano-tracking analysis: NTA, differential centrifugal sedimentation: DCS, transmission electron microscopy: TEM) were used to determine and compare changes in hydrodynamic/Stoke's diameter d_H/d_s, particle size distribution (PSD), aggregation and stability. Experimental duration was again over 2 weeks (336h) and changes in nanoparticle properties when suspended and exposed to unstressed EPS (those created naturally by algae/cyanobacterial species when organisms are healthy and growing) and stressed EPS (those created when organisms are exposed to a toxicological stressor) were compared along with plain MBL data as observed in Chapter 5. The eventual aim was to discern the impact of each of the EPS treatments on particle stability and whether these techniques were suitable to detect EPS effects on these NPs. The effect of NP coatings was also observed to understand if these alter when suspended in media with biological EPS.

6.1.2 Materials and Methods

6.1.2.1 Particles

Alkane coated Ag-NPs (AG1) and Citrate/PVP stabilised Ag-NPs (AG2) as described in Chapter 3 were used for these experiments.

6.1.2.2 Preparation of Media

MBL Woodshole algal media[9] was used for the suspensions. Preparation and composition is described in Chapter 3.

6.1.2.3 Preparation of algal EPS

Green algae species *C.reinhardtii,* exposed to 5µg/L of $AgNO_3$ to create stressed EPS (CR^-) along with unexposed *C.reinhardtii* (CR^+) and unexposed cyanobacteria species *S.Leopoliensis* (SL^+) were set up as in a 72 hour growth inhibition test in MBL Woodshole media[10]. After 72 hours duration algal material was spun out and separated from the other constituents using centrifugation tubes leaving EPS (stressed and unstressed). Full procedure is described in Chapter 3.

6.1.2.4 Preparation of suspensions

Preparation of NP suspensions was based on PROSPECT: Protocol for Nanoparticle Dispersion[11] and described in Chapter 3.

6.1.2.5 Characterisation

Table 6-1. Summary of Characterisation Measurements

Technique	Parameters Measured	Measurement Times	Notes
DLS (Dynamic Light Scattering)	Hydrodynamic diameter (d_H), Particle Size Distribution (PSD) (nm)	0h, 24h, 48h, 72h, 168h, 336h	Used Malvern Zetasizer
ZP (Zeta Potential)	Zeta Potential (mv)	0h, 24h, 48h, 72h, 168h, 336h	Used Malvern Zetasizer. Complimentary pH values taken using electron pH meter
NTA (Nano-Tracking Analysis)	Mode Hydrodynamic diameter (d_H), Particle Size Distribution	0h, 24h, 48h, 72h, 168h, 336h	Used Nanosight

	(PSD) (nm)		
DCS (Differential Centrifugal Sedimentation)	Stokes diameter (d_s), Particle Size Distribution (PSD) (nm)	0h, 24h, 48h, 72h, 168h, 336h	Used CPS Disc Centrifuge
TEM (Transmission Electron Microscopy)	Particle Size, Aspect Ratio, Cluster Size, %age Aggregates	0h, 336h	Used Jeol 2010 TEM. Qualitative visual counterpoint to other techniques

Summary of characterisation techniques is given in Table 6-1. Experimental techniques and measurement protocols are described in greater detail in Chapter 3. Each EPS treatment as well as plain MBL were also characterised to discern differences in the media before introduction of AG1 and AG2 particles

6.2 Results

6.2.1 Plain Media with/without EPS: NTA data.

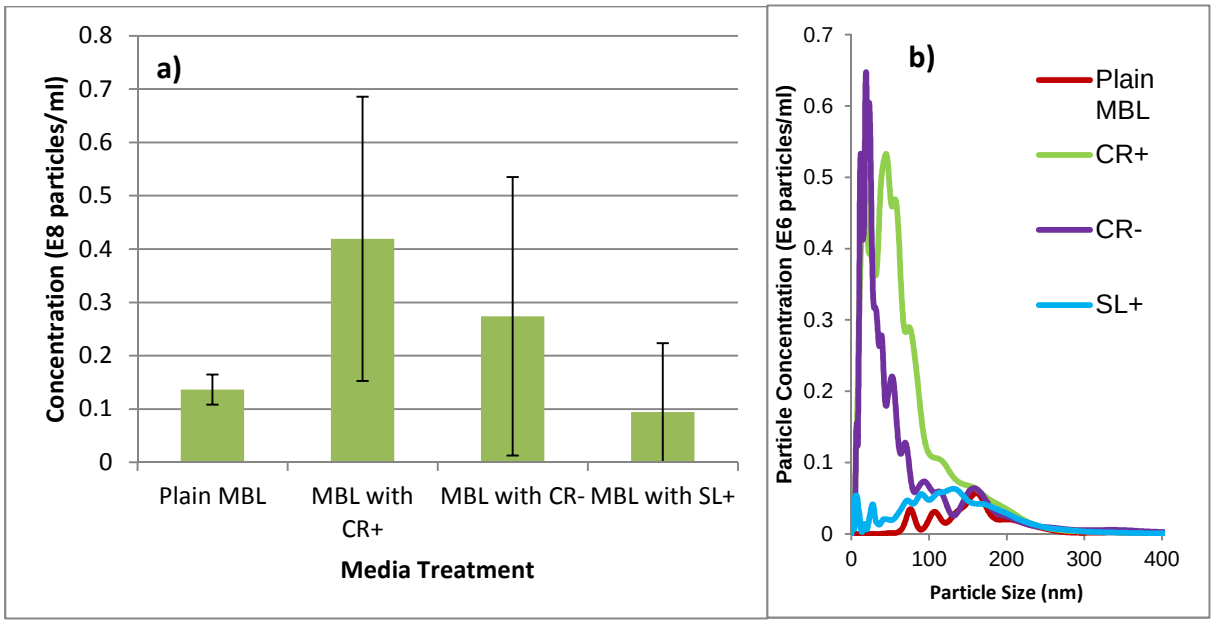

Figure 6-1. a) Concentration and b) Size distribution of MBL media treatments without particles as measured by NTA system: Plain MBL media, MBL media with unstressed

***C.reinhardtii* EPS (CR^+), MBL media with stressed *C.reinhardtii* EPS (CR^-), MBL with unstressed *S.leopoliensis* EPS (SL^+).**

EPS treatments without NPs present were assessed in DLS, DCS and NTA however the former two techniques were unable to detect a signal. This is likely due to low concentration of suspended material and the density dependent acquisition in DCS. NTA can detect low concentrations of suspended material and can be used to give concentrations of that material (no. of particles/ml). This was used to give an idea of the concentrations of just EPS in suspension which aids analysis when nanoparticles are added to the suspensions. Relative concentrations and PSDs of EPS in plain MBL media were detected by NTA (Figure 6-1). Although there was high error, it can be seen that CR^+ showed the highest average concentration followed by CR^-. SL^+ showed little difference from plain MBL media although greater error indicates that a population of suspended material was present but variable. PSD data shows that all EPS in every treatment were ~0-300nm (Figure 6-1b). EPS concentration data acquired using NTA was very variable due to the low refractive index of biological material as well as the very low concentration of suspended material. As such these values cannot be taken as absolute concentration but can be compared in relative terms with each other.

6.2.2 DLS and Zeta Potential data

6.2.2.1 AG1 Particles

The data shows there is no statistically conclusive increasing or decreasing trend in d_H over the duration of the experiment when exposed to any of the EPS at any concentration (Figure. 6-2). The hydrodynamic diameters given for each type of exudate however do differ. AG1 exposed to CR^+ gave d_H at 143-172nm for 100mg/L, 185-217nm for 10mg/L and 241-252mg/L for 1mg/L (Figure 6-1a), which are all much larger than the d_H seen when AG1 was

exposed to SL^+ (124-134nm: Figure 6-1b) and CR^- (120-121nm: Figure 6-1c) and plain MBL media (Figure 5-1). Manufacturer stated primary particle size of 3-8nm was not observed for any suspension.

The only suspension where different concentrations were compared was for CR^+ and it can be seen that d_H increased with decreasing concentration (Figure 6-1a).

ZP data (Figure. 6-3) shows AG1 particles exposed to all three treatments were negatively charged for the experimental duration. Exposure to CR^+ resulted in different effects at different concentrations. 100mg/L AG1 NPs ZPs increased from ~-30mV to ~-22mV, 10mg/L ZP values remained constant at ~-12mV, while 1mg/L ZPs were stable at ~-10mV until 336h where values decreased to -16mV. AG1 10mg/L exposed to SL^+ showed a slight increase (~-40->~-34mV) while 10mg/L NP exposed to CR^- were stable from 2h to 336h (~-33->-35mV). pH remained fairly stable for all AG1 samples over the duration of the experiment with measurements remaining within 0.16 pH values of each other.

6.2.2.2 AG2 Particles

PVP-stabilised AgNPs (AG2) exposed to all three EPS exhibited d_H values at 69-86nm in DLS (Figure. 6-4) and were stable for the experiment duration. Only AG2 in CR^+ showed different behaviour with a slightly higher d_H than the other two exudate treatments for the duration of the experiment possibly relating to the greater concentration of EPS present for this treatment as seen in Figure 6-1a. No overt differences were seen in d_H between SL^+ and CR^- exposures.

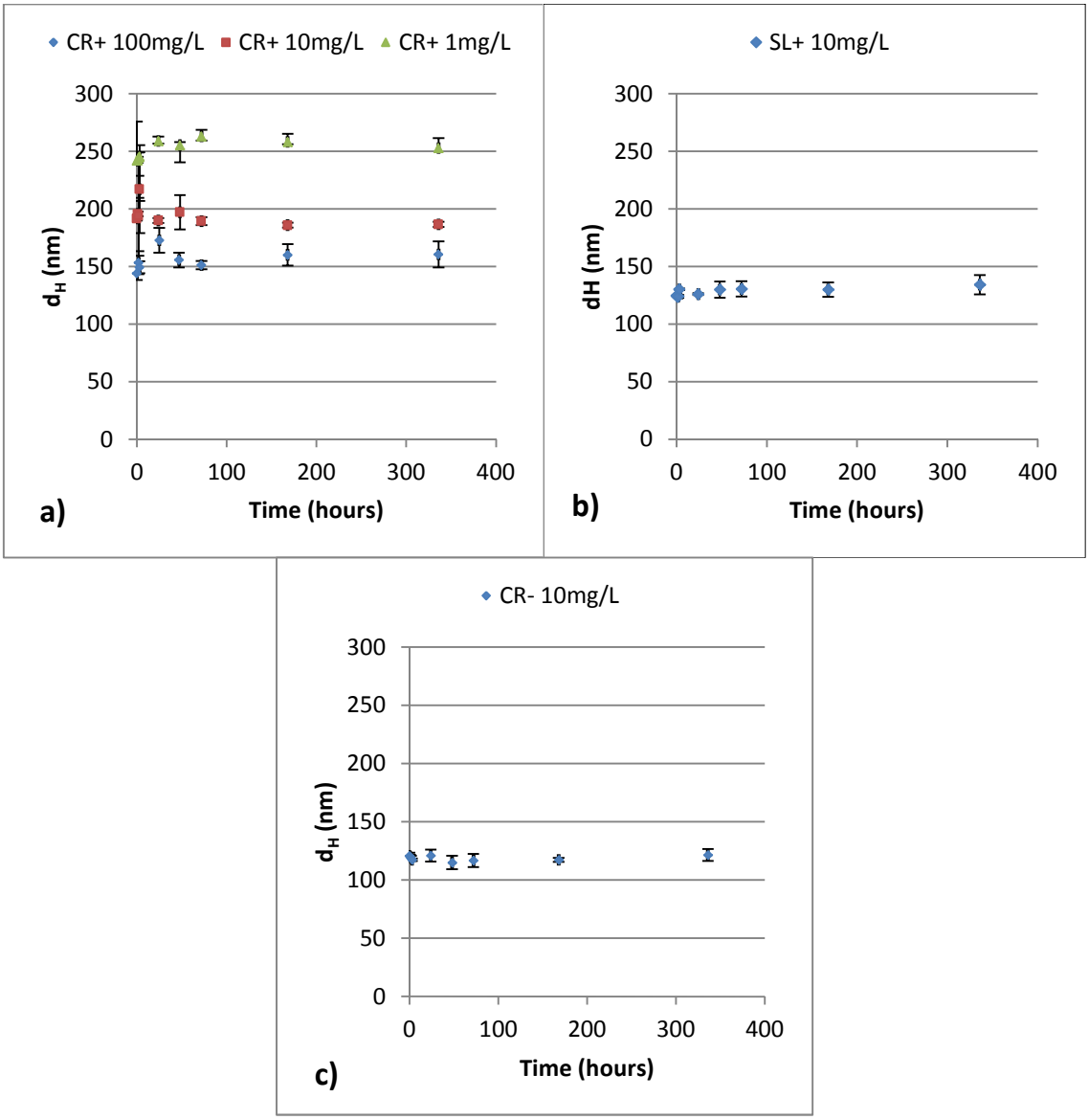

Figure 6-2. AG1 Mean Z-average d_H (nm) vs. time (hours) in: a) MBL media with unstressed *C.reinhardtii* EPS (CR^+) b) MBL with unstressed *S.leopoliensis* EPS (SL^+) c) MBL media with stressed *C.reinhardtii* EPS (CR^-).

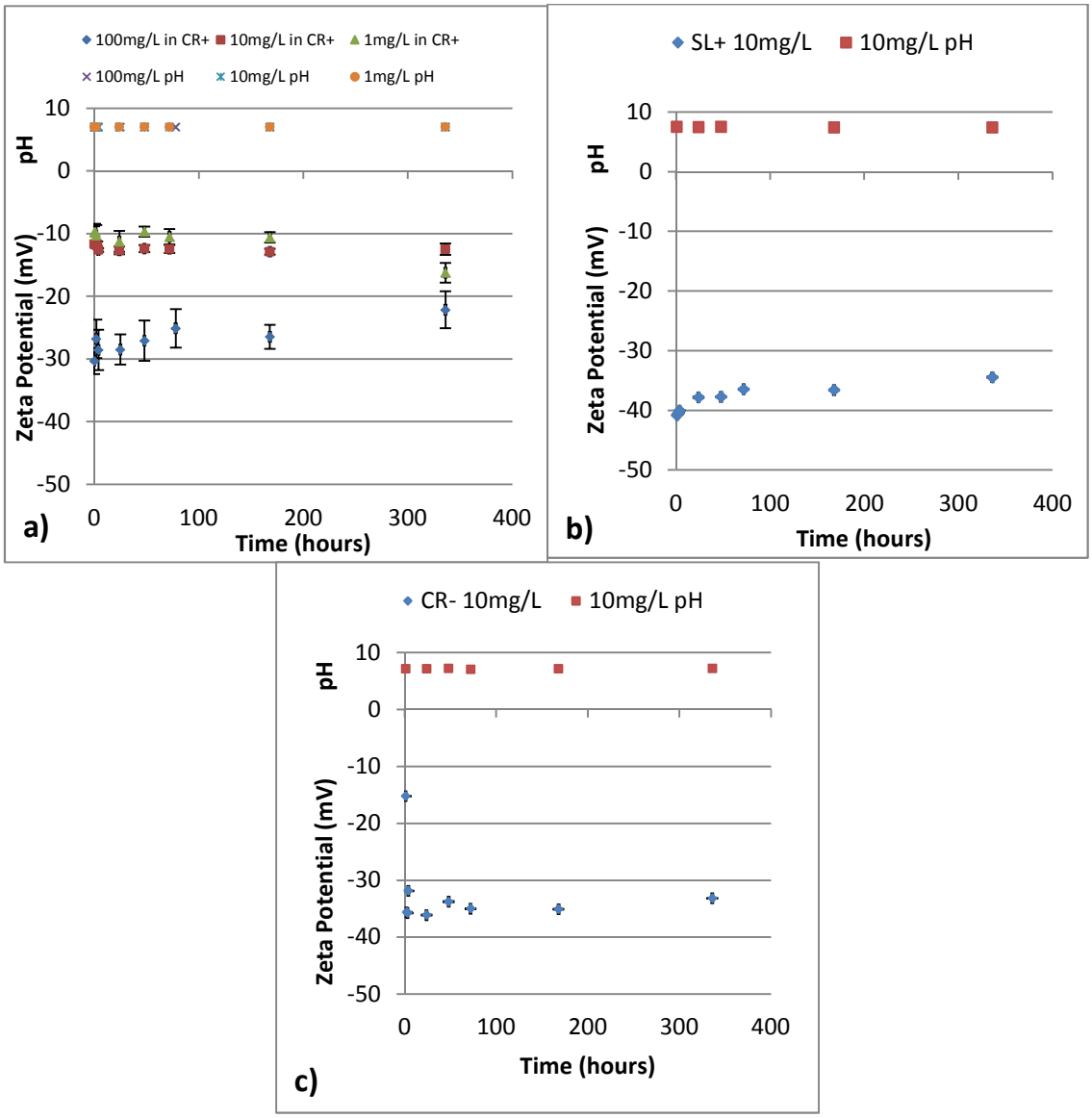

Figure 6-3. AG1 Mean Zeta Potential (mV) and pH values vs. time (hours) in: a) MBL media with unstressed *C.reinhardtii* EPS (CR^+) b) MBL with unstressed *S.leopoliensis* EPS (SL^+) c) MBL media with stressed *C.reinhardtii* EPS (CR^-)

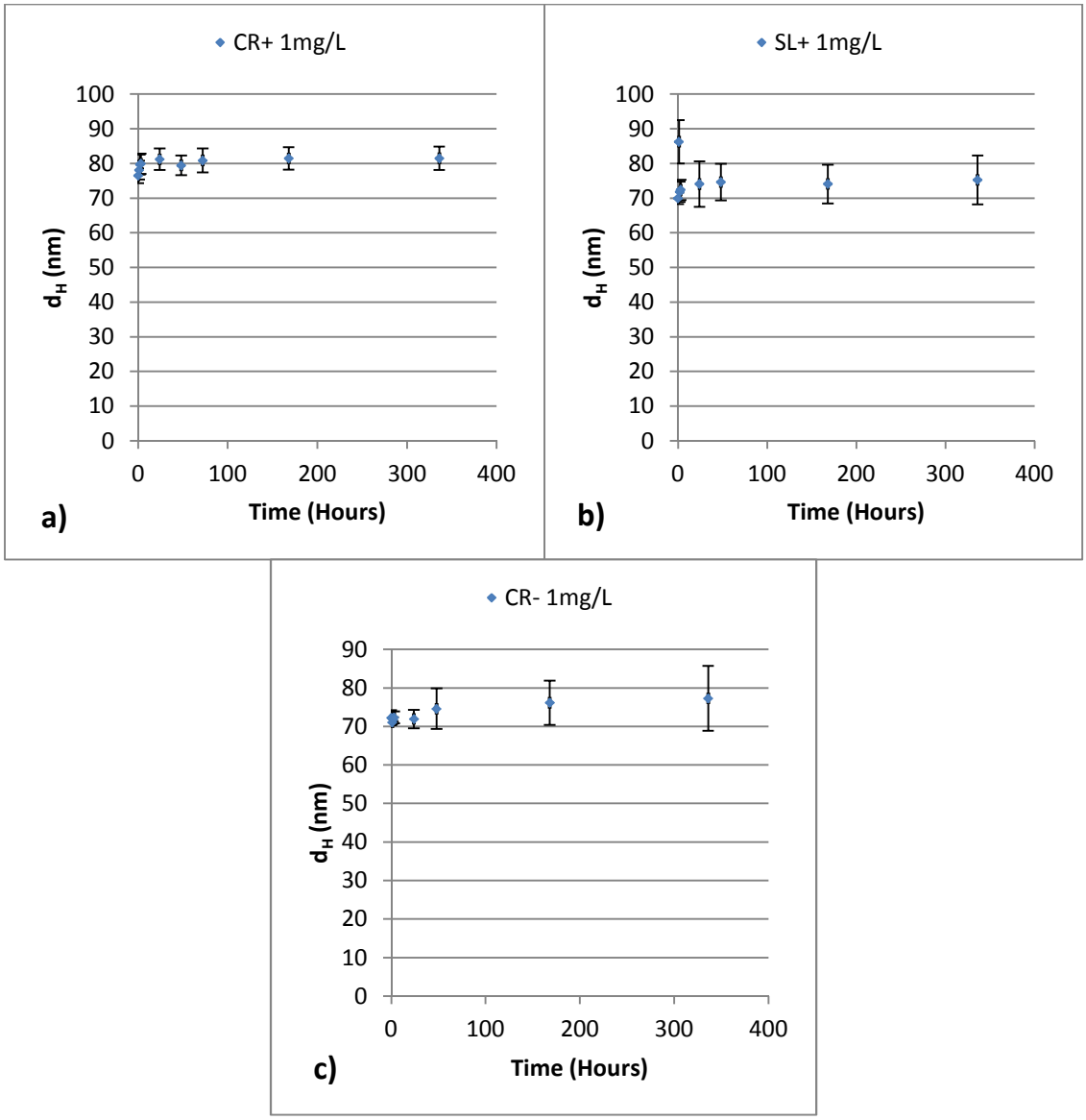

Figure 6-4. AG2 Mean Z-average d_H (nm) vs. time (hours) in: a) MBL media with unstressed *C.reinhardtii* EPS (CR^+) b) MBL with unstressed *S.leopoliensis* EPS (SL^+) c) MBL media with stressed *C.reinhardtii* EPS (CR^-).

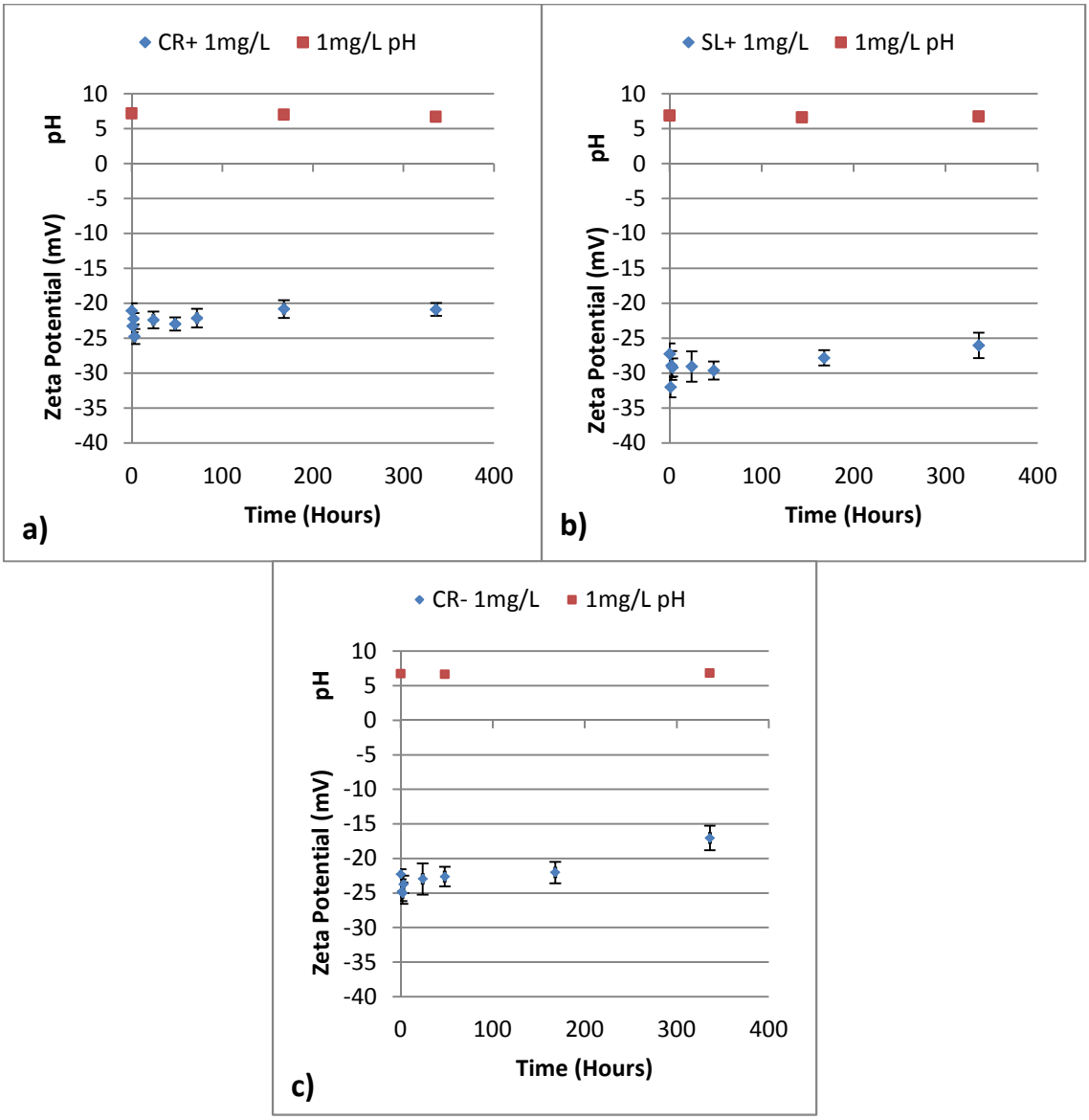

Figure 6-5. AG2 Mean Zeta Potential (mV) and pH values vs. time (hours) in: a) MBL media with unstressed *C.reinhardtii* EPS (CR^+) b) MBL with unstressed *S.leopoliensis* EPS (SL^+) c) MBL media with stressed *C.reinhardtii* EPS (CR^-).

1mg/L AG2 NPs were negatively charged in all exposures (Figure. 6-5). ZPs in CR^+ exposures ranged between ~-24mV and ~-20mV, SL^+ exposures between ~-32mV and ~-26mV and CR^- exposures between ~-24mV and ~-17mV. All showed a slight increase over the duration of the experiment but remained within the realm of moderate stability. pH remained within 0.5 of 7 for the experiment duration.

6.2.3 Nano-Tracking Analysis (NTA)

6.2.3.1 AG1 Particles

NTA size data for AG1 exposed to CR^+ at 1mg/L showed a mode d_H over the duration of the experiment at 81nm ± 13.51 (decrease from ~95nm to ~68nm) while 10mg/L showed a decrease in d_H but from ~56 to ~51nm (54.14nm ± 1.76) (Table 6-2a,b). PSD for both concentrations was similar for the duration of the experiment at 3-250nm with majority of diameters within 0-200nm (Table 6-2a, b).

AG1 exposed to SL^+ at 10mg/L showed a stable mode d_H at 32.5 ± 0.68nm and PSD at ~7-187nm for the duration of the experiment with the majority of particle diameters within 7-100nm (Table 6-2c).

10mg/L AG1 in CR^- showed a mode d_H of 32.6 ± 2.32nm and PSD at ~8-171nm over the duration of the experiment with the majority of particle diameters within 8-100nm (Table 6-2d).

6.2.3.2 AG2 Particles

AG2 particles suspended in all EPS treatments at 1mg/L showed no significant differences in mode d_H and PSD for the duration of the experiment (Table 6-3). Mode d_H values were ~16-22nm, lower than seen for primary particles in TEM (Figure 6-9, 6-10, 6-11), also seen in Chapter 5 (Table 5-3). PSDs remained between ~4-315nm with the majority of NP between ~3-80nm (Table 6-3).

Table 6-2. NTA data AG1: Mean (mode estimated) diameter and standard deviation (nm), Maximum range in size of PSD (nm) and mean peak width and standard deviation in different media treatments over 2 weeks (336h). Corresponding figures show the mean NTA detected PSD from up to 10 replicates for (a) CR^+ 1mg/L (b) CR^+ 10mg/L (c) SL^+ 10mg/L (d) CR^- 10mg/L. Figures are given to allow visualisation of the distributions. Note variable concentrations were due to variability in operator defined measurement conditions and have little effect on the PSD.

Treatment	Conc. (mg/L)	Mode diameter (d_H) (nm +/- 1 SD)	Maximum PSD range (nm)	Peak width (nm ± 1 SD)	Notes
CR^+	1mg/L	81 ± 13.51 (decrease from ~95-68nm)	3-247nm	225 ± 17	Distribution has shoulder at higher particle sizes. Majority of particles within 3-200nm (Figure (a))
CR^+	10mg/L	54.14 ± 1.76 (decrease from 56-51nm)	8-247nm	221 ± 13	Distribution has shoulder at higher particle sizes. Majority of particles within 8-200nm (Figure (b))
SL^+	10mg/L	32.5 ± 0.68	7-187nm	155.3 ± 14.76	Stable Distribution. Distribution has shoulder at higher particle sizes. Majority of particles within 7-100nm (Figure (c))
CR^-	10mg/L	32.6 ± 2.32	8-171nm	137.5 ± 15.64	Stable Distribution. Distribution has shoulder at higher particle sizes. Majority of particles within 8-100nm (Figure (d))

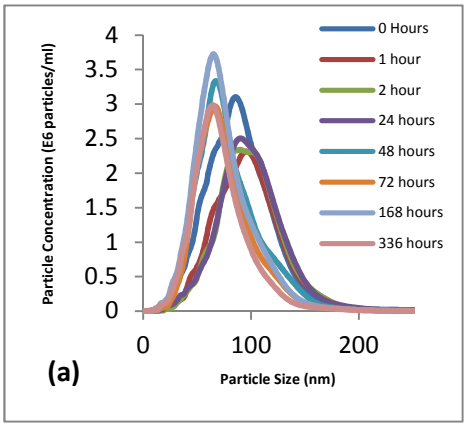

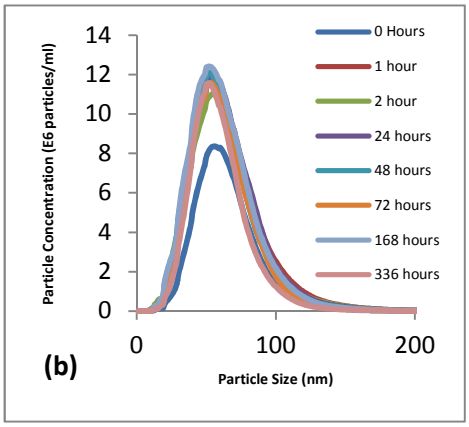

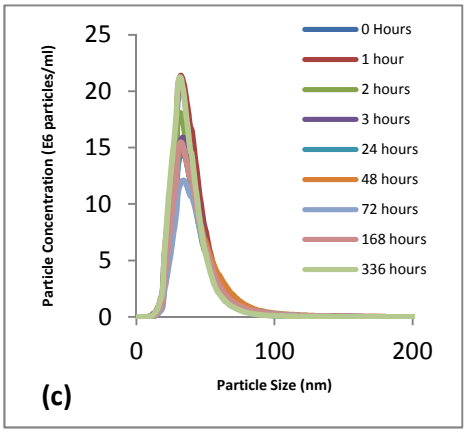

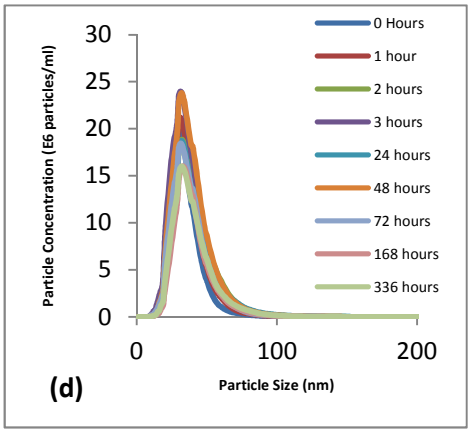

Table 6-3. NTA data AG2: AG1: Mean (mode estimated) diameter and standard deviation (nm), Maximum range in size of PSD (nm) and mean peak width and standard deviation in different media treatments over 2 weeks (336h). Corresponding figures show the mean NTA detected PSD from up to 10 replicates for (a) CR^+ 1mg/L (b) CR^+ 10mg/L (c) SL^+ 10mg/L (d) CR^- 10mg/L. Figures are given to allow visualisation of the distributions. Note variable concentrations were due to variability in operator defined measurement conditions and have little effect on the PSD.

Exposure	Conc. (mg/L)	Mode diameter (d_H) (nm +/- 1 SD)	Maximum PSD range (nm)	Peak width (nm ± 1 SD)	Notes
CR^+	1mg/L	19.46 ± 1.13	3-239nm	176 ± 44	Unchanging distribution (majority particles within 0-80nm) (Figure (a))
SL^+	1mg/L	17.23 ± 0.87	3-256nm	216 ± 36.5	Unchanging distribution (majority particles within 0-80nm) (Figure (b))
CR^-	1mg/L	18.63 ± 0.97	4-315nm	252 ± 36.6	Unchanging distribution (majority particles within 0-80nm) (Figure (c))

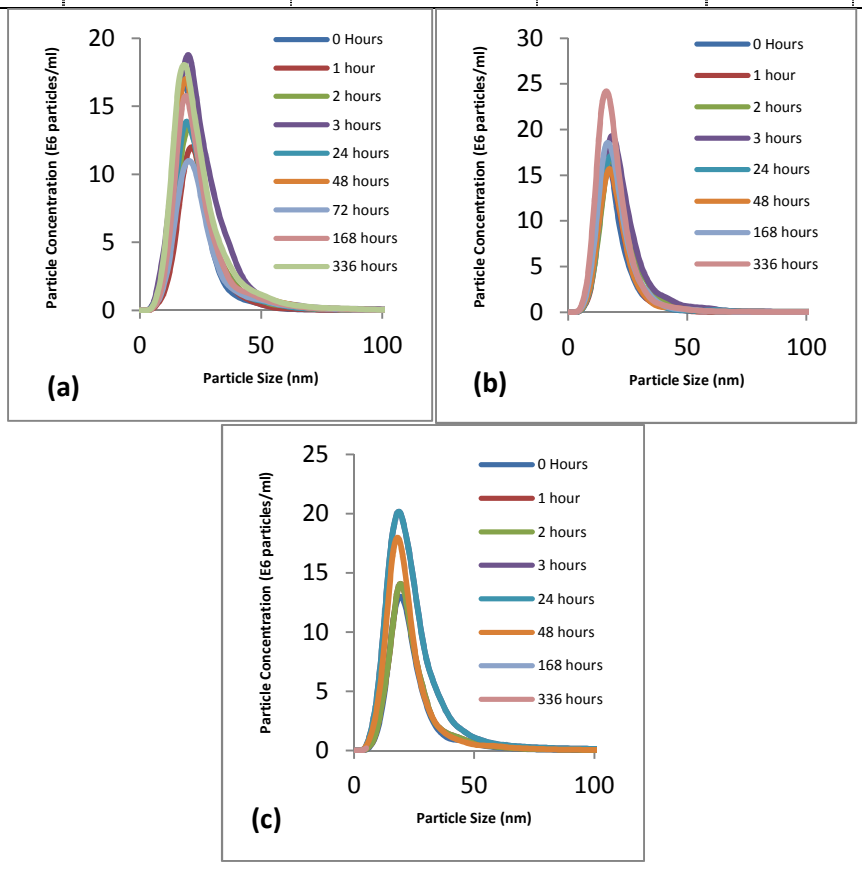

6.2.4 Differential Centrifugal Sedimentation

Table 6-4. DCS data: Particle Size Distributions (PSD: nm) and d_s (nm) values for AG1 and AG2 in all media treatments.

Particle	Treatment	Conc (mg/L)	PSD (nm)	d_s (Mode diameter: nm)
AG1	CR^+	1	~5-297	~20-30
	CR^+	10	~5-298	~35
	CR^+	100	~5-298	~40
	SL^+	10	~10-299	~30-45
	CR^-	10	~10-300	~35-40
AG2	CR^+	1	~14-298	~50
	SL^+	1	~10-298	~50
	CR^-	1	~10-297	~50

AG1 suspensions showed very similar PSDs (~5-298nm) and roughly the same d_s (~20-45nm) for the duration of the experiment in all algal exposures (Table 6-4). Most particles fell between 5-200nm in the PSD. Slight differences occurred in AG1 at 1mg/L in CR^+ which showed a greater variability of d_s than at 10mg/L and 100mg/L.

AG2 particles also showed constant PSD (~10-298nm) and mode d_s (~50nm) in all treatments for the duration of the experiments. Most particles fell between ~30-100nm in the PSD (Table 6-4).

6.2.5 Transmission Electron Microscopy

Table 6-5 shows particle size data from the analysis of TEM images (Figure 6-6, 6-7, 6-8) of AG1 in CR^+, SL^+ and CR^- media treatments at 0h and 2 weeks (336h). All the images show primary particles with diameters (d_{pp}:~7-11nm) as well as two types of clusters, loosely associated clusters (agglomerates) and tightly bound spherical clusters (aggregates).

Table 6-5. AG1 in in MBL with CR^+, SL^+ and CR^- : TEM data Primary particle (d_{pp}) and cluster diameters (d_{AGG}), size ranges, aspect ratios of primary particles (S_{pp}) and clusters (S_{AGG}) and percentage of clusters in aggregate form (tightly bound and fused together).

Media	Time (h)	Conc. (mg/L)	d_{pp} (nm/no. of particles)	d_{pp} range (nm)	S_{pp} (range)	d_{AGG} (nm/no. of clusters)	d_{AGG} range (nm)	S_{AGG} (range)	%Aggregates (%/no. of clusters)
CR^+	0	10	7.76±3.34/106	4.94-15.20	1.22±0.48 (1.00-2.24)	32.11±11.28/40	12.32-57.56	1.28±0.23 (1.01-2.00)	37.5% (40)
	336	10	7.81±3.36/104	4.81-12.65	1.17±0.48 (1.00-2.25)	43.60±17.32/37	14.22-88.74	1.26±0.43 (1.00-3.30)	51.351% (37)
SL^+	0	10	9.45±4.31/102	4.49-22.98	1.21±0.45 (1.00-1.87)	63.31±56.35/31	16.8-333.73	1.23±0.29 (1.00-2.36)	58.065% (31)
	336	10	10.40±4.70/92	3.48-21.28	1.27±0.49 (1.00-2.15)	44.72±16.60/36	18.38-94.89	1.28±0.26 (1.02-2.05)	63.89% (36)
CR^-	0	10	9.17±3.59/107	4.64-19.01	1.30±0.46 (1.01-2.57)	48.33±35.96/37	17.53-189.37	1.21±0.23 (1.01-2.06)	48.649% (37)
	336	10	7.84±3.48/102	4.21-15.19	1.15±0.46 (1.00-1.52)	48.64±24.45/38	14.26-133.61	1.12±0.13 (1.00-1.60)	76.315% (38)

NOTE – TEM samples were made with new batch of EPS-media and therefore were different to samples used for other characterisation techniques. As a result exact concentrations of biological EPS were different however stocks were created in using the same protocol and therefore results were comparable.

No conclusive trends could be noted from any of the TEM measured NP properties as the standard deviation was high and allowed for overlap in values. Average primary particle diameter (d_{pp}) remained ~7-11nm in all media at both measurement times however a decrease was seen in CR^- while an increase was noted in CR^+ and SL^+ from 0h to 336h. Decreases in primary particle aspect ratio (S_{pp}) were noted in CR^+ and CR^- but a slight increase was noted in SL^+. Similar trends were noted for the cluster diameter (d_{AGG}) and aspect ratio (S_{AGG}).

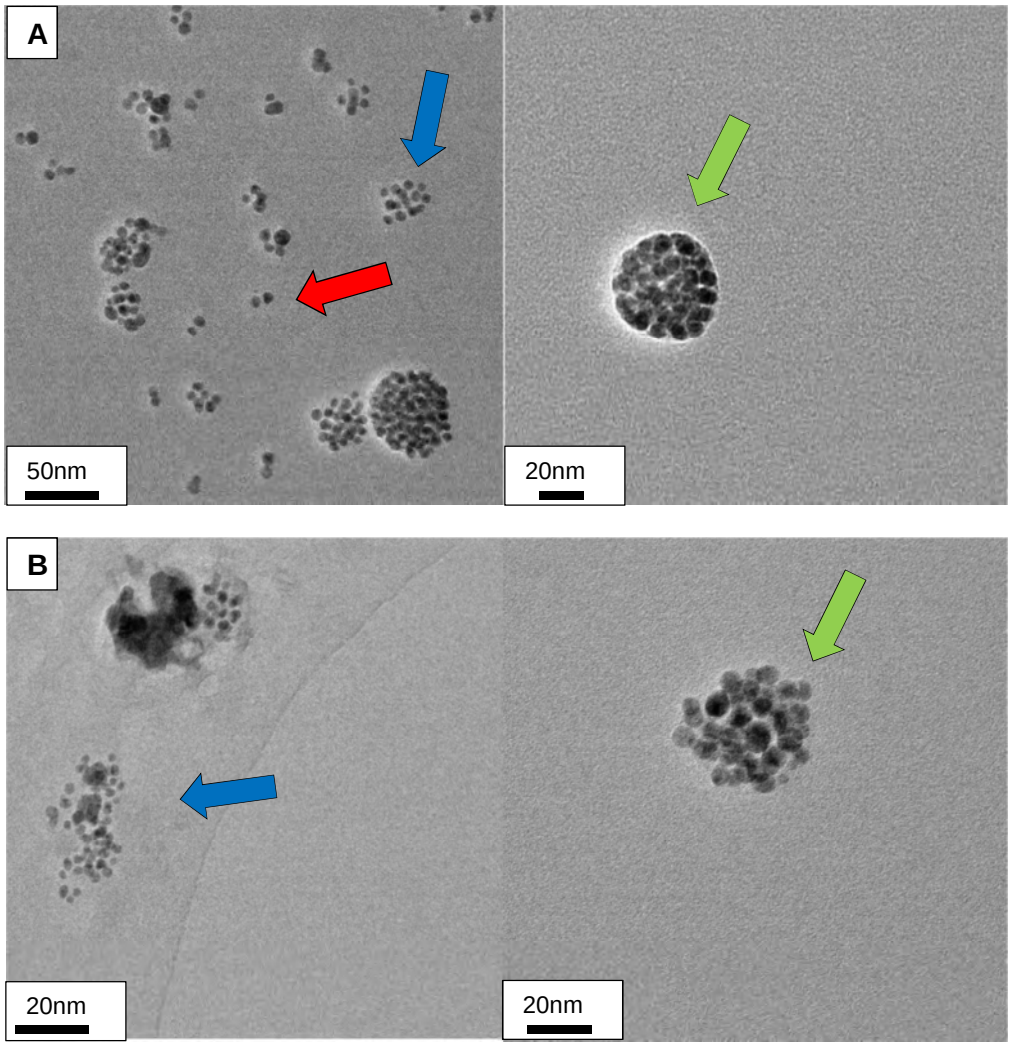

Figure 6-6. TEM image of 10mg/L AG1 in CR^{+}: a) 0 h (scale bars 50nm & 10nm) b) 2 weeks (scale bars 50nm and 50nm). Arrows indicate primary particles (red), loose clusters (agglomerates) (blue) and tight clusters (aggregates) (green)

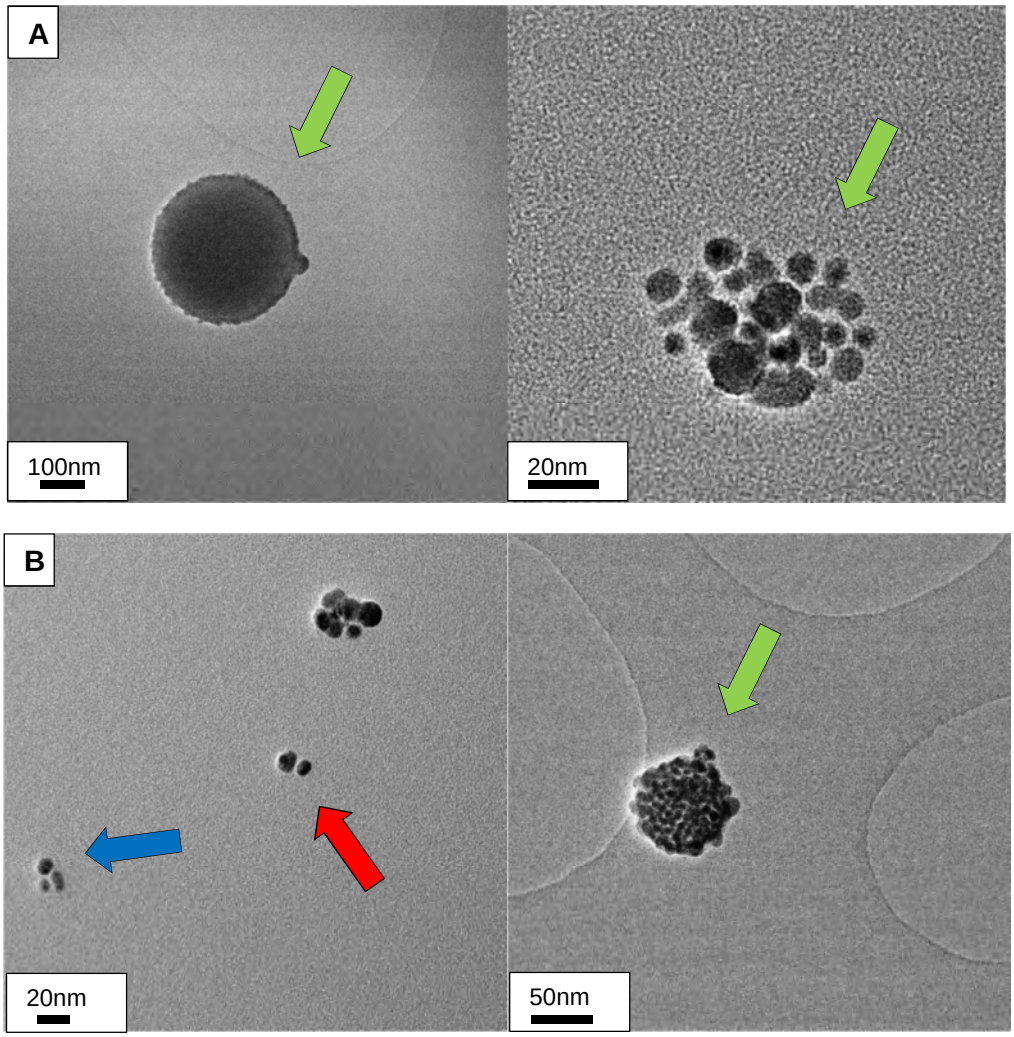

Figure 6-7. TEM image of 10mg/L AG1 in SL^{+}: a) 0 h (scale bars 50nm & 10nm) b) 2 weeks (scale bars 50nm and 50nm). Arrows indicate primary particles (red), loose clusters (agglomerates) (blue) and tight clusters (aggregates) (green)

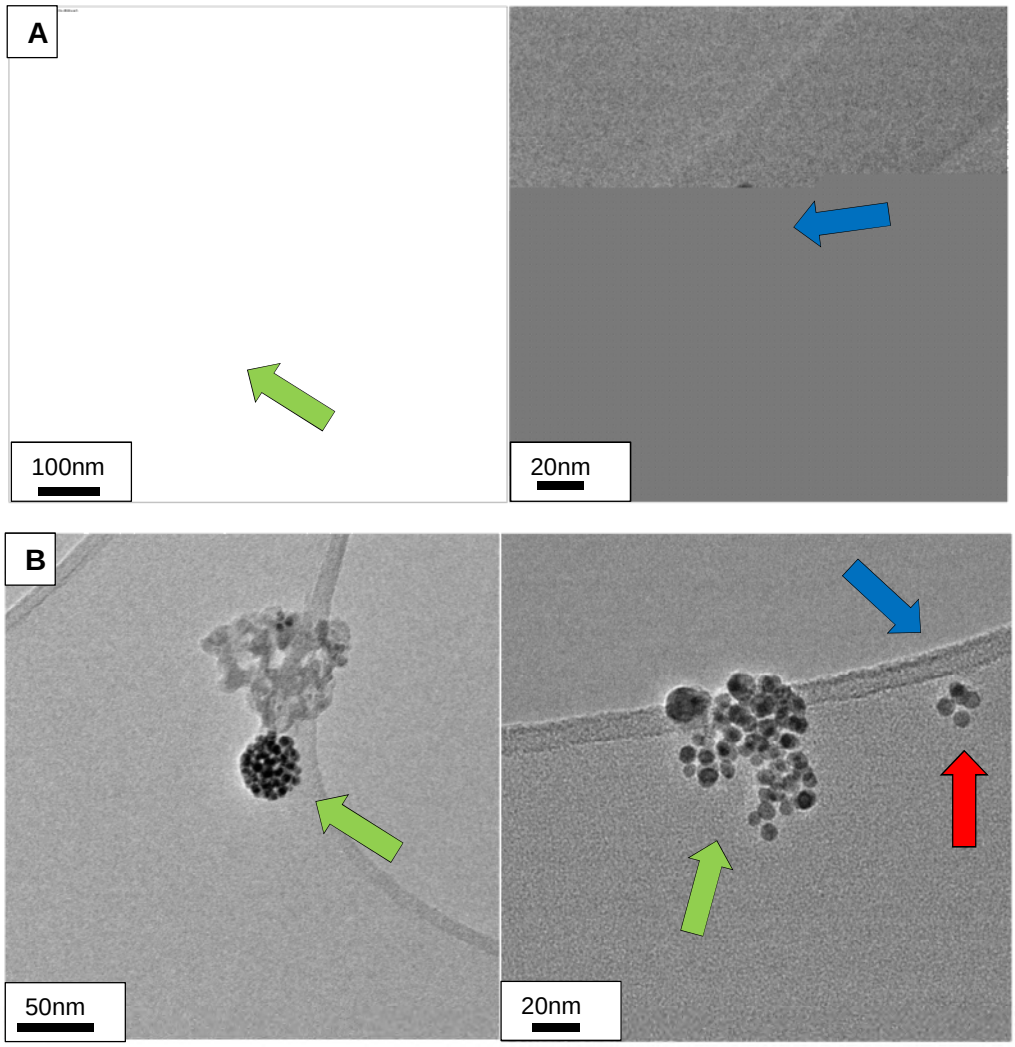

Figure 6-8. TEM image of 10mg/L AG1 in CR$^-$: a) 0 h (scale bars 50nm & 10nm) b) 2 weeks (scale bars 50nm and 50nm). Arrows indicate primary particles (red), loose clusters (agglomerates) (blue) and tight clusters (aggregates) (green)

Table 6-6. AG2 in MBL with CR^+, SL^+ and CR^- : TEM data. Primary particle (d_{pp}) and cluster diameters (d_{AGG}), size ranges, aspect ratios of primary particles (S_{pp}) and clusters (S_{AGG}) and percentage of clusters in aggregate form (tightly bound and fused together).

Media	Time (h)	Conc. (mg/L)	d_{pp} (nm/no. of particles)	d_{pp} range (nm)	S_{pp} (range)	d_{AGG} (nm/no. of clusters)	d_{AGG} range (nm)	S_{AGG} (range)	%Aggregates (%/no. of clusters)
CR^+	0	10	50.51±14.50 /52	21.31-96.15	1.18±0.09 (1.02-1.39)	99.73±50.28/12	39.29-215.29	1.57±0.55 (1.13-2.84)	0% (12)
	336	10	60.92±20.82 /56	26.74-130.08	1.19±0.14 (1.01-1.64)	154.08±98.51/7	72.38-365.93	1.59±1.59 (1.08-5.95)	0% (7)
SL^+	0	10	56.12±18.45 /51	16.99-133.39	1.21±0.13 (1.02-1.70)	0/0	0	0 (0)	0% (0)
	336	10	75.73±53.49 /39	35.08-313.12	1.28±0.24 (1.02-1.98)	0/0	0	0 (0)	0% (0)
CR^-	0	10	54.84±15.95 /54	26.52-104.53	1.18±0.13 (1.00-1.48)	131.23±81.88/4	73.97-249.35	1.82±0.69 (1.13-2.71)	0% (4)
	336	10	54.29±13.42 /51	32.62-109.67	1.20±0.13 (1.02-1.72)	91.09±47.40/7	55.10-191	1.97±0.47 (1.20-2.81)	0% (7)

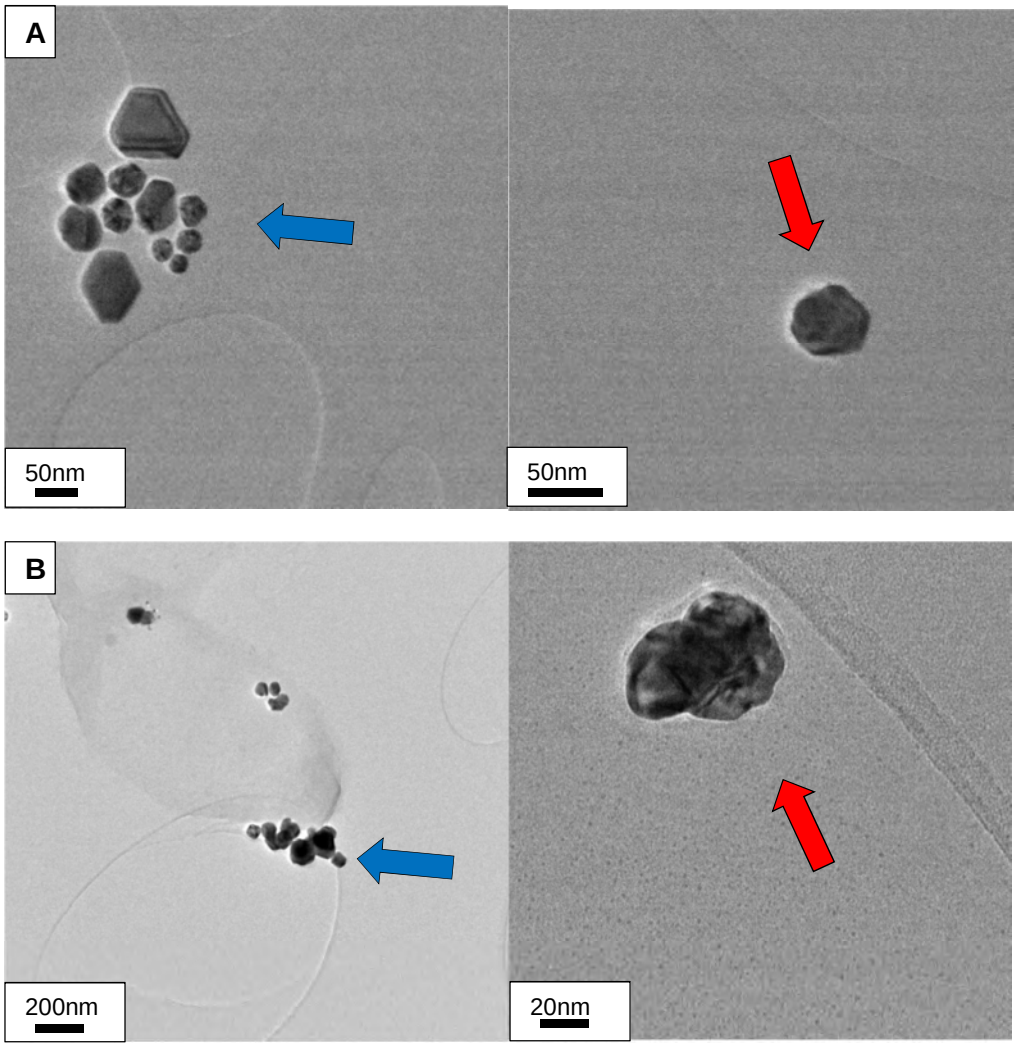

Figure 6-9. TEM image of 10mg/L AG2 in CR^+: a) 0h (scale bars 20nm & 50nm) b) 2 weeks (50nm & 50nm). Arrows indicate primary particles (red), loose clusters (agglomerates) (blue) and tight clusters (aggregates) (green).

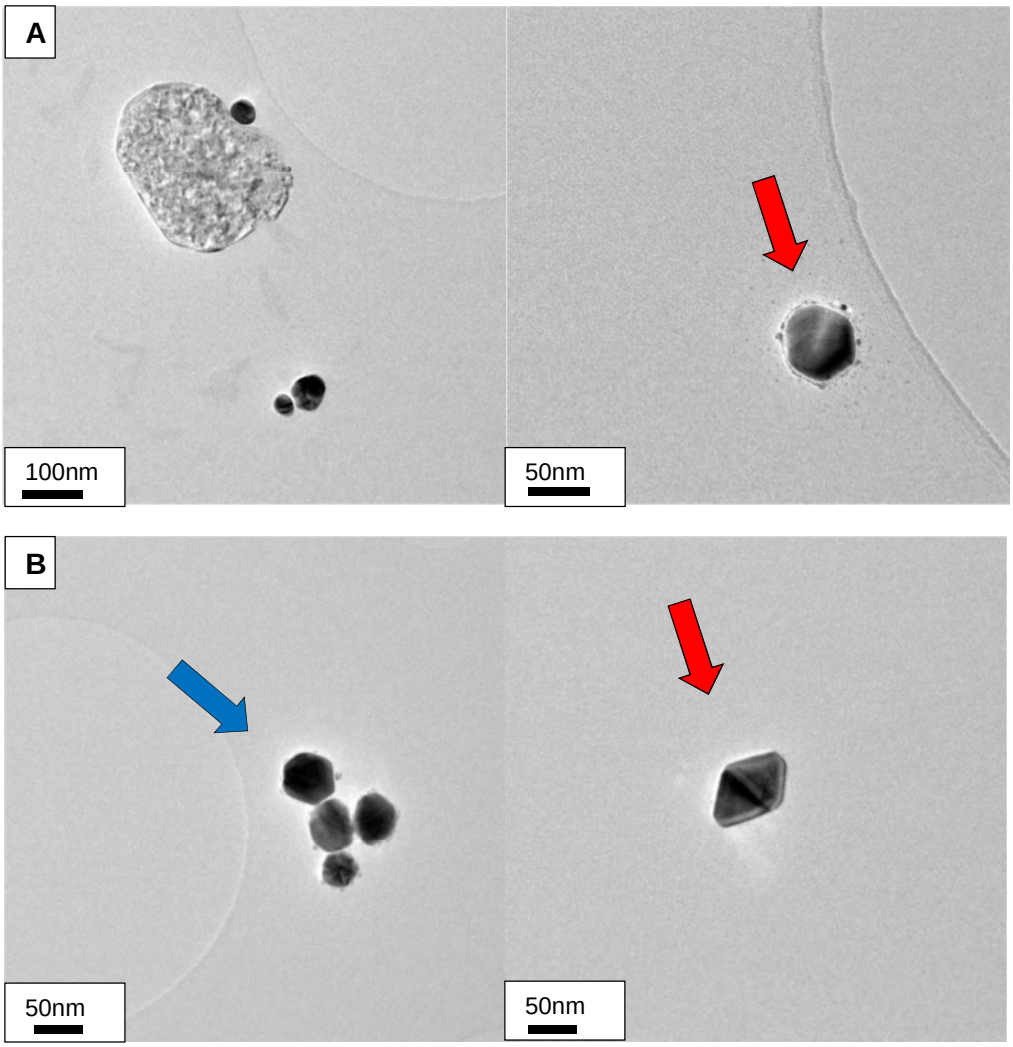

Figure 6-10. TEM image of 10mg/L AG2 in SL^+: a) 0h (scale bars 20nm & 50nm) b) 2 weeks (50nm & 50nm). Arrows indicate primary particles (red), loose clusters (agglomerates) (blue) and tight clusters (aggregates) (green).

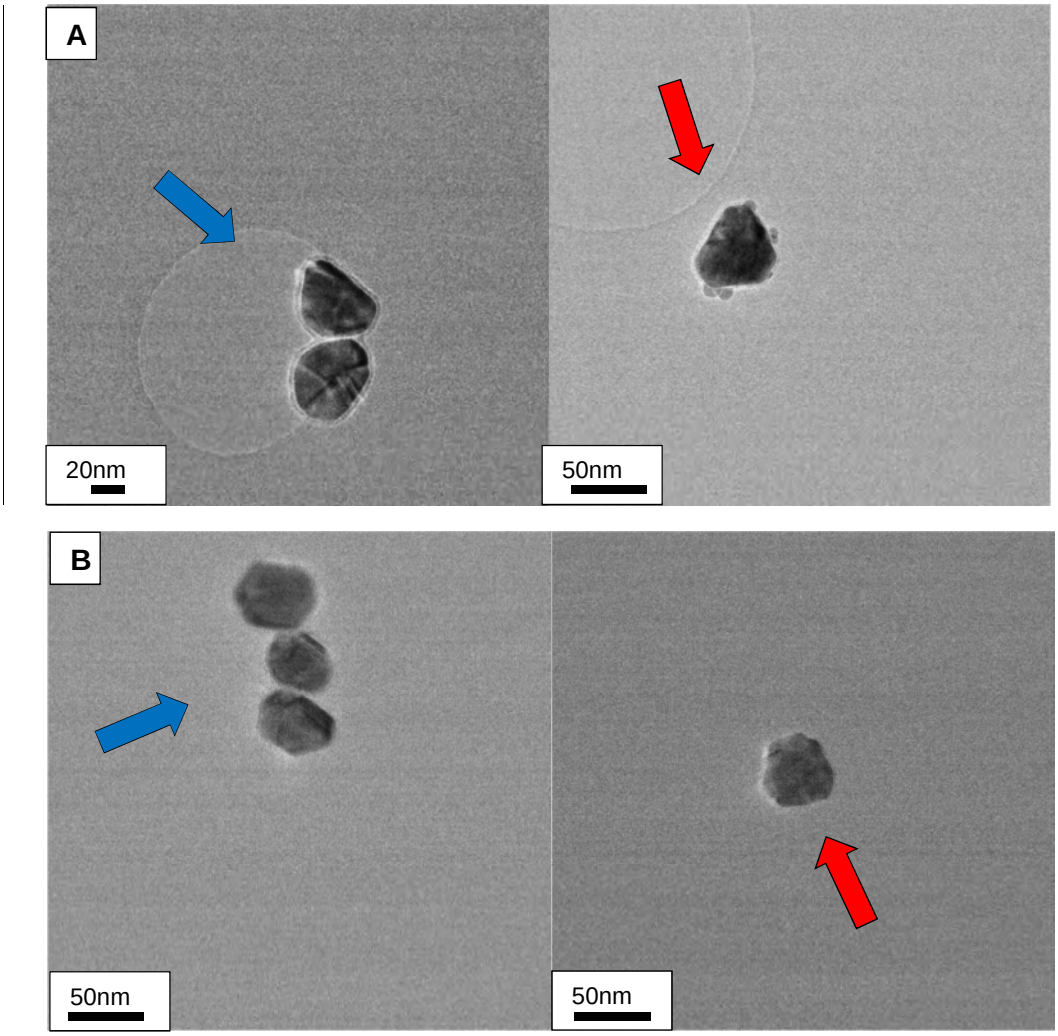

Figure 6-11. TEM image of 10mg/L AG2 in CR^-: a) 0h (scale bars 20nm & 50nm) b) 2 weeks (50nm & 50nm). Arrows indicate primary particles (red), loose clusters (agglomerates) (blue) and tight clusters (aggregates) (green).

Table 6-6 shows particle size data from the analysis of TEM images (Figures 6-9, 6-10, 6-11) of AG2 in CR^+, SL^+ and CR^- media treatments at 0h and 2 weeks (336h). NPs were present mainly as primary particles of ~50nm and any clusters were loosely associated agglomerates of primary particles however there were very few agglomerates present in any of the images. The images show that the majority of particles have a thin coating present on the outside of primary particles and clusters which is probably PVP. d_{pp} for AG2 in all three media at both times was always between 50-75nm and no significant difference could be seen after 336h for any of the samples, as with aspect ratio (S_{pp}) and ranges. Cluster size

and aspect ratio were variable but numbers were very low so no conclusions could be drawn from this data.

6.3 Discussion

6.3.1 Suitability of techniques

As with previous chapters the four characterisation techniques give different d_H/d_s and PSD values as expected per their fundamental theoretical differences (described in Chapter 3 and 5). DLS gives the largest d_H or d_s of all the characterisation techniques due to the tendency of polydisperse samples to push the z-average d_H to that of the larger objects in suspension. As seen in Chapter 5, AG1 was much more polydisperse than AG2 and therefore gives high values in DLS. NTA gives lower mode d_H in all treatments than DLS owing to its calculation of particle size distributions by counting individual point scatterers rather than intensity signals. DCS with its density dependent size calculations again gave different values to DLS and NTA. TEM was again used to visualise and interpret the size distribution data obtained in the other techniques as well as give morphological information.

6.3.2 Ability of Characterisation techniques to detect influence of EPS

The interaction of EPS and NPs is complicated and can result in a number of different associations (described in greater detail in 6.3.5). AG1 hydrodynamic diameters measured by DLS and NTA are larger in CR^+ treatment than in SL^+, CR^- (Figure 6-2, Table 6-2) and plain MBL (Chapter 5).

Larger AG1 d_H (observed using DLS and NTA) in CR^+ than in SL^+, CR^- and plain MBL as well as larger NTA measured AG1 CR^+ PSDs are probably due to the higher concentrations

of NTA detectable solid EPS (sEPS) present in the CR^+ treatment (Figure 6-1a). Greater likelihood of sEPS-particle interactions and more adsorption potential is expected at higher concentrations of suspended organic matter. The size of the sEPS (~0-300nm: Figure 6-1b) could also have had an effect on the signal from the light scattering techniques, as the upper range is larger than the expected primary particle/cluster size for both AG1 and AG2 and could therefore raise the upper value for d_H. However, AG2 particles in DLS showed increases in d_H in all EPS treatments from that of plain MBL, the greatest increase coming in the CR^+ treatment possibly due to higher concentrations of EPS in that treatment coating the particles. It may be that the nature of the coatings for AG2 (citrate+PVP) are responsible for the different levels of EPS adsorption to the particle surface than AG1. As in Chapter 5 the presence of ~20nm diameter particles was noted in NTA in all treatments (no different in size from those in plain MBL) which again likely resulted from the presence of high concentrations of loose PVP micelles in suspension (as noted in [12]). It is possible that when measuring these samples in NTA that any effect due to EPS is dwarfed by the concentrations of loose AG2 coating.

When using DCS or TEM little significant effect from any of the EPS treatments for either AG1 or AG2 was discerned over that of plain MBL. In DCS, differences to plain MBL or between treatments would be expected if coating of the NPs resulted in an alteration of particle density. As no such differences occurred it is unlikely that any surface attachment of sEPS resulted in changes to particle density. Either, concentrations of the sEPS were too low to alter density or attachment of the organics to the NP surfaces could have been weak and they became dislodged when introduced to the spinning gradient. It was not possible to extract trends from the TEM size or aspect ratio data owing to the large error bars associated with each value and the low number of particles counted resulting in inconclusive statistics. Therefore, potential morphological changes relating to dissolution of the particles could not be discerned. An increase in primary particle (or cluster) size in TEM image for CR^+ was expected from coating or association of the NPs by EPS owing to the larger d_H

values noted in DLS and NTA. However no statistically conclusive difference between any of the treatments was noted against that of plain MBL in TEM images (Chapter 5). Individual particles in AG1 were not found to be coated in biological material however some particles were shown to be associated and embedded in biological material in CR^+ and CR^- treatments (Figures 6-6, 6-8). If this embedding occurred as a result of evaporative TEM sample preparation issues it could not be discerned. The lack of individual particle coatings noted in TEM possibly backs up the fact that no differences were noted in the DCS results due to poor association of NPs with EPS. AG2 particles associated with biological material were not seen for any of the treatments in TEM.

Overall it can be stated that DLS and NTA are the techniques most affected by the presence of sEPS in suspension with AgNPs, while DCS and TEM did not detect any differences between treatments/plain MBL and had high statistical noise respectively. DLS and NTA effects possibly stem from the variation of size and morphology of sEPS with laser light causing flickering signals difficult to constrain by the software algorithms. EPS, as well as having a solid suspended fraction (sEPS), will also have a dissolved fraction (dEPS). The effect of dEPS cannot be discerned by any of the techniques as separate from the sEPS fraction for these samples and these techniques. This is likely due to the strong stabilising effect of the NP coatings and the low concentrations of suspended organic matter preventing changes in particle size being detected over that of experimental noise. Therefore for these NPs and EPS treatments it is not possibly to demonstrate a conclusive influence of EPS on nanoparticle properties as detected by this suite of characterisation techniques.

6.3.3 Interaction of EPS with different NP concentrations

The effect of concentration of AG1 NPs when exposed to EPS was assessed in the CR^+ treatment. As in Chapter 5, lower concentrations resulted in greater d_H detected by DLS and

NTA (but not d_s in DCS). As stated in 5.3.2. these differences likely relate to the paraffin stabiliser being diluted and stripped from the particle surface during sample creation. At lower concentrations AgNPs, more coating is removed and therefore more aggregation/agglomeration occurs. EPS may subtly affect this initial diameter distribution by interaction with the particles surfaces but this cannot be concluded from this data. Higher d_H in NTA at the lower concentration of AG1 (1mg/L) was not seen when assessing AG1 in the plain MBL. It is possible that EPS are a greater fraction of the sample suspension at lower NP concentrations and hence have a greater effect on the d_H and PSD.

6.3.4 Impact of EPS on Zeta Potential and Stability

Zeta Potential is used as a proxy for stability of particles in suspension. The results for AG1 and AG2 in all media with the exception of 1mg/L and 10mg/L in CR^+ show highly stable to moderately stable zeta potentials with minimal change in pH indicating that particles were electrostatically stable for the duration of the experiment (Figure 6-3, 6-5). As was the case in Chapter 5, the increasing ZP trend over the duration of the experiment in most treatments could be due dissolved CO_2 from contact with ambient laboratory air (a parameter that was not controlled for during these experiments). Dissolved CO_2 has been noted to make suspensions more acidic which could raise the ZP value, however the HCO_3^- ion that can be formed from dissolved CO_2 in water has been shown to cause more negative ZPs[13]. pH does not drastically change over the experiment therefore it is possible that ionic media effects, dissolved CO_2, organic matter and potential particle dissolution are all having an effect on ZP and these parameters should investigated systematically in future studies.

The hydrodynamic diameter and PSD data for AG1 and AG2 NPs indicate that by and large the particles are stable for the duration of the experiment. This agrees with the zeta potential data for 100mg/L AG1 and both concentrations of AG2 particles in all media treatments.

However, the low electrostatic stability indicated by ZPs of 1mg/L and 10mg/L AG1 samples in CR^+ (between -16->-9mV) would suggest particle aggregation should have occurred and not the stable d_H and PSD data seen for these samples.

The low ZPs at 1mg/L and 10mg/L AG1 are unexpected when exposed to the EPS as algal exudates have been shown in the literature to have strong negative zeta potentials at roughly the pH of this study (~pH7)[14,15]. Were these EPS to coat the suspended NPs, it would be expected that the negative zeta signal would become greater rather than increasing towards 0mV as the biological EPS would impart negative charge onto the particle surfaces. The close to neutral ZPs for 1-10mg/L AG1 (-16 to -9mV) in CR^+ do not reflect this. Indeed, it has been shown in the literature that positively charged NPs upon interaction with bacterial exo-polysaccharides become negatively charged with greater concentrations of EPS[16]. The lack of additional negative charge could imply that EPS concentration is too low to enact a change in the magnitude of NP surface charge, or that the interactions with the particle coatings are preventing this from occurring.

It is possible that the cause of lower ZP in these samples (AG1: 1-10mg/L) is that the paraffin coating leftover from the AG1 stock suspension is thicker than for the 100mg/L concentration sample. This is unexpected as the 100mg/L AG1 in CR^+ would in theory have a greater concentration of stabiliser present and hence a thicker coating and therefore show similar effects. However, this treatment shows greater negative ZP which suggests that the thickness of the coating after sample creation isn't purely controlled by the initial concentration of stock suspension added to the dilute media. It should be noted that the ZP of 100mg/L AG1 in MBL (Chapter 5) is more negative than in the CR^+ treatment indicating that whatever is causing the low zeta potential for 1+10mg/L in CR^+ may also be having an effect at 100mg/L. It could be that the suspended sEPS and dEPS prevent the organic stabiliser from being washed off the NPs upon sample creation and therefore enable the paraffin stabiliser to block charge from the Ag core. This may have a greater effect at lower concentrations because lower concentrations of NPs should show less overall charge and as

such is simpler to block. Furthermore, complex chemical interactions between CR^+ EPS, particle coating, particle core and the ionic media may be resulting in positive cations being generated which would raise the ZP. Despite the ZP indicating electrostatic instability (ZP close to 0mV), the unchanging PSD and d_H for 1-10mg/L AG1 in CR^+ also gives credence to AG1 particles having a steric component (also discussed in Chapter 5) to the paraffin coating allowing them to remain in suspension.

Lack of a similar effect for AG2 ZPs indicates that type of particle coating is important to NP stability. Comparable zeta potentials to plain MBL for both particles in the other EPS treatments indicate that the low concentration of sEPS and possibly dEPS are probably having little effect on these values. pH does not change drastically for any of the treatments however subtle localised effects relating to small incremental changes in pH cannot be discounted.

6.3.5 Impact of EPS on NP Stability

EPS have previously been shown to have an effect on the stability of nanomaterials in suspension. Bacterial EPS (250mg/L) stabilised 20mg/L silver nanoparticles in water over 72 hours[16] while polysaccharide brown algae exudates were seen to stabilise hematite nanoparticles[17]. Other types of natural organic matter (NOM) such as humic acids have also been shown to keep fullerene nanomaterials in suspension[18].

The ways in which EPS interact with NPs and influences their stability in liquid matrices include electrostatic, steric (gel stabilisation) as well as chemical interactions such as intermolecular bridging and ligand-complexation.

Electrostatic interactions resulting from particle coatings have been shown to result in stabilisation of NPs in suspension due to repellent charge. Coating of NPs in negatively charged EPS would likely result in repulsion and therefore continued stability. Negatively

charged suspended free EPS and NPs will also be individually susceptible to electrostatic repulsion and would be expected to repel each other preventing EPS from conferring additional stability to the particles. In this study both AG1 and AG2 and suspended EPS are likely negatively charged so it might be expected that there was repellent effect between the two. No d_s increase in the DCS data for all EPS treatments compared to plain MBL and the lack of EPS coating noted on TEM analysed primary particles indicate a lack of sEPS coating and likely repulsion between NPs and EPS. It has been found however that negatively charged particles with individual citrate and PVP coatings which should have been electrostatically repelled have adsorbed to surfaces coated with different organics (humic and fulvic acids as well as dextran to represent low molecular weight compounds) indicating that steric and hydrophobic interactions are also likely to be important for EPS-NP associations. These interactions are thought to be dependent on the types of organics and types of coating[19,20].

It has been hypothesised in the literature that rigid biopolymers such as polysaccharides and peptidoglycans produced by algae and bacteria could also induce aggregation through gel formation[21,22]. However, it was noted in an atomic force microscopy (AFM) study that Ag NPs and their aggregates joined with fibrillar polysaccharides exuded from marine diatoms and rather than altering their organic network by inducing crosslinking of proteins or altering the size of the fibrils the particles became embedded in the existing gel network and were prevented from further aggregation[23]. This effect can allow NPs to remain in suspension even if in aggregated form. The authors indicate that this embedding could relate to drying effect during sample preparation. As some TEM images for AG1 in the EPS treatments (CR^+ and CR^-) show NPs situated within biological material it may be that sEPS further contributes to particle stability by support from the gel network or this may just result from sample preparation effects (Figures 6-6a, 6-8). Other studies have also shown NP stability in a gel matrix[24] and greater stabilisation of BH_4^- coated NPs at greater ionic strengths when organic matter is present[25].

The literature indicates that interaction of ionic species such as those in MBL media and NOM is complicated, with chemical and surface charge effects coming into play. Only a few studies have investigated the interaction of surface stabilisers and suspended organics[19,26]. A major mechanism by which NOM is thought to alter NP surfaces is by complexation-ligand exchange[26]. The formation of strong covalent bonds (stronger than the N- or O- bonds that attach the particles original coating to the surface)[19,26] can occur with silver NP surfaces which result in replacement of the existing particle coatings (such as citrate or PVP) with organic molecules. Numerous studies have noted replacement of the PVP coating with NOM such as cysteine[27], hydrosulfide groups[26], humic acids[28] and fulvic acid[19]. Desorption of particle coatings is thought to cause destabilisation of the NPS. These interactions can be complex depending on the ionic makeup of the suspension media. Humic acid and Ca^{2+}, whilst showing little destabilisation separately have been shown to cause aggregation of NPs media possibly due to ion-carboxylic complexation causing changes in particle surface charge[28]. Smaller d_H values in DLS have been noted in the literature when NP coatings were replaced by organic matter[26]. In SL^+ and CR^-, AG1 DLS initial d_H values (120nm-135nm) were actually lower than seen in plain MBL (~150nm) at the same concentration (10mg/L). However, NTA results for the same treatments on AG1 gave comparable d_H values and PSDs between the two treatments and plain MBL indicating that any decrease in d_H between treatments was only present in DLS. It is likely that media composition, concentration and type of suspended material and particle coatings define the initial d_H value upon sample creation.

Even though NTA data for AG1 in CR^+ indicated a larger d_H than in SL^+ and CR^- treatments (and plain MBL), it did show a decrease in d_H over the experiment duration at both 1mg/L and 10mg/L concentrations (Table 6-2a, b). This decrease could relate to coating being desorbed and replaced with organic material. A similar effect was not noted in any other characterisation technique but it is possible that they cannot detect these subtle effects.

For AG1 and AG2 particles in ionic MBL media with EPS, there was no definitive evidence for instability therefore it is unlikely that particle-ligand complexation caused by EPS is occurring to the extent that destabilisation would occur. This could relate to a number of factors. The concentration of both the EPS and the multivalent ions in the media are possibly too low to elicit a reaction of sufficient energy or quantity to cause aggregation. It is also very likely that the particles coatings are providing a strong stabilising effect which will mitigate any destabilising reactions from EPS. Bridging reactions in Liu et al.[28] were stated to have caused aggregation of EPS-coated NPs however in this study no conclusive evidence was seen that EPS had coated the NPs. TEM data showed no obvious biological coating in the majority of images while DCS data seem to indicate no difference in d_s from plain MBL. Results from the light scattering techniques cannot conclusively state that an increase in d_H has occurred owing to their potential for skewing to larger sizes. If EPS are not coating the particles it is likely that any bridging reactions between OM and ionic species in the media are not affecting the particles leaving them stable in suspension.

6.3.6 Impact of EPS composition

Algal and cyanobacterial EPS have been shown to consist of a number of different constituents with varying molecular weights including proteins, lipids, nucleic acids and polysaccharides of which the latter is thought to be the major component[19]. Indeed the composition of EPS will influence the interaction with coated particle surfaces as it will determine which of molecules are most likely to come into contact with the surface. Yang et al.[26] noted that humic acid and cysteine increased electro-phoretic mobility and replaced PVP coating on Ag NPs. Lau et al.[19] also noted particle coatings were influential with fulvic acid having different levels of effect on citrate coated AgNPs and PVP coated NPs after analysis using NMR relaxation rates. It has been stated that stress imparted onto microorganisms can result in different levels and composition of EPS[2].

Paraffin-coated AG1 and citrate+PVP coated AG2 particles indicated no obvious change in stability when exposed to stressed green algae, unstressed green algae and cyanobacteria EPS over the duration of the experiment in media of 5.53mM ionic strength. The results obtained about the type and levels of EPS in this study are discussed in Chapter 7. SL^- EPS were not able to be analysed but it was noted that CR^- (created using 5µg/L $AgNO_3$ stressor) and CR^+ EPS exhibited little difference in composition with the majority of the EPS being high molecular weight organics (Figure 7-9). Therefore the lack of compositional difference between the two treatments of EPS may be a factor in the lack of detectable difference between each media treatment. High molecular weight organics such as humic acid have been shown to promote stability[26] therefore the CR^+ and CR^- EPS may be promoting stability however the influence of this in relation to concentration and particle coatings was not analysed and cannot be confirmed.

6.3.7 Environmental Implications

With both AG1 and AG2 particles showing stability in the presence of algal and cyanobacterial EPS it is likely that these particles would remain in a bioavailable form to microorganisms in an eco-toxicity exposure. Agglomeration of particles has been shown to result in less toxicity owing to a number of factors including less available surface area for interaction and larger particles being unable to enter the algal cell wall.

The behaviour of NPs in aquatic environments especially with algal EPS and general organic matter present requires much more study, especially into the fundamental mechanisms of attachment and surface interactions of each component of the EPS. This is necessary to truly understand the fate of nanomaterials in the environment as these interactions will govern the probability of a particle remaining in a bioavailable form and hence will determine the particle's fate[21]. In greater ionic strengths and organic matter concentrations present in

the environment it is possible that stripping of particle coatings could occur resulting in less particle stability. However in some cases, particles may remain in suspension owing to steric interaction with fibrillar OM. Stability over the 2 week time frame of this experiment indicates that particles may remain in a form dangerous to microorganisms for a substantial period. Dissolution may also be important as the ability of the particle to release ions will also impact on bioavailability and toxicity. The presence of EPS can mitigate toxic effects from ions[29].

6.4 Conclusions

Table 6-7. Summary of conclusions from each technique for AG1 and AG2.

Particle	DLS	NTA	DCS	TEM	Overall
AG1 **(in CR^+, SL^+, CR^-)**	PSD and d_H constant for all media treatments. CR^+ gives larger d_H than other treatments.	PSD constant for all media treatments. d_H unchanging in CR^- and SL^+. CR^+ shows larger and variable d_H	PSD constant for all media treatments.	No significant increase in primary particle size, cluster size or aspect ratio. %age of clusters as aggregates increases after 2 weeks (note. Chapter 5 indicates plain MBL media also increases number of aggregate clusters to a greater extent than EPS treatments)	Greater EPS concentration in CR^+ likely affecting DLS/NTA measurements. All EPS treatments may be affecting clusters over time but less so than plain ionic MBL media. More work needed to detect subtle changes.
AG2 **(in CR^+, SL^+, CR^-)**	Constant PSD and d_H for all treatments. CR^+ gives larger d_H than other treatments	Constant PSD and d_H for all treatments. Low NTA size values likely due to PVP micelles	Constant PSD and ds for all treatments	No significant increase in primary particle size, cluster size and aspect ratio. No increase in aggregates as %age of total clusters measured.	EPS not seen to affect AG2 particles with these techniques as size is constant. Larger size in CR^+ in DLS may relate to greater EPS concentration but requires more investigation

An overview of the particle behaviour in each technique is given in Table 6-7. The techniques DLS, NTA, DCS and TEM were on the whole able to detect general stability trends for both AG1 and AG2 particles. However subtle effects due to the presence of EPS were unable to be conclusively identified. The effects due to larger suspended EPS (sEPS) and dissolved EPS (dEPS) were unable to be discerned using this suite of techniques and more investigation is needed to understand the effect each of these types of organic matter has on particles behaviour.

The high stability of both AG1 and AG2 particles for the duration of the experiment is likely due to a number of reasons. Most likely the strength of particle coatings with both electrostatic and steric components is providing stabilisation. The concentration of EPS is likely to be too low to be having a major effect on the stability. However, it is possible that some displacement of both coatings was occurring as EPS could potentially displace the paraffin or citrate-PVP coatings through covalent interactions. If stripping of either coating is occurring, it is not occurring at such a magnitude to alter the stability of the particles. The double stabilising effect of citrate and PVP for AG2 is likely too great to allow organics to interact with the silver surface while the paraffin coating of AG1 likely defines the initial d_H during creation of the sample but owing to the stability of the particle does not change drastically over the experiment duration. Concentration of each of the components (EPS, ionic species in the media, particle surface stabiliser) is hence important and further study would result in investigating these properties and constraining them before attempting a similar experiment. Dissolution was not assessed in this chapter and some particles may show morphological changes however the techniques used in this study were unable to detect any conclusive trends. This is investigated in Chapter 7.

6.5 References

1. McIntyre, a M. & Guéguen, C. Binding interactions of algal-derived dissolved organic matter with metal ions. *Chemosphere* **90,** 620–6 (2013).

2. Ozturk, S. & Aslim, B. Modification of exopolysaccharide composition and production by three cyanobacterial isolates under salt stress. *Environ. Sci. Pollut. Res.* **17,** 595–602 (2010).

3. Unrine, J. M., Colman, B. P., Bone, A. J., Gondikas, A. P. & Matson, C. W. Biotic and abiotic interactions in aquatic microcosms determine fate and toxicity of Ag nanoparticles. Part 1. Aggregation and dissolution. *Environ. Sci. Technol.* **46,** 6915–24 (2012).

4. Bone, A. J. *et al.* Biotic and abiotic interactions in aquatic microcosms determine fate and toxicity of Ag nanoparticles: part 2-toxicity and Ag speciation. *Environ. Sci. Technol.* **46,** 6925–33 (2012).

5. Wilkinson, K. J., N, J. & Buffie, J. Coagulation of colloidal material in surface waters : the role of natural organic matter. *J. Contam. Hydrol.* **26,** 229–243 (1997).

6. Kim, J. S. *et al.* Antimicrobial effects of silver nanoparticles. *Nanomedicine Nanotechnology, Biol. Med.* **3,** 95–101 (2007).

7. Soldo, D., Hari, R., Sigg, L. & Behra, R. Tolerance of Oocystis nephrocytioides to copper: intracellular distribution and extracellular complexation of copper. *Aquat. Toxicol.* **71,** 307–17 (2005).

8. Chen, P., Powell, B. a, Mortimer, M. & Ke, P. C. Adaptive interactions between zinc oxide nanoparticles and Chlorella sp. *Environ. Sci. Technol.* **46,** 12178–85 (2012).

9. Nichols, H. W. in *Handb. Phycol. Methods* (ed. Stein, J. R.) 16–17 (Cambridge University Press, 1973). at <http://www.marine.csiro.au/microalgae/methods/Media CMARC recipes.htm#MBL>

10. OECD. Test No 201: Freshwater Alga and Cyanobacteria, Growth Inhibition Test. *OECD Guidel. Test. Chem.* **Section 2,** 25 (2011).

11. PROSPECT. Protocol for Nanoparticle Dispersion. (2010). at <http://www.nanotechia.org/sites/default/files/files/PROSPECT_Dispersion_Protocol.pdf>

12. Fatisson, J., Quevedo, I. R., Wilkinson, K. J. & Tufenkji, N. Physicochemical characterization of engineered nanoparticles under physiological conditions: effect of culture media components and particle surface coating. *Colloids Surf. B. Biointerfaces* **91,** 198–204 (2012).

13. Wang, N., Hsu, C., Zhu, L., Tseng, S. & Hsu, J.-P. Influence of metal oxide nanoparticles concentration on their zeta potential. *J. Colloid Interface Sci.* **407,** 22–8 (2013).

14. Henderson, R. K., Baker, A., Parsons, S. a & Jefferson, B. Characterisation of algogenic organic matter extracted from cyanobacteria, green algae and diatoms. *Water Res.* **42,** 3435–45 (2008).

15. Planchon, M. *et al.* Influence of exopolysaccharides on the electrophoretic properties of the model cyanobacterium Synechocystis. *Colloids Surf. B. Biointerfaces* **110,** 171–7 (2013).

16. Khan, S. S., Mukherjee, A. & Chandrasekaran, N. Impact of exopolysaccharides on the stability of silver nanoparticles in water. *Water Res.* **45,** 5184–90 (2011).

17. Chen, K. L. & Elimelech, M. Influence of humic acid on the aggregation kinetics of fullerene (C60) nanoparticles in monovalent and divalent electrolyte solutions. *J. Colloid Interface Sci.* **309,** 126–134 (2007).

18. Chen, K. L. & Elimelech, M. Aggregation and deposition kinetics of fullerene (C60) nanoparticles. *Langmuir* **22,** 10994–1001 (2006).

19. Lau, B. L. T., Hockaday, W. C., Ikuma, K., Furman, O. & Decho, A. W. A preliminary assessment of the interactions between the capping agents of silver nanoparticles and environmental organics. *Colloids Surfaces A Physicochem. Eng. Asp.* **435,** 22–27 (2013).

20. Huynh, K. A. & Chen, K. L. Aggregation kinetics of citrate and polyvinylpyrrolidone coated silver nanoparticles in monovalent and divalent electrolyte solutions. *Environ. Sci. Technol.* **45,** 5564–71 (2011).

21. Quigg, A. *et al.* Direct and Indirect Toxic E ff ects of Engineered Nanoparticles on Algae: Role of Natural Organic Matter. *ACS Sustain. Chem. Eng.* **1,** 686–702 (2013).

22. Buffle, J., Wilkinson, K. J. & Stoll, S. A Generalized Description of Aquatic Colloidal Interactions : The Three-colloidal Component Approach. *Environ. Sci. Technol.* **32,** 2887–2899 (1998).

23. Pletikapić, G., Žutić, V., Vrček, I. V. & Svetličić, V. Atomic force microscopy characterization of silver nanoparticles interactions with marine diatom cells and extracellular polymeric substance. *J. Mol. Recognit.* **25,** 309–317 (2012).

24. Planchon, M. *et al.* Exopolysaccharides protect Synechocystis against the deleterious effects of titanium dioxide nanoparticles in natural and artificial waters. *J. Colloid Interface Sci.* **405,** 35–43 (2013).

25. Delay, M., Dolt, T., Woellhaf, A., Sembritzki, R. & Frimmel, F. H. Interactions and stability of silver nanoparticles in the aqueous phase: Influence of natural organic matter (NOM) and ionic strength. *J. Chromatogr. A* **1218,** 4206–12 (2011).

26. Yang, X., Lin, S. & Wiesner, M. R. Influence of natural organic matter on transport and retention of polymer coated silver nanoparticles in porous media. *J. Hazard. Mater.* **264,** 161–168 (2014).

27. Gondikas, A. P. *et al.* Cysteine-Induced Modifications of Zero-valent Silver Nanomaterials: Implications for Particle Surface Chemistry, Aggregation, Dissolution, and Silver Speciation. *Environ. Sci. Technol.* **46,** 7037–7045 (2012).

28. Liu, X., Jin, X., Cao, B. & Tang, C. Y. Bactericidal activity of silver nanoparticles in environmentally relevant freshwater matrices : Influences of organic matter and chelating agent. *J. Environ. Chem. Eng.* **2,** 525–531 (2014).

29. Miao, A.-J. *et al.* The algal toxicity of silver engineered nanoparticles and detoxification by exopolymeric substances. *Environ. Pollut.* **157,** 3034–41 (2009).

Chapter 7. Mechanisms of Silver Nanoparticle Toxicity to Green Algae and Cyanobacteria Species

7.1 Introduction

Aquatic microorganisms such as algae and cyanobacteria play an important role in nutrient cycling and the health of freshwater ecosystems. They are amongst the most sensitive species to toxicants and as such they often drive risk assessment and fate studies[1]. Predicted levels of nanosilver in the environment have been placed at 0.01-80ng/L[2] for surface waters and up to 127ng/L for effluent from wastewater treatment plants (WWTP)[3,4] while experimental evidence for WWTP effluents have placed values at an average of 100ng/L[5,6].This value is only likely to increase with currently increasing production of silver containing products[7].

Toxicity of engineered nanoparticles (NPs) has been noted in numerous studies and greater concentrations will likely result in higher risks to organisms. As well as concentration, the form of silver NPs aquatic organisms encounter is important. Size, stability, morphology, aggregation state, composition of surrounding medium, suspended material concentration/composition and dissolution are all likely to play a role in determining toxicity. It is important to delineate the effects of these properties to understand the mechanisms through which nanomaterials impart toxicity.

7.1.1 Aims and Objectives

This study investigated the extent of toxicity of two types of coated Ag NPs (AG1: 3-8nm primary particles stabilised by an organic paraffin coating, AG2: ~50nm particles stabilised

by both PVP and citrate) to one green algae species (*Chlamydomonas reinhardtii*) and one cyanobacterial species (*Synechococcus leopoliensis*) using flow cytometry (FC). The effect was compared to that of ionic silver ($AgNO_3$) to separate the effects of ionic and nanoparticulate silver. With this in mind, the dissolution levels of the two particles were also measured over the duration of the experiment to try and delineate effects of ionic silver produced by nanoparticle dissolution from that of just the nanoparticles.

Furthermore, fluorescence markers were used to investigate specific cellular endpoints to gain an understanding of the mechanisms involved in nanoparticle toxicity to the algal population growth rates. Fluorescein diacetate (FDA) was used to detect cellular viability (i.e. direct killing of the cells), while Hydroethidium (HE) and Dichlorofluorescein (DCF) were used to detect sublethal effects in terms of reactive oxygen species (ROS) production by the test organisms.

Through these methods the aims were to first gauge the toxicity of two manufactured silver NPs with different intrinsic properties, one of which AG1 is used in industry and is such a realistic 'real world' sample and one model particle, AG2 which was synthesized for eco-toxicology studies. Second was to understand the causes and mechanisms of toxicity linked to specific properties of particles using fluorescence indicators and analytical dissolution data. Finally species specific responses to toxicants were also recorded such as production of extracellular polymeric substances (EPS) which will add to the growing database of nano-ecotoxicology.

7.2 Materials and Methods

7.2.1 Toxicants:

Alkane coated Ag-NPs (AG1) and Citrate/PVP stabilised Ag-NPs (AG2) as described in Chapter 3 were used in conjunction with silver nitrate ($AgNO_3$) powder dissolved in Milli-Q water as ionic silver control for fluorescence experiments.

7.2.2 Preparation of Samples:

The effect of each toxicant on both species was assessed by exposing the organism to a range of concentrations of each stressor (AG1, AG2, $AgNO_3$) over 72 hours according to a modified version of the OECD 201 Guideline[8] described in Chapter 3. Samples were created by addition of 9ml of dosed MBL Woodshole medium to 1ml algal culture (prepared as described in 3.3.7.3.). Growth rate inhibition was calculated as described below (7.2.5.)[8]

Fluorescence samples were created according to 3.3.5.6. Algal culture (6ml) was exposed to the growth rate EC_{70} concentration (concentration at which 70% inhibition of growth occurs) of each toxicant for 30-40 minutes before addition of fluorescent stains: Fluorescein diacetate (FDA), Hydroethidium (HE) and Dichlorofluorescein (DCF), and subsequent equilibration time (described in Table 3-11). Each experiment was repeated three times to ensure reproducibility of the results with H_2O_2 used as a positive control to test the efficacy of the stains.

7.2.3 Analytics Experiments

Levels of dissolved silver released by the NP samples were measured to give greater insight into toxic effect of particles vs. that of ions. Total and dissolved silver was analysed for both AG1 and AG2 at two nominal concentrations at 0 hours and 72 hours in each microorganism

culture using Atomic Absorption Spectroscopy (AAS) (see Chapter 3 for description). Nominal concentrations used are given in Table 7-2 along with the measured total and dissolved values. Nominal concentrations were taken from early EC_{20} and EC_{50} values estimated by eye (Fitting curves to the dose-response experiments (7.2.4.) resulted in different values in the final data set: Table 7-3). Nominal concentrations of Ag NPs added to the cultures were compared with measured total silver concentrations in Figure 7-4. The dissolved silver measurements as a percentage of the total silver concentrations are shown in Figure 7-5. Samples were prepared as described in 3.3.7.5. Charts for the analytical data (Figure 7.4 and 7.5) were plotted using OriginPro 9.1.

7.2.4 Dose-response Curves

1ml of each sample was measured using flow cytometry (FC) as described in 3.2.8.3. Dot plots of FL4 detection channel auto-fluorescence (*C.reinhardtii*) and FL1 detection channel auto-fluorescence (*S.leopoliensis*) both against side scatter (SS) were employed to measure the algal populations. Numeric values were obtained by gating the area around an expected algal population on each dot plot using the FC software and recording the counts. An example is shown in Figure 7-1. Decreases in population density were assessed from the differences in measured cell numbers within that area.

7.2.5 Growth inhibition calculations

Using an adapted OECD 201 guideline[8] the growth rate inhibition of the green algae and cyanobacteria were calculated. Percentage growth rate inhibition was measured as the percentage difference between the control growth rate and sample growth rate as calculated

from changes in cell density between cultures exposed to a toxicant and that of an untreated control. Full method is described in 3.3.7.2.

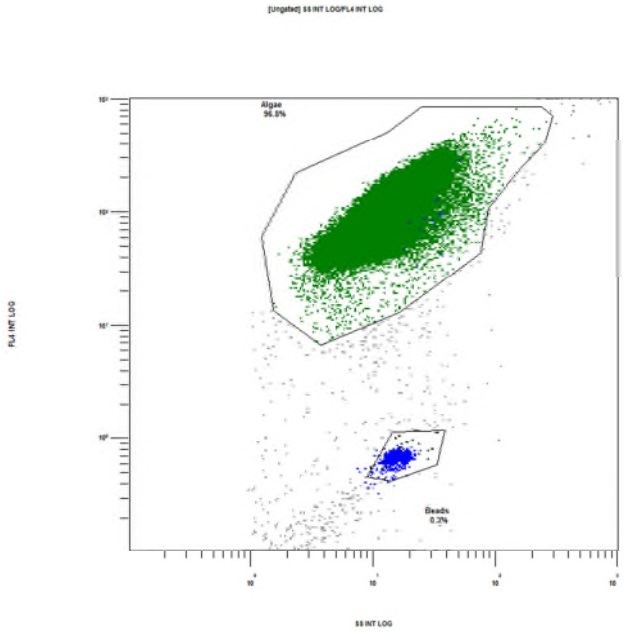

Figure 7-1. FL4 vs. SS dot plot for *C.reinhardtii* sample. Green area is the green algae population while the blue area shows the population of fluorescent beads added to sample for calibration. Software measures the number of algae within each gate.

7.2.6 Dose Response Curves Data Analysis

Growth rate inhibition against toxicant concentration curves were plotted using R (an example is shown in Figure 7-2). A log-logistic four parameter curve was fitted to each plot to obtain EC_x values using the *drc* R package[9,10] (equation 7-1). EC_{20}, EC_{50} and EC_{70} of each toxicant for each species are given in Table 7-3.

$$f(x,(b,c,d,e)) = c + \frac{d-c}{1+exp\{b(log(x)-log(e))\}}$$

Equation 7-1 – log-logistic four parameter curve with parameters *b,c,d,e.* The four parameters (*b,c,d,e*) were the EC_x value (*e*) which is the dose-response half-way between the upper limit (*d*) and the lower limit (*c*) with (*b*) giving the relative slope around (*c*).

7.2.7 Fluorescence Experiments

Mechanistic toxicity experiments using fluorescent stains were also undertaken using flow cytometry. Fluorescent stains were introduced to cultures exposed to each toxicant for a specific equilibration time. Counts were obtained of populations within a pre-defined gated area. FDA and DCF stained samples were plotted on a FL1 vs. SS dot plot while HE was plotted on FL2 vs. SS dot plots.

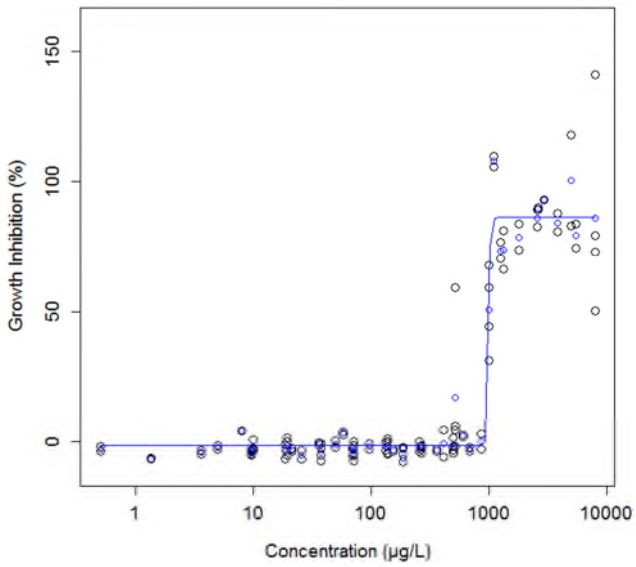

Figure 7-2. Example dose-response curve plotted in R. Growth rate inhibition (%) caused by AG1 on *C.reinhardtii* against concentration in µg/L. The data set was assembled from repeat growth inhibition ecotoxicology experiments over a range of different concentrations. Each data point was normalised to the mean growth rate control group from its own experiment (control: n=3). Values below 0% and above 100% arise due to inter-replicate growth rate variability within the control group.

For each measurement the 'non-stressed' control population exposed to the stain was gated and the level of response was gauged by movement of the population out of the pre-defined gate (Figure 7-3). The population in the 'non-stressed' control gate or the 'stressed' gate were plotted as a percentage against the total cells measured to assess the effect of each toxicant on the endpoints defined by the stains (cell viability and ROS generation). Each

experiment (individual algal population) had three replicates and experiments were repeated a minimum of 3 times to create the data set. The efficacy of each stain was tested using a H_2O_2 positive control (data not shown but example in Figure 7-3).

7.2.8 Fluorescence Experiments Data Analysis

Each data set is shown in bar plots with error bars of one standard deviation plotted using Microsoft Excel (Figures 7.6, 7.7, 7.8).

Significant differences between each treatment and the control in a data set were analysed using the raw stressed and unstressed alga count data rather than percentages. The ratios of stressed to unstressed alga for each treatment were natural log-transformed and compared to the control using a linear model. The p-values indicate the probability that no relationship exists between the treatment and the control with p-values below 0.05 indicating significance and therefore likely a difference between the variables. Significant differences from the control were indicated on the bar charts with asterisks. Table 7-4 indicates the p-values for each treatment against the control for each stain for both species.

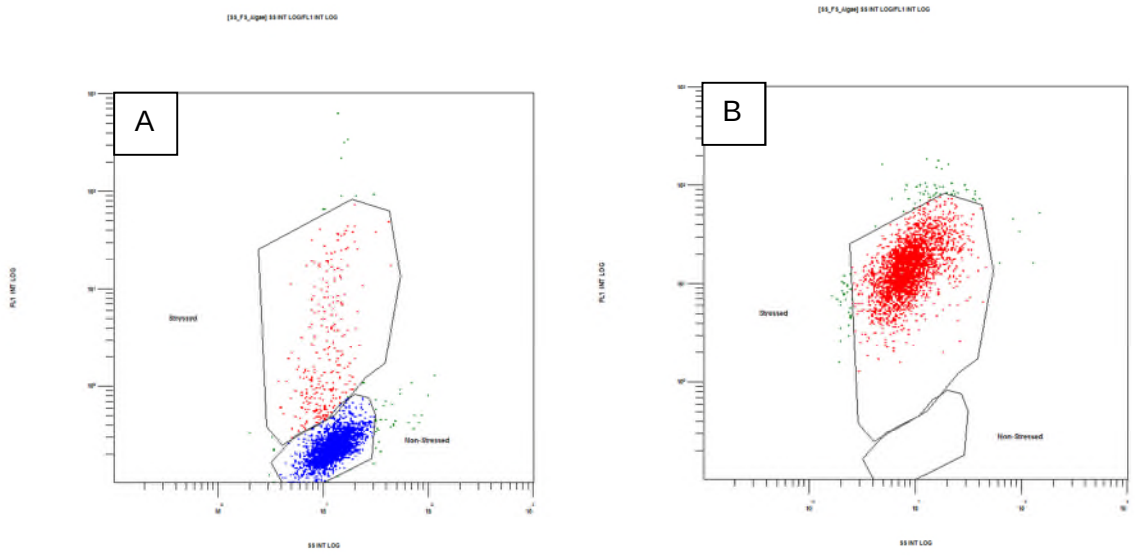

Figure 7-3. Dot plots of FL1 detected auto-fluorescence vs. Side scatter (SS) obtained by flow cytometry showing a control population stained using FDA (A) and the effect of H_2O_2 on the population (B).

7.2.9 Exudates Analysis

Algal extracellular polymeric substances (EPS) were analysed using liquid chromatography-organic carbon detection-organic nitrogen detection (LC-OCD-OND), a type of size-exclusion chromatography (SEC) which works by separating different organic fractions based upon their retention times in a column[11]. Higher molecular weight (MW) organics leave the column faster than lower molecular weight materials and as such have lower retention times. Sample preparation is described in 3.3.7.6 with the exposure doses for each toxicant for each species stated in Table 7-1. Samples were processed in a manner similar to Stewart et al.[11] in which different molecular weight classes were identified via retention time from a chromatogram. The signal intensity for each retention time grouping (molecular weight class) for the *C.reinhardtii* exposures is indicated in Figure 7-9.

Table 7-1. Concentrations (µg/L) used for each toxicant for EPS characterisation studies for both species.

Toxicant	Concentration (µg/L)	
	C.reinhardtii	*S.leopoliensis*
AG1	300	5, 969
AG2	600	1624, 2500
$AgNO_3$	9.2	5, 23

7.3 Results

7.3.1 Total and Dissolved Silver

Table 7-2. Total and Dissolved silver levels (mean ± 1SD, *n=2*) at Control, EC_{20} and EC_{50} values at the start and end of algae toxicity test for AG1 and AG2 particles for both *C.reinhardtii* and *S.leopoliensis*.

Species	Particle	Nominal Concentration (µg/L)	Total Silver (µg/L)		Dissolved Silver (µg/L)	
			0h	72h	0h	72h
C.reinhardtii	n/a	Control	-0.203 (±0.093)	-0.312 (±0.0375)	0.058 (±0.190)	-0.303 (±0.0863)
	AG1	700	41.093 (±1.524)	46.9 (±2.051)	5.754 (±1.797)	34.075 (±2.355)
		800	34.305 (±1.428)	46.79 (±0.495)	7.259 (±0.180)	37.045 (±3.698)
	AG2	1500	96.48 (±99.165)	170.55 (±141.634)	1.461 (±0.167)	17.866 (±19.876)
		1700	31.88 (±1.280)	837.275 (±525.699)	3.345 (±2.490)	4.921 (±1.153)
S.leopoliensis	n/a	Control	0.03 (±0.0226)	-0.294 (±0.010)	0.178 (±0.463)	-0.244 (±0.0368)
	AG1	97	34.46 (±0.113)	28.59 (±2.284)	0.765 (±0.0078)	-0.123 (±0.081)
		225	41.978 (±0.0177)	54.575 (±0.672)	1.733 (±0.019)	2.305 (±3.338)
	AG2	502.5	56.775 (±3.995)	96.75 (±23.193)	1.501 (±0.649)	-0.123 (±0.081)
		1100	61.625 (±1.803)	103.425 (±14.602)	1.277 (±0.215)	9.857 (±2.776)

AAS was used to measure the total silver levels present in algal and cyanobacterial cultures after addition of AG1 and AG2 NPs at 0 hours and 72 hours. Values for total silver are shown in Table 7-2. Values were also plotted against nominal concentrations to show the difference in recovery in both cultures (Figure 7-4). Total silver levels of both NPs obtained from both *C.reinhardtii* and *S.leopoliensis* cultures at both 0 and 72 hours are much lower than nominal concentrations introduced to the cultures. Measured total silver concentrations were all roughly equal regardless of the nominal concentration level with the exception of AG2 1500µg/L values and AG2 1700µg/L at 72h in *C.reinhardtii* cultures which were higher. Total silver in controls for both cultures were below AAS detection limits.

Measured total silver, as well as being much lower than the nominal values, also showed variation over the duration of the experiment. All total measured silver values with the exception of AG1 700µg/L in *C.reinhardtii* cultures, AG1 97µg/L in *S.leopoliensis* cultures and controls showed an increase between 0 hours and 72 hours (Figure 7-4a,b). The largest differences were seen for AG2 in *C.reinhardtii* cultures in the 1500µg/L sample and particularly in the 1700µg/L sample (Figure 7-4a). These increases likely relate to issues during sample preparation, such as additional sample transfer steps which were not always controlled, resulting in retention of silver by the plastic container. High analytical variability between small numbers of samples (n=2) may also be responsible for these differences.

Dissolved silver levels were also assessed using AAS after ultrafiltration of the same samples measured for total silver. Dissolved silver levels are shown in Table 7-2 and the percentage of the total measured silver signal in the form of dissolved silver at 0h and 72h of the experiment are shown in Figure 7-5.

In *C.reinhardtii* cultures, AG1 dissolved silver levels were between 10-20% at 0h for both concentrations (700µg/L and 800µg/L) and increase dramatically at 72h to ~70-75% (Figure 7-5a). For AG2 particles dissolved silver was low for both concentrations (1500µg/L and 1700µg/L) at 0h and 72h with no conclusive trend (Figure 7-5a). In *S.leopoliensis* cultures dissolved silver levels at all concentrations and for both particles were low (0-10% of total measured silver) at both 0h and 72h (Figure 7-5b).

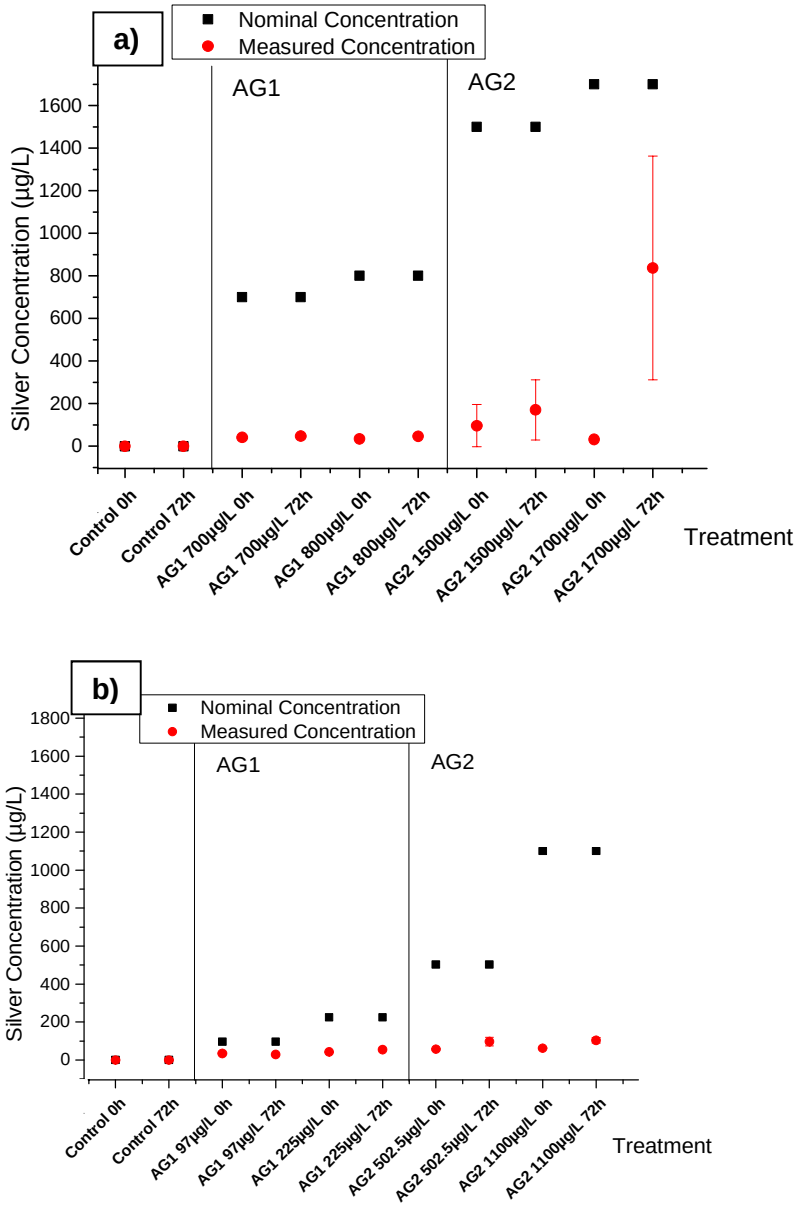

Figure 7-4. Nominal Vs. Measured Total silver concentrations for all treatments in a) *C.reinhardtii* cultures and b) *S.leopoliensis* cultures at T=0h and 72h. Values shown in Table 7-2 (Measured Values: mean ± 1SD, *n=2*).

7.3.2 Toxicity of AgNPs and $AgNO_3$

EC_x is the concentration at which X% of the culture analysed has been affected with respect to a particular endpoint. The EC_{20}, EC_{50} and EC_{70} values of each toxicant are displayed in Table 7-3 to show both the magnitude of toxicity of each toxicant to each species and also to give an idea of the steepness of the dose-response curves, which could indicate a difference

in toxic mechanism involved. For both species $AgNO_3$ was more toxic than both NPs, and there was no difference in the sensitivity to $AgNO_3$ between *C.reinhardtii* and *S.leopoliensis*. However, while for *S.leopoliensis* the $AgNO_3$ was roughly 2-3 times more toxic than both AG1 and AG2 based on EC_{50} (with little difference between the two NPs) then for *C.reinhardtii* the toxicity of AgNPs were 20-50 times lower than that of $AgNO_3$ and AG1 appeared twice as toxic as AG2, demonstrating species specific and NP specific effects. Furthermore, the data indicated that *C.reinhardtii* response curves for all toxicants were steeper than for *S.Leopoliensis.* For *C.reinhardtii,* AG1 and $AgNO_3$ curves were comparable and steeper than AG2 while for *S.leopoliensis* the AG1 curve was steeper than $AgNO_3$ and both were steeper than AG2 (Table 7-3).

7.3.2.1 Cell Viability

Cell viability was assessed using the FDA stain. Data is shown in Figure 7-6. Even in healthy control cultures there were a number of cells which fell ouside of the non-stressed gate during flow cytometry which results in the deviation of the control samples from 100% (Figure 7-6). Data for *C.reinhardtii* indicated that each treatment had a similar effect on the % viable cells with a decrease in ~20-30% for each treatment compared to the total measured cell count (Figure 7-6a). All three treatments also had a significant effect on cell viability compared to the control (Table 7-4) for *C.reinhardtii.* Values *for S.leopoliensis* were different. $AgNO_3$ showed ~75% decrease in viability compared to the control while AG1 indicate a ~10% decrease from control, both significant, while AG2 showed no significant effect (Figure 7-6b and Table 7-4).

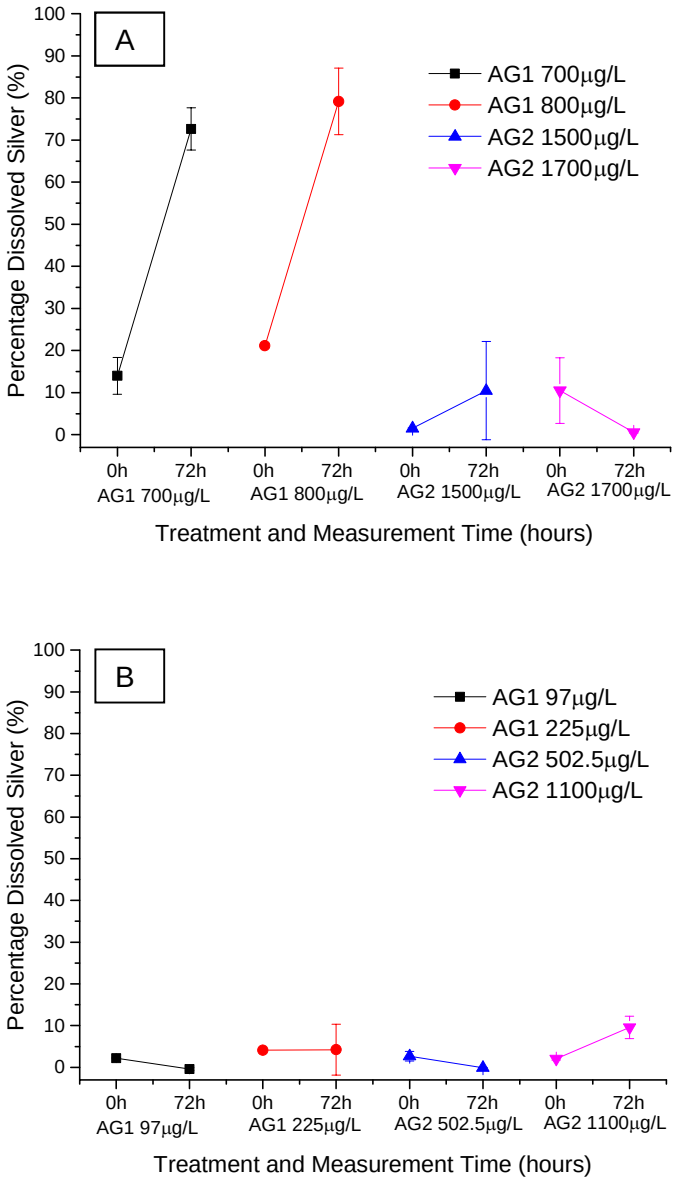

Figure 7-5. Dissolved silver as a percentage of total measured silver concentrations for all treatments in A) *C.reinhardtii* cultures and B) *S.leopoliensis* cultures at T=0h and 72h. Mean ± 1SD (*n=2*).

Table 7-3. EC_{20}, EC_{50}, EC_{70} values for each toxicant exposed to both species. Values are estimated from fitting a log-log 4 parameter fit to dose response data sets. Data sets were assembled from independent growth inhibition ecotoxicology experiments with two replicates per concentration concentrations. EC_x values given as nominal dose ± 1 standard error

N= number of experiments used to create curve, n=total number of data points used to create curve, R=replicates within each experiment. *C.reinhardtii* AG1: N=7, n=111, R=2. AG2: N=4, n=64, R=2, $AgNO_3$: N=6, n=48, R=2. S*.leopoliensis* AG1: N=6, n=94, R=2. AG2: N=6, n=93, R=2. $AgNO_3$: N=3, n=43, R=2.

	C. reinhardtii			***S. leopoliensis***		
EC_x	AG1 [µg/L]	AG2 [µg/L]	$AgNO_3$ [µg/L]	AG1 [µg/L]	AG2 [µg/L]	$AgNO_3$ [µg/L]
20	970 ± 23.4	1624 ± 180	24 ± 5.8	95 ± 23.3	33 ± 19	9.3 ± 5
50	993 ± 7	1819 ± 62	43 ± 7.7	164 ± 27	184 ± 59.8	66.9 ± 65
70	1008 ± 7	1950 ± 117	63 ± 13	228 ± 53	531 ± 267	223 ± 342

7.3.3 Fluorescence Data

Table 7-4. P-values for comparison of log-transformed ratios of stressed to unstressed algal populations against the control for each treatment (EC_{70} level exposures of AG1, AG2 and $AgNO_3$) and species using a linear model. Values indicate the likelihood that no relationship exists between the treatments. Asterisks indicate the significance of the relationship: no asterisk is no significance (≥0.05), '*' is low significance (≤0.05), '' is moderately significant (≤0.01), '***' is highly significant (≤0.001).**

Species	***C.reinhardtii***			***S.leopoliensis***		
	p-values					
	Stain			**Stain**		
Treatment (Endpoint)	FDA (Cell Viability)	HE (ROS)	DCF (ROS)	FDA (CELL VIABILITY)	HE (ROS)	DCF (ROS)
AG1	1.40e-10 ***	0.0940	0.0655	0.00597 **	0.001964 **	0.0139 **
AG2	4.28e-09 ***	0.75376	0.7780	0.06039	0.1114885	0.16605
$AgNO_3$	2.38e-10 ***	0.00151 **	3.08e-09 ***	<2e-16 ***	0.000583 ***	0.04060 *

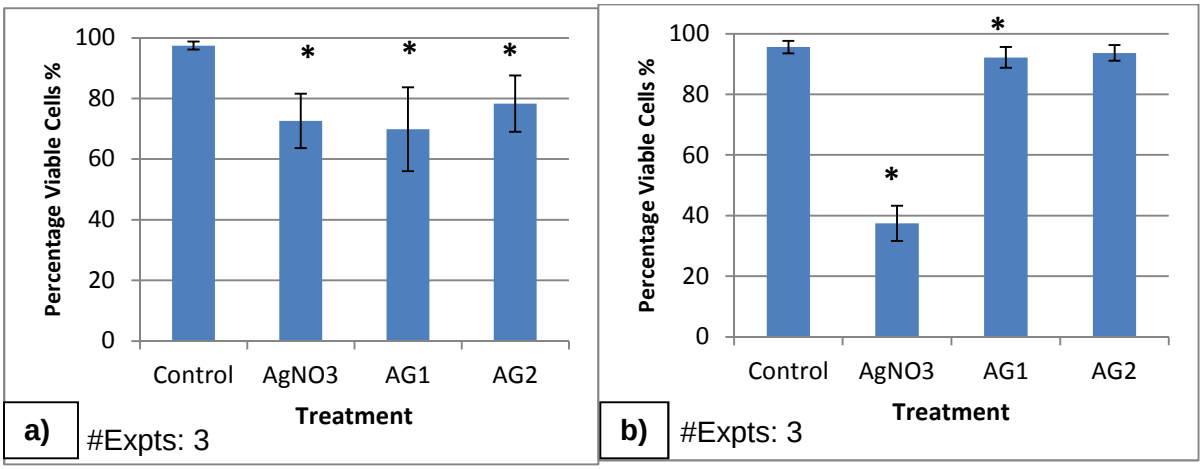

Figure 7-6. Percentage viable cells of measured population when exposed to EC_{70} $AgNO_3$, AG1 and AG2 for a) *C.reinhardtii* cultures and b) *S.leopoliensis* cultures. Means +/- 1SD for the means of 3 replicates for 3 experiments. Asterisks indicate significant effect compared to the control.

7.3.3.1 Reactive Oxygen Species

Both HE and DCF stains detect ROS production in cells (as intracellular hydrogen peroxide and superoxides respectively). As with cell viability, the control value deviated from 0% ROS because even in healthy cultures some cells fall into the stressed gate (Figure 7-7, Figure 7-8).

In the HE experiments (Figure 7-7a) for *C.reinhardtii*, $AgNO_3$ showed the highest production of ROS (~30%) which was significantly higher than the controls and both AG1 and AG2 NPs (~10-20%). AG1 had a greater effect, although neither NP showed significantly different results from the controls. HE results for *S.leopoliensis* indicated little ROS was produced for any toxicant but $AgNO_3$ and AG1 produced the most (~10%) and were significant compared to the control (Figure 7-7b). Again, AG2 produced no significant difference from the controls. The order of effect for both species went $AgNO_3$>AG1>AG2.

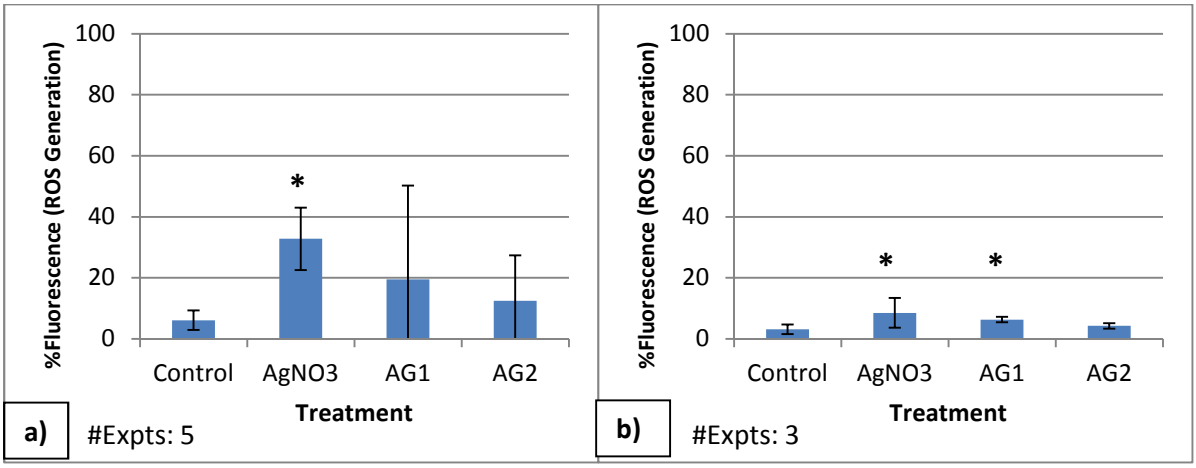

Figure 7-7. Percentage HE fluorescence (ROS detection) of measured population when exposed to EC_{70} $AgNO_3$, AG1 and AG2 for a) *C.reinhardtii* cultures and b) *S.leopoliensis* cultures. Means +/- 1SD for the means of 3 replicates for 5 experiments (*C.reinhardtii*) and 3 experiments (*S.Leopoliensis*) respectively. Asterisks indicate significant effect compared to the control.

DCF stain is used to measure superoxide ROS and can prove a useful counterpoint to the HE stain. DCF *C.reinhardtii* exposures indicated that as with HE, $AgNO_3$ resulted in significantly greater ROS effect than the controls, while the effects seen in the AgNPs were much lower. AG1 was seen to have a greater effect than AG2 but both were not significantly different to the controls (Figure 7-8a, Table 7-4). For the cyanobacteria experiments only a small amount of (<20%) ROS was produced for any of the toxicants. While AG1 produced more ROS than AG2, and both produced more than the controls, only the difference between the AG1 and controls was significantly different (Figure 7-8b, Table 7-4). Contrastingly, the $AgNO_3$ results for *S.leopoliensis* showed a significantly lower HE ROS value than the control (Figure 7-8b, Table 7-4). This lower value was not likely due to lower ROS production by the stressed alga cells, but more likely due to fewer stressed alga compared to unstressed alga for some of the replicates, possibly due to issues in experimental setup.

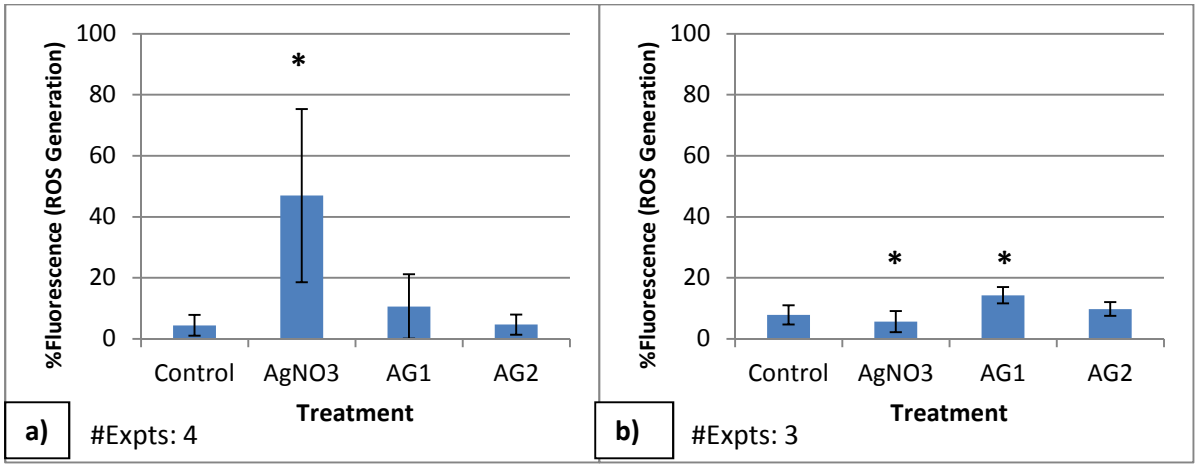

Figure 7-8. Percentage DCF fluorescence (ROS detection) of measured population when exposed to EC_{70} $AgNO_3$, AG1 and AG2 for a) *C.reinhardtii* cultures and b) *S.leopoliensis* cultures. Means +/- 1SD for the means of 3 replicates for 4 experiments (*C.reinhardtii*) and 3 experiments (*S.Leopoliensis*) respectively. Asterisks indicate significant effect compared to the control

7.3.4 Exudates Analysis

Chromatograms for toxicant analysis of *S.leopoliensis* are not included as only one control was usable. *C.reinhardtii* data is shown in Figure 7-9 which indicates the levels of organic material released within each retention time frame. Each time frame incorporates a different fraction of organic matter with the highest molecular weight (MW) material released from the column at the lowest retention time frame (28-45 minutes) while lowest MW material is released after the longest retention times (58.5-75 minutes).

The control, as well AG1 (50µg/L), AG2 (3500µg/L) and $AgNO_3$ (5µg/L) showed a high level of high MW materials (low retention times 28-45 minutes) and decreasing levels of lower MW organics over the longer retention times (Figure 7-9). In contrast *C.reinhardtii* cultures exposed to AG1 (969µg/L), AG2 (1624µg/L) and $AgNO_3$ (23µg/L) had low levels of high MW organics present, but higher levels of lower MW weight organics (Figure 7-9).

Therefore it can be noted that despite the low number of replicates, higher concentrations of toxicant (toxic stress) resulted in the production of less high MW organics and more low MW organics compared to the unstressed controls. The outlier from this pattern in this experiment is the AG2 3500µg/L exposure which while it did reduce the high MW organics

production failed to induce elevated production levels of the low MW organics in line with the other high concentration exposures. This may imply that a mild toxic stress (nominal EC_{20}) may produce different types of organic matter to a large toxic stress (>nominal EC_{70}) and that beyond a certain stress level the EPS composition is similar to control again because the ability to produce the extra low MW organic becomes impaired. These differences could potentially relate to the magnitude and rate of nanoparticle dissolution as dose and mechanistic data seemed to indicate that silver ions were playing the defining role in controlling toxicity with dissolved silver levels of AG1 after 72hours (Table 7-2) showing equivalent concentrations to ionic silver ($AgNO_3$) that caused toxicity between EC_{20} and EC_{50} levels to *C.reinhardtii* (Table 7-3). More work is required to check the EPS data owing to the low number of replicates, and possibly with a greater number of doses.

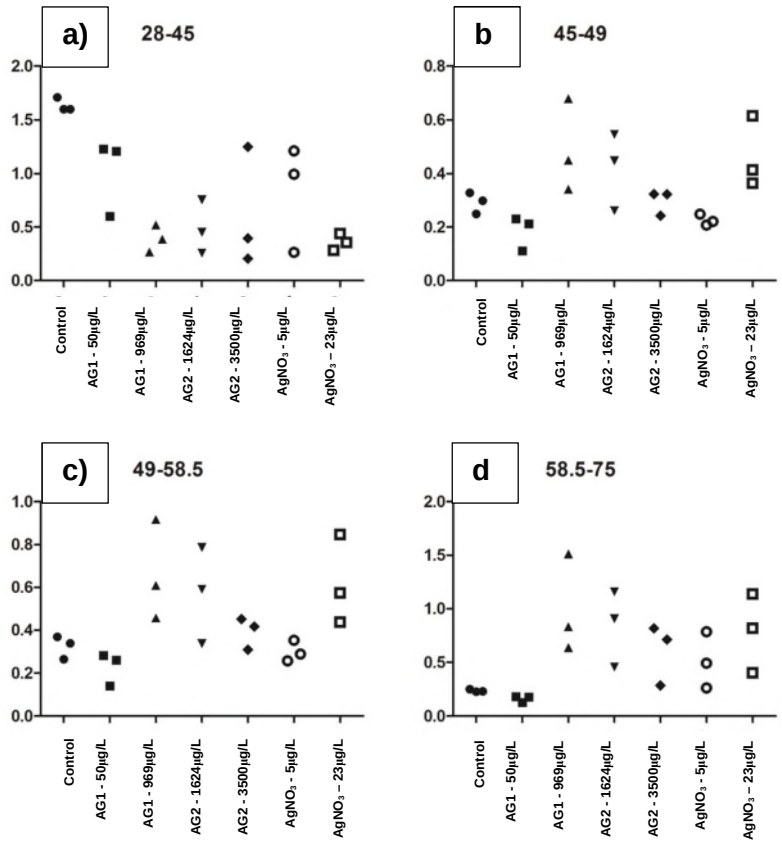

Figure 7-9. Each chart indicates the relative amounts of the EPS obtained from retention time frame for each exposure. X-axis is the sample and concentration and the y-axis is the signal intensity taken from the chromatogram from each time frame. The time frames are: a) 28-45 minutes (highest molecular weight material) b) 45-49 minutes c) 49-58.5 minutes d) 58.5-75 minutes (lowest molecular weight material).

7.4 Discussion

7.4.1 Total Silver vs. Nominal Silver

Total measured silver levels were seen to be much lower than the nominal concentrations introduced to the exposures (Figure 7-4). This would imply that either the particles were not evenly dispersed within the exposure or that they stuck to the walls of the exposure flask and were removed from suspension. It is also possible that the concentrations of the initial stock suspensions of each NP were wrongly prepared. AG2 stocks were created by weighing out NPs with PVP/citrate coatings as dry powder and then adding milli-Q water. It is possible that coating takes up a higher percentage of the mass leading to underestimation of the silver. Manufacturer stated AG1 stock concentration of 1000ppm was checked beforehand by AAS and the nominal silver concentration was matched and correct.

7.4.2 Dissolved Silver

Understanding dissolution behaviour of AgNPs in algal and cyanobacterial cultures gives valuable insight into the speciation and likely form in which NP derived metals interact with organisms. Silver that was able to travel through a 10kDa filter (assumed to be ionic silver from dissolved NPs) was measured using AAS to obtain µg/L concentrations of ionic silver released from AG1 and AG2 NPs (Table 7.2). Low levels of dissolved silver (<10%) for all treatments except AG1 in *C.reinhardtii* cultures could be due to experimental limitations. Ultrafiltration devices were soaked in copper nitrate (0.1M) to block the binding sites and therefore prevent adsorption and loss of silver in the filter therefore any silver retained in the filter is probably due to silver being adsorbed to algal and cyanobacterial cells and EPS which cannot travel through. The fact that 80% of total measured silver passed through the filters as dissolved silver (Figure 7-5a) despite the higher levels of low MW EPS noted in the

969mg/L AG1 EPS experiment is likely due to the high concentrations of silver and low relative concentration of EPS present (Figure 7-9).

The consistent low levels of recovery despite the wide range of concentrations used could indicate an experimental issue such as retention of silver on the inside walls of the plastic exposures flasks. Nanoparticles have been shown to adhere to certain experimental containers and as such it is necessary to check the suitability of laboratory ware before use[12]. It can be difficult to find containers that are suitable for both microorganism growth and for nanoparticle exposures and this should be considered when undertaking experiments of this nature. Poor presentation of the silver in the exposure flasks due to adsorption may have resulted in an underestimation of the toxic magnitude of the two nanoparticles as the observed toxic effects resulted from silver levels much lower than the nominal concentrations. Future experiments should attempt a more extensive quantification of the possible silver retention effect for this experimental setup.

It is also known that physicochemical properties of the NPs affect their dissolution including size, aggregation, concentration and surface stabilisers and coatings. Ma et al.[13] looking at the effects of size, synthesis method and coating on 5-80nm sized AgNPs noted that the former had the biggest effect on particle solubility with the latter two having little effect. Another study showed dissolution between same-sized particles (7nm) with different coatings (PVP, citrate and gum arabic) was variable indicating a coating mediated effect on ionic release from NPs rather than size[14]. The particles in this study were different sizes with AG1 having primary particles in the range of 3-10nm and the AG2 particles in the range of ~40-80nm in both MBL media and MBL media with algal and cyanobacterial EPS (see Chapter 5 and 6 for characterisation information). The AG1 particles show dissolution behaviour increasing to ~70-80% of the total silver signal when in the *C.reinhardtii* culture possibly due to size related solubility. High solubility has been seen to occur with ~7nm particles, consistent with the AG1 primary particle size[13]. Smaller sized particles are likely to be more soluble according to the Ostwald-Freundlich equation[15]. Many of the AG1 particles

are also present in tightly bound 30-100nm spherical clusters (see Chapter 5 and 6). Aggregation of particles has been seen to have no effect on the dissolution of citrate or PVP coated particles[16]. The low dissolution of the AG2 particles may relate to their larger size however the coating of these particles is also likely to play a part in the lack of dissolution. Citrate and PVP coatings have been studied in the literature, but their effect on dissolution has not yet been fully constrained as some studies have indicated that citrate coated silver particles show little dissolution compared to PVP coatings[14,17] while others have shown PVP to have a greater protective effect[18]. The PVP coating and citrate stabiliser are likely contributing partly to these particles lack of dissolution.

Whilst particle physico-chemical properties are likely influencing the dissolution of the AgNPs, external conditions could also have an impact on the dissolution. It has been shown that particle media properties will alter the dissolution of NPs such as the presence of chloride ions in solution that can result in increased NP dissolution[19]. Chloride is a constituent of the MBL Woodshole media used for exposures in this study however the effect is likely not applicable in this study as both cultures were grown in the same media and similar behaviour would be expected. Low dissolution of the AG1 particles in *S.leopoliensis* cultures but not *C.reinhardtii* cultures indicates a potential species specific effect. It is possible that AgNPs and ionic Ag released from the NPs were interacting with biological extracellular polymeric substances (EPS) exuded by both species. EPS have been shown to provide binding ligands for free ion toxicants released from NPs and influence intracellular accumulation and distribution[20]. The *S.leopoliensis* culture had a slightly higher starting cell concentration than *C.reinhardtii* and it is possible that the EPS from the former interact with ionic species produced from dissolution of AG1 particles which results in them becoming stuck in the filter during preparation meaning they do not reach AAS analysis. The type of EPS may also be a factor as different molecular weight products have been shown to have different binding behaviour to NPs[21]. However, as *S.leopoliensis* EPS samples could not be characterised, the EPS from both species could not be compared.

7.4.3 General Toxicity

The toxicity of two engineered AgNPs and an ionic $AgNO_3$ control to two aquatic microorganisms was investigated using growth rate inhibition as an end point with the aim of increasing the understanding of silver nanoparticle toxicity to relevant aquatic species.

All three forms of silver were toxic to both species as a decrease in growth rate after 72 hours was noted. $AgNO_3$ (assumed to in mainly ionic form of silver) was most toxic and there was no difference in toxicity between species, with EC_{50}s (±SE) of 43 ± 7.7 and 66.9 ± 65 µg/L for *C.reinhardtii* and *S.leopoliensis*, respectively. In contrast results from the AG1 and AG2 exposures (Table 7-3) showed both species and NP specific effects. The toxicity of two NPs were comparable, and only slightly less toxic than $AgNO_3$ to cyanobacteria *S.leopoliensis*, while for *C.reinhardtii* the toxicity of AgNPs were 20-50 times lower than that of $AgNO_3$ and AG1 appeared twice as toxic as AG2.

Other studies have also found species specific effects for nanoparticles. Ribeiro et al.[22] used $AgNO_3$ and the same AG1 silver NPs used in this study and found interspecies divergence in the toxicity level to three species from different trophic levels (green algae *Pseudonmonas subcapitata*, water flea *Daphnia magna* and zebrafish *Danio rerio*). While for *P.subcapitata* their EC_{50} value for $AgNO_3$ (33.79±2.96µg/L SE) at 72 hours is comparable to that of *C.reinhardtii* in this study (43.36µg/L ±7.66 SD), their EC_{50} for AG1 (32.40±2.09µg/L SE) is almost two magnitudes lower than ours (993.09±7.33 SD). Another study which used photosynthetic yield as the end point over much shorter time periods (1-5 hours) similarly found lower EC_{50} values than the current study for $AgNO_3$ (21.25-31.94µg/L) and carbonate coated 25±13nm AgNPs (89.42µg/L at 5hours, 356µg/L at 1 hour) of which ~1% of total nanoparticle silver was in dissolved form up to 8 days[23]. Kim and Hwang[24] noticed that cyanobacteria *Microcystis aureginosa* was much more sensitive to inhibitory effects by AgNPs than green algae and showed 87% inhibition at 1mg/L, which is of comparable sensitivity to the current study (EC_{70} of 228 ± 53 and 531 ± 267 µg/L for AG1 and AG2,

respectively). Differences between cyanobacteria *Synechococcus sp*. and marine diatom *Thalassiosira pseudonana* were also discovered however NP effect concentrations were actually an order of magnitude higher than those found in this study for *S.leopoliensis* (a member of the synechococcus family) as 50% growth inhibition occurred at concentrations (356-539µg/L)[25].

The higher sensitivities for *S.leopoliensis* to the AgNPs than for *C.reinhardtii* observed both in the present study and similar differences between green algae and cyanobacteria in the literature studies highlighted above, could be due to physical and/or biological reasons. *S.leopoliensis* are smaller organisms than *C.reinhardtii* and as such a greater surface area per volume is available allowing greater interaction or uptake of toxicants. The difference in size also results in thinner cell walls in cyanobacteria which for *Synechococcus* species tends to be ~10nm[24]. There are also biological differences in the makeup of the cell walls in each species with green algae having cellulose as the main structural constituent while cyanobacterial cell walls consist mainly of peptides, peptidoglycan in particular[24]. This could result in differences in affinity and non-specific interactions with silver species. Cell walls for *C.reinhardtii* have been to seen to be important when gauging AgNP toxicity in the literature[26].

Pore sizes in the cell walls of algal species tend to range from 5-20nm[27] which could result in greater ease of entry for smaller nanoparticles. This along with the higher dissolution of AG1, could be one reason for the greater observed toxicity of AG1 compared with AG2 seen here for *C.reinhardtii* as the primary AG1 particles in those cultures are roughly 3-10nm (Chapter 5 and 6) and could pass through the pore space to reach the cell membrane. While cell wall pore sizes are small it has been noted that NPs can cause pores to become larger which would allow even larger NPs such as AG2 to pass through to be internalised in the cells by endocytosis[23].

The type of EPS produced could also be important. *C.reinhardtii* EPS samples indicated that a concentration dependent toxic response may have occurred with more low molecular weight EPS released by stressed organisms than unstressed organisms (Figure 7-9). Unfortunately, this could not be compared with cyanobacteria EPS as the *S.Leopoliensis* samples could not be analysed. Yang et al.[21] have shown that different molecular weight organics interact in different ways with nanomaterials and as such toxicity contrasts between *C.reinhardtii* and *S.Leopoliensis* may be due in part to EPS differences. More work is required to ascertain the absolute effects of EPS on nanoparticle toxicity. Chapter 6 discusses EPS effect on nanoparticle stability.

7.4.4 Toxicity Mechanisms

Cellular mechanisms of toxicity of silver NPs on aquatic microorganisms are still not fully understood. The prominent debate in the literature is whether the toxic effects are defined by the physical/chemical properties of the nanoparticles themselves, due to ionic species created from the dissolution of the nanoparticles or a combination of both. It has long been established that Ag^+ are among the more toxic metal ions to plant and algal organisms due to positive charge and strong interactions with various ligands present in aquatic environments[28].

Navarro et al.[23] found that toxicity of silver NPs on *C.reinhardtii* was determined by Ag ion release when measuring short-term toxic effects on photosynthetic yield. Miao et al.[20] noted that toxicity to marine diatom *Thalassiosira weissflogii* was mediated by Ag^+ release while Angel et al.[16] noted that toxicity of citrate and PVP coated AgNPs was less than that of micron sized silver and was mediated by ionic Ag release. Other studies have noted that while the dissolution of ions is likely having an effect, the toxicity of the particles cannot be explained entirely due to this mechanism. Stevenson et al.[29] found that toxicity imparted on early phase *C.reinhardtii* cultures could not be explained fully by ionic release from AgNPs and particle properties may have influenced the results. Burchardti et al.[25] proposed a dual

free Ag and AgNP effect in marine diatom *T.pseudonana* and cyanobacterial species *Synechococcus sp.* Other studies have also given similar conclusions[30].

While the concentrations used in the analytical experiments are different to the toxicity experiments in this study in order to meet the limits of detection it can be seen that at least a slight percentage of all the nominal NP concentrations exhibit a dissolved silver signal meaning that some ionic silver will be present in exposures at all times. AG1 in *C.reinhardtii* cultures in particular show a drastic increase in dissolved Ag ions after 72 hours which would mean a large ionic effect is likely occurring in these samples. However AG1 in *S.leopoliensis* cultures and AG2 in both cultures do not produce many ionic species (or ionic species do not remain in suspension); <10% of total silver. The EC_{50}s based on total masses were comparable to that of $AgNO_3$, which could indicate a predominantly particle based effect.

For the AG1 particle nominal exposures of 700 and 800µg/L in *C.reinhardtii* after 72h (Table 7-2), the measured total was only around 40µg/L of which 80-100% was dissolved. These values come close to the EC_{50} for the $AgNO_3$ ionic control (Table 7-3) which means that the released ions could possibly be the only toxic agent in these exposures, with the AG1 NPs being bound or sedimented out. AG2 particles for *C.reinhardtii* appear to be less analogous to $AgNO_3$ exposures as the dissolved silver levels are so low at the AG2 EC_{50} levels (Table 7-2, 7-3) that dissolved silver cannot account for all the toxicity and a particle specific effect may be occurring in conjunction.

For *S.leopoliensis,* the dissolved silver levels for both the AG1 and AG2 particles in these exposures are very low compared with the EC_{50} values found for $AgNO_3$ so assuming the silver in the AgNO3 is primarily present as ions this would indicate that ions are unlikely to be the only silver species responsible for the toxicity of these particles to this organism.

7.4.5 Cell Viability

The toxicity of NPs was investigated further with the use of fluorescent stains. FDA was used to investigate the cellular viability of the microalgal/cyanobacterial cell membranes exposed to EC_{70} doses obtained from the dose-response curves. FDA is able to enter viable cells where it breaks down in to fluorescein which remains trapped and fluoresces. In ruptured cells the fluorescein can escape and the fluorescence is no longer at the same level as the non-ruptured cells allowing the number of viable cells to be assessed.

All three toxicants had a similar and significant effect at EC_{70} to *C.reinhardtii* exposures, reducing cell viability by 30% when compared to the non-stressed control (Figure 7-6). This implies that damage to the cell membranes is likely to be an important mechanism of toxicity for this species for these toxicants. Toxic effects from AG2 despite the low dissolution of these particles may relate to other properties such as physical abrasion effects relating to size and aggregation state or particle coatings

S.leopoliensis cell viability data showed different effects to those for *C.reinhardtii* as significant differences from the control were only seen for $AgNO_3$ with a >60% reduction in viability. For AG1 only <10% reduction was observed and no effect at all on viability was seen for AG2 (Figure 7-6). This implies that any toxicity due to both AG1 and AG2 particles was not due to cell membrane damage while for $AgNO_3$ it was responsible for significant loss in cell viability. While dissolved silver was comparable for AG1 and $AgNO_3$ it is possible that the EPS produced by this species were removing much of the ionic silver produced by the AG1 particles as despite being significantly different to the control the cell viability levels for AG1 exposures were not comparable to $AgNO_3$. Greater loss of cell viability for $AgNO_3$ may indicate that due to the greater bioavailability of ionic silver it may have damaged cell membranes more quickly than ionic silver released by AG1 over the 45 minute exposure time. The lack of significant cell viability loss also indicates that physical abrasion effects for

both NPs were potentially affecting *S.leopoliensis* less than *C.reinhardtii*, and that a different mechanism of toxic action may be involved for the two species.

It has been known for a while that membrane damage can occur in algal and bacterial species when exposed to nanomaterials[1,31] and pits have been seen in cell walls when observed using microscope techniques[32]. No microscopy techniques were utilised in this study to assess algal-particle interactions and will be considered in any future work. Other studies have also used FDA to assess cell viability in aquatic organisms however it is hard to compare different studies owing the differences in NP physico-chemical properties, cell media properties, exposure time and methodology. Oukarroum et al.[33] showed an 80% decrease in cell viability compared to the control when assessing the impact of 0.1-10mg/L AgNPs on aquatic plant *Lemna gibba* after 7 days. While another noted 24 hours exposure of *Dunaliella tertiolecta* and *Chlorella vulgaris* to 1mg/L AgNPs resulted in 33% and 44% decrease in cell viability while exposure to 10mg/L resulted in 96% and 88%[26]. The 1mg/L results are comparable to those obtained in this study for both NPs on *C.reinhardtii* which were exposed to a similar concentration. However, different exposures time and specific concentrations were used in those experiments and hence results may not be directly comparable.

7.4.6 Reactive Oxygen Species

Reactive oxygen species (ROS) were determined using two different fluorescence indicators HE and DCF. ROS are reduced oxygen intermediates produced by algal and cyanobacterial metabolic processes which are known to increase when exposed to a stressor. HE measures intracellular hydrogen peroxide (H_2O_2) while DCF measures superoxides (O_2^-), two forms of ROS with different valence states. The presence of either type was used as a proxy for overall levels of ROS.

The variations in the levels of ROS produced by *S.leopoliensis* when exposed to EC_{70}s of all toxicants were low, although unlike AG2 both $AgNO_3$ and AG1 caused significant difference to the control for both indicator stains (Figure 7-7, 7-8). DCF ROS values for $AgNO_3$ were not showing a significant increase compared to the control as the significance likely pertains to lower values than the control as described above (7.3.3.1.). However, $AgNO_3$ still gave significant difference from the control for the HE stain which indicated that it is possible that toxic mechanisms for silver ions for cyanobacteria resulted from intracellular hydrogen peroxide rather than superoxides. AG1 values showed significant change to the control unlike AG2 therefore ROS production potentially played a role in toxicity for one particle but not the other.

In the *C.reinhardtii* exposures $AgNO_3$ at the EC_{70} was seen to produce the most ROS (both intracellular H_2O_2 and superoxides) for both stains and gave the only significant differences to the control out of the three toxicants (Figure 7-7a, 7-8a, Table 7-4). Neither NP gave significant differences from the control indicating that ROS does not play a large mechanistic role in *C.reinhardtii* toxicity for these nanoparticles and ROS is unlikely to be the cause of the significant difference seen in cell viability from the control for both particles.

While HE and DCF stains have been used extensively in the eco-toxicity literature there was only one paper the author could find that used fluorescence markers to analyse the ROS levels of AgNPs on algal species. In this study ROS generation in freshwater *C.vulgaris* and marine *D.tertiolecta* after 24 hours exposure to different concentrations of AgNPs using DCF resulted in 44% and 123% (1mg/L) increase in ROS generation compared to the control and increases of 7 and 24 times the control for a larger concentration (10mg/L)[26]. While the lower concentrations were similar to those used in our study comparison is difficult owing to the different silver NPs and DCF exposure times. The lack of ROS effect noted for the particles in our study may be due to the fact that our exposures were only 45 minutes as opposed to the 24 hours used in Oukarroum et al.[26]. DCF was also used to assess ROS generation in *C.reinhardtii* using polymer coated core-shell copper oxide NPs and a large increase in

intracellular ROS after 6 hours exposure to 0.02g/L concentrations was seen. It was noted however that uncoated CuO NPs and the separate polymeric shell did not cause production of ROS and therefore an effect to change in morphology may have occurred. It was stated that uncoated particles may be aggregating and lowering surface area available for ROS to form[23,34].

Both AG1 and AG2 have been shown to be reasonably stable in plain MBL medium and in MBL medium containing algal and cyanobacterial EPS (Chapter 5 and 6) however direct interaction with the alga themselves was not assessed. This is likely important to future mechanistic studies.

Biological reasons could also account for the difference in ROS production. Microalgal and cyanobacteria species have both enzymatic and non-enzymatic oxygen scavenging defence mechanisms to prevent dangerous ROS free radicals from damaging the cells internal organs[35]. Wang et al.[36] noted that differences in the abilities of these defence mechanisms to scavenge ROS could account for differences in the levels of H_2O_2-stimulated ROS picked up by the DCF stain in cyanobacteria *M.aureginosa* and green algae *P.subcapitata*.

In this study levels of ROS were comparable for NPs between the two species (despite the significant effect of AG1 to ROS production in cyanobacteria) however levels of ROS produced for $AgNO_3$ despite significance were much lower in *S.leopoliensis*. Therefore species-specific defence mechanisms (such as EPS production) may have had an effect on ROS production.

Another potential reason for lower cyanobacteria ROS levels may relate to the penetration depth of the DCF stain. Cell wall thickness and constituency may not allow equal levels of DCF to enter each cell[36,37]. It may be that the low values of ROS for $AgNO_3$ in *S.leopoliensis* were due to lower uptake of the DCF and HE stains than for *C.reinhardtii* owing to different thicknesses/chemical constituents of the cell walls.

As with the FDA stain it could also be that concentrations of NPs and $AgNO_3$ are too low or not exposed for long enough to elicit a strong ROS signal able to be picked up by the stains. Finally, as mentioned above, it is possible that greater concentration of cyanobacterial cells and EPS may eliminate some of the ROS. EPS have been seen to protect against DNA damage and lipid peroxidation in other cyanobacterial species[38].

7.5 Conclusions

The toxicity of two different AgNPs (AG1 and AG2) with different coatings and sizes was compared to $AgNO_3$ ionic control for one green algae species and one cyanobacterial species. The order of toxicity was $AgNO_3$ > AG1 > AG2 for both species as ionic silver is able to internalised easily by aquatic microorganisms, while the smaller size and/or greater dissolution is likely to be the reason for AG1 causing higher toxicity than AG2. The steepness of the toxicity curves were variable between both species and all toxicants indicating possible differences in toxic mechanism which were further investigated with fluorescent stains. Neither of the particles showed much dissolution with the exception of AG1 in *C.reinhardtii* cultures which increased over the test duration (72h) reaching ~80% of the total. The dissolution levels for AG2 in *C.reinhardtii* cultures and both NPs in *S.leopoliensis* cultures were too low to be responsible for the observed toxicities. The low detection of total and dissolved silver could however have been caused by binding to the experimental containers or through complexation with biomass and extracellular polymeric substances respectively, and may in fact have resulted in underestimation of the toxicity of both nanoparticles when expressed based on nominal total concentrations.

Fluorescent stains and flow cytometry were used to detect cell viability and reactive oxygen species production by all three toxicants and it was found that $AgNO_3$ always had a larger effect on cell viability than the AgNPs for both species on a mass basis, and produced more

ROS than the NPs with AG1 having a greater effect in most experiments than AG2. These differences in cell viability and ROS likely relate to biological differences in the two species with respect to the cell wall. As such, clear species specific differences in both sensitivities and mechanisms could be seen between toxicants used here.

The AG1 NPs used in this study are used in industry and are as such a useful example of particles likely to be released into the environment. The greater toxicity and apparent dissolution of AG1 implies that behaviour and effects of industry standard particles must be measured to accurately model NP toxicity in natural environments. With the increasing production levels of engineered nanomaterials, concentrations in the environment are expected to rise. Currently estimations of silver concentrations in European surface waters are in the range of 0.01-127ng/L[3,4,7] which are over two orders of magnitude lower than the EC_{20} values calculated in this study. Therefore it is unlikely that high acute toxicity will occur to green algae and cyanobacteria at the concentrations currently occurring in the environment except in extreme situations near point sources. In realistic environmental scenarios the EPS produced by aquatic microorganisms likely play a large role in mitigating the toxic effect of both ionic and particulate silver.

These conclusions are useful when considering the context of risk assessment. Models and legislation for risk and fate assessment require information which improves on the current understanding of toxicity and the levels of toxicity. Current risk assessment methods are fairly blunt with their incorporation of different mostly acute toxicological endpoints and simple metrics of toxicity. EC_x values such as those obtained in this study can be used in calculating species sensitivity distributions (SSDs) and assessment factors (AF) which are valuable in giving context to risk models[39]. Knowledge gaps in the toxicity literature which are being filled by data such as that from this study will improve risk models when considering release of nanomaterials into aquatic environments.

7.6 References

1. Navarro, E. *et al.* Environmental behavior and ecotoxicity of engineered nanoparticles to algae, plants, and fungi. *Ecotoxicology* **17,** 372–386 (2008).

2. Mueller, N. C. & Nowack, B. Exposure Modeling of Engineered Nanoparticles in the Environment. *Environ. Sci. Technol.* **42,** 4447–4453 (2008).

3. Gottschalk, F., Sonderer, T., Scholz, R. W. & Nowack, B. Modeled Environmental Concentrations of Engineered Nanomaterials (TiO2, ZnO, Ag, CNT, Fullerenes) for Different Regions. *Environ. Sci. Technol.* **43,** 9216–9222 (2009).

4. Gottschalk, F., Sonderer, T., Scholz, R. W. & Nowack, B. Possibilities and limitations of modeling environmental exposure to engineered nanomaterials by probabilistic material flow analysis. *Environ. Toxicol. Chem.* **29,** 1036–48 (2010).

5. Gottschalk, F., Sun, T. & Nowack, B. Environmental concentrations of engineered nanomaterials: review of modeling and analytical studies. *Environ. Pollut.* **181,** 287–300 (2013).

6. Mitrano, D. M. *et al.* Detecting nanoparticulate silver using single-particle inductively coupled plasma-mass spectrometry. *Environ. Toxicol. Chem.* **31,** 115–21 (2012).

7. Fabrega, J., Luoma, S. N., Tyler, C. R., Galloway, T. S. & Lead, J. R. Silver nanoparticles: behaviour and effects in the aquatic environment. *Environ. Int.* **37,** 517–31 (2011).

8. OECD. Test No 201: Freshwater Alga and Cyanobacteria, Growth Inhibition Test. *OECD Guidel. Test. Chem.* **Section 2,** 25 (2011).

9. Ritz, C. & Streibig, J. Analysis of Dose Response Data. (2013).

10. Ritz, C. & Streibig, J. C. Bioassay Analysis using R. *J. Stat. Softw.* **12,** (2005).

11. Stewart, T. J., Traber, J., Kroll, A., Behra, R. & Sigg, L. Characterization of extracellular polymeric substances (EPS) from periphyton using liquid chromatography-organic carbon detection-organic nitrogen detection (LC-OCD-OND). *Environ. Sci. Pollut. Res. Int.* **20,** 3214–23 (2013).

12. Handy, R. D. *et al.* Ecotoxicity test methods for engineered nanomaterials: practical experiences and recommendations from the bench. *Environ. Toxicol. Chem.* **31,** 15–31 (2012).

13. Ma, R. *et al.* Size-Controlled Dissolution of Organic-Coated Silver Nanoparticles. *Environ. Sci. Technol.* **46,** 752–759 (2011).

14. Yang, X. *et al.* Mechanism of silver nanoparticle toxicity is dependent on dissolved silver and surface coating in Caenorhabditis elegans. *Environ. Sci. Technol.* **46,** 1119–27 (2012).

15. Misra, S. K., Dybowska, A., Berhanu, D., Luoma, S. N. & Valsami-Jones, E. The complexity of nanoparticle dissolution and its importance in nanotoxicological studies. *Sci. Total Environ.* **438,** 225–32 (2012).

16. Angel, B. M., Batley, G. E., Jarolimek, C. V & Rogers, N. J. The impact of size on the fate and toxicity of nanoparticulate silver in aquatic systems. *Chemosphere* **93,** 359–365 (2013).

17. Kittler, S., Greulich, C., Diendorf, J., Köller, M. & Epple, M. Toxicity of Silver Nanoparticles Increases during Storage Because of Slow Dissolution under Release of Silver Ions. *Chem. Mater.* **22,** 4548–4554 (2010).

18. Huynh, K. A. & Chen, K. L. Aggregation kinetics of citrate and polyvinylpyrrolidone coated silver nanoparticles in monovalent and divalent electrolyte solutions. *Environ. Sci. Technol.* **45,** 5564–71 (2011).

19. Levard, C. *et al.* Effect of Chloride on the Dissolution Rate of Silver Nanoparticles and Toxicity to E. coli. *Environ. Sci. Technol.* **47,** 5738–5745 (2013).

20. Miao, A. J. *et al.* The algal toxicity of silver engineered nanoparticles and detoxification by exopolymeric substances. *Environ. Pollut.* **157,** 3034–41 (2009).

21. Yang, X., Lin, S. & Wiesner, M. R. Influence of natural organic matter on transport and retention of polymer coated silver nanoparticles in porous media. *J. Hazard. Mater.* **264,** 161–168 (2014).

22. Ribeiro, F. *et al.* Silver nanoparticles and silver nitrate induce high toxicity to Pseudokirchneriella subcapitata, Daphnia magna and Danio rerio. *Sci. Total Environ.* **466-467C,** 232–241 (2013).

23. Navarro, E. *et al.* Toxicity of Silver Nanoparticles to Chlamydomonas reinhardtii. *Environ. Sci. Technol.* **42,** 8959–8964 (2008).

24. Park, M. H., Kim, K. H., Lee, H. H., Kim, J. S. & Hwang, S. J. Selective inhibitory potential of silver nanoparticles on the harmful cyanobacterium Microcystis aeruginosa. *Biotechnol. Lett.* **32,** 423–428 (2010).

25. Burchardt, A. D. *et al.* Effects of Silver Nanoparticles in Diatom Thalassiosira pseudonana and Cyanobacterium Synechococcus sp. *Environ. Sci. Technol.* **46,** 11336–11344 (2012).

26. Oukarroum, A., Bras, S., Perreault, F. & Popovic, R. Inhibitory effects of silver nanoparticles in two green algae, Chlorella vulgaris and Dunaliella tertiolecta. *Ecotoxicol. Environ. Saf.* **78,** 80–5 (2012).

27. Bhatt, I. & Tripathi, B. N. Chemosphere Interaction of engineered nanoparticles with various components of the environment and possible strategies for their risk assessment. *Chemosphere* **82,** 308–317 (2011).

28. Hiriart-baer, P., Fortin, C., Lee, D. & Campbell, P. G. C. Toxicity of silver to two freshwater algae , Chlamydomonas reinhardtii and Pseudokirchneriella subcapitata, grown under continuous culture conditions: Influence of thiosulphate. *Aquat. Bot.* **78,** 136–148 (2006).

29. Stevenson, L. M. *et al.* Environmental feedbacks and engineered nanoparticles: mitigation of silver nanoparticle toxicity to Chlamydomonas reinhardtii by algal-produced organic compounds. *PLoS One* **8,** e74456 (2013).

30. Griffitt, R. J., Luo, J., Gao, J., Bonzongo, J.-C. & Barber, D. S. Effects of particle composition and species on toxicity of metallic nanomaterials in aquatic organisms. *Environ. Toxicol. Chem.* **27,** 1972–1978 (2008).

31. Rodea-Palomares, I. *et al.* An insight into the mechanisms of nanoceria toxicity in aquatic photosynthetic organisms. *Aquat. Toxicol.* **122-123,** 133–43 (2012).

32. Sondi, I. & Salopek-Sondi, B. Silver nanoparticles as antimicrobial agent: a case study on E. coli as a model for Gram-negative bacteria. *J. Colloid Interface Sci.* **275,** 177–182 (2004).

33. Oukarroum, A., Barhoumi, L., Pirastru, L. & Dewez, D. Silver nanoparticle toxicity effect on growth and cellular viability of the aquatic plant Lemna gibba. *Environ. Toxicol. Chem.* **32,** 902–7 (2013).

34. Wang, J., Zhang, X., Chen, Y., Sommerfeld, M. & Hu, Q. Toxicity assessment of manufactured nanomaterials using the unicellular green alga Chlamydomonas reinhardtii. *Chemosphere* **73,** 1121–8 (2008).

35. Rastogi, R. P., Singh, S. P., Häder, D. & Sinha, R. P. Detection of reactive oxygen species (ROS) by the oxidant-sensing probe 2', 7' -dichlorodihydrofluorescein diacetate in the cyanobacterium Anabaena variabilis PCC 7937. *Biochem. Biophys. Res. Commun.* **397,** 603–607 (2010).

36. Wang, Z., Li, J., Zhao, J. & Xing, B. Toxicity and Internalization of CuO Nanoparticles to Prokaryotic Alga Microcystis aeruginosa as Affected by Dissolved Organic Matter. *Environ. Sci. Technol.* **45,** 6032–6040 (2011).

37. Schrader, K. K., Dayan, F. E. & Nanayakkara, N. P. D. Generation of reactive oxygen species by a novel anthraquinone derivative in the cyanobacterium Planktothrix perornata (Skuja). **81,** 198–207 (2005).

38. Chen, L. Z. *et al.* UV-B-induced oxidative damage and protective role of exopolysaccharides in desert cyanobacterium Microcoleus vaginatus. *J. Integr. Plant Biol.* **51,** 194–200 (2009).

39. Van Vlaardingen, P. L. A. & Verbruggen, E. M. J. *Guidance for the derivation of environmental risk limits within framework of "International and national environmental quality standards for substances in the Netherlands" (INS). Revision 2007.* (2007).

Chapter 8. Conclusions, Wider Implications and Future Work

8.1 Reiteration of Thesis Aims

As part of the international NanoFATE project[1], this thesis investigated aspects pertaining to the life-cycle analysis of post-production engineered nanoparticles in environmental matrices.

The aims of this thesis were:

- To investigate the applicability and effectiveness of using different techniques to understand the size, stability and morphology of zinc oxide and silver NPs in media of varying properties and composition at long and short term timescales including exposure to algae produced extracellular polymeric substances (EPS)
- To investigate the influence and interrelatedness of particle surface coatings, media ionic strength, exudates from green algae and cyanobacterial microorganisms and concentration on the stability of silver NPs over a two week period
- To investigate the magnitude and mechanism of toxicity of two coated silver NPs on green algae and cyanobacterial species and how this can be related to measured particle properties.

8.2 Outcomes of Research

Particle Characterisation

ZnO ENPs are subject to rapid aggregation and sedimentation in all media studied hence would not fit any definition of nanoparticle. However, as TEM images show and toxicity

results suggest, the clusters of ENPs have high surface area and are thus more reactive / soluble than the solid form.

Silver nanoparticle coatings (paraffin and citrate+PVP) are more important to nanoparticle stability than either the ionic strength of the surrounding media (water and MBL/ISO ecotoxicology media), or the suspended algal/bacterial organic matter at concentrations studied. Zeta potential results suggest this is due to the steric component of each coating offsetting electrostatic instability as well as low concentrations of phycological extracellular polymeric substances (EPS). In general the silver ENPs were observed to retain their nano dimension in the media studied. Analysis of nanoparticle aspect ratio in TEM images in this thesis was limited nevertheless showed dissolution and reprecipitation is occurring.

This work studied the behavior of industrially manufactured particles, and use of a suite of ensemble techniques was shown to give reliable particle size, distribution and aggregation/agglomeration behaviour when used contemporaneously, despite their inherent limitations and with suspension concentrations within detection range. However the use of only one method can give misleading results. Necessity of multiple-method studies has been shown in the literature but these studies have mainly only been undertaken using laboratory synthesized samples[2–5]. Electron microscopy is invaluable for determining particle morphology.

Sample concentration and polydispersity are important factors when selecting techniques. At 1000mg/L ZN1 and ZN2 nanoparticles aggregated and sedimented in de-ionised water making DLS and DCS unsuitable for detecting subtle changes in behaviour. Lower concentration AG1 and AG2 samples (1-10mg/L) gave less variable results due to their smaller size distribution.

Ecotoxicology

Low recovery rates for silver nanoparticles were noted in this work. Selection of suitable culture flasks is important for nano-ecotoxicology studies to prevent this. Selection of appropriate equipment is difficult as it must be optimized for algal/bacterial growth and also to prevent unwanted metal retention.

The test organism's biological structure is important for nanoparticle toxicity. Cyanobacteria *S.leopoliensis* were more susceptible to $AgNO_3$ (ionic silver) and silver nanoparticle toxicity (AG1 and AG2) than green algae *C.reinhardtii*.

Ionic silver control ($AgNO_3$) was more toxic to both species of microorganism than either AG1 and AG2 silver nanoparticles, however a size effect was notable with smaller sized silver nanoparticles (AG1) having greater toxicity than larger (AG2) particles. Dissolution of nanoparticles and toxicity is dependent on both particle size and type of coating. AG1 particles are smaller than AG2 plus the thickness and coverage of the AG1 paraffin coating compared with the PVP coating and citrate stabiliser of the AG2 particles result in greater dissolution.

Species specific toxic mechanisms were detected by assessing cell viability and production of reactive oxygen species (ROS). $AgNO_3$ had the largest effect on these endpoints in both species. AG1 had a greater effect on all endpoints in *S.leopoliensis* than AG2 but only cell viability was significantly affected by both nanoparticles in *C.reinhardtii*.

Toxic stress to green algae *C.reinhardtii* resulted in the production of EPS of different composition to those produced when unstressed. EPS from *S.leopoliensis* were noted to remove ionic silver from suspension but this was still not enough to prevent greater toxicity to this species than to *C.reinhardtii.*

8.3 Wider Implications

Metal and metal oxide nanoparticles from consumer products could enter sewage systems via drainage channels and travel through waste-water treatment plants to the environmental through direct pipelines or in sewage sludge[6]. Studying the properties and speciation of NPs is important for improving risk assessment. Whilst the experiments in this thesis have contributed to understanding the basics of particle behavior in ionic and organic-exposed media, these conditions are much simpler than realistic environmental scenarios which would have variable ionic strengths, concentrations and composition of suspended materials, therefore nanoparticles would likely behave differently than in this work. Sterically coated nanoparticles (such as silver nanoparticles in this work) are less susceptible to ionic strength increases (with the exception of very high ionic strengths such as seawater[7]) and may retain stability in environmental systems. While algal and cyanobacterial EPS was shown to have little effect on particle stability in this study (possibly due to low concentrations), suspended organic matter (OM) has previously been shown to both improve or prevent stability depending on the coating and composition of OM[8–10]. Microcosm/mesocosm experiments similar to those attempted in the literature[11,12] may be useful to assess these particles in realistic scenarios in the future.

Assuming the stability measured in this work was maintained, AG1 and AG2 would likely remain suspended in the water column with a high percentage of the distribution at the nano-scale. Toxicity could result from interaction with aquatic species such as algae, insects or fish, and as such they remain highly relevant to risk assessment especially if they enter the environment at high concentrations i.e. via industrial spillage. However, the non-nano aggregates of ZN1 and ZN2 nanoparticles noted in this work would likely result in sedimentation making them too large to fall under the umbrella of nano and therefore nano-risk assessment. Nevertheless, the high aspect ratio of ZN2 particles may mean that the

surface of the aggregates still has some potential for toxicity to benthic organisms. This can also be applied to soil eco-toxicology whereby particles may be present in non-nano lumps.

Transformation of nanoparticles to different chemical phases has not been the focus of this research but as the literature shows these cannot be ignored especially for ecotoxicology media containing chloride ions. Silver nanoparticles have been shown to be transformed to silver sulfides and chlorides after coming through sewage treatment processes[13–16]. Dissolution of nanoparticles mean it is possible that ionic species or even particle surfaces could have been transformed/reprecipitated as different silver or zinc species[6].

Interaction with suspended organic materials such as algal EPS, which makes up a large proportion of dissolved organic carbon (DOC) pool, likely also affect nanoparticle behavior. Cyanobacterial EPS removed Ag^+ ions released from AG1 (Chapter 7). As such released ionic species from NPs may not last long in the water column due to interaction with EPS or other suspended organic matter.

Ionic silver was a defining toxicological parameter in this work. Nanoparticle risk from dissolved ions could be legislated as ionic silver rather than nano[5]. As such greater study into the dissolution kinetics of these NPs and assessing whether the solid particles still persist and impart particle-specific effects on environmental systems is necessary.

A benefit of this work is to show which characterization technique should be applied to which purpose. The choice of technique is dependent on the situation to which it is needed. Research labs will naturally have access to many techniques which makes a multi-method comparison possible and necessary, while others may need to select only one due to access and budgetary constraints. DLS and DCS would likely be more suitable for producers who are trying to create a product with low size distribution whereas NTA would be more suitable for regulators who wish to detect the presence of nano-materials at lower concentrations. Pettitt and Lead in a recent paper have suggested the minimum characterization needed during toxicity testing incorporating concentration, physical form and surface characteristics[5]

which should be used as a guideline. Access to low and also high-end techniques will always be required.

8.4 Future Work and Recommendations

Characterisation of NPs in Environmentally Relevant Scenarios.

A gap exists between the concentrations that can be detected by commonly used characterization techniques and environmentally relevant levels of nanomaterials. Concentrations detected in the environment are much lower (ng/L in natural to low µg/L in wastewater treatment plant – WWTP- effluent)[17] than those used in this thesis and as such behaviour may differ. Toxic effects to cyanobacteria were noted as low as 33µg/L in this work therefore it is pertinent for risk assessment to worry about WWTP effluents and direct spillages from industrial accidents. At lower concentration waters it is also wise to consider bioaccumulation effects potentially causing toxic effects up the food-chain.

Techniques that provide thorough and reliable detection of silver in nanoparticulate form at environmentally relevant concentrations (ng/L-µg/L[18]) in complex matrices have yet to be fully developed. More study into the development of high-throughput ensemble methods would be very useful as this would make analysis more robust and efficient. Counting methods such as single particle ICP-MS[19] are starting to gain traction with calls to change the definition of nano-materials to incorporate size distribution. Further development and access of these techniques is necessary.

The work indicates that nanoparticle behavior can be influenced by the properties and constituents of the surrounding medium. Systematic experiments that take into account each property in an eco-toxicological or environmental system are necessary to apply data to real scenarios and to constrain the effect of each property on particle fate. Protocols to

systematise measurements across multiple laboratories would allow comparison and creation of databases of particles properties which in turn could aid in fate predictions.

Interaction with EPS: Little work has been done to assess nanoparticle interactions with EPS. Dissolved silver removal by *S.leopoliensis* exudates (Chapter.7) indicate that EPS could play an important role in mitigating toxicity. Furthermore interaction of NP surface coatings/stabilisers with EPS is also important and systematic studies in which different concentrations and compositions of EPS from a range of species are needed. In depth analysis into algal EPS composition at different levels of toxic stress for a range of species and their affinity and kinetic interaction with NP surfaces (similar to protein coronas for human NP toxicology[5]) is also needed to link composition and NP interactions. These experiments would provide useful data for fate studies and risk assessment. Additionally further work could be attempted by spinning EPS-coated NPs out of suspension to measure the total organic carbon (TOC) present on the surface of these nanomaterials and the nature of these surface interactions.

Persistence in the Environment: Although particles retain a constant PSD after 6 months, eventually their coating may degrade allowing nanoparticle transformation. Studies to predict and measure the long-term mobility and persistence of engineered nanoparticles are needed and for this measurement data of nanoparticle properties over longer time periods are useful. Studies have begun into using aged nanoparticles to simulate these effects but much work is still needed in this field.

More analysis of Coatings: Both nanoparticles and their potential stabilisers/coatings have intrinsic properties and interaction between the two could result in either suppression or enhancement of these properties. Analysis into these interactions and the resulting behavior in ecotoxicology and environmental systems is required. While it is likely impossible to know and understand every coating used on every engineered nanomaterial coatings it may be possible to categorise coatings by type or chemical composition with respect to safety

legislators such as REACH. Prediction of stability, mobility and toxicity of an industrially relevant nanoparticle (such as AG1 in this work) in a natural system based upon its coating could be possible. This will also fit into the work investigating EPS interaction as different coatings will likely have affinity for different organic matter.

Toxicity Mechanisms: Species specific toxic effects were noted in Chapter 7 however the mechanisms behind these are still not fully elucidated. Further research into specific endpoints such as cell viability and generation of reactive oxygen species and how these relate to the genetics and physical properties of the algae are likely to help. It is apparent that ROS is one of the most important toxicity mechanisms, and conversion of NPs into other species such as AgCl or Ag_2S is an outcome of NPs entering an environmental system. It may be that redox potential is the determinant property of particle fate[5].

8.5 References

1. NanoFATE. NanoFATE Website. (2014). at <https://wiki.ceh.ac.uk/display/nanofate/Home>

2. Domingos, R. F. *et al.* Characterizing Manufactured Nanoparticles in the Environment : Multimethod Determination of Particle Sizes. *Environ. Sci. Technol.* **43,** 7277–7284 (2009).

3. Mahl, D., Diendorf, J., Meyer-Zaika, W. & Epple, M. Possibilities and limitations of different analytical methods for the size determination of a bimodal dispersion of metallic nanoparticles. *Colloids Surfaces A Physicochem. Eng. Asp.* **377,** 386–392 (2011).

4. Anderson, W., Kozak, D., Coleman, V. A., Jämting, Å. K. & Trau, M. A comparative study of submicron particle sizing platforms: Accuracy, precision and resolution analysis of polydisperse particle size distributions. *J. Colloid Interface Sci.* **405,** 322–330 (2013).

5. Pettitt, M. E. & Lead, J. R. Minimum physicochemical characterisation requirements for nanomaterial regulation. *Environ. Int.* **52,** 41–50 (2013).

6. Ma, R. *et al.* Fate of zinc oxide and silver nanoparticles in a pilot wastewater treatment plant and in processed biosolids. *Environ. Sci. Technol.* **48,** 104–12 (2014).

7. Keller, A. A. *et al.* Stability and aggregation of metal oxide nanoparticles in natural aqueous matrices. *Environ. Sci. Technol.* **44,** 1962–7 (2010).

8. Lau, B. L. T., Hockaday, W. C., Ikuma, K., Furman, O. & Decho, A. W. A preliminary assessment of the interactions between the capping agents of silver nanoparticles and environmental organics. *Colloids Surfaces A Physicochem. Eng. Asp.* **435,** 22–27 (2013).

9. Yang, X., Lin, S. & Wiesner, M. R. Influence of natural organic matter on transport and retention of polymer coated silver nanoparticles in porous media. *J. Hazard. Mater.* **264,** 161–168 (2014).

10. Liu, X., Jin, X., Cao, B. & Tang, C. Y. Bactericidal activity of silver nanoparticles in environmentally relevant freshwater matrices : Influences of organic matter and chelating agent. *J. Environ. Chem. Eng.* **2,** 525–531 (2014).

11. Bone, A. J. *et al.* Biotic and abiotic interactions in aquatic microcosms determine fate and toxicity of Ag nanoparticles: part 2-toxicity and Ag speciation. *Environ. Sci. Technol.* **46,** 6925–33 (2012).

12. Unrine, J. M., Colman, B. P., Bone, A. J., Gondikas, A. P. & Matson, C. W. Biotic and abiotic interactions in aquatic microcosms determine fate and toxicity of Ag nanoparticles. Part 1. Aggregation and dissolution. *Environ. Sci. Technol.* **46,** 6915–24 (2012).

13. Lowry, G. V *et al.* Long-term transformation and fate of manufactured ag nanoparticles in a simulated large scale freshwater emergent wetland. *Environ. Sci. Technol.* **46,** 7027–36 (2012).

14. Lowry, G. V, Gregory, K. B., Apte, S. C. & Lead, J. R. Transformations of nanomaterials in the environment. *Environ. Sci. Technol.* **46,** 6893–9 (2012).

15. Levard, C. *et al.* Effect of Chloride on the Dissolution Rate of Silver Nanoparticles and Toxicity to E. coli. *Environ. Sci. Technol.* **47,** 5738–5745 (2013).

16. Levard, C. *et al.* Sulfidation of silver nanoparticles: natural antidote to their toxicity. *Environ. Sci. Technol.* **47,** 13440–8 (2013).

17. Mitrano, D. M. *et al.* Detecting nanoparticulate silver using single-particle inductively coupled plasma-mass spectrometry. *Environ. Toxicol. Chem.* **31,** 115–21 (2012).

18. Fabrega, J., Luoma, S. N., Tyler, C. R., Galloway, T. S. & Lead, J. R. Silver nanoparticles: behaviour and effects in the aquatic environment. *Environ. Int.* **37,** 517–31 (2011).

19. Tuoriniemi, J., Cornelis, G. & Hassellöv, M. Size discrimination and detection capabilities of single-particle ICPMS for environmental analysis of silver nanoparticles. *Anal. Chem.* **84,** 3965–72 (2012).